TECHNISCHE UNIVERSTÄT MÜNCHEN

Fakultät Wissenschaftszentrum Weihenstephan für Ernährung,
Landnutzung und Umwelt

Lehrstuhl für Atmosphärische Umweltforschung

Annual variation of chemical composition and source apportionment of particulate matter in Beijing

Rongrong Shen

Vollständiger Abdruck der von der Fakultät Wissenschaftszentrum Weihenstephan für Ernährung, Landnutzung und Umwelt der Technischen Universität München zur Erlangung des akademischen Grades eines

Doktors der Naturwissenschaften

genehmigten Dissertation.

Vorsitzende: Univ-Prof. Dr. Annette Menzel

Prüfer der Dissertation:

1. Univ-Prof. Hans Peter Schmid, Ph.D.
2. apl. Prof. Dr. Stefan Emeis
   Universität zu Köln

Die Dissertation wurde am 05.09.2014 bei der Technischen Universität München eingereicht und durch die Fakultät Wissenschaftszentrum Weihenstephan für Ernährung, Landnutzung und Umwelt am 30.03.2015 angenommen.

Acknowledgements

First of all, I would like to express my appreciation to Prof. Dr. Klaus Schäfer who helped me a lot in the past five years. Without his patience, contribution, supporting and encouragement, I would never have finished my PhD thesis.

I would like to show my special thanks to Prof. Dr. Hans Peter Schmid who provided me financial aid during my fifth year which made finishing my PhD study to be a reality.

I also want to thank Prof. Dr. Stefan Emeis and Dr. Peter Suppan for their helps during these years. Whenever I needed them, they always stood behind me and supported me.

Thanks to Prof. Yuesi Wang for supporting PM sampling and experiments in Beijing.

Thanks to Prof. Longyi Shao and Prof. Kuang Cen for supporting PM sampling.

Thanks to Dr. Jürgen Schnelle-Kreis for discussing and supporting organic compound analysis, especially giving me many helpful comments on my PhD thesis.

Thanks to Dr. Gülcin Abbaszade for supporting organic compound analysis.

Thanks to Dr. Stefan Norra, Dr. Utz Kramar and Dr. Nina Schleicher for supporting inorganic elements measurement.

Thanks to Mr. Mathieu Fricker and Dr. Volker Dietze for supporting filter weighing.

Thanks to Dr. Richard Foreman for proofreading the manuscript of my PhD thesis and also for accompanying me for five years as an office colleague.

Thanks to China Scholarship Council and Karlsruhe Institute of Technology, Center of Climate and Environment for funding support.

Additionally, I would like to thank all other members of our group for always being nice to me. And also thank all my Chinese colleagues for making me away from homesick.

Finally, I want to show my greatest gratitude to my parents for supporting and caring me all the time and also to my husband, Cheng Gao, for his supporting and understanding. Without them, there would be no me.

Abstract

After the emission reduction measures during the Olympic Summer Games 2008, mass and number concentrations of fine airborne particulate matter (PM) in Beijing were still high, especially haze pollution became more and more frequent recently. In order to find out the long-term characteristics of PM in Beijing and to identify the main sources of PM, especially during haze episodes in different seasons and weather conditions, a continuously one year PM sampling from June 2010 till June 2011 and two month PM sampling from April 2013 till June 2013 were performed.

The chemical characteristics of PM in Beijing were investigated. EC, OC, elements, water soluble ions and organic compounds (hopanes, PAHs and levoglucosan) were analyzed. Organic matter and secondary inorganic ions (SO_4^{2-}, NO_3^- and NH_4^+) were found to be the major fractions of PM in Beijing which contributed 22-41% and 25-37% to PM mass, respectively, indicating that anthropogenic sources of PM are dominant in Beijing. In addition, meteorological parameters were also found to be an important influence on PM mass loading. High relative humidity and low MLH can enhance PM mass concentration while precipitation can reduce pollutant concentrations. Different wind directions have different influences, such as northerly winds transport dust to Beijing and southerly winds carry pollution from industrial area to Beijing. Visibility was mainly reduced by a high amount anthropogenic compounds, especially by secondary inorganic ions.

As classical pollution events in Beijing, haze and dust were also investigated. The comparison between haze, dust and clear days was performed. The results showed that PM mass concentration during both haze and dust days were 3-4 times higher than during clear days. Secondary inorganic ions were found to be the most important part of PM during haze days throughout the whole year. The variation of mass percentages of secondary inorganic ions showed the highest value during haze days, which indicated that haze was dominated by fine particles. This result was also found in the $PM_{2.5}/PM_{10}$ ratio. The backward trajectories were usually used to distinguish the sources of different dust events. So dust storms on 17 and 30 April 2011 were found to be originated from the sandy lands and Gobi deserts, respectively. The ratio of Mg/Al was used to identify the dust contribution from outside and inside Beijing.

Therefore, sources from outside and inside Beijing contributed 25% and 75% to the total mineral particles amount of PM, respectively, during the dust event on 19 May 2013.

Sources of PM were estimated by characteristics of compounds in PM. High levoglucosan concentrations in summer and autumn indicated that contributions of biomass burning to PM exposure are significant. The homohopane index, hopane index and diagnostic ratios of PAHs illustrated that coal and fuel oil combustion were the main sources for hopanes and PAHs in PM. Further, these results were supported by Positive Matrix Factorization (PMF) source apportionment. Seven sources of PM were obtained: industry, secondary nitrate formation, secondary sulfate formation, coal combustion, traffic, mineral dust and biomass burning.

High PM mass concentration is always found during haze episodes. The sources of PM during haze episodes are important. In general, PM during clear days was influenced by dust and traffic emissions while during haze days PM was dominated by secondary inorganic ions during the whole year. The different sources of particles during haze in different seasons were given in this study for the first time. Source apportionment showed that secondary inorganic ions formation and biomass burning were the main sources for haze in summer and autumn, winter haze was dominated by a mixture of different sources especially by coal combustion, while spring haze was mainly caused by mineral dust. These results were in good agreement with the analysis of the characteristics of the variation of the particles composition. In addition, backward trajectory cluster analysis was applied in this study. Generally, southerly air flow transport from industrial regions was found to be the main source of particles during haze in Beijing.

Consequently, this study gives a systematically comprehensive investigation on PM exposure in Beijing. It supplies the clear knowledge on sources of PM in all seasons, especially during haze episodes. These results may be useful to develop effective emission control strategies.

Zusammenfassung

Trotz der Emissionsreduktionsmaßnahmen anlässlich der Olympischen Sommerspiele 2008 sind die Massen- und Anzahlkonzentrationen der feinen luftgetragenen Partikel (PM) in Peking erhöht und die Smog(Dunst)-Ereignisse nehmen zu. Um die langfristigen Eigenschaften der Partikel in Peking zu erfassen und deren wesentlichen Quellen zu identifizieren, insbesondere während der Smogereignisse zu unterschiedlichen Jahreszeiten und Wettersituationen, wurden eine einjährige Messkampagne von Juni 2010 bis Juni 2011 sowie eine zweimonatige Messkampagne von April bis Juni 2013 zur Sammlung der Partikel durchgeführt.

Es wurden die chemischen Eigenschaften der gesammelten Partikel untersucht. Elementarer Kohlenstoff (EC), organischer Kohlenstoff (OC), Elemente, wasserlösliche Ionen und organische Komponenten (Hopan, PAH, Levoglucosan) wurden analysiert. Als Hauptbestandteile der Partikel in Peking wurden organische Substanzen und sekundäre anorganische Ionen (SO_4^{2-}, NO_3^- und NH_4) identifiziert, die zu 22–41% bzw. 25–37% zur Partikelmasse beitragen. Das bedeutet, dass anthropogene Quellen der Partikel in Peking dominieren. Zusätzlich haben meteorologische Parameter einen wesentlichen Einfluss auf die die Partikelmasse. Eine hohe relative Feuchte und eine niedrige Mischungsschichthöhe erhöhen die Partikelmassenkonzentrationen während Niederschlag deren Massenkonzentration verringert. Die verschiedenen Windrichtungen haben einen unterschiedlichen Einfluss auf die Partikelbelastung in Peking. Nördliche Winde verursachen einen Staubtransport, und südliche Winde ermöglichen einen Einfluss nahe gelegener Industrieregionen. Die Sichtweite wird im Wesentlichen durch den hohen Anteil anthropogen erzeugter Partikel, insbesondere sekundäre anorganische Ionen, reduziert.

Als klassische Luftbelastungen wurden Dunst- und Staubereignisse in Peking untersucht und mit der Situation an klaren Tagen verglichen. Die Ergebnisse zeigen, dass die Partikelmassenkonzentration an Dunst- und Staub-Tagen drei- bis viermal höher als an klaren Tagen ist. Als wesentlicher Bestandteil der Partikel an Dunst-Tagen wurden die sekundären anorganischen Ionen identifiziert. Der Massengehalt sekundärer anorganischer Ionen war den höchsten Wert während Dunst Tage. Das ist auch ein Hinweis darauf, dass Dunst vor allem durch feine Partikel gebildet wird. Dieses Ergebnis wird vom Massenkonzentrationsverhältnis $PM_{2.5}/PM_{10}$ bestätigt. Rückwärts-berechnete Trajektorien wurden zur Bestimmung der Quellen

der Partikel an Staub-Tagen genutzt. Damit wurde herausgefunden, dass die Staubstürme am 17. und 30. April 2011 ihren Ursprung in der Sandfläche bzw. Gobi-Wüste hatten. Das Verhältnis der Staubkomponenten Mg/Al wurde zur Bestimmung der Staubquellen außerhalb und innerhalb von Peking verwendet. Diese Quellen tragen mit 25% bzw. 75% zum Mineralstaubgehalt der Partikel bei einem Staubereignis am 19. Mai 2013 bei.

Auf der Grundlage der chemischen Zusammensetzung der Partikel wurden deren Quellen ermittelt. Hohe Levuglucosan-Konzentrationen im Sommer und Herbst weisen auf einen wesentlichen Beitrag der Biomasse-Verbrennung an der Partikelmassenkonzentration hin. Der Homohopan- und Hopan-Index sowie die diagnostischen Verhältnisse von PAHs sind Indikatoren für Kohle- und Heizölverbrennung als Hauptquellen von Hopan und PAHs. Die Quellzuordnung wurde außerdem mittels einer Positiven Matrix-Faktorisierung (PMF) berechnet. Damit wurden sieben Quellen erhalten: Industrie, Bildung von sekundäres Nitrat, Bildung von sekundäres Sulfat, Kohleverbrennung, Verkehr, Mineralstaub und Biomasseverbrennung.

Während Dunst-Episoden wurden stets hohe Partikelmassenkonzentrationen festgestellt, deren Quellen untersucht wurden. Generell sind während des ganzen Jahres die Bestandteile der Partikel an klaren Tagen durch Staub- und Straßenverkehrsemissionen verursacht sowie an Dunst-Tagen von sekundären anorganischen Ionen dominiert. Die verschiedenen Quellen der Partikel während Dunst-Episoden im Laufe eines Jahres wurden in dieser Arbeit das erste Mal bestimmt. Die Quellzuordnung zeigte, dass Bildung von sekundäre anorganische Ionen und Biomasseverbrennung die Hauptquellen des Dunstes im Sommer und Herbst sind. Im Winter dominiert eine Vielzahl von Quellen, und im Frühjahr ist die Hauptquelle Mineralstaub. Diese Ergebnisse sind in guter Übereinstimmung mit der Analyse der Variation der Zusammensetzung der Partikel. Schließlich hat die eingesetzte Rückwärts-Trajektorien-Analyse gezeigt, dass der Luftmassentransport aus den südlichen Industriegebieten eine Hauptquelle der Partikel während Dunstepisoden in Peking ist.

Somit ist diese Arbeit eine systematische, umfassende Untersuchung der Partikelbelastung in Peking. Es wird eine vertiefte Kenntnis der Quellen von Partikeln in allen Jahreszeiten, vor allem während Dunstepisoden, erlangt. Diese Ergebnisse sind eine wichtige Grundlage für die die Entwicklung effektiver Emissionskontrollstrategien.

Contents

Chapter 1 Introduction

1.1 State of the Art

Particulate matter (PM), the suspended mixture of solid and liquid particles in the air, is an important object which can influence the Earth's energy budget (Sokolik and Toon, 1996; Alpert et al., 1998; Satheesh et al., 2005), global climate (IPCC 2013), visibility (Doyle and Dorling, 2002; Jung and Kim, 2006; Cao et al., 2012) and human health (Schwartz, 1994; Pope and Dockery, 2006; Shao et al., 2006; Dimitrova et al., 2012). In the past years, many studies about particle characteristics have been done, such as physical characteristics and chemical composition, further source appointment, as well as health and environmental impacts.

1.1.1 Physical characteristics

The physical characteristics of PM include mass concentration, number concentration, size distribution, shape, surface description and optical parameters.

Mass concentration is an important parameter for assessing the air pollution level, so it is often used in air quality guidelines, which require the implementation of threshold values worldwide, such as from the World Health Organization (WHO) (source from http://www.who.int/mediacentre/factsheets/fs313/en/), the European Commission (EC) (source from http://ec.europa.eu/environment/air/quality/standards.htm), the United States Environmental Protection Agency (US-EPA) (source from http://www.epa.gov/air/criteria.html) and China (source from http://kjs.mep.gov.cn/hjbhbz/bzwb/dqhjbh/dqhjzlbz/201203/t20120302_224165.htm) (Table 1.1). For instance, PM_{10} (the particles with aerodynamic diameters less than 10 μm) concentrations in 86 Chinese cities were investigated on the basis of air pollution index (API) records by Qu et al. (2010). They concluded PM_{10} mass concentrations in northern cities (108 μg m^{-3}), central cities (95 μg m^{-3}) and southern cities (55 μg m^{-3}) and hence showed that

northern cities in China had more serious air pollution than southern cities. PM_{10} was observed in Leipzig, Germany for 5 years (2005-2009) by Engler et al. (2012), and they found that 232 days during the sampling period at roadside sampling site exceeded the 24 h mean PM_{10} threshold value from EC (50 μg m^{-3}). This example shows that European cities also suffer from high PM exposure. Jahn et al. (2013) collected ambient and personal $PM_{2.5}$ (the particles with aerodynamic diameter less than 2.5 μm) samples in Guangzhou during winter 2011 and found that the average ambient and personal $PM_{2.5}$ pollution during the whole sampling period was 78 ± 28 μg m^{-3} and 72 ± 33 μg m^{-3}, respectively, which were higher than the 24 h mean $PM_{2.5}$ threshold values of the WHO and US-EPA air quality guidelines (Table 1.1). All these results show that air pollution is a problem worldwide that will take time to be improved.

Table 1.1: Threshold values from air quality guidelines for PM around the world

	Annual mean (μg m^{-3})		24 hour mean (μg m^{-3})	
	PM_{10}	$PM_{2.5}$	PM_{10}	$PM_{2.5}$
WHO	20	10	50	25
EC	40	25	50	/
US-EPA	/	12	150	35
China (Grade I)	40	15	50	35
China (Grade II)	70	35	150	75

Monitoring number concentration and size distribution of PM is also very important for studying particles because ultrafine particles (the particles with aerodynamic diameter less than 100 nm) contribute less to PM mass concentration but much to number concentration (Morawska et al., 1998; Rodríguez et al., 2005). Finer particles, which have a larger number concentration, can penetrate deeper into the human respiratory tract and hence have a greater influence on human health when compared with coarser particles (Dockery et al., 1993; Schwartz et al., 1996), which indicates number concentration and size distribution can also affect human health (e.g. Penttinen et al., 2001). Many studies on number concentration and size distribution were carried out in the past. For instance, particle number concentration was found to be influenced by solar radiation, wind direction and wind speed (Wehner and Wiedensohler, 2003). Traffic activities was also found to be an important factor which influence PM number concentration temporal variation (Hussein et al., 2004). See et al. (2006) investigated PM during clear days and haze days in Singapore for one year and the results

showed that the mean number concentration of particles with diameters in the range 8 – 20,000 nm during clear days and haze days was $2.88 \times 10^4 \pm 1.42 \times 10^4$ cm^{-3} and $5.31 \times 10^5 \pm 8.33 \times 10^5$ cm^{-3}, respectively; and the number size distribution showed bimodal distributions during both clear (peaks at particle diameters of 10 nm and 35 nm) and haze days (peaks at particle diameters of 50 nm and 400 nm). This study demonstrated that during haze days, both the number and size of particles were increasing. Cusack et al. (2013) monitored PM_1 in the western Mediterranean and found that average number concentrations N increased from the nucleation mode in the size range 9 – 30 nm ($N_{9-30\,nm}$) at 616 cm^{-3}, to the accumulation mode ($N_{100-825\,nm}$) at 881 cm^{-3}, and then to the Aitken mode ($N_{30-100\,nm}$) at 1601 cm^{-3}, which indicated that Aitken mode was the dominant particle mode.

The morphology of particles, such as shape, size, surface area, volume, reflectivity and absorbance, has also been studied in the past. The main analysis methods are scanning electron microscope (SEM), energy dispersive X-ray (EDX) and transmission electron microscopy (TEM). For instance, SEM combined with EDX and TEM were used by Piña et al. (2002) to investigate the microscopic morphology of lead-rich particles in San Luis Potosi, Mexico. Li et al. (2011a) investigated the microscopic morphology of haze particles during winter time using TEM. The morphology of single particles in Macao was studied by SEM, where soot and roughly spherical particles were found to be the dominant fractions in PM (Li et al., 2011b). Fu et al. (2012) collected aerosol samples during October and November 2010 in Shanghai, and four types of carbonaceous matters including polymeric organic compound (POC), soot, tar ball, and biogenic particles were found by using TEM and EDX.

1.1.2 Chemical characteristics

The chemical composition of PM is very complex. The particles from both different sources and sizes have different composition. The chemical composition analysis of particles is currently one of the most common studies and includes water soluble ions, inorganic elements, carbonaceous matter, and organic compounds. The main analysis methods are proton-induced X-ray emission analysis (PIXE), inductively coupled plasma mass spectrometry (ICP-MS), ion chromatography (IC), atomic absorption spectrometry, atomic fluorescence spectrometry, energy dispersive X-ray fluorescence spectrometry as well as high performance liquid chromatography and gas chromatography–mass spectrometry (HPLC-MS and GC-MS).

Water soluble ions are considered to be an significant fraction of ambient PM, about one quarter or more of the total $PM_{2.5}$ mass (He et al., 2001; Yao et al., 2002; Chan and Yao, 2008; Shen et al., 2009). They can increase the hygroscopicity of particles (Tang et al., 1995), reduce visibility (Lee et al., 2005; Yuan et al., 2006), and influence climate change (Wang et al., 2005a). The dominated fractions in water soluble ions are secondary inorganic ions (sulfate (SO_4^{2-}), nitrate (NO_3^-) and ammonium (NH_4^+))(Yao et al., 2002; Xiao et al., 2004; Shon et al., 2012), which are mostly produced by chemical reaction processes from their precursor gases, such as sulfur dioxide (SO_2), nitrogen oxides (NO_x) and ammonia (NH_3) (Seinfeld and Pandis, 2006; Ianniello et al., 2011; Shon et al., 2012). Furthermore, the particle size distributions of water soluble ions have also been studied worldwide, such as in Dayalbagh, Agra (Parmar et al., 2001), Korea (Park and Kim, 2004), Canada (Zhang et al., 2008a), and Newark, USA (Zhao et al., 2008). All these results showed that SO_4^{2-} and NH_4^+ were in the fine mode while NO_3^- was in both fine and coarse modes.

Usually inorganic elements contribute a small fraction to the ambient PM mass, but some elements, especially trace elements, are reported to have an adverse affection on human health (e.g. Shao et al., 2006; Wu et al., 2012a) and the ecosystem (Duan et al., 2013). Because most toxic trace elements concentrate in the fine mode of particles (Yang et al., 2009; Li et al., 2012), they can float in the air with long lifetimes and influence a large scale area. Therefore, an investigation into the elements is also necessary. Richter et al. (2007) measured the elements in PM_{10} which were collected in Chile during winter from 1997 till 2003 and three groups of carbonates and oxides, mobile elements, and immobile elements were found. In all groups, mobile elements were found to have more influences on the environment and human health. Cao et al. (2008) focused on the variations of Cr, Cu, Cd, Pb and Zn concentrations during the past 40 years (1965-2005) in Shanghai and found that these five heavy metal mass concentrations increased with the increase in industry and traffic emissions. Chen et al. (2008) analyzed stable lead isotope ratios in Shanghai and found that stationary industrial emissions were the main source for lead pollution. Mutlu et al. (2012) investigated Cd mass concentrations in Korea over a period of 7 years and found that the annual mean levels of Cd decreased from port cities, through to industrial and inland cities. At the same time, the carcinogenic risk which was caused by Cd in port and industrial cities was found to be higher than that in inland cities. All these studies showed that industry is an important source for inorganic elements.

Organic carbon (OC), as a key component in cooling the atmosphere (IPCC, 2013), is caused by not only the primary emission, such as fossil fuel combustion and biomass burning (Duan et al., 2004, 2005), but also chemical conversion processes which produce secondary organic carbon (SOC) (Pandis et al., 1992). Elemental carbon, which originates from incomplete combustion, affects the visibility, climate and radiative forcing (Jacobson, 2001; Menon et al., 2002; Duan et al., 2005), and is also used to evaluate the environment and health influence from traffic (Keuken et al., 2012). Both OC and EC are important part of PM (Yang et al., 2011a, 2011b). Cao et al. (2007) found that both OC and EC showed the lowest mass concentrations in summer and the highest mass concentrations in winter. The same results, the highest OC and EC mass concentrations in winter, were also observed in Europe by Aymoz et al. (2007). EC and organic matter (OM) constitute carbonaceous matter (CM), which contribute 20 – 50% of particle mass (Rogge et al., 1993a; Lim and Turpin, 2002; Cao et al., 2007). With the exception of primary OC, secondary OC (SOC) has been investigated considerably and was found to have higher contribution to OC during summer than winter (Strader et al., 1999; Cao et al., 2007), but contrary result was also obtained (Dan et al., 2004; Zhao et al., 2013a). This different result could be caused by different meteorological conditions and emission sources.

The organic matters in PM contain more than 20,000 species which have been identified, such as alkanes, acids, polyols, aromatic compounds, polycyclic aromatic hydrocarbons (PAHs), and hopanes. Particulate organic matter (POM) originates from direct emission and also from gas-to-particles conversion. It is another large and important fraction of PM, which can account for 30% - 50% of Beijing's total fine particle mass (He et al., 2006). It can reduce visibility and change radiative transfer (He et al., 2006). It also has been found to affect human health, especially because it contains some carcinogenic and mutagenic compounds, such as, polychlorinated biphenyls (PCBs) and PAHs (He et al., 2006; Ross, 2004; Kim et al., 2013). In airborne particles, PAHs are one of the most important organic compounds which have been measured extensively in the past years, such as in Göteborg, Sweden (Brorström-Lundén and Lindskog, 1985), Upper Silesia, Poland (Bodzek et al., 1993), Massachusetts, USA (Allen, et al., 1996), Kuala Lumpur, Malaysia (Omar et al., 2002), and Shanghai, China (Gu et al., 2010). PAHs showed much higher mass concentrations in winter and autumn than in summer and spring due to higher emissions and meteorological conditions (Zheng and Fang, 2000; He et al., 2006; Tan et al., 2006; Gu et al., 2010). Hopanes and levoglucosan are also important organic compounds which are widely used as a tracer for fossil fuel combustion (Huang et al., 2006) and biomass burning (Zhang et al., 2008b; Wagener et al., 2012), respectively. The

homohopane index and hopane index were in particular used more often in the past to distinguish sources of particles (e.g. Oros and Simoneit, 2000; Schnelle-Kreis et al., 2007).

1.1.3 Source apportionment (SA)

1.1.3.1 Source types

In general, source types of PM can be summarized as follows:

(1) Natural and anthropogenic sources. PM can originate from natural sources, like volcanic eruptions, sea spray and dust storms, as well as from anthropogenic sources which are caused by human being's activities, such as fossil fuel combustion, vehicle and industrial emissions.

(2) Primary and secondary sources. PM can also be grouped into primary and secondary particles on basis of the formation mechanism. Primary PM is originated from direct emission of natural and anthropogenic sources, such as sea spray, dust storms, biomass burning, construction and fossil fuel combustion. Secondary particles are formed from chemical reactions, such as secondary sulfate and nitrate which are mostly formed from their precursors SO_2 and NO_x, respectively.

(3) Local and non-local sources. On a geographical scale, sources of PM can also be classified into local and non-local sources. Local sources imply that the particles are emitted from the sources in the studied area while non-local sources imply that the particles are transported from contiguous cities or even from thousands kilometers away. Air pollution is thus not strictly a local problem anymore, as it can be influenced by sources on a regional scale.

1.1.3.2 Source markers

EC, OC, secondary inorganic ions, inorganic elements and organic compounds are the main components in PM. Different compounds can originate from single or different sources. Many previous studies on source apportionment of PM used chemical composition tracers to characterize sources (e.g. Arditsoglou and Samara, 2005; Song et al., 2007; Gu et al., 2011). Therefore chemical composition tracers and certain ratios of compounds play an important

role on the source apportionment and the chemical composition, which is measured in this study and their possible sources are listed in Table 1.2.

1.1.3.3 Source apportionment models

In order to improve air quality, a better understanding of the sources of PM is necessary, such as the use of source appointment (SA). Dispersion models and receptor models, which are two major groups of SA techniques, have been used extensively for determining the distribution and contribution of different sources.

Dispersion models aim to simulate how the particles form, transport and deposit in the atmosphere and to also calculate particle concentrations at different locations by using particles emission inventories (Holmes and Morawska, 2006; Viana et al., 2008). The disadvantage of this kind of method is that detailed emission inventories are necessary but are not easily obtained.

Receptor models identify the sources of particles on the basis of their chemical composition concentrations at the monitoring sites. Mass conservation is assumed in receptor models so that the sources of PM can be identified using a mass balance analysis (Hopke et al., 2006).

Because receptor models are much easier to be implemented than dispersion models, many receptor models were developed during the last years, such as principal component analysis (PCA), factor analysis (FA), chemical mass balance (CMB), and positive matrix factorization (PMF). Many studies on SA have been done on the basis of these receptor models. Chen et al. (2010) used the Effective Variance Chemical Mass Balance (EV-CMB) receptor model to perform $PM_{2.5}$ SA in the United States. Wang et al. (2013) used the PCA and PMF receptor models to identify the sources of TSP over the Northern Yellow Sea and got similar results from both models. Yang et al. (2013) used PMF to identify the sources of $PM_{2.5}$ in Jinan, China and concluded six main sources. In addition to the use of particulate chemical composition to perform SA, particle size distribution data also was used. For instance, Gu et al. (2011) identified seven main sources of PM_{10} in Augsburg, Germany by PMF model on the basis of particle size distribution data.

Table 1.2: Source markers

Chemical composition	Sources	Reference
OC	Fossil fuels; Biomass burning; Chemical conversion processes	Pandis et al., 1992; Duan et al., 2004; Duan et al., 2005
EC	Fossil fuels; Biomass burning	Castro et al., 1999
Cl^-	Coal combustion; Biomass burning; Sea salt	Yao et al., 2002; Li et al., 2007
NO_3^-	Chemical reactions of precursor gases	Guo et al., 2010; Ianniello et al., 2011
SO_4^{2-}	Chemical reactions of precursor gases	Guo et al., 2010; Ianniello et al., 2011
NH_4^+	Chemical reactions of precursor gases	Guo et al., 2010; Ianniello et al., 2011
Mg	Crustal sources	Yang et al., 2005
Al	Crustal sources	Yang et al., 2005
K	Sea salt; Soil-derived; Biomass burning; Waste incineration	Zhang et al., 2008a; Zhang et al., 2010; Deng et al., 2011; Li et al., 2013
Ca	Construction dust	He, et al., 2001; Han et al., 2007
Ti	Crustal sources	Zhang et al., 2010
Fe	Crustal sources	Yang et al., 2005
V	Fuel oil combustion	Fang et al., 2010
Cr	Coal combustion; Industrial contaminants; Vehicle emission; Fuel oil combustion	Gao et al., 2002; Fang et al., 2010; Shi et al., 2010; Yang et al., 2013
Mn	Crustal sources; Iron smelters; Waste incineration	Zhang et al., 2010
Ni	Fuel oil combustion	Fang et al., 2010
Cu	Vehicle emission; Industrial emission; Brake and pump system; Waste incineration	Lee et al., 1999; Xu et al., 2012
Zn	Vehicle emission; Lubricant oil; Brake linings; Tires; Industrial contaminants; Waste incineration	Li et al., 2004; Song et al., 2006a; Shi et al., 2010; Xu et al., 2012
As	Coal combustion; Smelter and base-metal refinery industries	Tian et al., 2010; Wang and Mulligan, 2006
Sb	Brake wear	Pakkanen et al., 2001
Ba	Road dust	Viana et al., 2006
Pb	Vehicle emission; Ceramic industry; Manufacturing of insecticides; Paints; Glass; Storage batteries	Li et al., 2004; Soriano et al., 2012
Hopane	Fossil fuel combustion	He et al., 2006; Schnelle-Kreis et al., 2007
PAH	Fossil fuel combustion	Hou et al., 2006
Levoglucosan	Biomass burning	Zhang et al., 2008b; Wagener et al., 2012

However, in the receptor models mentioned above, the disadvantage of CMB models is that sometimes compelete source emission profiles which are needed in CMB models cannot be obtained or cannot be suitable in research area because they are from the U.S. (Song et al., 2006a). Therefore, the methods which can apportion sources without source profiles, such as PCA, FA and PMF, are used widely to avoid such problems. However, compared with PCA and FA, PMF can constrain the factors and their loadings to be non-negative in value and distribute different weight to each data according to their estimated uncertainties. Another advantage of PMF is it can handle missing data (Pattero and Tapper, 1994; Paatero, 1997).

1.1.4 Climate and environment effects

PM can influence the climate directly by scattering and absorbing solar radiation (Ramanathan et al., 2001). This is especially true of carbonaceous matter (BC or EC and OC) which are the major compounds which absorb and scatter solar radiation (Haywood and Boucher, 2000; Ramanathan et al., 2001). PM can also influence the climate indirectly by changing cloud lifetime, cloud properties (Lohmann and Feichter, 2005) and precipitation formation (Rosenfeld et al., 2008). EC and VOCs have a warming effect on climate while NH_3, OC and SO_2 have a cooling effect (IPCC, 2013). An increase in the particle number concentration can also cause climate cooling because solar radiation reflection increases with particle number concentration (Haywood and Boucher, 2000; Ramanathan et al., 2001).

In addition to the climate effects, PM can also affect visibility. Poor visibility affects not only human health but also air and ground transportation, so the understanding of the temporal variation of the visibility and the factors influencing it have become more important. Numerous studies carried out around the world indicate the negative correlation between particle mass concentrations and visibility (Doyle and Dorling, 2002; Deng et al., 2008; Chang et al., 2009). Che et al. (2007) and Gao et al. (2011) evaluated the trend of horizontal visibility across China and Yangtze River Delta region from 1981 till 2005, respectively. Wu et al. (2012b) analyzed the trends of visibility on sunny days in China from 1960 till 2009. All these studies found that the visibility decreased in China during recent years. On the other hand, Doyle and Dorling (2002) analyzed visibility data in the UK from 1950 to 1997 and found that visibility improved at most monitoring sites after 1973. Therefore, air quality in China has become more serious than in other countries. Cao et al. (2012) found that the effect of anthropogenic air

pollution on visibility was significant and that high secondary inorganic particle concentrations were the main reason for lower visibility (< 5 km).

1.1.5 Health effects

Airborne PM have gotten more attention during the last years because of the detection of their adverse effects on human health (e.g. Dockery et al., 1996). About 3.7 million global annual deaths were caused by urban outdoor air pollution in 2012 and about 16% of lung cancer deaths, 11% of chronic obstructive pulmonary disease deaths and 13% of respiratory infection deaths worldwide were caused by urban air pollution (WHO, 2014). The main properties of particles which can influence particle toxicity are: (1) mass and number concentration, (2) particle size, and (3) chemical composition.

Mass concentration is the first indicator of the air pollution level. Many epidemiological investigations pointed out adverse health effects, such as morbidity and mortality, increased as PM mass concentrations increased (Schwartz, 1994; Ostro et al., 2006; Pope and Dockery, 2006). Studies have shown that mortality rise by 1.4% with every increase in 10 μg m^{-3} of $PM_{2.5}$ (Borja-Aburto et al., 1998) and between 0.7% and 1.6% with every increase in 10 μg m^{-3} of PM_{10} (Pope et al., 1995).

As described in section 1.1.1, particle size also plays an important role in affecting human health, because finer particles are known to penetrate deeper into the human respiratory system than coarser particles (Schwartz et al., 1996; Ostro et al., 2006; Kan et al., 2007).

Some chemical compounds in particles, such as trace elements or PAHs, are considered to be harmful for human health. For instance, Zn can change pulmonary cell reactivity (Adamson et al., 2000) and cause plasmid DNA damage (Shao et al., 2006). Pb was found to change cardiac autonomic functioning (Magari et al., 2002). In addition to having the same affection on human health as Pb, V can also cause oxidative DNA damage (Sørensen et al., 2005) and mortality (Lippmann et al., 2006). It was also pointed out that Ni can change heart rate and cause mortality (Lippmann et al., 2006). As was found to accumulate in the human body and cause chronic poisoning (Finkelman et al., 1999), and may even cause liver cancer (Kang et al., 2011). Even constant elements were also found to have an adverse influence on human health, such as, Mg and Ca have effects on cardiovascular health (Wu et al., 2012a), Al and Fe can also

damage plasmid DNA (Shao et al., 2006). PAHs are found to be a kind of compound with carcinogenicity and mutagenicity (Wei et al., 2010), and most PAHs were found in the fine fraction of particles (Guo et al., 2003; Bi et al., 2005) which can penetrate into the respiratory system of human beings easily, thereby causing immunogenic toxicity and lung cancer (Kim et al., 2013).

1.2 PM studies in Beijing

Beijing (Figure 1.1) with a total area of 16140 km^2 is situated at the North China Plain and is shielded by mountains to the North (Yanshan Mountains), Northwest (Yinshan Mountains) and West (Taihangshan Mountains). The Mongolian and Gobi Deserts lie to the Northwest of Beijing while the Bohai Sea is around 150 km away to the Southeast. Industry mainly gathers in the Southwest and South of Beijing and agricultural activities, such as wheat, cotton and corn, encircle Beijing (Guinot et al., 2007). Tianjin Municipality, Tangshan city, Baoding city and Shijiazhuang city, which are industrial cities, are located to the South of Beijing. The meteorological conditions in Beijing are characterized as windy and sandy springs, hot and wet summers, clear autumns, and cold and dry winters (Pang et al., 2009).

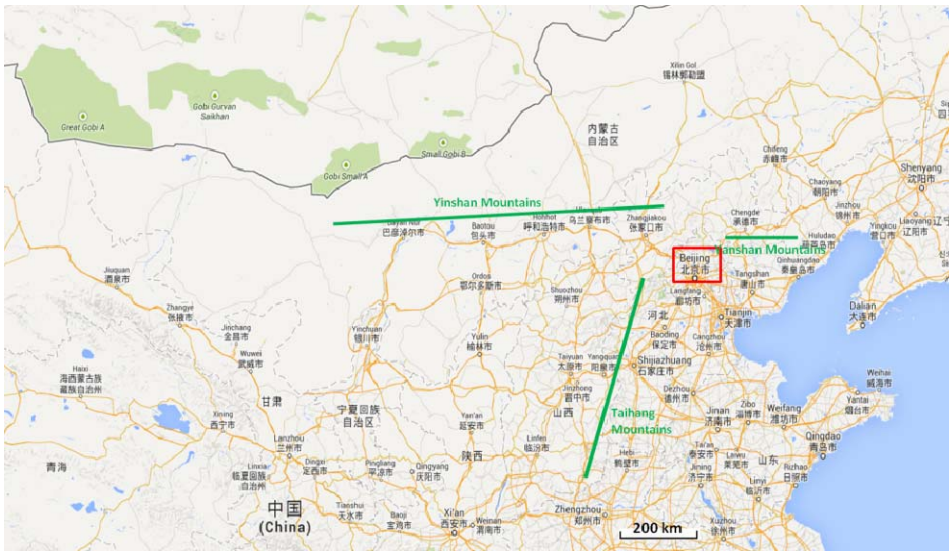

Figure 1.1: The orographic condition and surrounding of Beijing (Source: Google map)

As a mega-city, Beijing had a population of approximately 20.7 million and 5.2 million vehicles in 2012 (Beijing Municipal Bureau of Statistics, 2013). In the past ten years, population and the number of vehicles have increased rapidly (Figure 1.2), leading to the increase in the air pollutants from vehicle emission and human being's activities. The consumption of standard coal equivalent (SCE) also increased during these years. In 2012, the total energy consumption in Beijing was 71.8 million tonnes of SCE, which is over 1.5 times the SCE in 2003. Even though cleaner energy, such as natural gas and electricity, has been used in the urban area of Beijing instead of coal since 1999 (Zhao et al., 2013b), coal is still used in the rural area of Beijing. Additionally, the air pollution is not a local problem anymore and has become a more regional scale phenomenon. Especially coal is still the primary fuel in most areas of both the Hebei Province, which surrounds Beijing, and the Tianjin Municipality which is located to the Southeast of Beijing. In 2012, coal accounted 88.8% of primary energy consumption in Hebei Province (Hebei economic yearbook, 2013) and 53.0 million tonnes of coal in Tianjin Municipality, making it the most consumed energy source (Tianjin statistical yearbook, 2013). Currently, the Beijing-Tianjin-Hebei (BTH) region has become one of the most polluted areas in China. The changing of energy consumption structure and interaction of air pollution on a regional scale have made the understanding and controlling of air quality more complicated and difficult.

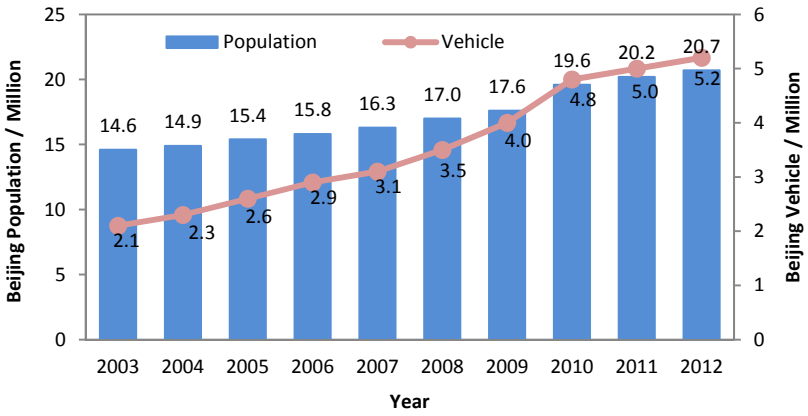

Figure 1.2: The variation of population and vehicle number in Beijing during the past ten years (Data source: Beijing Statistic Yearbook, 2004-2013)

PM, as the major air pollutant in Beijing, has received attention since the 1980s due to the rapid increase in economic activity and urbanization (Huang et al., 2006; Chan and Yao, 2008;

Garland et al., 2009). Annual $PM_{2.5}$ mass concentration before the 2008 Olympic Summer Games in Beijing ranged around 100 μg m^{-3} (He et al., 2001; Shi et al., 2003; Duan et al., 2006), which was much higher than the Grade II annual average of the Chinese Ambient Air Quality Standard (35 μg m^{-3}). In order to improve air quality, significant emission reduction measures were undertaken during the Olympic Summer Games in 2008 (Stone, 2008; Wang et al., 2010a; Zhou et al., 2010), which reduced mainly coarse particles in the ambient air (Schleicher et al., 2011). However, more pollution control measures will still be needed to further reduce air pollution. Therefore, a clear understanding of the particle characterization and sources, especially of the fine particles, is necessary for improving the air quality of Beijing.

Many papers about particles in Beijing have been published in comparison with other megacities in China. The general chemical characteristics and variation of $PM_{2.5}$ (He et al., 2001; Shi et al., 2003, Sun et al., 2004a; Song et al., 2012; Zhao et al., 2013b) and certain specific species, such as carbonaceous components (Duan et al., 2004, 2005; Lin et al., 2009; Yang et al., 2011a; Zhao et al., 2013a), inorganic elements (Shi et al., 2005; Yang et al., 2005; Yang et al., 2012), inorganic ions (Yao et al., 2002; Guo et al., 2010; Ianniello et al., 2011) and organic matters (Pang et al., 2009; Guo et al., 2012, 2013; Sun et al., 2012; Wang et al., 2012), were reported. In addition, the health effects of particles in Beijing were also investigated (Shi et al., 2004; Shao et al., 2006, 2007a; Wang et al., 2008a; Guo et al., 2009; Li et al., 2010a).

The understanding of $PM_{2.5}$ sources is important and essential for making and developing effective control strategies. Different receptor models, such as CMB (e.g. Zheng et al., 2005), PMF (e.g. Song et al., 2007; Zhang et al., 2007), and PCA (e.g. Song et al., 2006b; Duan et al., 2012), have been applied to identify possible sources of PM in Beijing during the past years. The common sources obtained from these studies were coal combustion, vehicle emissions and dust including road dust and construction dust. In addition, secondary ions, industry and biomass burning were also found. Therefore these six sources are the main sources of PM in Beijing.

Additionally, due to the increase in emissions from motor vehicles and the secondary particles formation, haze become progressively conspicuous (Zhao et al., 2013b). Haze is one kind of air pollution phenomenon which is formed from primary and secondary particles in the atmosphere and can cause atmospheric visibility to decrease to less than 10 km (Sun et al., 2006). Haze days are usually accompanied with high PM mass concentration (Zhao et al., 2013c). Numerous studies on haze pollution in Beijing were done in the past (e.g. Sun et al.,

2006; Wang et al., 2006a; Li et al., 2010b; Sun et al., 2013a), especially on the January 2013 haze pollution event (e.g. Wang et al., 2014a; Wang et al., 2014b; Zhang et al., 2014a; Zhang et al., 2014b). The results from the above studies showed that secondary inorganic ions were the dominant part in PM during haze days. Except the increasing secondary inorganic ion mass concentrations, the size was also found to increase, from the condensation mode to the droplet mode (Sun et al., 2013a). Additionally, agricultural biomass burning is another important source for haze (Li et al., 2010b). The contribution from southerly direction air flow to haze was significant, much higher than other directions (Sun et al., 2006). Compared with previous haze events, the reasons for extreme heavy haze pollution in January 2013 could be summarized as follows: unusual meteorological conditions, which were not favorable for the dispersion of pollutants, abnormally high NOx concentrations, which accelerated the formation of secondary ions, and regional influences which indicated that a reduction of pollution on a regional scale should be under consideration (Wang et al., 2014a).

In addition to haze, dust storm is another classical air pollution event in Beijing because of its location which is downwind of Asian dust source regions, such as the Gobi, Mongolian, and Taklimakan deserts and the Loess plateau in Northern China (Sun et al., 2005). Over the past decade, many studies on the dust events in Beijing have been published, such as on mass concentrations (e.g. Zhuang et al., 2001), size distributions (e.g. Zhuang et al., 2001), chemical composition (e.g. Sun et al., 2005; Shao et al., 2007b), optical properties (e.g. Xie et al., 2008; Huang et al., 2010) and source appointment (e.g. Sun et al., 2004b; Yuan et al., 2008). In general, the PM mass concentration during a dust storm increases rapidly and can reach extremely high mass concentration into thousands μg m^{-3}. Coarse particles are the dominant part of PM during dust storms but still there is a large fraction of fine particles (Zhuang et al., 2001). Crustal element mass concentrations, such as Al, Ca, Fe, Mg and Na, always increase during dust storms. But anthropogenic element concentrations, such as Zn, Pb, As, have also been found to increase. This indicates that dust storm can also transport anthropogenic pollutants over long distances (Sun et al., 2005). Dust particles have significant correlation with optical properties, especially water soluble ions in fine mode, while crustal elements are found in coarse mode (Huang et al., 2010). As the sources of dust storms are very different, usually a back trajectory approach will be used to trace the origin area. Additionally, the ratio between elements, such as Mg/Al, can also be used as a source indicator .

1.3 Open questions

As mentioned above, many studies about chemical characterization and source appointment of PM in Beijing have been done during the past years (e.g. He et al. 2001; Zheng et al., 2005; Duan et al., 2006; Zhang et al., 2006; Duan et al., 2012; Sun et al., 2013b) and the results showed that PM is very complex and variable. On the other hand, the duration of sampling in these studies are not continuous, focusing only on single haze events. Therefore, a systematic and comprehensive investigation of the complete chemical composition of continuously long term collected $PM_{2.5}$ and source appointment based on these data is needed. There are still questions related to PM characteristics needing to be answered. For instance:

- How to study the qualitative and quantitative parameters of PM_1 and nano-particles?
- What is the contribution of anthropogenic PM to the total PM exposure within the greater Beijing region?
- What are the sources of haze during different seasons and in the course of the last years?

1.4 Structure of work

My work will be described in the following chapters. Chapter 2 will depict the objectives of my study and the scope of my thesis. Chapter 3 will focus on the methodology. Chapter 4 will describe the characteristics of PM and its chemical composition. Chapter 5 will put emphasis on describing special pollution events, such as haze and dust. Chapter 6 will perform source apportionment of PM in Beijing using the PMF model. Chapter 7 will give the conclusions and outlook.

Chapter 2 Motivation and scope

2.1 Motivation

A number of contributions to answer some of the open questions mentioned in Chapter 1.3 were performed in this study. In particular, to be studied are the changes in PM characteristics in Beijing after the "Blue sky project" and the emission reduction measures for the Olympic Summer Games 2008.

Considering coarse particles were more efficiently reduced during the emission reduction measures for the Olympic Summer Games in 2008 (Schleicher et al., 2011) and haze pollution became much more frequent recently (Wang et al., 2006a), the following hypotheses are given in this study:

1) The sources of fine particles are not only local, but also regional and from long range transported.
2) Fine and anthropogenic particles are major fractions of haze particles.
3) Due to seasonal variations in emissions and meteorological parameters, there are seasonal variations in the processes forming haze.

Based on these hypotheses, $PM_{2.5}$ sampling and analyses in Beijing were planned. Two high volume $PM_{2.5}$ samplers were used to collect continuously one year PM samples in parallel. The sampling site was chosen at ground-level in an urban background area where people spend most of their time for working and living. In order to obtain the characteristics and sources of PM, EC/OC, water soluble ions, inorganic elements and organic compounds were analyzed. The whole measured composition was used to perform source appointment.

There are however still some questions which should be answered in future work, for instance:

1) How to study the qualitative and quantitative parameters of PM_1 and nano-particles?

2) How are our results from source apportionment related to required emission reduction measures?
3) Which improvements in emission inventories are required following our source apportionment results?
4) What are the human health influences of PM we collected and analyzed in the urban background?
5) How to perform emission reduction measures in the future?

2.2 Scope

The scope of this study is to perform a systematically comprehensive investigation of PM in Beijing during one year. The work flow chart of this study is given in Figure 2.1.

The focus areas of this study are:

1) Characteristics of PM concentrations and chemical composition in Beijing
    - What is the concentration and composition of PM in Beijing on the basis of a continuous investigation during one year?
    - How are the temporal variations of PM and its composition in Beijing from day to day?
    - How do meteorological parameters influence temporal variations of particle mass concentration and composition?
2) Characteristics of PM during haze and dust episodes
    - What are the characteristics of PM during haze episodes?
    - What are the characteristics of PM during dust events?
    - What are the differences in particle composition during haze, dust and clear days?
    - What are the differences in particle composition during haze days in different seasons of the year?
3) Source appointment of PM in Beijing
    - What are the most important geogenic and anthropogenic sources of particles?
    - What are the main sources for haze particles?
    - Which kind of sources of different dust events can be identified?

These questions will be discussed in detail in chapters 4, 5, and 6, respectively. Finally, it will be stated if the hypotheses formulated above are correct or not together with conclusions in chapter 7.

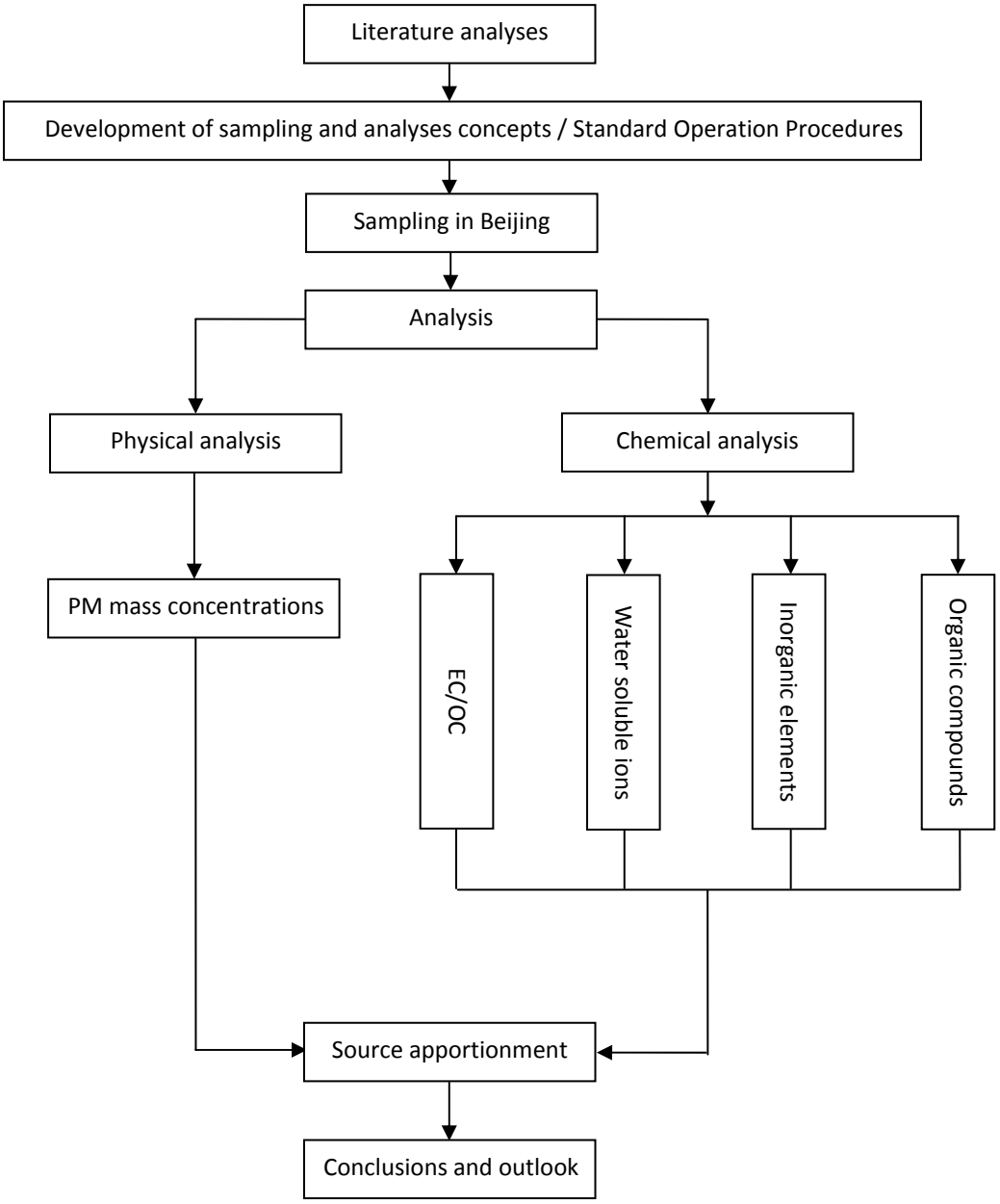

Figure 2.1: Flow chart of the research

Chapter 3 Methodology

In order to get better understanding of the topics which are listed in Chapter 2, two PM sampling campaigns were performed in Beijing from 2010 till 2013. The first campaign was conducted at the campus of the China University of Geosciences (Beijing) (CUGB) from June 2010 till June 2011 and the second one was carried out at the Institute of Atmospheric Physics, Chinese Academy of Sciences (IAP, CAS) from 10 April 2013 till 8 June 2013. Both sampling sites, analytical methods and problems which happened during the campaigns are described in this chapter.

3.1 Sampling strategy

3.1.1 Sampling sites

3.1.1.1 China University of Geosciences (Beijing) (CUGB) (2010.06.21 - 2011.06.20)

Daily mean ambient PM samples were collected at the campus of the China University of Geosciences (Beijing) (CUGB), from 21 June 2010 till 20 June 2011. The sampling site, which is close to the North 4th Ring Road, is located a distance of about 10 m from the walk-way (in the South) of the east entrance of the university and a distance of approximately 10 m from the 6 lane Xueyuan road (to the East, separated by a wall) (Figures 3.1, 3.2, 3.3). As the sampling site is surrounded by trees, covered by grassland and shielded by a 2.5 m high wall to the Xueyuan road, it could be characterized as an “urban background site” but not a traffic site. This characterization was checked by ultra-sonic anemometer measurements (USA1, Metek, Elmshorn, Germany) at the measurement site (see Figure 3.3) and it was found that the local wind directions were mainly from the open area but not from the Xueyuan road. The sampler inlet tubes were installed at a 2 m height above ground, indicative of the level of human exposure. Another reason for choosing this site to collect PM is that it is at a distance of 10 – 20 m from the instrumentation of the Air Quality Department, Research Center Human

Biometeorology, German Meteorological Service, Freiburg, Germany (DWD) and the Institute of Mineralogy and Geochemistry, Karlsruhe Institute of Technology, Karlsruhe, Germany (KIT/IMG), which is visible in the background of Figure 3.3 and has been tasked with investigation of the inorganic composition of $PM_{2.5}$ based on weekly passive and active sampling in a continuous measurement series since 2005 (Schleicher et al., 2012).

Figure 3.1: The location of the sampling sites in Beijing (Source: Google maps): CUGB is the China University of Geosciences (Beijing); IAP is the Institute of Atmospheric Physics; ZBAA is the code for monitoring site from where can obtain the meteorological data on the website of the University of Wyoming, USA

Figure 3.2: The location of the sampling site at the CUGB in Beijing from 21 June 2010 till 20 June 2011 (Source: Google maps)

Figure 3.3: The location of the sampling site at the CUGB in Beijing from 21 June 2010 till 20 June 2011: sampler A and B as well as an ultra-sonic anemometer used to check the local transport conditions

Figure 3.4: The location of the sampling site at the IAP in Beijing from 10 April 2013 till 08 June 2013

3.1.1.2 Institute of Atmospheric Physics (IAP) (2013.04.10 - 2013.06.08)

The second campaign was operated with the same two $PM_{2.5}$ samplers for daily mean sampling on the roof of the two story institute building which is close to the 325 m measurement tower of the IAP (Figures 3.1 and 3.4) at about 10 m above ground, from 10 April 2013 till 08 June 2013. This site is located about 1 km away from the outside of the 3rd Ring Road. The North-South G6 Jingzang Expressway and the East-West Beitucheng West Road are located 300 m to the East and 50 m to the North of the sampling site, respectively. Apart from the traffic, this

site is also surrounded by residential areas, parks, trees and institutes. Therefore, as with the site at the CUGB, this site could also be regarded as a "residential site" or "urban background site". This site was selected as a sampling site because many studies have been done at this site in the past and they showed that this site is representative of the urban background (e.g. Wang et al., 2001; Liu et al., 2013; Sun et al., 2013c).

3.1.2 PM sampling methods

Two sequential High Volume Samplers (HVS, Digitel DHA-80, Hegnau, Switzerland) (Figure 3.5), A and B in Figures 3.1 and 3.4, were operated to collect $PM_{2.5}$ samples in parallel automatically (VDI guideline 2463). The samplers were running at a flow rate of 500 l min^{-1} for 24 hours per day (00:00 – 24:00). At the IAP sampling site, the time resolution of sampling was changed from 24 h into 4 h during haze periods. Quartz fiber filters (Munktell T293, Falun, Sweden) with 150 mm diameter were used as collection substrate. The field blank samples of both samplers were collected every second week. Seven or eight filters with filter holders were stored in the sampler to change the filter magazine once per week. One point should be mentioned here, unless otherwise noted, all time used in the following chapters is local time (UTC+08).

The filters of sampler A were used for analysis of organic composition, EC/OC and water soluble ions. All filters of sampler A, which were wrapped in aluminum foils before and after sampling, were heated at 500°C for 6 hours before sampling to release any possible organic compounds. The filters of sampler B were used for mass determination and analysis of inorganic elements. Before sampling, all filters of sampler B were weighed in the conditioning room at the DWD and then wrapped in paper envelops during the first campaign and in aluminum foils cleaned by acetone before use during the second campaign. All filters of both samplers were stored in a clean environment at room temperature before sampling. After sampling, all loaded filters were stored in a clean deep freezer at -20°C before chemical analysis. All filters of sampler A were divided in the Joint Mass Spectrometry Centre, Cooperation group "Comprehensive Molecular Analytics", Helmholtz Zentrum München, Neuherberg, Germany (HMGU) for different experiments (Figure 3.6). Organic compounds, EC/OC and ions were only involved in this study from all these different measurements. All bottles and dishes used for storing the filter parts were cleaned by methanol and dried at 60°C for 2 hours. Standard Operation Procedures (SOPs) were developed for these work.

Figure 3.5: $PM_{2.5}$ high volume sampler DHA-80 (Source: Manual from DIGITEL Elektronik AG)

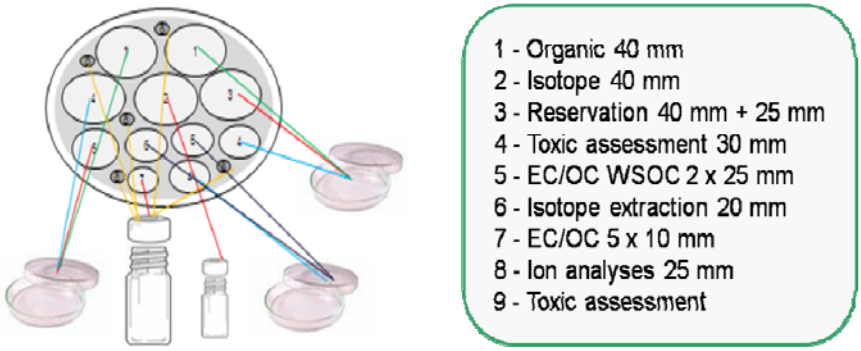

Figure 3.6: Partition of sampler A loaded filters

3.2 Analytical Methods

Because the first campaign at the CUGB and the second campaign at the IAP were independent sampling campaigns, the analytical methods in these two campaigns were also independent from each other and partly decided by corresponding cooperation partners, funding and available instruments. All the analytical methods used in these two campaigns are described in the following sections. All the measurements and facilities are listed in Table 3.1.

Table 3.1: Measurements and facilities

Facility	Campaign	Sampling period	Measurement	Executive	Executor
DHA–80 $PM_{2.5}$ sampler	CUGB	2010.06-2011.06	Collection of PM samples	China University of Mining and Technology (Beijing) (CUMTB)	Jing Wang, Jianying Wang
Tapered Element Oscillating Microbalance	CUGB	2010.06-2011.06	$PM_{2.5}$ and PM_{10} online data	IAP	Dr. Zirui Liu
Ceilometer CL31	CUGB	2010.06-2011.06	Mixing Layer Height	IAP	Dr. Guiqian Tang
Mettler Analysenwaage AE240	CUGB	2010.06-2011.06	Filter mass weighing	DWD	Rongrong Shen
Thermal/Optical Carbon Analyzer	CUGB	2010.06-2011.06	EC/OC	University of Rostock, Germany (UR)	Hendryk Czech, Dr. Thorsten Streibel
Polarized Energy Dispersive X-ray Fluorescence	CUGB	2010.06-2011.06	Inorganic elements	KIT/IMG	Rongrong Shen, Dr. Utz Kramar
Ion chromatography and Continuous Flow Analyzer	CUGB	2010.06-2011.06	Water soluble ions	HMGU	Heidi Witte, Prof. Dr. Bernhard Michalke
Gas chromatography-mass spectrometry	CUGB	2010.06-2011.06	Organic compounds	HMGU	Rongrong Shen, Dr. Guelcin Abbaszade, Dr. Jürgen Schnelle-Kreis
DHA–80 $PM_{2.5}$ sampler	IAP	2013.04-2013.06	Collection of PM samples	IAP	Rongrong Shen
Tapered Element Oscillating Microbalance	IAP	2013.04-2013.06	$PM_{2.5}$ and PM_{10} online data	IAP	Dr. Zirui Liu
Ceilometer CL31	IAP	2010.06-2011.06	Mixing Layer Height	IAP	Dr. Guiqian Tang
Mettler Analysenwaage AE240	IAP	2013.04-2013.06	Filter mass weighing	DWD	Rongrong Shen
Thermal/Optical Carbon Analyzer	IAP	2013.04-2013.06	EC/OC	IAP	Rongrong Shen
Inductively coupled plasma mass spectrometry	IAP	2013.04-2013.06	Inorganic elements	Capital Normal University, China	Rongrong Shen
Ion chromatography	IAP	2013.04-2013.06	Water soluble ions	IAP	Rongrong Shen
Gas chromatography-mass spectrometry	IAP	2013.04-2013.06	Organic compounds	HMGU	Dr. Guelcin Abbaszade, Dr. Jürgen Schnelle-Kreis

3.2.1 Gravimetric determination of PM mass concentration

All filters of sampler B from CUGB and IAP were weighed before and after sampling with an analytical balance (Mettler Analysenwaage AE240, reading precision 0.1 mg) after equilibration for 48 h in a conditioning room (temperature 22°C ± 0.2, relative humidity 42% ± 0.5) at the DWD. The PM mass concentration was determined by the following equation:

$$C = \frac{(W_2 - W_1) * 1000}{F * t} \quad (3\text{-}1)$$

where C is the mass concentration of PM, μg m^{-3}; W_2 is the weight of the filters after sampling, μg; W_1 is the weight of the filters before sampling, μg; F is the normalized sampling volume at standard condition (0°C/1013mbar), l min^{-1}; t is the sampling period, min.

Each filter was weighed at least 3 times before and after sampling. More details are described in the Standard Operation Procedure for Filter Weighing (Appendix A).

3.2.2 Tapered Element Oscillating Microbalance (TEOM)

$PM_{2.5}$ and PM_{10} TEOM (TEOM Series 1400a, Thermo Fisher Scientific Environmental Instrument Co. Ltd) data were collected by the IAP. TEOM works on the basis of the frequency of oscillation. With increasing particle mass on the filters, the frequency of oscillation decreases. According to the relationship between particle mass and the frequency of oscillation, the mass of particles can be calculated. More details can be found in Cyrys et al. (2001) and Green et al. (2006). TEOM data was used as a comparison with our filter weighing data. But because the working temperature of TEOM Series 1400a is 50°C, the loss of volatile substances can occur. Previous studies pointed out PM determined by TEOM underestimates PM mass by 15% - 50% when compared with gravimetric determination of PM mass concentration (Eatough et al., 2003; Hitzenberger et al., 2004). All daily mean TEOM data in this study was averaged from hourly data.

3.2.3 Polarized Energy Dispersive X-ray Fluorescence (PEDXRF)

As a sensitive, fast, highly recommended and non-destructive technique, PEDXRF is often used to determine the chemical inorganic elements of various types of samples (Misra et al., 2002; Kadıoğlu et al., 2010). In this study, loaded samples from CUGB were analyzed for 15 chemical elements including S, K, Ca, Ti, Cr, Mn, Fe, Ni, Cu, Zn, As, Sn, Sb, Ba and Pb by PEDXRF (Epsilon 5, PANalytical, the Netherlands) at the Laboratory for Electron Microscopy (LEM) of KIT in Karlsruhe, Germany. All the results of the loaded filters were initially subtracted by field blank filters.

A silicon with lithium (Si (Li)) detector and tungsten (W) - anode X-ray tube (100 KV, max 600 W) were used for all elemental analyses. Ca, Fe, KBr, Mo, Ag and Al_2O_3 were used as secondary / polarization targets. All loaded filters were analyzed as thin layer samples. Calibration of the system was performed by using the results from a portion of the filters previously analyzed by inductively coupled plasma mass spectrometry (ICP-MS) as a reference for estimating the homogeneous particle loading of the filters. More details are described in a previous study (Kramar, 1999). The limits of quantification (LOQ) of all measured elements are listed in Table 3.2.

Table 3.2: Limits of quantification (LOQ) of all measured elements in PM samples at the CUGB

Element	LOQ	Element	LOQ	Element	LOQ
Fe	0.19 µg m^{-3}	Mn	0.01 µg m^{-3}	As	3.1 ng m^{-3}
S	0.11 µg m^{-3}	Cr	15.4 ng m^{-3}	Sn	7.1 ng m^{-3}
K	0.16 µg m^{-3}	Ni	1.6 ng m^{-3}	Sb	6.4 ng m^{-3}
Ca	0.24 µg m^{-3}	Cu	9.0 ng m^{-3}	Ba	3.9 ng m^{-3}
Ti	0.01 µg m^{-3}	Zn	9.6 ng m^{-3}	Pb	15.8 ng m^{-3}

Note: Volume – 240 m^3

3.2.4 Inductively coupled plasma mass spectrometry (ICP-MS)

Loaded quartz fiber filters from IAP were punched into a 20 mm round diameter and were digested in Teflon vessels with 6 ml concentrated HNO_3, 2 ml HCl and 0.2 ml HF by using microwave digestion system (MARS 5, CEM Corporation, Matthews, NC, USA). The digested solution was diluted with de-ionized water (Milli-Q, 18.2 MΩ • cm) to 50 ml and then was

analyzed by the Agilent 7500a ICP-MS (Agilent, USA) for K, Ca, Na, Mg, Al, Fe, V, Cr, Mn, Ni, Cu, Zn, As, Cd, Ba, Tl and Pb. No.5183-4688 Environmental Calibration Standard (Agilent, USA) was used as external standard and Sc, Ge, Y, In, Tb and Bi with a concentration of 1 μg L^{-1} in 2% HNO_3 were used as internal standards for calibration. Quality control was done by a parallel analysis of the soil reference material GBW07403. Results from field blank filters were subtracted from all the results from the loaded filters. This method was also described in a previous work (Pan et al., 2013). The LOQ of all measured elements are also listed in Table 3.3.

Table 3.3: Limits of quantification (LOQ) of each element in $PM_{2.5}$ at the IAP (unit: ng m^{-3})

Element	LOQ	Element	LOQ	Element	LOQ
Na	2.8	Cr	0.02	Zn	0.3
Mg	0.7	Mn	0.008	As	0.01
Al	1.6	Fe	1.5	Cd	0.001
K	0.1	Co	0.005	Ba	0.3
Ca	1.9	Ni	0.01	Tl	0.001
V	0.005	Cu	0.025	Pb	0.004

Note: Volume – 720 m^3

3.2.5 Ion chromatography (IC) and Continuous Flow Analyzer (CFA)

Four water soluble ions of PM samples from CUGB were analyzed at the Research Unit Analytical BioGeoChemistry (BGC), HMGU, Neuherberg, Germany. Chloride (Cl^-), NO_3^- and SO_4^{2-} were analyzed by IC (ICS-1500, Dionex, USA) and NH_4^+ was analyzed by CFA (Scan^{++}, Skalar, The Netherlands). Loaded quartz fiber filters were punched into 25 mm round diameter and extracted by 5 ml de-ionized water (Milli-Q, 18.2 MΩ • cm) in an ultrasonic bath for 15 minutes. After extraction, the solution was filtered by using a 0.45 μm filter. The 15 ml extracted solution for each sample was obtained after three times extraction. Anions (Cl^-, NO_3^- and SO_4^{2-}) were analyzed with an Ionpac AS4A-SC with guard column AG4A-SC, ASRS 300-4 mm suppressor and a mixture of 1.8 mM $NaCO_3$ and 1.7 mM $NaHCO_3$ isocratic eluent. The LOQ as calculated by volume of 240 m^3 for Cl^-, NO_3^-, SO_4^{2-} and NH_4^+ were 0.196 μg m^{-3}, 0.196 μg m^{-3}, 0.196 μg m^{-3} and 0.392 μg m^{-3}, respectively. Field blank filters were also measured and subtracted from the loaded filters.

3.2.6 Ion chromatography (IC)

Eight water soluble ions, including three anions (Cl^-, $NO_3^-$and SO_4^{2-}) and five cations (sodium (Na^+), NH_4^+, potassium (K^+), magnesium (Mg^{2+}) and calcium (Ca^{2+})), of the loaded $PM_{2.5}$ samples from IAP were analyzed by IC (ICS-90, Dionex, USA). Loaded quartz fiber filters were punched into a 30 mm round diameter and shaken for 30 minutes with 25 ml de-ionized water (Milli-Q, 18.2 MΩ • cm) in an ultrasonic bath. Before being analyzed by IC, the shaken liquid was filtered by syringe filter with pore size of 0.22 μm (Xiboshi, China). An Ionpac AS14A 4 × 250 mm analytical column, ASRS 300-4 mm suppressor and $NaCO_3$/$NaHCO_3$ eluent were used for analyzing anions. Cations were measured by using an Ionpac CS12A 4 × 250 mm analytical column, CSRS 300-4 mm suppressor and methane sulfuric acid (MSA) (chromatogram class, EGC II MSA, Dionex, USA) eluent. The flow rate of eluent for both anions and cations were 1.0 ml min^{-1}. Field blank filters were measured and subtracted from the loaded filters. This method was also described in a previous work (Li et al., 2013). The LOQ were calculated by volume of 720 m^3 for Cl^-, NO_3^-, SO_4^{2-}, Na^+, NH_4^+, K^+, Mg^{2+} and Ca^{2+} were 0.002 μg m^{-3}, 0.004 μg m^{-3}, 0.009 μg m^{-3}, 0.001 μg m^{-3}, 0.001 μg m^{-3}, 0.002 μg m^{-3}, 0.001 μg m^{-3}, and 0.002 μg m^{-3}, respectively.

3.2.7 Thermal/Optical Carbon Analyzer (IMPROVE A – Protocol)

OC and EC in PM collected at the CUGB and the IAP were analyzed by the thermal/optical carbon analyzer (DRI Model 2001A, Desert Research Institute, USA) on the basis of the IMPROVE (Interagency Monitoring of Protected Visual Environments) A protocol. The thermal optical reflection method (TOR) is used in this protocol, which has been described in previous studies (e.g. Chow et al., 1993, 2001, 2007; Cao et al., 2007; Li et al., 2012). The 8 mm round diameter filter part was punched from each loaded sample and heated gradually at different temperatures in the oven of the instrument. Different OC and EC fractions were measured at different temperatures and in different carrier gases, which are shown in Table 3.4. OC1, OC2, OC3, and OC4 were measured in pure helium (He) at 140°C, 280°C, 480°C, 580°C, respectively while EC1, EC2, and EC3 were determined in He containing 2% oxygen (O_2) at 580°C, 740°C, 840°C, respectively. OC and EC have been corrected by the value of optical pyrolyzed carbon (OPC). OC is calculated by the sum of OC1, OC2, OC3, OC4 and OPC while EC is calculated by excluding OPC from the sum of EC1, EC2, and EC3. Calibration should be done twice, before and after analysis, by using standard CH_4/CO_2. Field blank filters were measured and subtracted from the loaded filters. The LOQ for OC and EC during the first campaign (volume of

240 m^3) and the second campaign (volume of 720 m^3) were 0.53 μg m^{-3} and 0.12 μg m^{-3}, 0.18 μg m^{-3} and 0.04 μg m^{-3}, respectively.

Table 3.4: EC/OC fractions at different temperatures and in different carrier gases

Fractions	Temperature (°C)	Carrier gases
OC1	140	Helium
OC2	280	Helium
OC3	480	Helium
OC4	580	Helium
EC1	580	Helium / 2% Oxygen
EC2	740	Helium / 2% Oxygen
EC3	840	Helium / 2% Oxygen

3.2.8 Gas chromatography-mass spectrometry (GC-MS)

PM samples from CUGB and IAP were analyzed by in situ derivatization direct thermal desorption gas chromatography time-of-flight mass spectrometry (IDTD-GC-TOFMS) for the organic compounds. Agilent 6890 gas chromatograph (Agilent, USA) was used. All the filters were divided into 13.5 mm × 2.1 mm (Length × Width) stripes. One stripe with non-polar and polar internal standards which were used for compounds quantification was put into the goose-neck of a GC liner, above which glass wool, which was used to keep the particles from dropping into the capillary column, had already been put. After that, all GC liners were sealed by poly tetra fluoro ethylene (PTFE) caps. 10 μl N-methyl-N-trimethylsilyltrifluoroacetamide (MSTFA, Macherey-Nagel, Germany), which was injected into the filter stripe in each liner before analyzing the samples, was used for derivatization. Data evaluation was done by using the Pegasus III TOFMS (LECO, St. Joseph, MI, USA). More details of this method were described in a previous study (Orasche et al., 2011). The filed blank filters were also measured and the value of blank filters were subtracted from the results of loaded filters.

In this study, levoglucosan, eleven hopane substances including 18α(H)-22,29,30-Trisnorneohopane (Ts), 17α(H)-22,29,30-Trisnorhopane (Tm), 17β(H)-22,29,30-Trisnorhopane (27b), 17α(H)21β(H)-30-Norhopane (29ab), 17β(H)21α(H)-30-Norhopane (29ba), 17α(H)21β(H)-Hopane (30ab), 17β(H)21α(H)-Hopane (Moretan) (30ba), 22S-17α(H)21β(H)-Homohopane (31abS), 22R-17α(H)21β(H)-Homohopane (31abR), 22S-17α(H)21β(H)-

Bishomohopane (32abS), 22R-17α(H)21β(H)-Bishomohopane (32abR), and fifteen PAHs including phenanthrene (PHE), anthracene (ANT), pyrene (PYR), fluoranthene (FLU), benz(a)anthracene (BAA), chrysene (CRY), benz(bk)fluoranthene (BBKF), benzo(e)pyrene (BEP), benzo(a)pyrene (BAP), perylene (PER), dibenz(a,h)anthracene (DAH), indeno(1,2,3,c,d) pyrene (IND), picene (PIC), benz(g,h,i)perylene (BGH), coronene (COR) were measured. However, the low molecular weight (LMW) PAHs (3 and 4 rings PAHs) such as PHE, ANT, PYR and FLU are considered to be semi-volatile and thus mainly present in the gas phase. As the mass concentrations of these compounds determined in PM samples are highly driven by the gas phase concentrations during the last minutes of sampling, PHE, ANT, PYR and FLU are excluded from discussion in this study. The LOQ for organic compounds from CUGB and IAP are listed in Table 3.5.

Table 3.5: Limit of quantification (LOQ) of all measured organic substances in PM (unit: ng m^{-3})

Substance	CUGB	IAP	Substance	CUGB	IAP	Substance	CUGB	IAP
levoglucosan	0.23	0.08	31abS	0.11	0.04	BAP	0.09	0.03
Ts	0.11	0.04	31abR	0.11	0.04	PER	0.05	0.02
Tm	0.11	0.04	32abS	0.11	0.04	DAH	0.05	0.02
27b	0.11	0.04	32abR	0.11	0.04	IND	0.11	0.04
29ab	0.11	0.04	BAA	0.05	0.02	PIC	0.11	0.04
29ba	0.11	0.04	CRY	0.05	0.02	BGH	0.11	0.04
30ab	0.11	0.04	BBKF	0.09	0.03	COR	0.23	0.08
30ba	0.11	0.04	BEP	0.09	0.03			

Note: Volume – 240 m^3 at the CUGB and 720 m^3 at the IAP

3.3 Meteorological data

Meteorological parameters including temperature (T), atmospheric pressure (P), relative humidity (RH), visibility, wind speed (WS) and wind direction (WD) were obtained from the weather station ZBAA (see Figure 3.1) where the data are available at an internet page of the University of Wyoming, USA (http://weather.uwyo.edu/upperair/sounding.html). ZBAA is an International Civil Aviation Organization airport code of Beijing Capital International Airport.

Here it is used as the name of weather station on the website of the University of Wyoming, USA. The visibility data are only available up to 10 km.

At the same time, an automatic weather station Milos 520 (Vaisala, Finland) located on the same place as our samplers were located during the second campaign, was also used to observe meteorological parameters.

The important point should be mentioned here that visibility is only acquired at the ZBAA while precipitation and mixing layer height (MLH) are only detected at the IAP. MLH was determined by a ceilometer CL31 (Vaisala GmbH, Hamburg, Germany), which is an eye-safe and hands-off mini-lidar system. It is designed as a single lens lidar system which uses the same lens for transmitting and receiving light. The maximum altitude which it can reach is 7700 m. The backscatter profile is used to identify the vertical height of aerosol layers, which is the so called "the gradient method". All details were described by Münkel (2007).

The temperature, atmospheric pressure, relative humidity, wind speed and wind direction are obtained at both sites. T, RH and P data from ZBAA are highly consistent with IAP data (Figure 3.7). WS and WD were not compared, because the IAP site is located in the city and is thus surrounded by buildings which makes the WS and WD more locally determined.

During these two campaigns, the regional transport should be considered. Therefore, the meteorological data, including T, P, RH, WS, WD and visibility from ZBAA were used. Precipitation and MLH data, which were only obtained from IAP, were used for both campaigns.

3.4 Source characterization methods

3.4.1 Selection of source apportionment method

The application of analytical methods, described in Chapter 3.2, provided 361 daily mean $PM_{4.3}$ samples with 47 species collected at the CUGB from June 2010 till June 2011 and 60 daily mean $PM_{2.5}$ samples with 29 species collected at the IAP from 10 April till 08 June 2013. As described in Chapter 1.1.3.3, a quantification of single emission sources of these composition data by chemistry-transport modelling would require a-priori knowledge of all the emission sources of these species. Unfortunately, such a-priori information is not available at all.

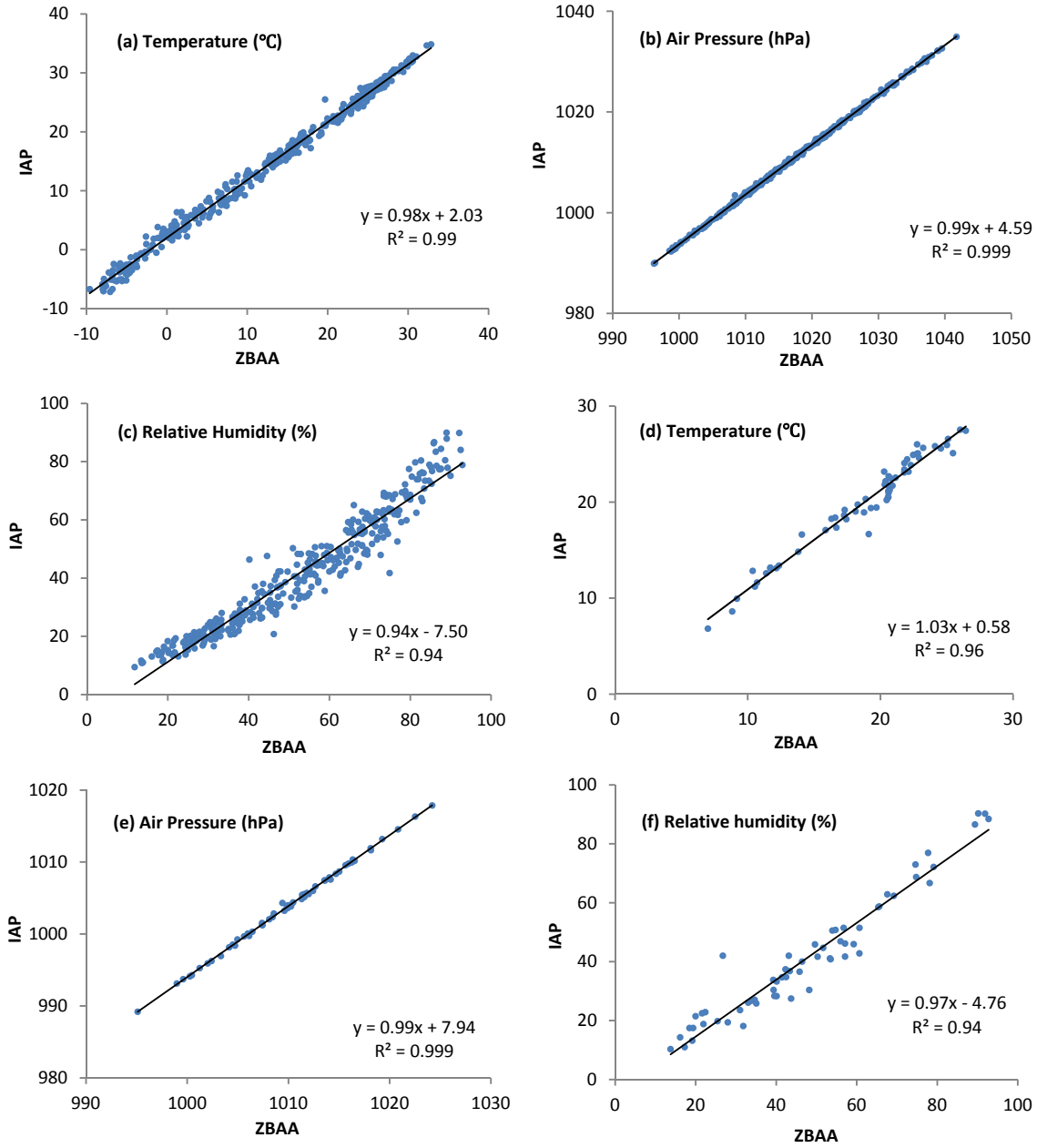

Figure 3.7: Correlations between meteorological parameters at the ZBAA and the IAP. (a) To (c) show the correlations between temperature, air pressure and relative humidity at the ZBAA and the IAP from 2010.06.21 till 2011.06.20. (d) To (f) show the correlations between temperature, air pressure and relative humidity at the ZBAA and the IAP from 2013.04.10 till 2013.06.08

Receptor models for source apportionment need known emission profiles which are also not available. Consequently, a multivariate statistical method like PMF which can group a large amount of variables into few variables which can be interpreted as factors (sources) will be applied which enables the source apportionment on the basis of the measured PM compound concentrations and their uncertainties only.

3.4.2 Positive matrix factorization (PMF)

3.4.2.1 The theory of PMF

PMF is one kind of multivariate factor analysis methods (Paatero and Tapper, 1994; Paatero, 1997) which can be used to produce factor profiles and factor contributions by decomposing a matrix of measured data into these two matrices. Specifically, the method of PMF can be written as:

$$X = G \times F + E \tag{3-2}$$

X is the matrix of measured species mass concentrations [µg m^{-3}], G is the matrix of factor contributions [µg m^{-3}], F is the matrix of factor profiles [g g^{-1}], and E is the residual of the factor analyses [µg m^{-3}]. So the equation (3-2) can also be written as follows:

$$x_{ij} = \sum_{k=1}^{p} g_{ik} f_{kj} + e_{ij} \tag{3-3}$$

where x_{ij} is the measured concentration of compound j in sample i, p is the total number of factors, g_{ik} is the contribution of factor k to sample i, f_{kj} is the profile of compounds j of factor k, and e_{ij} is the residual for the compounds j in sample i. Factor profiles obtained from PMF are interpreted as sources on the basis of a-prior knowledge of source markers (see Chapter 1.1.3.2) (Reff et al., 2007).

The aim of the PMF method is to find the minimum weighted sum of the squared residual function Q value (Equation 3-4) by using least-squares fitting (Paatero and Tapper, 1993, 1994). The solution obtained at the minimum Q value is considered to be a reasonable result. The equation is as follows:

$$Q = \frac{X-E}{U} = \sum_{i=1}^{n} \sum_{j=1}^{m} \left[\frac{x_{ij} - \sum_{k=1}^{p} g_{ik} f_{kj}}{u_{ij}} \right]^2 \tag{3-4}$$

Here, U or u_{ij} is the uncertainty of X or x_{ij}, n is the total number of samples, and m is the total number of measured compounds.

The U.S. EPA PMF 3.0 software was used in this study (http://www.epa.gov/heasd/research/pmf.html). Two input files are required by PMF: species mass concentrations X and corresponding uncertainties U in each sample (Figure 3.8). The Multilinear Engine (ME) algorithm was applied to calculate minimum Q value. The initial matrices G_0 and F_0 were randomly selected by model and minimum Q was obtained by multiple iterations using conjugate gradient approach. Due to the randomly selection of the starting point, minimum Q can be not only global minimum, but also local minimum. In order to reach the global minimum, the model should run 20 times at different starting points (base model run) to check if the minimum Q is constant. After finding the minimum Q, 100 bootstraps were conducted with a random starting point to check the stability of the solution. Factor contributions from bootstraps were compared with those from base run and if correlation coefficient (R^2) was higher than 0.6, then the solution was mapped, otherwise it was not unmapped. 10% unmapped results for each factor were acceptable.

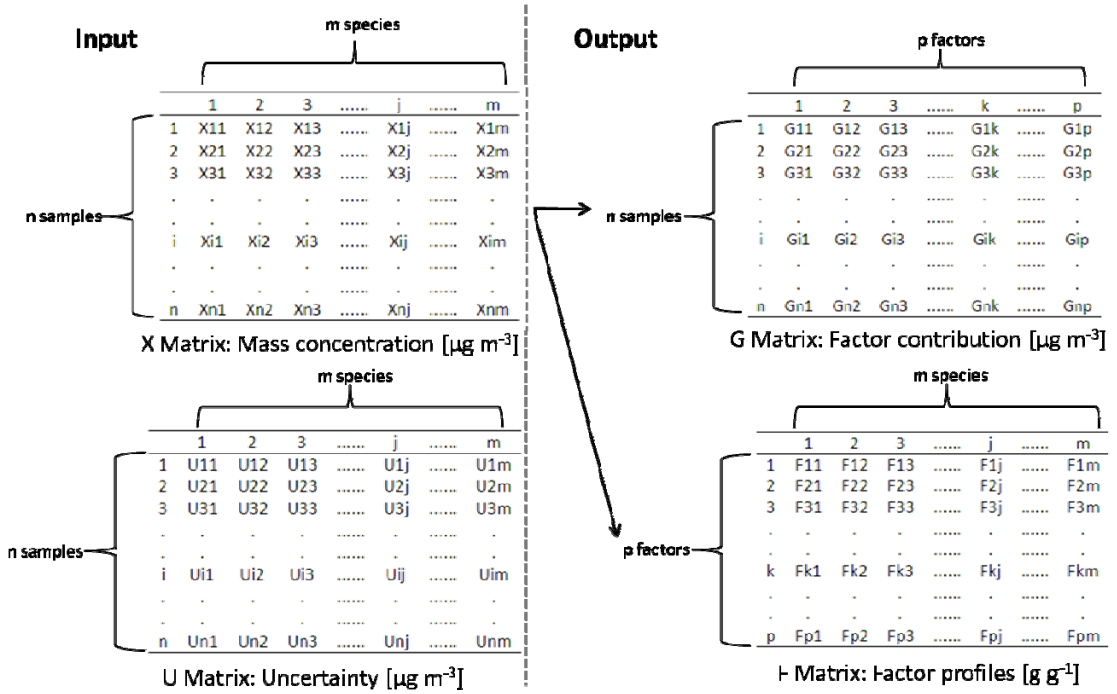

Figure 3.8 Input and output data file in PMF

Choosing the right number of factors is very important and difficult. Unfortunately, there is no criteria for choosing this number. The bigger the measured data matrix X is, the larger the number of factors can be. Therefore, different numbers of factors should be tested in the PMF, and the number of factors with the most meaningful results was chosen. The general flow chart of PMF is shown in Figure 3.9. More details about this method can be referred in Reff et al. (2007).

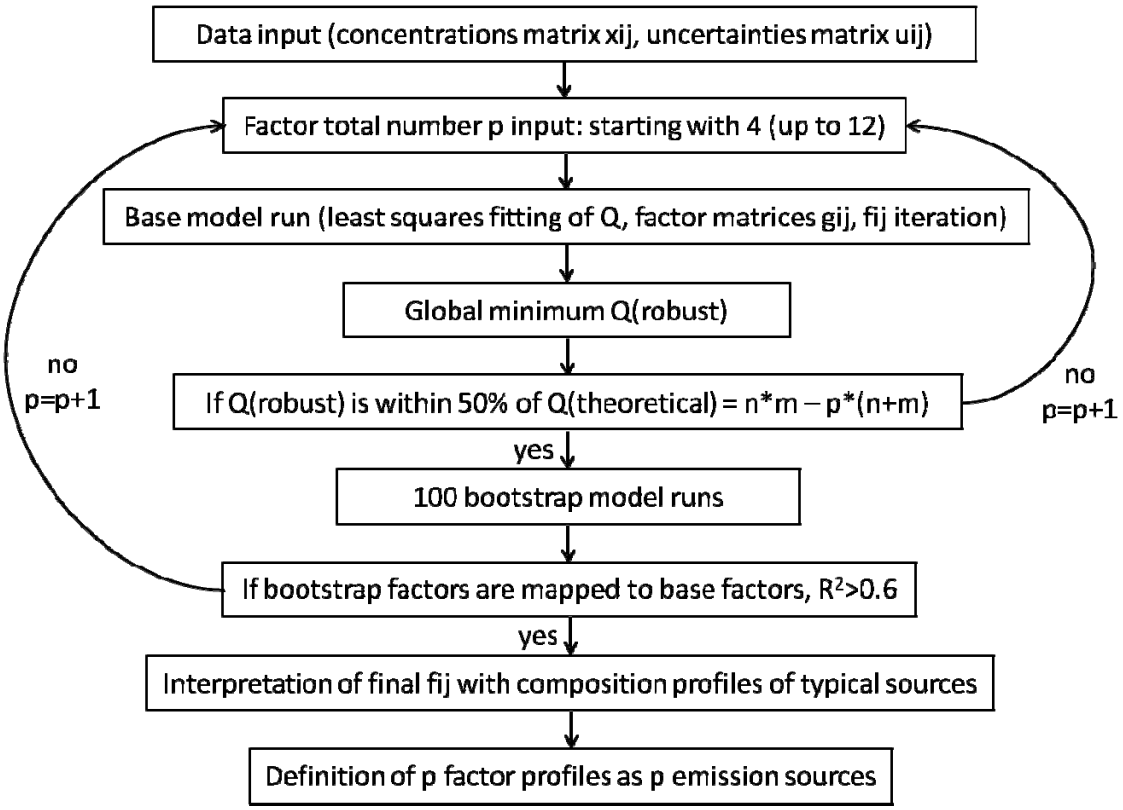

Figure 3.9 Flow chart of PMF

The output data contain G and F (Figure 3.8). Here the time series of factor contributions and factor profiles were selected to demonstrate the PMF results (see Figures 6.3 and 6.4). The source types are determined from the factor profiles on the basis of literature knowledge of source markers, ratios of compounds or composition profiles of typical source types (see chapter 1.1.3.2, Table 1.2 and their transformation into Table 3.6) and temporal variation of

each factor. The best modelled number of factors, p, is decided by the best coincidence of modelled factor profiles with those from literature.

In order to get better solution, the following information should be checked: (1) Comparison between Q_{robust} (base run without outliers), Q_{true} (base run with outliers) and $Q_{theoretical}$ (freedom of dataset); (2) Good fitness should be checked by comparison between observed (input data) and predicted (modelled) PM compound concentrations; (3) Residual analysis of each PM compound; (4) Comparison between each factor contribution.

Table 3.6: Source markers

		EC	OC	SO_4^{2-}	NO_3^-	NH_4^+	Cl^-	K	Fe	Mg	Al	Ca	Ti	Mn	Ba	Cr	Mn	Cu	Zn	As	Pb	Sb	V	Ni	Hopane	PAHs	levoglucosan
1	Biomass burning	√	√				√	√																			√
2	Chemical formation		√	√	√	√																					
3	Fossil fuel combustion	√	√																						√	√	
4	Mineral dust							√	√	√	√	√	√	√	√												
5	Industry													√		√	√	√	√	√	√						
6	Coal combustion						√									√				√							
7	Vehicle emission															√		√	√		√						
8	Brake																	√	√			√					
9	Fuel oil combustion															√							√	√			
10	Sea salt						√	√																			
11	Waste incineration							√						√				√	√								

3.4.2.2 PMF input data treatment

During the first campaign at the CUGB and the second campaign at the IAP, inorganic elements, water soluble ions, EC/OC, hopanes and PAHs were measured. Levoglucosan was only available during the first campaign. The criteria to select the input data for PMF suggested by Reff et al. (2007) are summarized as follows:

(1) Species which cannot represent any source should be excluded from the PMF data set.

(2) A duplication data input should be avoided, for instance, Na and Na^+, Ca and Ca^{2+}, Mg and Mg^{2+}, S and SO_4^{2-}, OC and organic compounds. In this study, elements were chosen because ions only include the water soluble part. OC and organic compounds were both used in PMF, because the more organic compounds used can show more detail as opposed to only using OC.

(3) Data lower than or equal to the limit of quantification (LOQ) were replaced by half of the LOQ and their uncertainties were set as 5/6 of the LOQ (Polissar et al., 1998). If the concentration is higher than the LOQ, the uncertainties were given as follows (Norris et al., 2008):

$$u_{ij} = (((\text{Error Fraction})*x_{ij})^2 + LOQ_{ij}^2)^{0.5} \quad (3\text{-}5)$$

where the error fraction (%) which is estimated from both sampling error and analytical error. In this study, an error fraction of 8-10% for trace element, 8% for EC and OC, 12-15% for water soluble ions, and 12-20% for organic compounds were estimated for the PMF analysis. If a large number of certain species are lower than the LOQ, then they are deleted from PMF analysis.

(4) The missing data was replaced by the mean value of that species and the uncertainties were set as three times of the mean value (Gu et al., 2011).

(5) Signal-to-noise (S/N) ratios were used to categorize a species, especially for poor or unknown data. Three categories which are "bad"(S/N<0.2), "weak"(0.2<S/N<2), and "strong" (S/N>2) can be obtained (Pattero and Hopke, 2003). "Bad" means this species will be excluded from PMF model. "Weak" means the uncertainty of this species will be increased by model in order to reduce the influence of this species.

In this study, the modeling uncertainty was set as 5% according to the suggestion from Norris et al. (2008). Species were discarded from the model if sum of the number of missing data and the number of data with values below the LOQ is more than 1/3 of the samples.

3.4.3 Backward trajectory and cluster analysis

The HYSPLIT4 (Hybrid Single Particle Lagrangian Integrated Trajectory, Version 4) model, which was developed by US National Oceanic and Atmospheric Administration (NOAA) Air Resources Laboratory, is often used to calculate backward trajectories of air flow for tracing its transport pathways (http://ready.arl.noaa.gov/HYSPLIT.php). In this study, meteorological data provided by the Global Data Assimilation System (GDAS) were applied in HYSPLIT4 model. The model computed air trajectories with a 1 h interval. The furthest emission sources are the dust regions like Taklamakan desert (about 3000 km). Wind speeds during dust events mainly range

between 8-18 m s^{-1}. The lifetime of $PM_{2.5}$ in the air is more than 3 days (Raes et al., 2000). Consequently, such particles can be in Beijing by wind driven transport within about 3 days. Considering 72 h backward trajectory is enough to cover all possible surrounding emission sources of Beijing on horizontal scale, including dust storms (Zhu et al., 2011). Additionally, the longer the backward trajectory time is used, the higher uncertainty it has (Wang et al. 2010b). So 72 h backward trajectories were used in this study. In order to combine backward trajectories and daily mean PM mass concentrations together, so only one backward trajectory can be used for each day. Because MLH has the highest value at early afternoon which is favorable for the mixing of air pollutants, the time ending at 06:00 UTC (local time 14:00) was selected for backward trajectory. A height of 500 m above ground level (AGL) at the ending point was selected because pollutants can be well mixed at this height and it can avoid the influences of the buildings when comparing with 100 m. This height was also found to be used in some previous studies (e.g. Zhang et al., 2009, Ji et al., 2014). In addition, according to the air flow speed and direction, backward trajectories are grouped into different clusters. So the main mean cluster backward trajectories can be obtained by HYSPLIT4.

3.5 Quality assurance / quality control (QA/QC)

In order to get high sampling quality, all filter holders and rings were cleaned in de-ionized water twice in an ultrasonic bath for 20 min before being used every time, then washed with de-ionized water individually again. After that, they were baked at 110°C in an oven for 1 h. The tweezers were cleaned by de-ionized water first and then by methanol before being used every time. The field blank filters were collected every two weeks, and all the experimental results were corrected by deducting the blank filter values. More details were described in the Standard operation procedures (SOPs) which were developed for all important operations: the standard operation procedure for filter weighing (Appendix A) and the standard operation procedure for sampling (Appendix B).

After a one year sampling campaign at the CUGB, PM mass concentrations from the CUGB by DHA-80 samplers (high volume sampler, HVS) were compared with TEOM data from IAP (Figure 3.10), and relative low PM mass concentrations from HVS were found.

At the same sampling period, weekly $PM_{2.5}$ samples were collected by a Mini-Volume Sampler (MVS, Leckel, Berlin) which was operated by KIT/IMG at a flow rate of 200 l h^{-1} at the same

sampling site (Schleicher et al., 2010). Quartz fiber filters with a 50 mm diameter (MN QF 10, Macherey-Nagel) were used. The comparison between HVS and MVS was also done (Figure 3.11). The correlation coefficient (R^2) between MVS data and HVS data was 0.85 with a slope of 1.82.

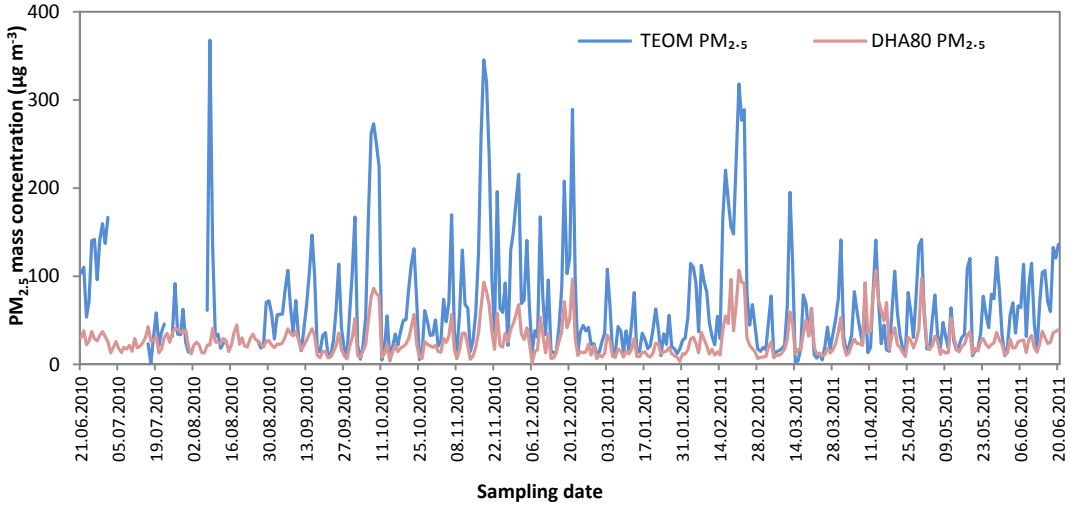

Figure 3.10: Comparison of $PM_{2.5}$ daily mean mass concentrations between HVS (CUGB) and TEOM (IAP)

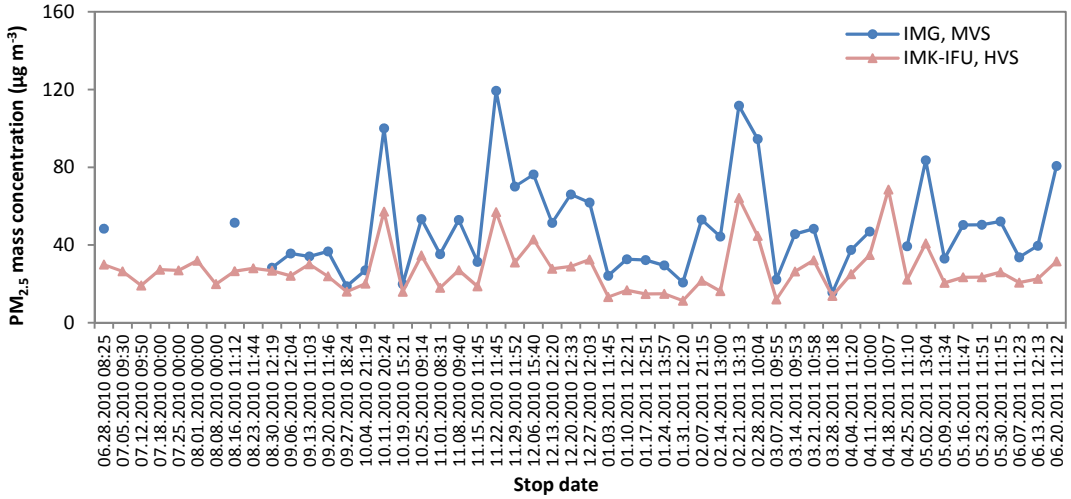

Figure 3.11: Comparison of $PM_{2.5}$ weekly mass concentration between HVS and MVS

One important point should be mentioned here is that even though the PM mass concentration determined by HVS during the first campaign at the CUGB was lower than the TEOM data and the MVS data, similar temporal variations were nonetheless found.

In order to maintain high quality in the results from sampling, the reasons for these differences should be carefully considered. The difference between HVS and TEOM could be caused by the different sampling sites. The reason for the difference between HVS and MVS could be that HVS were surrounded by trees and grass which can absorb some particles. Compared with HVS, MVS was much closer to the main entrance and the main road of CUGB which leads to a higher exposure of re-suspended road dust. Additionally, the different volumes and velocities of these two different kinds of samplers can also influence the collected PM mass. Because of the suction of samplers, some particles can pass through the filter. Therefore, filter collection usually will lose some particles. Especially HVS has stronger suction than MVS which indicates that the loss of HVS is higher than of MVS (Fu et al., 2008). In other words, a lower velocity results in a better deposition of the particles. Fu et al. (2008) compared the Andersen HVS with the low volume sampler (LVS), and found that PM concentrations determined by HVS are smaller than by LVS (Figure 3.12). In our study, the temperature of HVS inside where the collected filters were stored was about 10°C higher than outside which can cause a greater loss of volatile compounds, like volatile organic compounds (VOCs).

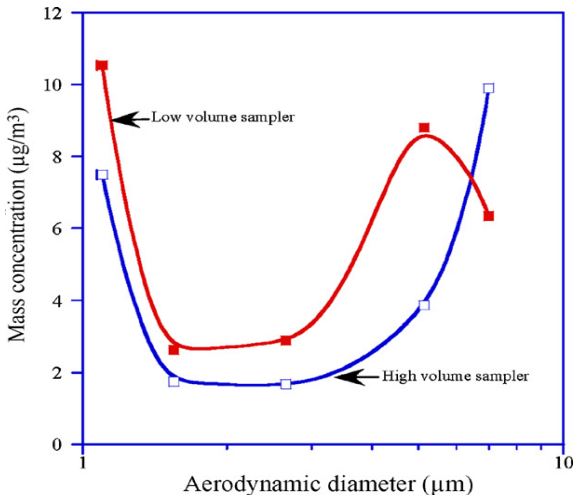

Figure 3.12: Comparison of PM mass concentrations between Andersen HVS and LVS (Source: Fu et al., 2008)

In order to get more details about the reasons for such big differences, both DHA-80 samplers were checked by Riemer Messtechnik first to make sure if the samplers were working well or not, and two problems with these two samplers were found: (1) Sampling in Beijing was done without baffle pots; (2) The tube between the sampling head and filter loading place was in the wrong position in both samplers. Therefore, a comparison campaign (Table 3.7) between two HVS and a LVS (volume is 2.3 $m^3 h^{-1}$, and quartz fibre filters of 4.7 cm ø) of KIT/IMG was conducted in Karlsruhe from June till August 2012. The aims of this comparison campaign are to find out the influences of sampling without a baffle pot and of sampling with the wrong tube position on the particle loading.

Table 3.7: Comparison campaign in Karlsruhe, 2012, among high volume samplers HVS A, HVS B and low volume sampler (LVS)

	Date	HVS A	HVS B	LVS	Remarks
1st week	6.22 - 6.29	Daily mean	Daily mean	Daily mean	HVS A and HVS B: no baffle pot and wrong tube position
2nd week	6.29 - 7.06	Weekly	Weekly	Weekly	
3rd week	7.20 - 7.27	Weekly	Weekly	Weekly	HVS A: with baffle pot and correct tube position HVS B: without baffle pot and correct tube position
4th week	7.27 - 8.03	Weekly	Weekly	Weekly	
5th week	8.03 - 8.10	Weekly	Weekly	Weekly	
6th week	8.10 - 8.17	Daily mean	Daily mean	Weekly	

3.5.1 Baffle pot

The principle of the impactor design is that when the aerosol stream passes through the nozzle, the coarse particles with larger inertia will impact upon the creamed baffle pot, and smaller particles will pass with the aerosol stream into the tube and be collected on the filters (Marple and Willeke, 1976).

The baffle pot is of a U-style and there is an annular heating plate under it (Figure 3.13). During the first campaign at the CUGB, grease (silicon high vacuum grease, Merck, Germany) was put on the heating plate. The vertical distance between tube jet exit and heating plate is 1 mm more than it is between tube jet exit and baffle pot (Figure 3.13 and Figure 3.14). Figure 3.13 shows the picture of the head of $PM_{2.5}$.

To check whether there is any difference when particles impact on the heating plate instead of the baffle pot, information from the German VDI as well as from the literature were checked.

Figure 3.13: DIGITEL $PM_{2.5}$ inlet opened for maintenance (Source: www.digitel-ag.com)

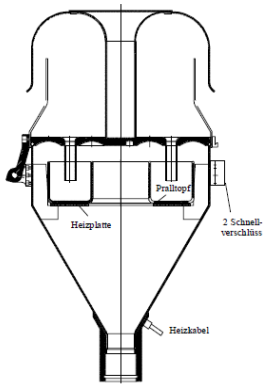

Figure 3.14: Head of DHA-80 $PM_{2.5}$ sampler (Bedienungsanleitung High Volume Sampler DIGITEL DHA-80, Source: www.riemer-mt.de)

The ratio of jet-to-plate distance to jet width (S/W), Reynolds number (Re), and the ratio of nozzle throat length to jet width (T/W) are the decisive factors for the cut point of the sampler head (Marple and Willeke, 1976) (Figure 3.15).

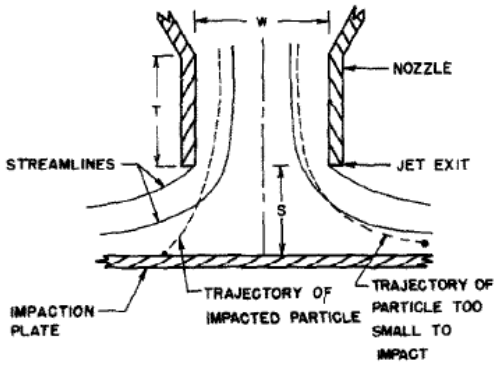

Figure 3.15: Particle trajectories and parameters for sampler impactor (Source: Marple and Willeke, 1976)

DHA-80 $PM_{2.5}$ impactor parameters are shown in Figure 3.16. T is 24 mm, S/W is 3.6 and T/W is 4.3. For the round impactor, if S/W value is bigger than 1.0, then the small variations in S will not change the value of the cut point (Marple and Willeke, 1976). This means there is no difference between sampling with and without a baffle pot. This is not only found from theoretical calculation, but also from the real sampling results during the comparison campaign.

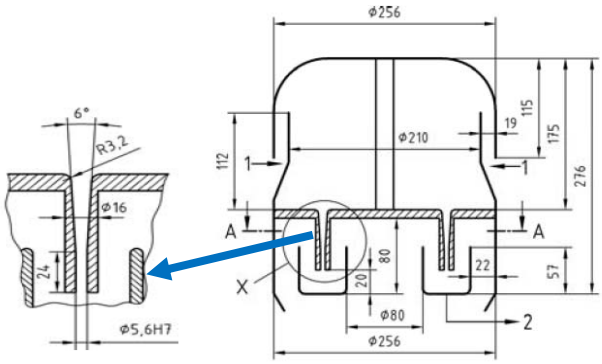

Figure 3.16: Parameters of $PM_{2.5}$ impactor of DHA-80 (Unit: mm, Source: VDI/DIN 14907)

From the 3rd week until the 6th week of the comparison campaign in Karlsruhe, HVS A was operated with a baffle pot and HVS B was operated without a baffle pot. Both samplers were with the correct tube position. The results from the comparison are shown in Figure 3.17 and

show that sampling with a baffle pot or not does not influence the $PM_{2.5}$ mass concentration loading.

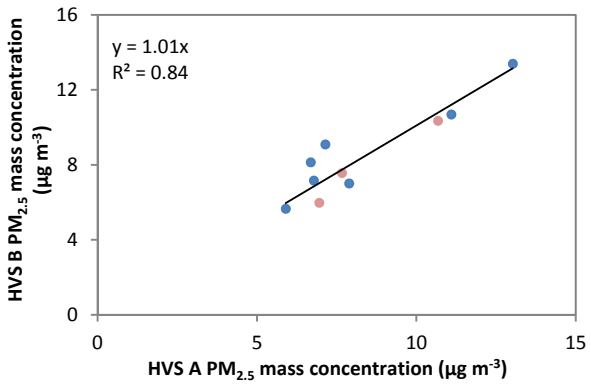

Figure 3.17: Comparison of measurement results between HVS A (with baffle pot) and HVS B (without baffle pot) (red ones are weekly samples and blue ones are daily samples)

3.5.2 Tube problem

The tube was found in the wrong position in both samplers due to an unknown reason during the first campaign at the CUGB in Beijing. The tube inside had dropped down about 2 cm (Figure 3.18).

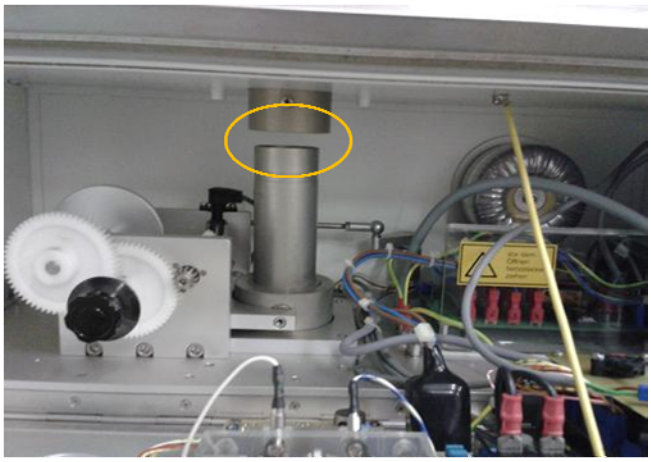

Figure 3.18: Wrong tube position of HVS

During the comparison campaign in Karlsruhe, the PM mass concentration between HVS and LVS was compared. During the first two weeks, HVS A and HVS B were setup similarly to that during the CUGB sampling campaign (wrong tube position and without baffle pot). The ratio of PM mass concentration as determined from the HVS to the LVS was 0.25. During the following four weeks, HVS A and HVS B were changed to their correct tube position, while HVS A was with a baffle pot while HVS B was without a baffle pot. The ratio of PM mass concentration as determined from the HVS to the LVS was found to have increased to 0.84. Obviously, the mass concentration of HVS with the correct tube position is about 3 times of that with the wrong tube position.

In order to get more details on the differences between the sample collection with the wrong tube position and the correct tube position, a 2nd comparison campaign was done at the KIT/IMK-IFU in Garmisch-Partenkirchen (Table 3.8). During this campaign, sampler A was operated with the correct tube position but sampler B was operated with the wrong tube position. For the first 3 weeks, both samplers were installed inside a vehicle hall and after that, both samplers were installed next to the entrance of KIT/IMK-IFU for the following 7 weeks.

Table 3.8: Comparison campaign in Garmisch-Partenkirchen, 2012, between high volume sampler HVS A with correct tube position and HVS B with wrong tube position

	Date	HVS A	HVS B	Location
1st week	08.31 - 09.07	Weekly	Weekly	Inside vehicle hall
2nd week	09.07 - 09.14	Weekly	Weekly	
3rd week	09.20 - 09.27	Weekly	Weekly	
4th week	09.28 - 10.05	Weekly	Weekly	Ambient air, near to the entrance
5th week	10.05 - 10.12	Weekly	Weekly	
6th week	10.16 - 10.23	Weekly	Weekly	
7th week	10.23 - 10.30	Daily means	Daily means	
8th week	10.30 - 11.06	Daily means	Daily means	
9th week	11.06 - 11.13	Daily means	Daily means	
10th week	11.14 - 11.21	Daily means	Daily means	

From this comparison campaign, the difference in particle loading at the baffle pot was found. Figure 3.19 shows that particle loading at the HVS A baffle pot is much more than that at HVS B

baffle pot which means more coarse particles passed with the aerosol stream into the tube and were collected on the filters of HVS B. In other words, the size of particles which were collected by filters of HVS B was changed.

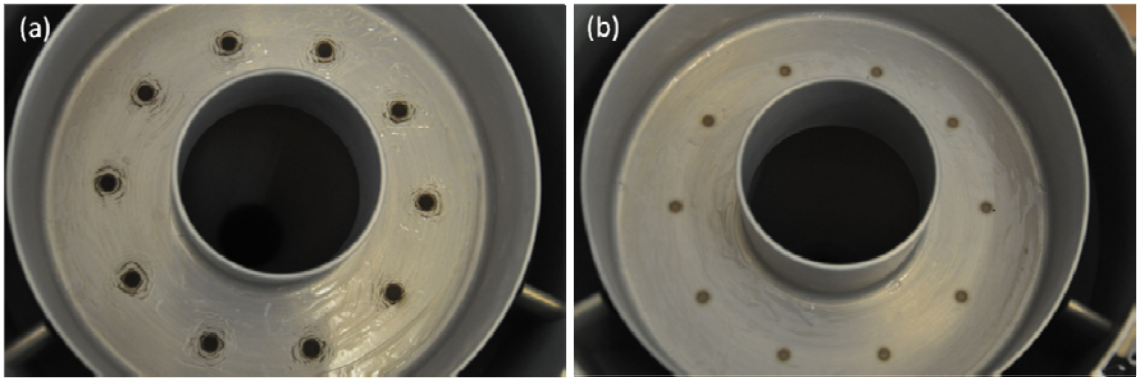

Figure 3.19: Comparison between particle loading on (a) HVS A baffle pot (correct tube position) and (b) HVS B baffle pot (wrong tube position) in Garmisch-Partenkirchen, 2012

Apart from the difference with the baffle pot, a large temperature difference between the ambient temperature and the temperature inside the tube of the sampler was also found (Figure 3.20). The mean temperature difference between ambient temperature and the inside sampler temperature was about 12°C for HVS B, but only 5°C for HVS A. The reason for the higher temperature difference in HVS B was the wrong tube position because the air was heated by the turbine and collected in a cycle. That means the air in the tube went through the filters and arrived at the turbine, and then the air was heated by the turbine as some of the exhaust air was sucked back into the tube via the tube gap of 2 cm (Figure 3.21). Because such air had been cleaned by the filter already, it does not influence the particle loading on the filter during the next cycle but would raise the temperature inside the sampler.

One important point should be mentioned here, after one year sampling, no obvious dust was found inside of both samplers which means there was no leaking from outside of samplers happened. In other words, passing the tubes of sampler head was the only way for air to go into the samplers.

During the Karlsruhe comparison campaign, both HVS were operated with the correct tube position from the 3rd week until the 6th week. As shown in Figure 3.22, the mean temperature

difference between ambient temperature and the inside temperature of both HVS was below 6°C.

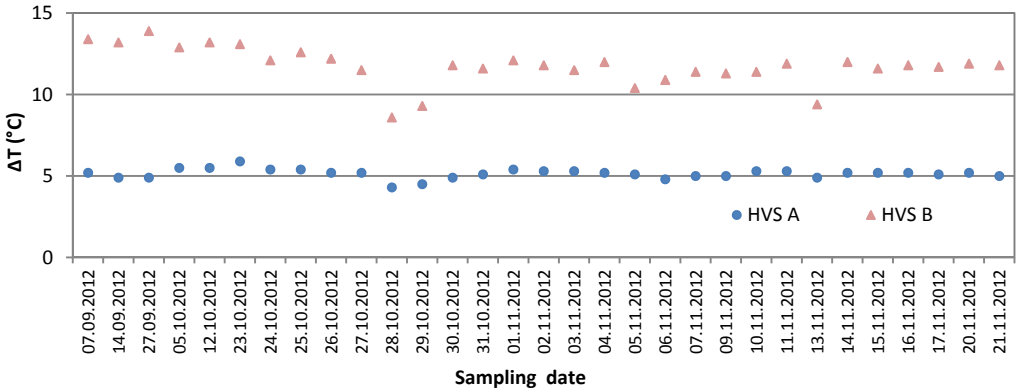

Figure 3.20: Comparison of temperature difference between ambient temperature and temperature inside of HVS A with correct tube position and HVS B with wrong tube position in Garmisch-Partenkirchen, 2012

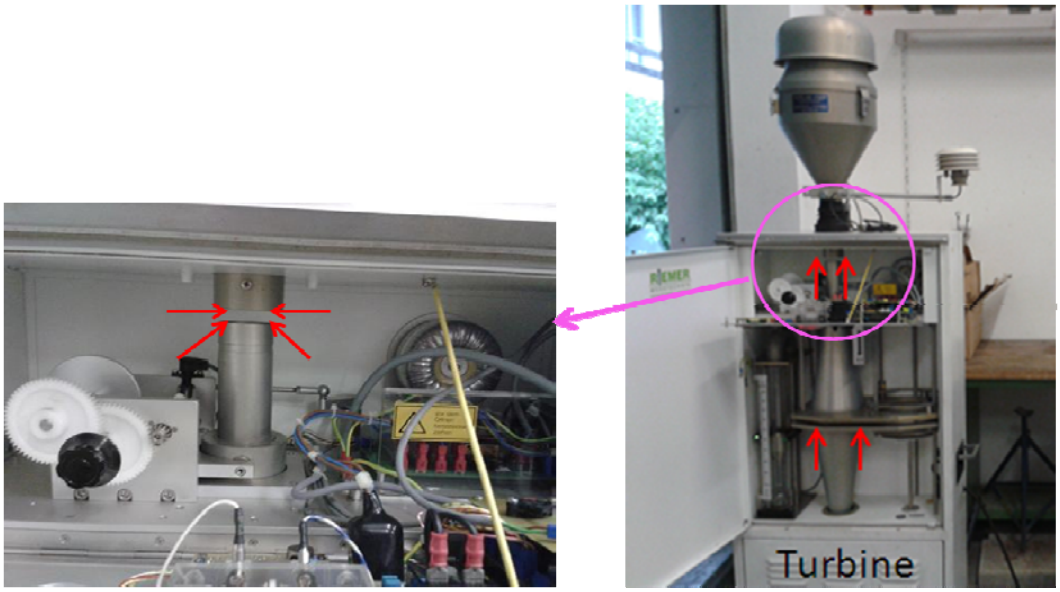

Figure 3.21: The direction of air flow inside of sampler with wrong tube position

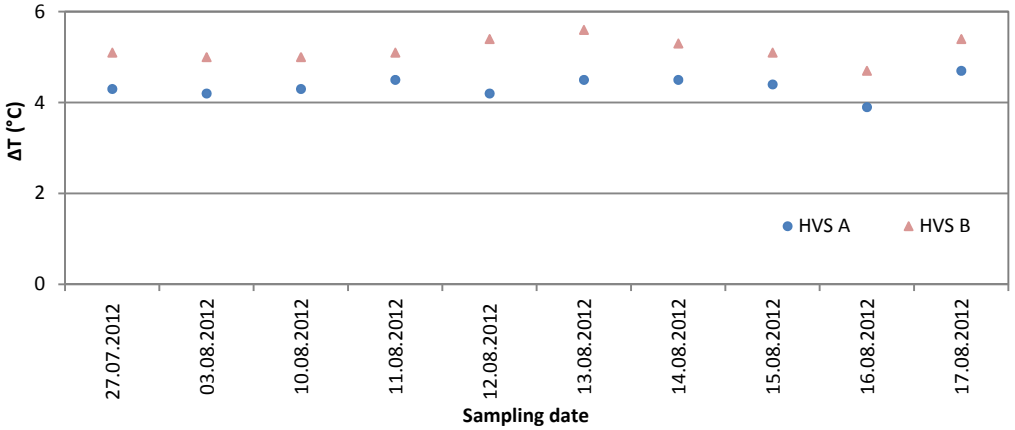

Figure 3.22: Comparison of temperature difference between ambient temperature and temperature inside of HVS A and HVS B when both HVS were operated with the correct tube position in Karlsruhe, 2012

Considering the lowered tube, the sample collection flow rate changed. Therefore, a measurement of flow volume through the sampling head with the wrong tube position was done by Digitel and a reduced sample collection flow of 10 $m^3 h^{-1}$ was measured. When the flow volume is reduced, the cutoff point of the samplers would also be changed, which means the size of the collected particles on the filters changed. This is in agreement with the result from baffle pot comparison between HVS A with the correct tube position and HVS B with the wrong tube position (Figure 3.19). So the recalculation of the cutoff point was necessary.

Following the impactor design theory (Gussman, 1969; Marple and Liu, 1974; Marple and Willeke, 1976), the equation is given as:

$$Stk_{50}=\frac{4\rho_p Q C {D_{50}}^2}{9\pi n \mu W^3} \quad (3\text{-}6)$$

Here, Stk_{50} is the stokes number at 50% collection efficiency, ρ_p is the particle density (ρ_p = 1 g cm^{-3}), Q is the total volume passing through the sampler, C is the Cunningham slip correction factor, D_{50} is particle diameter at 50% collection efficiency, n is the number of nozzles, μ is the fluid viscosity ($\mu = 1.81 \times 10^{-4}$ kg s^{-1} m^{-1}) and W is the jet width.

Because Stk_{50} is relatively constant when S/W ratio (see section 3.5.1) is larger than 1.0 (Marple and Willeke, 1976), the cutoff size of particles $C^{0.5}D_{50}$ can be recalculated by the following equation:

$$\frac{4\rho_p Q_1 C_1 {D_1}_{50}^{\ 2}}{9\pi n\mu W^3} = \frac{4\rho_p Q_2 C_2 {D_2}_{50}^{\ 2}}{9\pi n\mu W^3} \quad (3\text{-}7)$$

In our case, the flow rate of HVS with the correct tube position is 500 l min^{-1} which means Q_1 is 30 $m^3 h^{-1}$ and with the wrong tube position is 10 $m^3 h^{-1}$ (Q_2), n of HVS is 10, W of HVS is 5.6 mm, $C_1^{0.5}D_{1\,50}$ is 2.5 µm. According to the formula 3-6, the cutoff size $C_2^{0.5}D_{2\,50}$ of particles which were collected during the first campaign at the CUGB was found to be 4.3 µm which means $PM_{4.3}$ was collected at the CUGB.

Chapter 4 Characteristics of particulate matter concentration and chemical composition

PM mass concentration is an important parameter for assessing the pollution level and many studies have been done during the past years (e.g. Chan et al., 2008; Cusack et al., 2013; Huang et al., 2013; Jahn et al., 2013). As described in Chapter 1.1.2, chemical compounds in PM play very important role on environment pollution, climate change and human health. Therefore, in order to study the influences of PM on the environment pollution, climate change and human health, the analysis of the chemical composition of PM such as carbonaceous matter, inorganic elements, water soluble ions and organic compounds is required.

In this chapter, comprehensive data on EC, OC, water soluble ions, inorganic elements and particulate organic compounds in PM collected in Beijing is described. The samples collected at the CUGB from 21 June 2010 till 20 June 2011 and at the IAP from 10 April 2013 till 8 June 2013 are discussed.

4.1 Results from long-term daily mean $PM_{4.3}$ sampling at the CUGB (2010.06.21 – 2011.06.20)

4.1.1 $PM_{4.3}$ mass concentration

As discussed in Chapter 3, the size of particles collected at the CUGB was recalculated as $PM_{4.3}$. $PM_{4.3}$ mass concentrations determined from daily mean sampling at the monitoring site of the CUGB in Beijing from 21 June 2010 till 20 June 2011 are shown in Figure 4.1. They ranged from 18 μg m^{-3} to 321 μg m^{-3}, with an annual average value of 83 μg m^{-3}. Significant variation of monthly $PM_{4.3}$ mass concentrations was observed (Figure 4.2). The $PM_{4.3}$ mass concentration

decreased continuously from June 2010 till September 2010, then increased from October 2010 till November 2010, and decreased again after December 2010, reached the lowest value of 44 µg m^{-3} in January 2011, and the highest value of 117 µg m^{-3} in April 2011. Seasonal variation of $PM_{4.3}$ mass concentration was also examined (Figure 4.3). The seasons were defined as follows: summer – June till August; autumn – September and October; winter – November till March; spring – April and May (He et al., 2001). Only 20 days were observed in summer 2011 (from 1 June till 20 June 2011), but 70 days in summer 2010 (21 June to 31 August 2010). The time periods were not overlapping, so that one cannot fully compare both summer periods. Another point is that the 20 samples in the beginning of June 2011 are not representative for summer 2011. So in the following sections or chapters, the data of these 20 samples (summer 2011) will be shown but excluded in the discussion of seasonality. Figure 4.3 shows that $PM_{4.3}$ mass concentrations reached the highest value at 95 µg m^{-3} during spring 2011, decreased through the winter 2010, summer 2010 and tended to be the lowest in autumn 2010 (80 µg m^{-3}), but there was no very obvious seasonal variation of $PM_{4.3}$ mass concentrations during the whole sampling year.

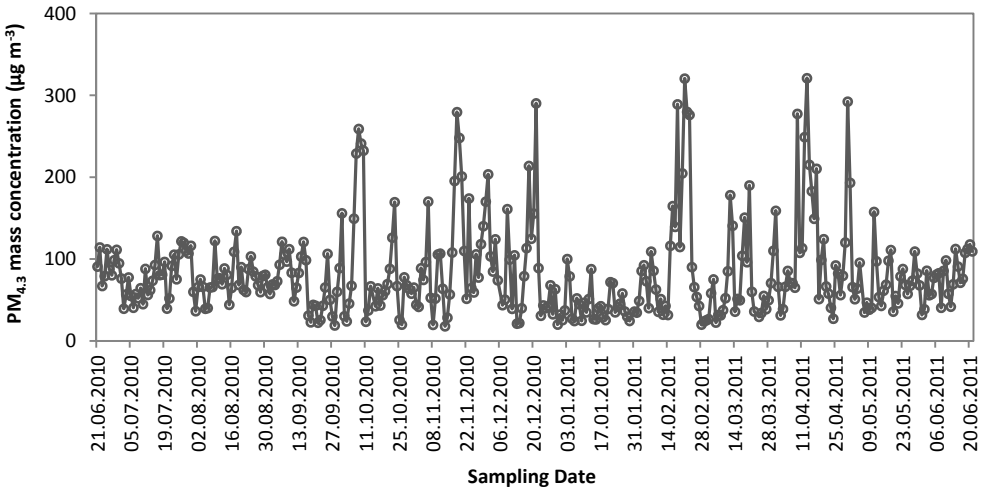

Figure 4.1: Annual variation of daily mean $PM_{4.3}$ mass concentrations at the CUGB from 2010.06.21 till 2011.06.20

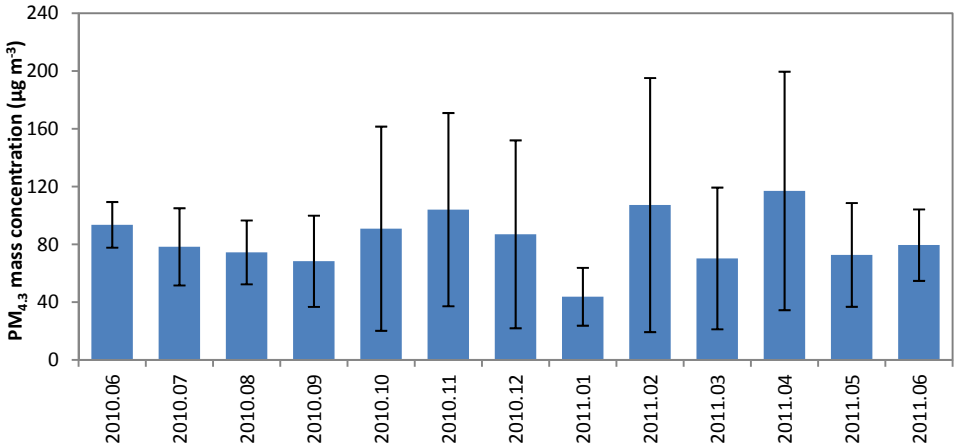

Figure 4.2: Monthly variation of $PM_{4.3}$ mass concentrations at the CUGB from 2010.06.21 till 2011.06.20

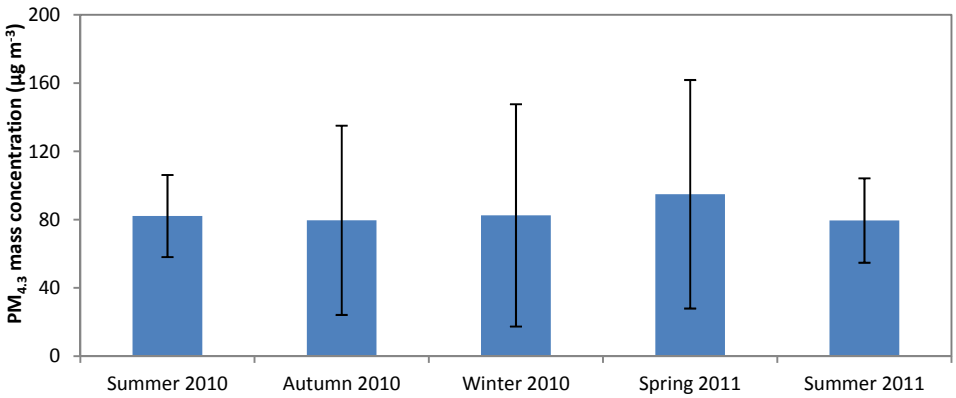

Figure 4.3: Seasonal variation of $PM_{4.3}$ mass concentrations at the CUGB from 2010.06.21 till 2011.06.20

4.1.2 EC and OC

Annual variations of daily mean EC and OC mass concentrations in $PM_{4.3}$ are shown in Figure 4.4. One year, 365 daily mean samples were collected. Complete EC and OC data sets were achieved from 335 samples.

The total carbon (TC, sum of OC and EC) contributed about 30.8% to $PM_{4.3}$ mass in this study. This result is similar to the result from $PM_{2.5}$ in Beijing by He et al. (2001), who found a contribution of 29.1% from TC.

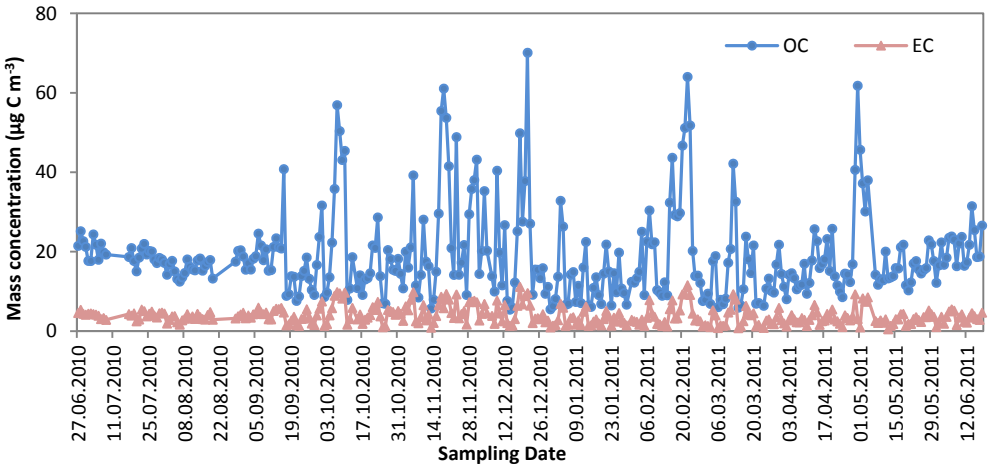

Figure 4.4: Annual variations of daily mean EC and OC mass concentrations in $PM_{4.3}$ at the CUGB from 2010.06.21 till 2011.06.20 (335 samples)

Daily mean OC mass concentrations varied from 5.4 to 70.1 µg C m^{-3} and EC mass concentrations ranged from 0.5 to 11.6 µg C m^{-3}. From Figures 4.1 and 4.4, one can see that OC and EC mass concentrations vary synchronously with $PM_{4.3}$ mass concentrations. The annual average mass concentrations of OC and EC were 18.9 ± 10.9 µg C m^{-3} and 3.8 ± 2.1 µg C m^{-3}, respectively, and contributed 25.5 ± 8.2% and 5.3 ± 1.9% to $PM_{4.3}$ mass, respectively. The seasonal average concentration of OC was the highest at 19.2 ± 13.5 µg C m^{-3} in winter 2010 and the lowest at 18.0 ± 9.7 µg C m^{-3} in spring 2011. OC mass concentrations were also found to be the highest in winter by other studies (e.g. He et al., 2001; Zhao et al., 2013a; Zhang et al., 2013). The reason could be the increase in local emissions, such as coal combustion for heating. However, our results showed lower value than that determined by other studies in the Beijing urban area, for instance, 31.5 µg C m^{-3} by He et al. (2001), 26.8 µg C m^{-3} by Zhao et al. (2013b), 24.9 µg C m^{-3} by Zhang et al. (2013). The reason is that OC concentrations were the lowest in January 2011, resulting in a low average during the winter period because these values could not be compensated by November, December 2010 and February 2011 when relatively high OC concentrations were detected. For EC, the highest mass concentration was 4.3 ± 2.2 µg C m^{-3} in autumn 2010 and the lowest mass concentration was 3.2 ± 1.8 µg C m^{-3} in spring 2011 (Figure 4.5). The mass percentages of OC and EC in $PM_{4.3}$ showed no big variation in different seasons, 25.8%, 26.3%, 25.4% and 23.5% for OC and 5.2%, 5.9%, 5.4% and 4.3% for EC in summer 2010, autumn 2010, winter 2010 and spring 2011, respectively. Monthly variations of OC and EC are shown in Figure 4.6. The highest OC mass concentration was in November 2010 and the lowest was in January 2011. EC exhibited the same variation as OC.

Carbonaceous matter (CM) can be calculated by the sum of organic matter (OM) and EC while OM is normally estimated by OC. The ratio between OM and OC was found to range from 1.4 to 1.8 depending on the oxidative state of the aerosol which may lead to a seasonally dependent ratio. In this study, a ratio of 1.6 was used based on the following formula (Turpin and Lim, 2001):

$$CM = 1.6 \times OC + EC \quad (4\text{-}1)$$

CM contributed 45.4%, 48.1%, 45.8% and 38.4% to $PM_{4.3}$ mass in summer 2010, autumn 2010, winter 2010 and spring 2011, respectively and the annual average mass percentage of CM in $PM_{4.3}$ was 45.6% which shows that CM is an important constituent in $PM_{4.3}$.

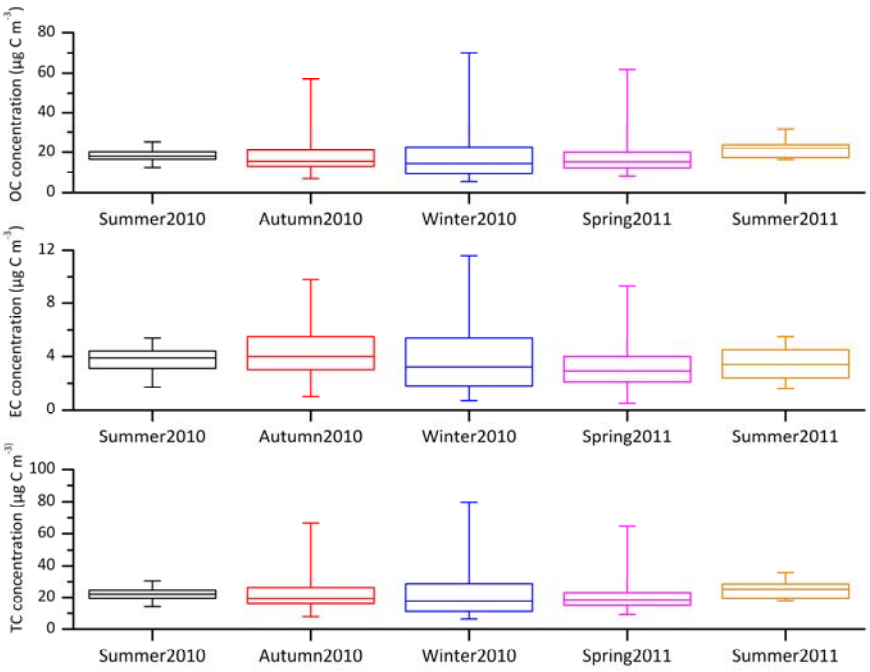

Figure 4.5: Box plots of daily mean OC, EC and TC mass concentrations at the CUGB from 2010.06.21 till 2011.06.20 (335 samples). The lower end of the box is represented by the lower quartile, the upper end of the box is the upper quartile, and the median value is shown by the line inside the box. Whiskers represent the complete data range (minimum to maximum)

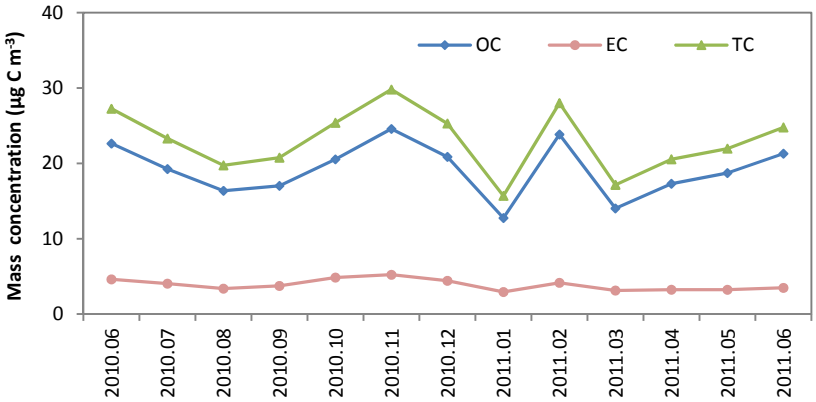

Figure 4.6: Monthly variations of OC, EC and TC mass concentrations in $PM_{4.3}$ at the CUGB from 2010.06.21 till 2011.06.20

4.1.3 Water soluble ions

Water soluble ions were measured in nearly all loaded $PM_{4.3}$ filters at the CUGB (328 samples). The seasonal average mass concentrations of Cl^-, NO_3^-, SO_4^{2-} and NH_4^+ are listed in Table 4.1.

Table 4.1: Seasonal average mass concentrations of the ions in $PM_{4.3}$ at the CUGB from 2010.06.21 till 2011.06.20 (unit: µg m^{-3})

Ion	Minimum	Maximum	Annual average (N=328)	2010 Summer (N=48)	2010 Autumn (N=60)	2010 Winter (N=142)	2011 Spring (N=60)	2011 Summer (N=18)
Cl^-	NA	24.3	2.0 ± 3.0	0.07 ± 0.2	0.5 ± 0.7	3.0 ± 3.5	0.9 ± 1.7	0.03 ± 0.04
NO_3^-	0.2	216	8.6 ± 21.2	1.7 ± 1.0	9.9 ± 17.4	11.7 ± 28.8	7.5 ± 11.3	2.6 ± 1.6
SO_4^{2-}	0.5	181	12.8 ± 19.3	21.9 ± 16.3	12.8 ± 16.3	10.9 ± 23.7	9.9 ± 10.7	14.0 ± 10.9
NH_4^+	NA	90.2	4.6 ± 8.6	5.6 ± 4.3	5.8 ± 9.9	4.6 ± 10.6	2.8 ± 4.0	3.2 ± 2.7

NA: < LOQ

In $PM_{4.3}$ at the CUGB, the sum of NO_3^-, SO_4^{2-} and NH_4^+ mass concentrations contributed by an annual average value of 24.3% (ranging from 2.1% to 85.3%) to the total $PM_{4.3}$ mass concentration. NO_3^- had the highest mass concentration at 11.7 µg m^{-3} in winter 2010 and the lowest mass concentration in summer 2010 (1.7 µg m^{-3}) while SO_4^{2-} showed the highest mass

concentration in summer 2010 with the value of 21.9 μg m^{-3} and the lowest mass concentration (9.9 μg m^{-3}) in spring 2011. Seasonal variation of NH_4^+ mass concentration showed the highest value in autumn 2010, followed by summer 2010, winter 2010, and spring 2011. Cl^- contributed a minor fraction to $PM_{4.3}$ mass concentration in comparison with NO_3^-, SO_4^{2-} and NH_4^+, at only 2.2%. It was found that 69.7% of Cl^- mass concentrations in summer 2010 were lower than the LOQ, while Cl^- mass concentrations during winter 2010 showed an noticeably high value of 3.0 μg m^{-3}.

4.1.4 Inorganic elements

For the assessment of air quality, the average seasonal mass concentrations of 15 elements including Fe, S, K, Ca, Ti, Mn, Cr, Ni, Cu, Zn, As, Sn, Sb, Pb and Ba, which were analyzed from the $PM_{4.3}$ samples, are listed in Table 4.2. 358 samples were valid analyzed in all loaded filters.

Table 4.2: Seasonal average mass concentrations of the chemical elements in $PM_{4.3}$ at the CUGB from 2010.06.21 till 2011.06.20 (unit: ng m^{-3})

Element	Min	Max	Annual average (N=358)	2010 Summer (N=69)	2010 Autumn (N=60)	2010 Winter (N=148)	2011 Spring (N=60)	2011 Summer (N=21)
Fe	20	9439	1455 ± 1198	1155 ± 368	1227 ± 605	1494 ± 1169	2103 ± 2013	969 ± 296
S	33	20799	2960 ± 3479	5107 ± 4242	2805 ± 3116	2363 ± 3447	1900 ± 1814	3587 ± 2591
K	129	13220	1569 ± 1740	1163 ± 827	1070 ± 771	1899 ± 2318	1585 ± 1370	1963 ± 1634
Ca	NA	16102	2340 ± 2048	1534 ± 544	1747 ± 862	2540 ± 1898	3587 ± 3494	1682 ± 581
Ti	8	918	102 ± 101	67.3 ± 22.9	72.6 ± 36.8	107 ± 77.6	175 ± 190	65.8 ± 22.0
Mn	NA	255	52.3 ± 37.4	37.6 ± 13.1	46.8 ± 23.3	61.0 ± 42.8	60.7 ± 48.9	31.6 ± 11.6
Cr	NA	83.4	16.3 ± 13.0	17.5 ± 11.0	14.3 ± 8.7	17.8 ± 15.5	14.3 ± 11.4	12.3 ± 13.9
Ni	NA	4.1	1.0 ± 0.7	0.9 ± 0.6	0.7 ± 0.5	1.1 ± 0.8	1.0 ± 0.7	0.7 ± 0.7
Cu	NA	210	35.5 ± 30.9	28.8 ± 16.8	37.0 ± 28.3	39.9 ± 37.8	31.0 ± 27.5	26.5 ± 12.9
Zn	NA	1723	326 ± 301	350 ± 219	328 ± 296	313 ± 351	326 ± 295	328 ± 186
As	NA	145	15.6 ± 19.6	13.1 ± 13.1	12.7 ± 13.4	17.2 ± 24.6	16.8 ± 19.9	17.1 ± 12.0
Sn	NA	16.2	5.3 ± 3.6	5.0 ± 3.5	4.1 ± 3.3	5.3 ± 3.5	6.0 ± 3.8	7.4 ± 2.8
Sb	NA	10.6	2.8 ± 1.9	2.6 ± 2.0	2.7 ± 2.0	3.0 ± 2.0	2.7 ± 1.8	2.9 ± 1.4
Ba	NA	149	22.5 ± 18.8	17.8 ± 5.8	18.9 ± 9.5	23.1 ± 18.4	32.6 ± 31.5	14.9 ± 4.4
Pb	1.0	593	105 ± 98.8	96.6 ± 56.2	97.3 ± 80.6	116 ± 122	99.2 ± 103	93.1 ± 53.4

NA: < LOQ. Min is minimum and Max is maximum.

In all elements, S had the highest annual average mass concentration of 2960 ng m^{-3} and the lowest was Ni with 1.0 ng m^{-3}. S had a high concentration level over the whole year, with the highest mass concentration in summer 2010 and it was found to have a significant positive correlation with SO_4^{2-} (R=0.83), therefore the reason for the highest mass concentration of S during summer could be the secondary sulfate formed by photochemical reactions, especially in summer with strong solar radiation and high temperature (Seinfeld and Pandis, 2006). Fe, Ca, Ti and Ba, which are generally related to the crustal sources (Yang et al., 2005), accounted for 49.1% of all elemental mass, and showed similar variational patterns over the whole year with many coinciding peaks in mass concentration. For instance, the highest mass concentrations of these four elements occurred in spring 2011 which was likely due to a dust storm contribution (Figure 4.7 (a)). The other non-crustal elements, such as Zn, As, Sn, Sb and Pb, which are generally considered to originate from anthropogenic sources, showed no large difference from season to season. Figure 4.7 (b) shows that Zn, As and Pb followed similar patterns during the whole measurement period and had the lowest mass values in January 2011.

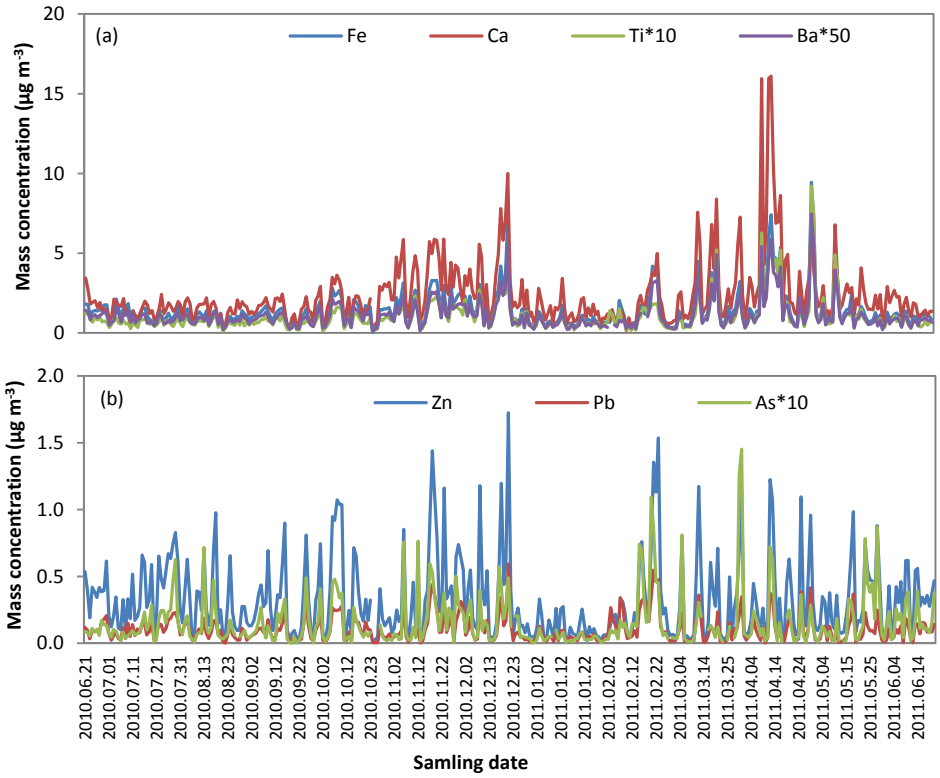

Figure 4.7: Annual variations of (a) Fe, Ca, Ti and Ba and (b) Zn, Pb and As daily mean mass concentrations in $PM_{4.3}$ at the CUGB from 2010.06.21 till 2011.06.20

4.1.5 Organic compounds

In all loaded $PM_{4.3}$ filters at the CUGB, 340 samples were measured for organic compounds effectively. Levoglucosan, eleven hopane substances including Ts, Tm, 27b, 29ab, 29ba, 30ab, 30ba, 31abS, 31abR, 32abS, 32abR, and eleven PAH substances including BAA, CRY, BBKF, BEP, BAP, PER, DAH, IND, PIC, BGH, COR were measured. Annual variations of levoglucosan, hopane substances and PAHs are shown in Figures 4.8, 4.9 and 4.10, respectively. Seasonal average mass concentrations of all these organic compounds in $PM_{4.3}$ at the CUGB are listed in Table 4.3. Because 27b mass concentrations in most samples were lower than LOQ, the data of 27b was excluded in this chapter.

Table 4.3: Seasonal average mass concentrations of organic compounds in $PM_{4.3}$ at the CUGB from 2010.06.21 till 2011.06.20 (unit: ng m^{-3})

Substance	Min	Max	Annual average (N=340)	2010 Summer (N=52)	2010 Autumn (N=61)	2010 Winter (N=151)	2011 Spring (N=58)	2011 Summer (N=18)
Levoglucosan	7.9	2443	406±352	667±462	568±451	369±262	176±131	278±268
Hopanes								
Ts	NA	7.0	1.5±1.0	1.5±0.9	1.7±0.9	1.3±0.9	1.5±0.9	2.7±1.5
Tm	NA	14.4	2.4±2.2	1.1±0.5	1.6±0.8	3.4±2.7	1.3±0.6	2.5±0.8
29ab	0.87	33.7	5.6±4.2	4.6±1.6	5.3±2.3	6.6±5.5	3.4±1.9	8.4±3.0
29ba	NA	18.8	2.9±3.2	0.9±0.5	1.3±0.5	4.5±3.7	0.9±0.8	2.5±0.8
30ab	0.37	24.0	5.6±3.7	5.2±1.8	6.0±2.5	5.7±4.4	4.0±2.7	9.9±4.2
30ba	NA	19.0	2.6±3.0	0.8±0.3	1.4±0.5	4.0±3.6	0.9±0.6	2.2±0.7
31abS	NA	8.9	2.1±1.1	2.3±0.6	2.4±0.8	1.9±1.1	1.5±0.9	3.9±1.6
31abR	NA	8.7	1.9±1.1	1.7±0.4	1.7±0.6	2.2±1.4	1.2±0.9	2.9±1.2
32abS	NA	6.5	1.6±0.9	1.4±0.4	1.6±0.4	1.8±1.0	1.0±0.9	2.34±1.1
32abR	NA	6.7	1.4±0.9	1.3±1.0	1.1±0.4	1.5±0.9	0.9±1.0	1.8±1.0
PAHs								
BAA	NA	33.3	2.1±4.0	0.1±0.1	0.4±0.4	4.4±5.1	0.3±0.2	0.2±0.1
CRY	NA	72.7	5.6±8.6	0.8±0.4	1.9±1.9	10.8±10.8	1.4±1.0	1.2±0.4
BBKF	0.15	82.1	7.5±10.8	1.3±0.5	3.6±2.9	14.0±13.5	2.2±1.8	1.4±0.7
BEP	0.05	26.7	2.3±3.3	0.4±0.2	1.2±0.9	4.2±4.1	0.7±0.6	0.5±0.3
BAP	0.02	29.2	2.6±3.8	0.3±0.2	1.1±1.0	4.7±5.0	1.2±0.5	1.3±0.5
PER	NA	7.1	0.7±0.9	0.06±0.03	0.4±1.1	1.0±0.9	0.2±0.1	NA
DAH	NA	5.3	0.7±0.8	0.2±0.1	0.4±0.3	1.1±0.8	1.1±1.3	0.2±0.1
IND	NA	34.8	3.4±4.4	0.8±0.5	2.0±1.4	5.9±5.4	1.3±1.0	0.9±0.4
PIC	NA	4.5	0.9±0.8	0.1±0.05	0.5±0.3	1.2±0.8	0.5±0.5	0.2±0.04
BGH	NA	23.5	2.5±3.2	0.6±0.2	1.6±1.2	4.3±3.9	1.0±0.9	0.7±0.3
COR	NA	18.0	2.6±2.4	1.0±0.8	1.4±1.2	3.8±2.6	1.0±0.8	1.0±0.5

NA: < LOQ. Min is minimum and Max is maximum.

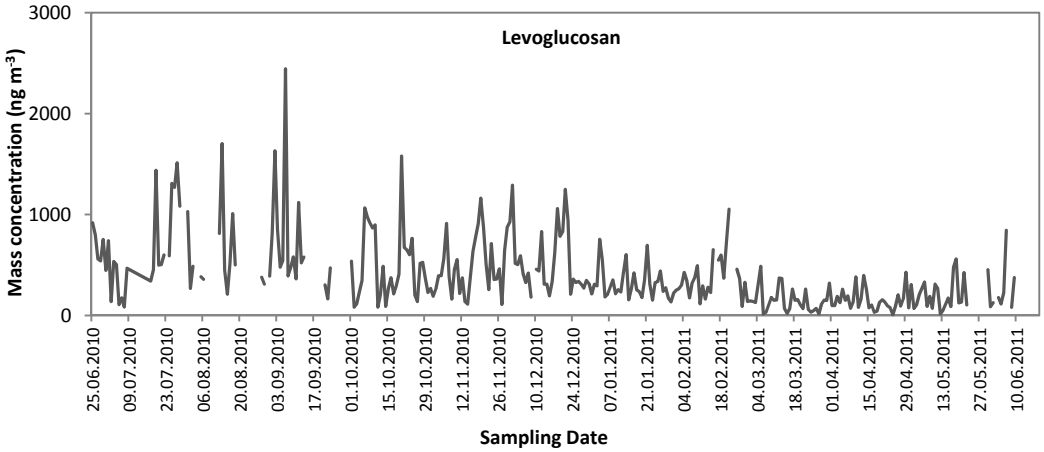

Figure 4.8: Annual variation in daily mean mass concentrations of levoglucosan in $PM_{4.3}$ at the CUGB from 2010.06.21 till 2011.06.20

Levoglucosan was the dominant compound in all measured organic compounds. Levoglucosan daily mean mass concentrations ranged from 7.9 ng m^{-3} to 2443 ng m^{-3}, with an annual average value of 406 ng m^{-3} and contributed 0.6% (average value) to $PM_{4.3}$ mass (Figure 4.8). The seasonal variation of levoglucosan mass concentration (Table 4.3) showed that the highest mass concentration was in summer 2010 (667 ng m^{-3}), followed by autumn 2010 (568 ng m^{-3}), winter 2010 (369 ng m^{-3}), and the lowest was in spring 2011 (176 ng m^{-3}).

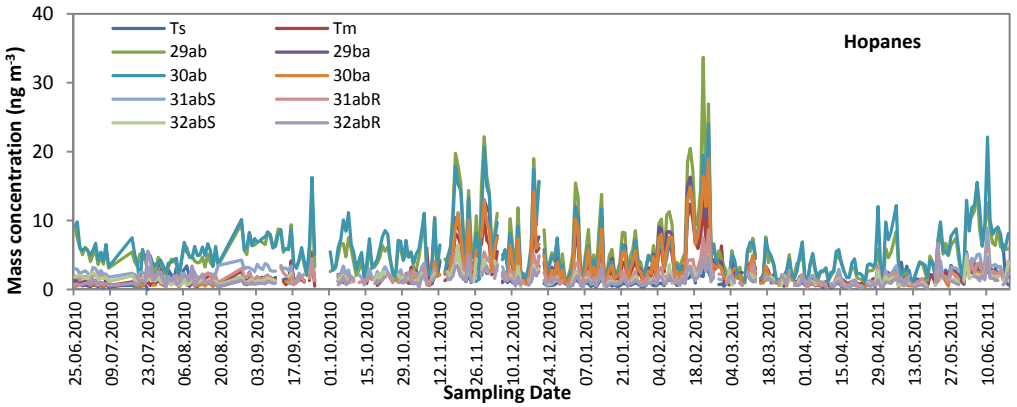

Figure 4.9: Annual variation in daily mean mass concentrations of hopane substances in $PM_{4.3}$ at the CUGB from 2010.06.21 till 2011.06.20

Annual average mass concentrations of daily mean Ts, Tm, 29ab, 29ba, 30ab, 30ba, 31abS, 31abR, 32abS and 32abR were 1.5 ng m^{-3}, 2.4 ng m^{-3}, 5.6 ng m^{-3}, 2.9 ng m^{-3}, 5.6 ng m^{-3}, 2.6 ng m^{-3}, 2.1 ng m^{-3}, 1.9 ng m^{-3}, 1.6 ng m^{-3}, and 1.4 ng m^{-3}, respectively (Table 4.3). For seasonal variation, except for Ts, 30ab and 31abS which all showed the highest mass concentrations in autumn 2010, all the other hopane substances had a higher mass concentration in winter 2010 than in other seasons. Ts was the only substance which had a lower mass concentration in winter 2010 than in other seasons while Tm and 30ba had the lowest mass concentrations in summer 2010. The mass concentrations of 29ab, 30ab, 31abS, 31abR, 32abS and 32abR were the lowest in spring 2011 compared with other seasons. The dominant substances were 29ab and 30ab in all hopane compounds, which contributed by annual average value of 22.9% and 24.2% to all measured hopanes mass, respectively.

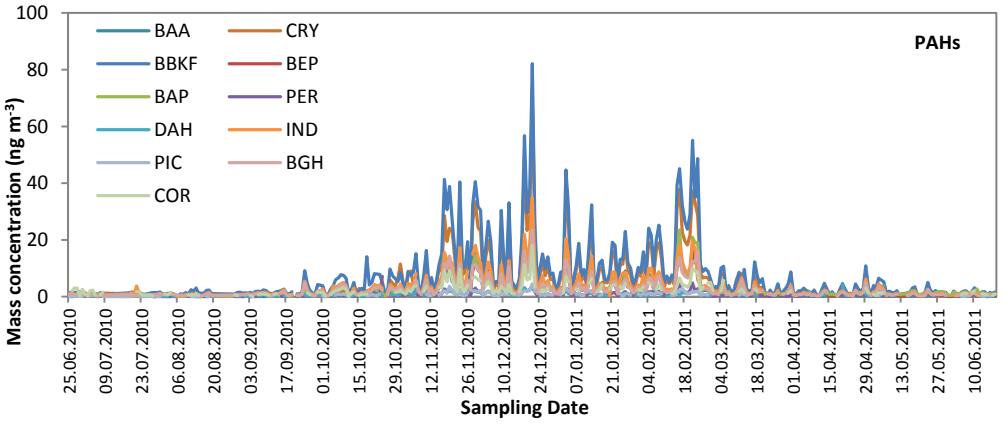

Figure 4.10: Annual variation in daily mean mass concentrations of PAH substances in $PM_{4.3}$ at the CUGB from 2010.06.21 till 2011.06.20

The total PAHs mass concentrations were in the range of 1.1 – 332 ng m^{-3} during the whole year. The sum of PAHs mass concentrations was the lowest in summer 2010 (5.2 ng m^{-3}), relatively higher in spring 2011 with an average value of 8.3 ng m^{-3} and autumn 2010 with an average value of 13.4 ng m^{-3}. PAHs mass concentrations increased rapidly during winter time as also observed in previous studies (e.g. He et al., 2006; Huang et al., 2006), with a average measured mass concentration of 53.2 ng m^{-3} which was around 9 times higher than in summer 2010. Generally, 5-ring PAHs, including BBKF, BEP, BAP, PER, DAH and PIC, were the most abundant compounds in total PAHs and constituted 48.9% (annual average) of all PAHs mass.

BBKF were the dominant compounds in 5-ring PAHs with a average contribution of 53.6% to 5-ring PAHs mass.

4.1.6 $PM_{4.3}$ mass balance

The mass balance of $PM_{4.3}$ is shown in Figure 4.11. Organic matter was calculated on the basis of formula 4-1. The sum of Fe, Ca, Ti and Ba is considered as crustal elements. Trace elements include Cr, Ni, Zn, As, Pb, Sn, Cu and Sb. From Figure 4.11, organic matter was the largest fraction of $PM_{4.3}$ with the mass contribution of 41%. NO_3^-, SO_4^{2-} and NH_4^+ contributed 25% to $PM_{4.3}$ mass. The other unknown part was the third highest fraction of $PM_{4.3}$ mass with the contribution of 23%. Inorganic elements constituted 6% of the $PM_{4.3}$ mass.

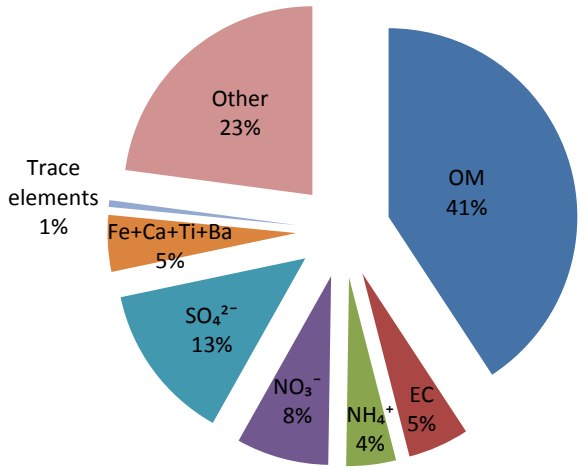

Figure 4.11: Mass balance of $PM_{4.3}$ on the basis of daily mean samples at the CUGB during 2010-2011

4.2 Results from short-term daily mean $PM_{2.5}$ sampling at the IAP (2013.04.10 – 2013.06.08)

In this campaign, EC, OC, three water soluble anions (Cl^-, SO_4^{2-} and NO_3^-), five water soluble cations (Na^+, NH_4^+, K^+, Mg^{2+} and Ca^{2+}) and eighteen inorganic elements (Na, Mg, Al, K, Ca, Fe, V, Cr, Mn, Co, Ni, Cu, Zn, As, Cd, Ba, Tl and Pb) were measured. Organic compounds, were only analyzed from 10 April till 31 May because the GC-MS machine was out of order. Eleven

hopane substances including Ts, Tm, 27b, 29ab, 29ba, 30ab, 30ba, 31abS, 31abR, 32abS, 32abR, and eleven PAH substances including BAA, CRY, BBKF, BEP, BAP, PER, DAH, IND, PIC, BGH, COR were measured. Levoglucosan data cannot be available in this campaign. Average values of all compounds from their daily mean mass concentrations are shown in Table 4.4. Because 27b mass concentrations in most samples were lower than the LOQ, the data of 27b was excluded in all discussion. Considering that only 8 sampling days (from 1 June till 8 June 2013) were in summer following the definition of seasons in the section 4.1, spring 2013 was used as the name of the whole sampling period during this campaign in the following discussion.

Table 4.4: Average values of all measured compounds from daily mean mass concentrations in $PM_{2.5}$ samples collected at the IAP in spring 2013 (unit: μg m^{-3}, from V to COR unit: ng m^{-3})

Species	Minimum	Maximum	Average	Species	Minimum	Maximum	Average
$PM_{2.5}$	16	182	89.4±42.7	Cd	NA	15.5	2.2±2.6
EC	1.0	7.6	3.2±1.3	Ba	0.6	694	31.6±46.3
OC	4.2	23.6	11.4±4.0	Tl	0.1	4.3	1.7±1.0
Cl^-	0.07	4.8	1.1±1.2	Pb	7.7	556	178±125
NO_3^-	0.5	45.6	12.3±10.4	Ts	NA	1.0	0.4±0.3
SO_4^{2-}	1.6	47.9	15.3±12.6	Tm	NA	0.5	0.2±0.1
Na^+	0.08	0.6	0.3±0.1	29ab	0.1	2.0	0.7±0.4
NH_4^+	0.6	28.5	9.0±7.7	29ba	NA	0.8	0.2±0.2
K^+	0.1	1.8	0.8±0.4	30ab	0.2	2.7	1.0±0.5
Mg^{2+}	0.03	0.3	0.12±0.07	30ba	NA	0.5	0.2±0.1
Ca^{2+}	0.2	5.6	1.5±1.2	31abS	NA	1.0	0.4±0.2
Na	0.09	2.3	0.7±0.4	31abR	NA	0.9	0.3±0.2
Mg	0.08	2.2	0.7±0.5	32abS	NA	0.6	0.2±0.1
Al	0.06	5.9	1.4±1.1	32abR	NA	0.5	0.2±0.1
K	0.2	2.5	1.1±0.5	BAA	0.06	4.5	0.4+0.6
Ca	0.2	7.8	2.2±1.7	CRY	0.2	7.9	1.0+1.1
Fe	0.3	4.6	1.4±0.8	BBKF	0.6	16.7	2.7±2.5
V	0.5	15.6	5.1±3.5	BEP	0.2	8.9	1.3±1.2
Cr	1.4	20.7	7.1±4.0	BAP	0.1	8.2	0.8±1.1
Mn	13.9	129.5	62.7±25.4	PER	NA	1.9	0.1±0.3
Co	0.06	1.8	0.7±0.4	DAH	NA	0.6	0.1±0.1
Ni	0.2	14.9	4.2±2.7	IND	0.03	2.9	0.5±0.4
Cu	4.6	62.9	26.9±13.8	PIC	NA	0.6	0.1±0.1
Zn	13	875	238±181	BGH	0.2	5.6	1.0±0.8
As	NA	153	16.9±24.0	COR	NA	2.0	0.5±0.4

NA: < LOQ.

4.2.1 $PM_{2.5}$ mass concentration

From 10 April till 8 June 2013, daily mean $PM_{2.5}$ samples were collected at the IAP sampling site. During the haze episodes, the sampling temporal resolution was changed from 24 h to 4 h, and the daily average $PM_{2.5}$ mass concentration was calculated based on 4 h $PM_{2.5}$ mass concentrations. On 16 May, the electricity supply to sampler B was turned off, so there was no sample for determining mass concentration on that day.

The variation of $PM_{2.5}$ mass concentrations is shown in Figure 4.12. Daily mean $PM_{2.5}$ mass concentration varied from 16 to 182 μg m^{-3} with the average value of 89 μg m^{-3}. This value is obviously approximately 2.5 times higher than the annual average of Chinese Ambient Air Quality Standard for $PM_{2.5}$ (Grade II: 35 μg m^{-3}) (China State Environmental Protection Administration (SEPA), 2012).

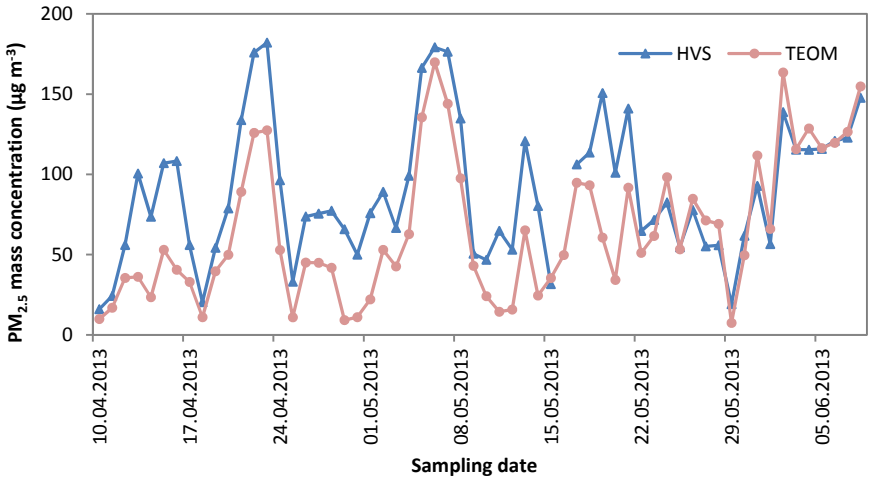

Figure 4.12: $PM_{2.5}$ daily mean mass concentrations measured by HVS and TEOM at the IAP from 2013.04.10 till 2013.06.08

The difference of $PM_{2.5}$ mass concentrations obtained from HVS and from TEOM is shown in Figure 4.12. Most $PM_{2.5}$ mass concentrations determined by TEOM were lower than by HVS, which is in agreement with the discussion in Chapter 3. The reasons for the temporal variation of the difference could be the influence of humidity and temperature upon the measurement methods. But obviously, $PM_{2.5}$ mass concentrations from HVS and TEOM showed the same variational pattern.

Three obvious PM accumulation processes during haze episodes were found in this short-term campaign. They happened from 18 April till 25 April, 3 May till 9 May and 1 June till 8 June, which are shown as peaks in Figure 4.12. During these three haze episodes, the maximum daily mean $PM_{2.5}$ mass concentration reached 182 μg m^{-3}, 179 μg m^{-3}, and 148 μg m^{-3}, respectively. Haze pollution will be discussed further in Chapter 5.

4.2.2 EC and OC

The OC daily mean mass concentrations were from 4.2 to 23.6 μg C m^{-3} while EC daily mean mass concentration changed from 1.0 to 7.6 μg C m^{-3} (Figure 4.13). The average mass concentrations of OC and EC were 11.4 ± 4.0 and 3.2 ± 1.3 μg C m^{-3}, respectively. These results are close to the observed results from Zhang et al. (2013) who collected $PM_{2.5}$ in Peking University from April 2009 till January 2010 and showed that OC and EC average mass concentrations were 13.7 ± 4.4 μg C m^{-3} and 2.8 ± 1.1 μg C m^{-3} in spring, respectively. The average mass percentages of OC and EC in $PM_{2.5}$ were 14.5% and 3.9%, respectively. OC and EC showed the same variation with $PM_{2.5}$ mass concentration and also showed peaks during haze events (Figures 4.12 and 4.13).

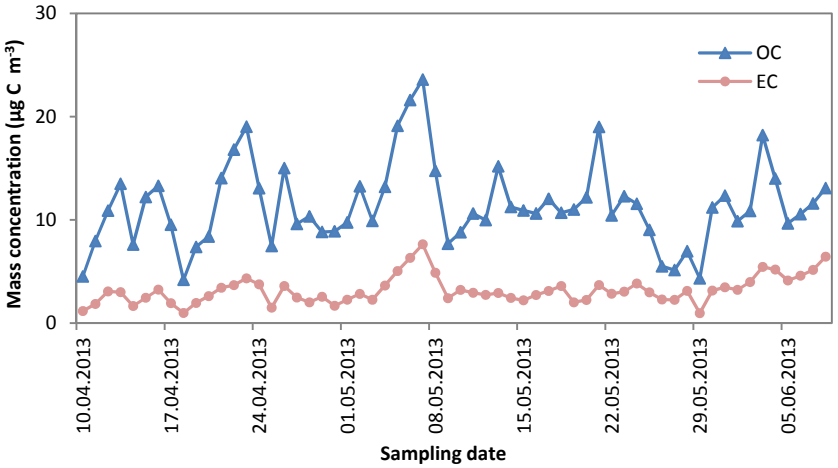

Figure 4.13: Variation in daily mean mass concentrations of EC and OC in $PM_{2.5}$ at the IAP from 2013.04.10 till 2013.06.08

Carbonaceous matter was also calculated according to the formula 4-1, the average fraction of CM in $PM_{2.5}$ varied from 13.0% to 62.2% with an average value of 27.2%.

4.2.3 Water soluble ions

The average mass concentrations of various ions during the whole sampling period at the IAP are listed in Table 4.3. The sum of all measured ions mass contributed an average value of 42.2% to the $PM_{2.5}$ mass.

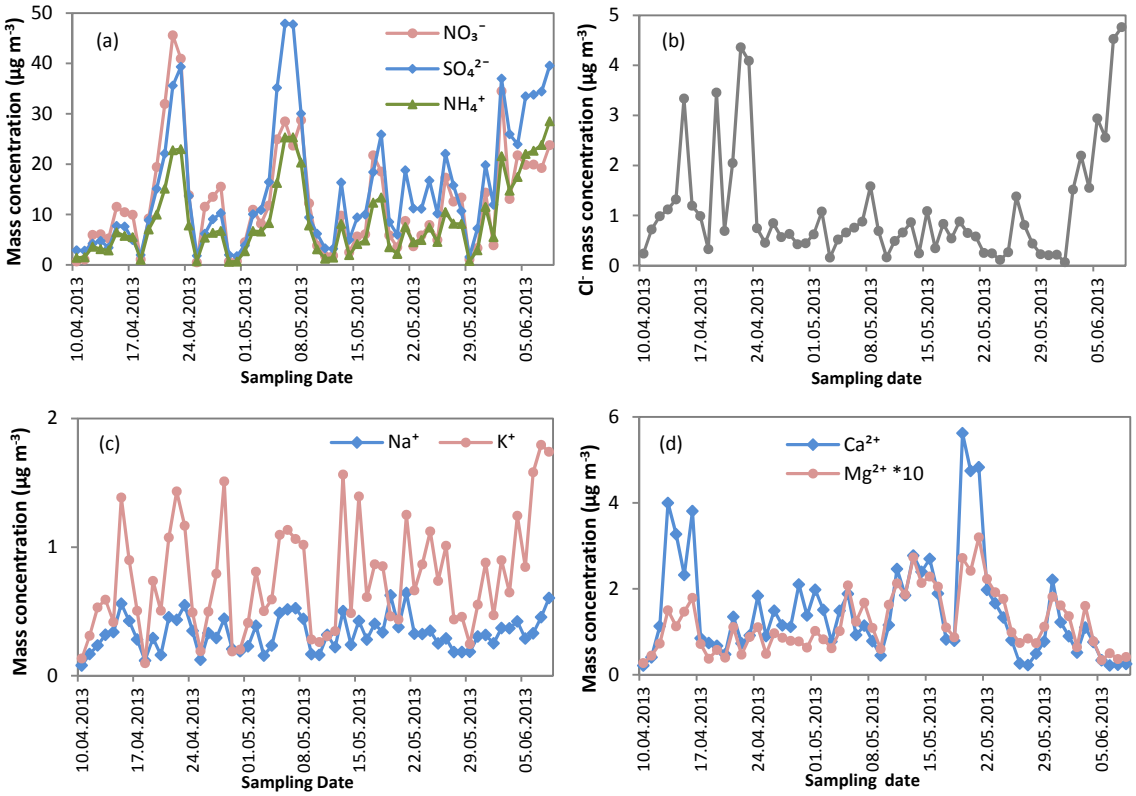

Figure 4.14: Variation in daily mean mass concentrations of water soluble ions in $PM_{2.5}$ at the IAP from 2013.04.10 till 2013.06.08

In $PM_{2.5}$ at the IAP, the maximum daily mean mass concentrations of NO_3^-, SO_4^{2-} and NH_4^+ were 45.6 µg m^{-3}, 47.9 µg m^{-3}, and 28.5 µg m^{-3}, respectively (Figure 4.14 (a)). The sum of NO_3^-, SO_4^{2-} and NH_4^+ mass contributed an average value of 37.6% and 84.9% to the total $PM_{2.5}$ mass and

total ions mass, respectively. The similar results were also found by previous studies. Yao et al. (2002) collected $PM_{2.5}$ samples in Beijing from 1999 till 2000, measured the same eight ions as this study and found that NO_3^-, SO_4^{2-} and NH_4^+ accounted for 85% of the total ions mass. He et al. (2012) also measured the same eight water soluble ions in $PM_{2.5}$ at Beijing and Chongqing and found that NO_3^-, SO_4^{2-} and NH_4^+ contributed 85-90% to the total ion mass in both cities.

Compared to the above major ionic species, Cl^-, Na^+, K^+, Ca^{2+} and Mg^{2+} were a minor contributor to the water soluble species with an average fraction of 15.1%. Chloride mass concentrations varied from 0.07 to 4.8 μg m^{-3} with an average value of 1.1 μg m^{-3} (Figure 4.14(b)). Na^+ had no big variation during the whole sampling period (Figure 4.14(c)), and showed a similar variation as K^+. The average daily mean mass concentrations of Na^+ and K^+ were 0.3 μg m^{-3} and 0.8 μg m^{-3}, respectively. Ca^{2+} had the highest mass concentration of 5.6 μg m^{-3} on 19 May 2013 (Figure 4.14(d)). Because Ca^{2+} and Mg^{2+} are mostly in the coarse fraction of particles (Shen et al, 2009; Li et al, 2013), and only contributed 7.5% and 0.6% to the total mass of all measured ions, respectively. The average mass concentrations of Mg^{2+} and Ca^+ were 0.1 μg m^{-3} and 1.5 μg m^{-3}, respectively.

4.2.4 Inorganic elements

The average mass concentrations of inorganic elements are also listed in Table 4.3. Ca was the most abundant crustal element in $PM_{2.5}$ samples. The average mass concentration was 2.2 μg m^{-3} and the highest mass concentration reached 7.8 μg m^{-3}. Ca, Mg, Al and Fe showed similar variational patterns and had peak concentrations during the re-suspended dust event on 19 May 2013, indicating that they might have originated from similar sources (Figure 4.15(a)), i.e. crustal sources. The summed mass of these four elements accounted for 66.6% of all elemental mass. Ca had another two peaks in mass concentration between 10 April and 17 April 2013, because of both rebuilding activities of a nearby wall and the observed high wind speeds during this period. Because there were further re-construction activities in this city area, Ca is usually used as a tracer for construction dust in Beijing (He et al., 2001; Han et al., 2007). Zinc was the most abundant trace element in $PM_{2.5}$ samples, with an average mass concentration of 238 ng m^{-3} and a maximum mass concentration of 875 ng m^{-3}. Zn, As and Pb followed similarly varying patterns during the measurement time period, especially the peaks in mass concentration during the haze events (Figure 4.15(b)).

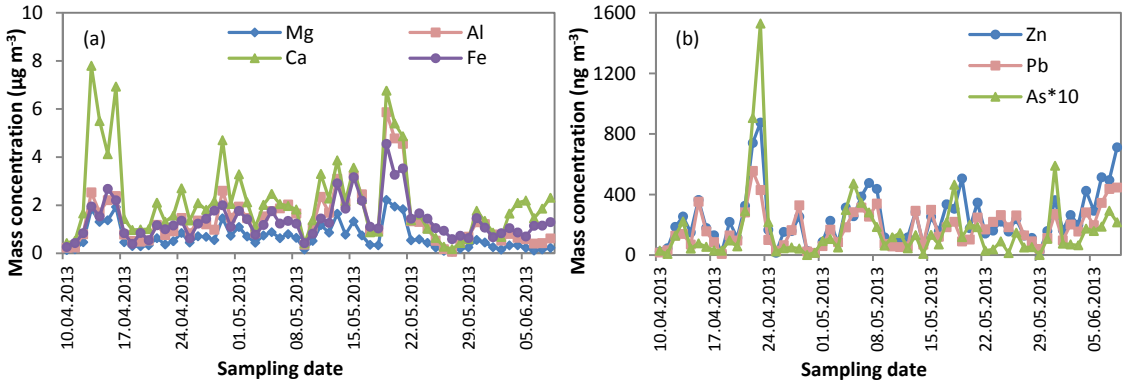

Figure 4.15: Variations in daily mean mass concentrations of (a) Mg, Al, Ca and Fe and (b) Zn, As and Pb in $PM_{2.5}$ at the IAP from 2013.04.10 till 2013.06.08

4.2.5 Organic compounds

Variations of hopanes and PAHs are shown in Figures 4.16 and 4.17, respectively. Average daily mean mass concentrations of Ts, Tm, 29ab, 29ba, 30ab, 30ba, 31abS, 31abR, 32abS and 32abR were 0.4 ng m^{-3}, 0.2 ng m^{-3}, 0.7 ng m^{-3}, 0.2 ng m^{-3}, 1.0 ng m^{-3}, 0.2 ng m^{-3}, 0.4 ng m^{-3}, 0.3 ng m^{-3}, 0.2 ng m^{-3}, and 0.2 ng m^{-3}, respectively. The dominant hopane substances were 29ab and 30ab, contributing 21.0% and 30.4% to the total hopane mass, respectively.

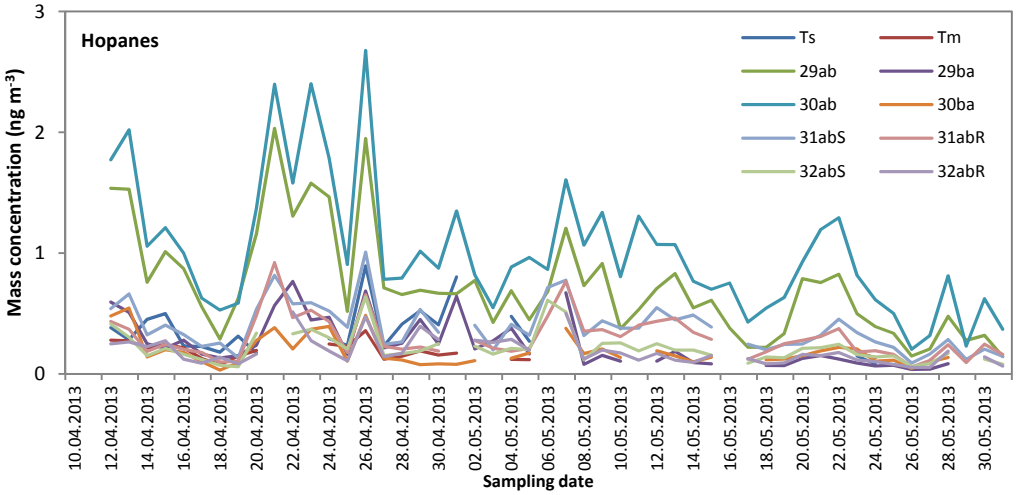

Figure 4.16: Variation in daily mean mass concentrations of hopane substances in $PM_{2.5}$ at the IAP from 2013.04.10 till 2013.05.31

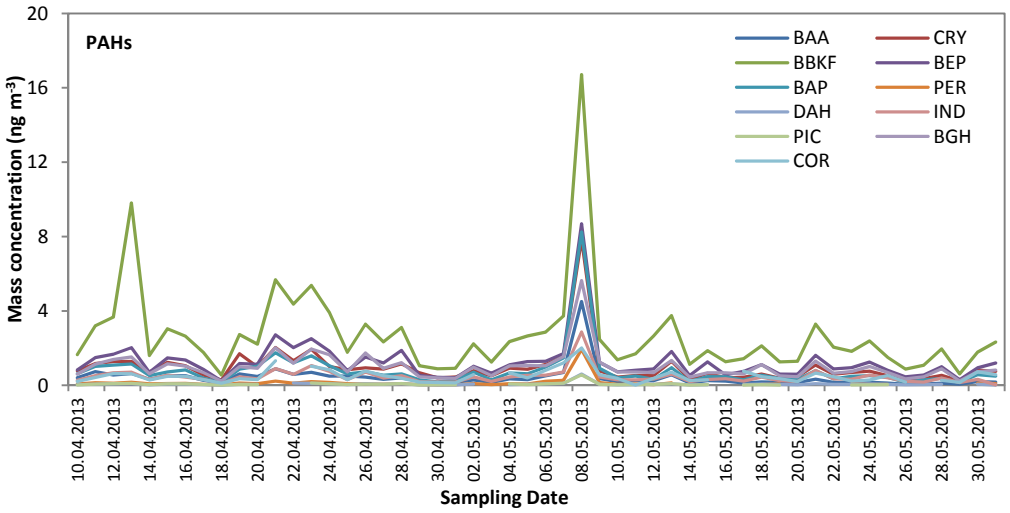

Figure 4.17: Variation in daily mean mass concentrations of PAHs in $PM_{2.5}$ at the IAP from 2013.04.10 till 2013.05.31

The total PAHs mass concentrations varied from 1.9 to 59.6 ng m^{-3} during spring 2013. Similarly to the results from $PM_{4.3}$ at the CUGB, 5-ring PAHs were found to be the most abundant PAH compounds in $PM_{2.5}$ at the IAP, with the average contribution of 59.2% to total PAHs mass. BBKF was the dominant compound in 5-ring PAHs with a contribution of 54.9% to 5-ring PAHs mass in $PM_{2.5}$. From Figure 4.17, PAHs peak mass concentration (59.6 ng m^{-3}) was obviously observed on 8 May 2013, with a small peak between 21 and 23 April during which haze was observed. This indicates the accumulation of PAHs happened during haze days.

4.2.6 $PM_{2.5}$ Mass balance

Figure 4.18 shows the contributions of different fractions to $PM_{2.5}$ mass at the IAP. Compared with $PM_{4.3}$ at the CUGB, the contribution of OM decreased to 22% of $PM_{2.5}$ mass. The mass percentage of NO_3^-, SO_4^{2-} and NH_4^+ increased to an average value of 37%. The undefined fraction of $PM_{2.5}$ constituted the highest part with the average value of 29%.

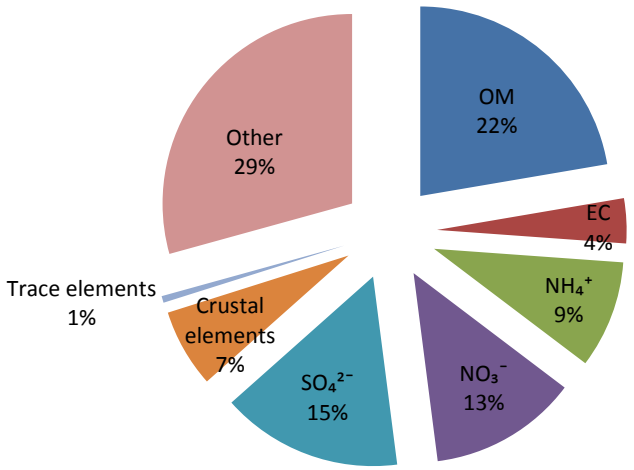

Figure 4.18: Mass balance of $PM_{2.5}$ on the basis of daily mean samples at the IAP during spring 2013

4.3 Discussion

4.3.1 Secondary organic carbon (SOC)

OC originates not only from primary sources like fossil fuel combustion and biomass burning, but also from the formation of low volatile particulate organic compounds from volatile organic precursor compounds, which is so-called SOC. EC is considered as a primary pollutant from the incomplete combustion (Castro et al., 1999), and often used to estimate SOC (Turpin et al., 1991; Turpin and Huntzicker, 1991; Strader et al., 1999; Lin and Tai, 2001; Cao et al., 2007).

The origins of carbonaceous compounds can be indicated by the correlations between OC and EC (Chow et al., 1996; Park et al., 2001; Cao et al., 2007). Correlations between OC and EC in this study are listed in Table 4.5. OC and EC had a significant positive correlation in autumn 2010 (R^2=0.83) and winter 2010 (R^2=0.84) at the CUGB, which indicated that OC and EC might originate from the similar sources (Park et al., 2001; Cao et al., 2007). OC mass concentrations were weakly correlated with EC in summer 2010 (R^2=0.46), spring 2011 (R^2=0.33) at the CUGB and spring 2013 (R^2=0.60) at the IAP which implied a mixture of sources (Cao et al., 2007).

Table 4.5: Relationships between OC and EC concentration at the CUGB and the IAP

Season	PM	Location	Sampling period	OC(y) = a × EC(x) + b	R^2
Summer 2010	$PM_{4.3}$	CUGB	2010.06-2010.08	y = 2.23x + 9.75	0.46
Autumn 2010	$PM_{4.3}$	CUGB	2010.09-2010.10	y = 4.45x - 0.34	0.83
Winter 2010	$PM_{4.3}$	CUGB	2010.11-2011.03	y = 4.85x - 0.10	0.84
Spring 2011	$PM_{4.3}$	CUGB	2011.04-2011.05	y = 3.03x + 8.21	0.33
Spring 2013	$PM_{2.5}$	IAP	2013.04-2013.06	y = 2.35x + 3.95	0.60

An OC/EC mass ratio higher than 2 indicates the presence of SOC (Chow et al., 1996). The seasonal average OC/EC ratios are shown in Table 4.6, all data from different seasons had the values higher than 2. Daily mean OC/EC ratios in $PM_{4.3}$ at the CUGB varied from 2.7 to 48.6 with an average value of 5.3. The seasonal variation showed that the lowest OC/EC ratio was 4.4 in autumn 2010 and the highest value was 5.6 in spring 2011. OC/EC ratios in $PM_{4.3}$ at the CUGB were higher than the results from other studies in the past (Table 4.6). The scatter plots for OC and EC mass concentrations in $PM_{4.3}$ at the CUGB are shown in Figure 4.19. There were some really high OC/EC values, especially on 30 April and 1 May 2011. The OC/EC ratios at these two days reached 20.2 and 48.6. This is because a dust event happened during these two days and relatively high OC concentrations had originated from organic soil material (Zhao et al., 2013a). In $PM_{2.5}$ at the IAP during spring 2013, OC/EC ratios were in the range of 2.0 to 5.5 with an average ratio of 3.8 (Figure 4.20), which suggested that the SOC contributed much to the composition of OC in Beijing during spring 2013.

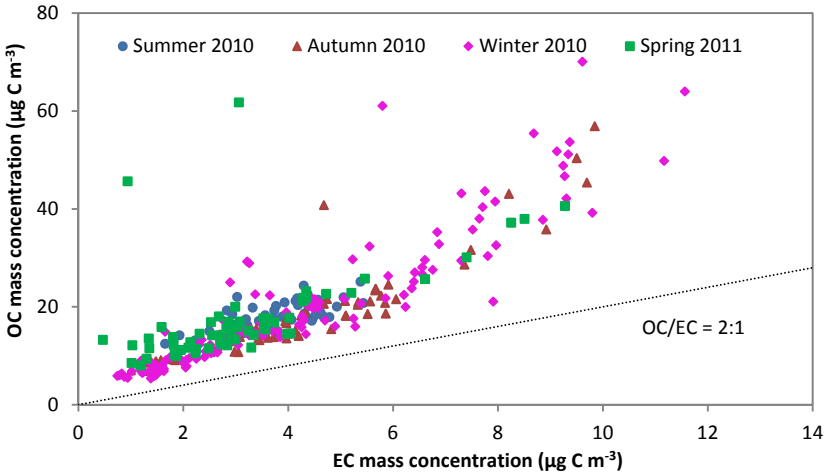

Figure 4.19: Correlation between OC and EC daily mean mass concentration in $PM_{4.3}$ at the CUGB

Table 4.6: Comparisons between OC and EC mass concentration (μg C m^{-3}) in this study and results from other studies

Location	Season	Sampling period	PM	OC	EC	OC/EC	Reference
Downtown Beijing, China	Autumn	1999.09-1999.10	$PM_{2.5}$	28.8	10.2	2.8	He et al.(2001)
	Winter	1999.11-2000.03		31.5	11.1	2.8	
	Spring	2000.03-2000.05		18.2	6.7	2.7	
	Summer	2000.06-2000.08		13.4	6.3	2.1	
Urban Beijing, China	Summer	2002.06-2002.07	$PM_{2.5}$	10.7	5.7	2.2	Dan et al. (2004)
	Winter	2002.12		36.7	15.2	3.5	
Sub-Beijing, China	Autumn	2002.09-2002.10	PM_{10}	17.8	4.7	3.8	Duan et al. (2005)
	Winter	2002.11		25.6	10.5	2.4	
Urban Beijing, China	Winter	2003.01	$PM_{2.5}$	27.2	7.1	3.7	Cao et al. (2007)
	Summer	2003.06-2003.07		17.2	4.6	4.4	
Urban Beijing, China	Spring	2009.04	$PM_{2.5}$	13.7	2.8	4.9	Zhang et al. (2013)
	Summer	2009.07		11.1	4.2	2.6	
	Autumn	2009.10		17.8	5.3	3.4	
	Winter	2010.01		24.9	7.5	3.3	
Urban Beijing, China	Spring	2009.04-2009.05	$PM_{2.5}$	15.8	5.2	3.0	Zhao et al. (2013a)
	Summer	2009.07-2009.08		10.1	5.9	1.7	
	Autumn	2009.10-2009.11		20.2	7.1	2.8	
	Winter	2010.01-2010.02		26.8	7.1	3.8	
Urban Beijing, China	Summer	2010.06-2010.08	$PM_{4.3}$	18.2	3.8	4.8	This study (CUGB)
	Autumn	2010.09-2010.10		18.8	4.3	4.4	
	Winter	2010.11-2011.03		19.2	4.0	4.8	
	Spring	2011.04-2011.05		18.0	3.2	5.6	
Urban Beijing, China	Spring	2013.04-2013.06	$PM_{2.5}$	11.4	3.2	3.8	This study (IAP)

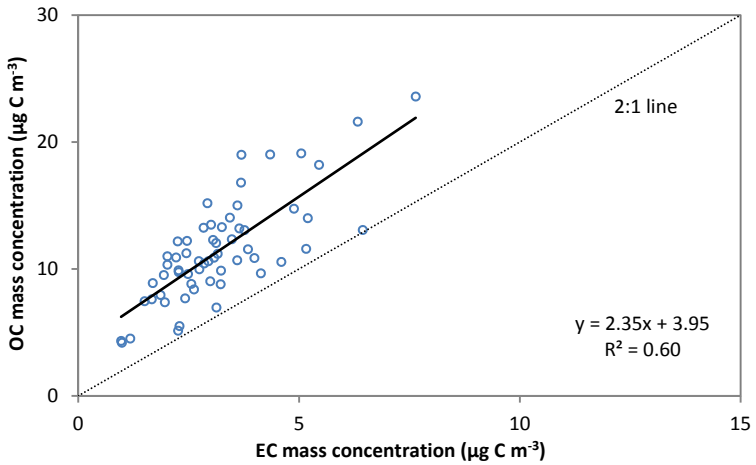

Figure 4.20: Correlation between OC and EC daily mean mass concentrations in $PM_{2.5}$ at the IAP

In order to evaluate the contribution of SOC to PM, OC/EC ratios were applied. SOC can be identified by the following equation (Turpin and Huntzicker, 1995):

$$SOC = OC_{total} - EC \times (OC/EC)_{primary} \quad (4\text{-}2)$$

where OC_{total} is the total organic carbon mass concentration and $(OC/EC)_{primary}$ is the ratio of primary OC to EC. From the formula $EC \times (OC/EC)_{primary}$, the primary OC mass concentration can be estimated. However, the estimation of the ratio of primary OC to EC is difficult because it is affected by the meteorological conditions (Dan et al., 2004), such as temperature and sunlight, which lead to the presence of the uncertainty.

Considering the problem mentioned above, formula 4-2 was replaced by the following formula (Castro et al., 1999; Zhang et al., 2008c):

$$SOC = OC_{total} - EC \times (OC/EC)_{minimum} \quad (4\text{-}3)$$

where $(OC/EC)_{minimum}$ is the minimum ratio of OC to EC. However, this estimate can only be used correctly when semi-volatile organic compounds take small faction in OM and when the sources for primary OC and EC are stable (Castro et al., 1999).

Because of semi-volatile organic compounds, the ambient temperature should be considered, but Castro et al. (1999) found that when temperature was lower than 150°C, lower than 10% of the total OC was volatilized, which means that the semi-volatile organic compounds have little influence on the calculation of SOC. However, the emission inventory for primary OC and EC is also difficult to obtain and therefore, the formula was improved again as follows:

$$SOC = OC_{total} - OC_{primary} = OC_{total} - (a \times EC + b) \quad (4\text{-}4)$$

where $OC_{Primary}$ is primary OC mass concentration, a is the calculated slope, and b is the calculated intercept. The lowest 20% OC/EC ratios were used to calculate the primary OC/EC ratios by using a least-squares regression (Cao et al., 2007; Zhao et al., 2013a).

In our study, considering the changing emission sources during different seasons, the lowest OC/EC ratios were calculated in different seasons separately. All data associated with special events (such as dust and precipitation) which can affect the OC/EC ratios significantly was excluded before calculating the lowest OC/EC ratio (Cabada et al., 2004; Cao et al., 2007). Because the amount of valid data in the different seasons was different, the amount of

suitable samples (lowest 20%) was also different. Therefore, ten samples with the lowest OC/EC ratios in each season were used to calculate the slope and intercept.

In $PM_{4.3}$, the seasonal variation of SOC/OC ratios showed that the highest was in winter 2010 (55%), followed by summer 2010 (47%), spring 2011 (25%), and the lowest in autumn 2010 (22%). The SOC/TC ratios had the same variation as SOC/OC, with ratios of 46%, 39%, 22% and 19%, respectively. Previous studies pointed out that the lower SOC fraction occurred during winter because of low temperatures and less solar radiation (Strader et al., 1999; Cao et al., 2007). For instance, Cao et al. (2007) showed that SOC accounted for 24% of TC during winter, less than during summer (36% of TC) in the northern Chinese cities. But the opposite result was presented by Dan et al. (2004) who showed that SOC had a higher contribution to $PM_{2.5}$ during winter than during summer in Beijing. This is a similar result to ours. The increase in coal combustion for heating during winter which can lead to an increase in emission of organic compounds and low mixing layer heights which can cause accumulation of SOC precursors and thus enhance the formation of SOC could be the reasons for higher SOC/OC ratios in winter in Beijing. Beside this, SOC was found to have a significant positive correlation with PM (R^2=0.81) during winter 2010 while there were no significant correlations observed during other seasons, indicating that the increase in SOC during winter 2010 was the main reason for the increase in PM.

In $PM_{2.5}$, the primary OC/EC ratio with a value of 2.09 is close to the result from Cao et al. (2007) who found a primary OC/EC ratio of 1.99 for northern cities of China in summer. By this estimation, SOC accounted for 42% of OC (ranged from 6% to 62%) and 34% of TC (ranged from 4% to 52%).

SOC could be an important compound of PM, and because all the SOC data were only estimated but not measured, further research on SOC is needed in China.

4.3.2 Ions

4.3.2.1 Secondary inorganic ions (NO_3^-, SO_4^{2-} and NH_4^+)

NO_3^-/SO_4^{2-} mass ratio has been widely used as an indicator for mobile or stationary sources of particles in the past (Arimoto et al., 1996; Yao et al., 2002; Wang et al., 2005b). In $PM_{4.3}$, NO_3^-/SO_4^{2-} mass concentration ratios ranged from 0.02 to 2.8 with an average value of 0.7 and was

the highest in winter 2010 with an average value of 0.9, followed by autumn 2010 (0.8), spring 2011 (0.7), and the lowest in summer 2010 (0.1). The reason for the lowest NO_3^-/SO_4^{2-} ratio in summer could be that NO_3^- is volatile under high temperatures. Therefore, using NO_3^-/SO_4^{2-} to indicate the dominant sources of pollutants has limitations. A previous study (Wang et al., 2005b) found that NO_3^-/SO_4^{2-} mass ratio to be 0.8 in spring, 0.6 in summer, 0.9 in autumn and 0.5 in winter during 2001-2003 in Beijing. Compared with this, our result in winter is relatively high while NO_3^-/SO_4^{2-} mass ratios in spring, summer and autumn are a little lower. In $PM_{2.5}$ at the IAP, the NO_3^-/SO_4^{2-} mass concentration ratio ranged from 0.2 to 2.0 with an average value of 0.8, similar to the results in spring as found from the CUGB measurements and a previous study (Wang et al., 2005b).

NO_3^-, SO_4^{2-} and NH_4^+ in $PM_{4.3}$ had the same variation during the whole sampling period, which suggested that they had likely originated from similar processes. It is the same situation in $PM_{2.5}$ (Figure 4.14(a)).

In the following paragraphs of this section, the equivalent concentrations (μeq m^{-3}) of all ions are used. The equivalent concentration is calculated as: the ion mass concentration divided by the atomic weight and multiplied by the charge number.

All correlation coefficients between the different ions in $PM_{4.3}$ at the CUGB and $PM_{2.5}$ at the IAP are shown in Tables 4.7 and 4.8, respectively. In both $PM_{4.3}$ and $PM_{2.5}$, NH_4^+ equivalent concentrations had strong correlations with NO_3^- and SO_4^{2-} equivalent concentrations.

Table 4.7: Correlation coefficients (R) between the daily mean water soluble ions in $PM_{4.3}$ at the CUGB

	Cl^-	NO_3^-	SO_4^{2-}
NO_3^-	0.43		
SO_4^{2-}	0.37	0.83	
NH_4^+	0.36	0.89	0.86

Table 4.8: Correlation coefficients (R) between the daily mean water soluble ions in $PM_{2.5}$ at the IAP

	Cl^-	NO_3^-	SO_4^{2-}	NH_4^+	K^+	Na^+	Ca^{2+}
NO_3^-	0.61						
SO_4^{2-}	0.54	0.85					
NH_4^+	0.66	0.88	0.97				
K^+	0.61	0.62	0.68	0.70			
Na^+	0.48	0.52	0.58	0.55	0.76		
Ca^{2+}	-0.22	-0.34	-0.32	-0.40	-0.07	0.42	
Mg^{2+}	-0.32	-0.26	-0.11	-0.25	0.09	0.44	0.78

The slope of linear regression between NH_4^+ and SO_4^{2-} equivalent concentrations in $PM_{4.3}$ and $PM_{2.5}$ are shown in Figures 4.21 (a) and 4.22 (a), giving 1.09 and 1.58, respectively. That they are both higher than unity reveals SO_4^{2-} was neutralized completely by NH_4^+. Additional NH_4^+ was inferred to react with NO_3^- and Cl^-. Previous studies pointed out that the reaction products of NH_4^+ forming order of priority is $(NH_4)_2SO_4$, followed by NH_4NO_3, and then NH_4Cl (Zhang et al, 2008a).

The ratio of NH_4^+ and $[SO_4^{2-}+NO_3^-]$ equivalent concentrations varied from 0.01 to 4.93 with the average ratio of 0.70 in $PM_{4.3}$ (Figure 4.21(b)), while it ranged from 0.65 to 1.31, with the average ratio of 0.98 in $PM_{2.5}$ (Figure 4.22(b)). When the ratio is smaller than unity, nitrate can be present in not only NH_4NO_3 but also other chemical forms. Due to NH_4NO_3 being volatile, only small amounts of NO_3^- can exist in PM under high temperature. But if not, this could be caused by high NH_3 mass concentrations which are enough to neutralize both H_2SO_4 and HNO_3 (Ianniello et al., 2011). So high NH_3 concentrations, high HNO_3 concentrations and low SO_4^{2-} concentrations are favor the formation of NH_4NO_3 (Seinfeld and Pandis, 2006; Zhao et al., 2013b). Moreover, high relative humidity is another important factor which can enhance NO_3^- and NH_4^+ mass concentrations in the PM, because a high RH can increase the dissolution of hydrosoluble compounds, such as HNO_3 and NH_3, on the surface of moist particles (Pathak et al., 2009; Ianniello et al., 2010, 2011).

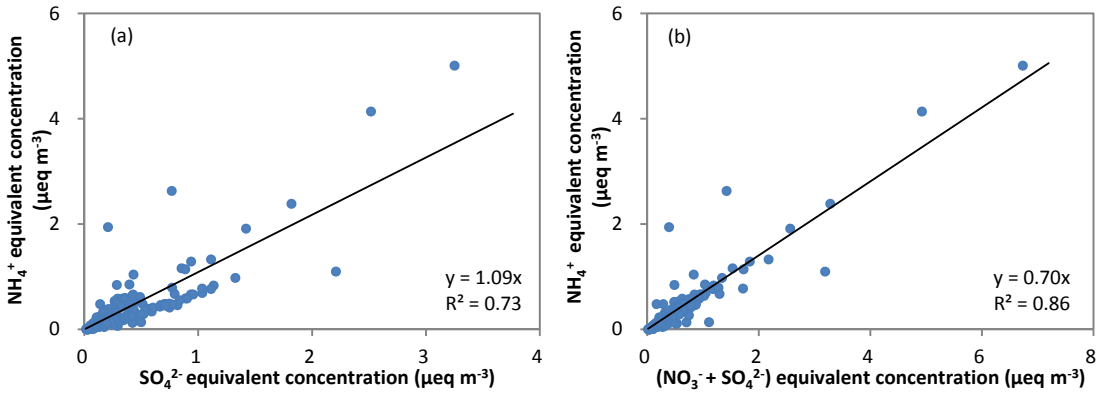

Figure 4.21: Correlations between equivalent concentrations of ions in $PM_{4.3}$ at the CUGB

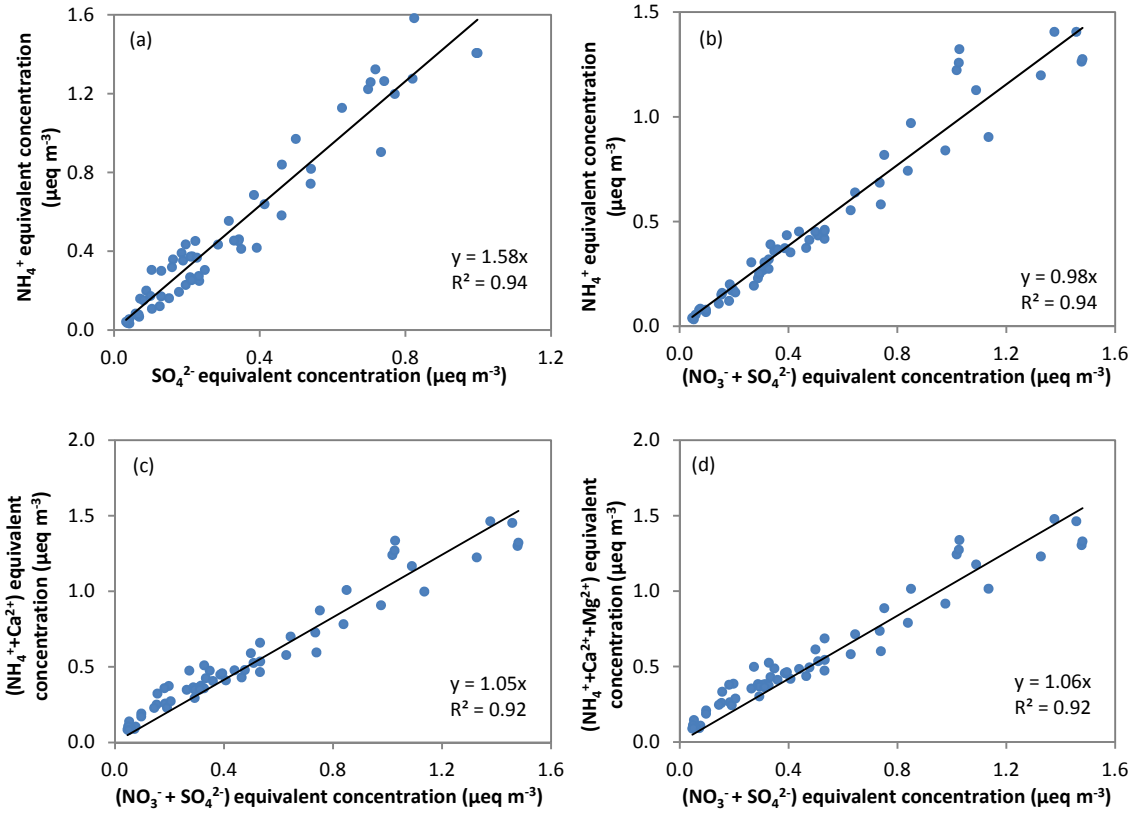

Figure 4.22: Correlations between equivalent concentrations of ions in $PM_{2.5}$ at the IAP

4.3.2.2 Chloride, sodium, potassium, magnesium and calcium

Chloride is mainly thought to originate from coal combustion (Yao et al., 2002), biomass burning (Li et al., 2007) and sea salt (Li et al., 2013). But in this study, the contribution from sea-salt could be not significant because the molar ratio of Cl^- to Na^+ in $PM_{2.5}$ during spring 2013 at the IAP was 2.13, i.e. higher than that in sea water of 1.17 (Chester, 1990; Zhang et al., 2013), which indicated Cl^- originated from other sources. In $PM_{4.3}$ at the CUGB, the highest mass concentration of Cl^- was in winter 2010 with the value being 3 μg m^{-3}, which was 43 times, 5 times and 2 times higher than that in summer 2010, autumn 2010 and spring 2011, respectively. Therefore, Cl^- in $PM_{4.3}$ at the CUGB could be from coal combustion.

Na^+, K^+, Mg^{2+} and Ca^{2+} were only available in $PM_{2.5}$ at the IAP. In this study, Mg^{2+} probably came from mineral dust because it had a good correlation with Ca^{2+} (R=0.78) which had the highest mass concentration on 19 May 2013 (Figure 4.14(d)) caused by re-suspended dust. The average molar ratio of Mg^{2+}/Na^+ in $PM_{2.5}$ was 0.74, which was larger than the average ratio of 0.23 in sea water (Chester, 1990; Zhang et al., 2013) indicating that sea salt could not be the source of Mg^{2+}. Mineral particles were found to have heterogeneous reactions with NO_x, HNO_3 and N_2O_5 (Li and Shao, 2009). The correlations between $[NH_4^+ + Ca^{2+}]$ and $[NO_3^- + SO_4^{2-}]$, $[NH_4^+ + Ca^{2+} + Mg^{2+}]$ and $[NO_3^- + SO_4^{2-}]$ (Figure 4.22 (c) and (d)) were significant with the same correlation coefficient (R^2=0.92), which indicated that nitrate was present in not only NH_4NO_3, but also $Ca(NO_3)_2$ and $Mg(NO_3)_2$ (Zhang et al., 2013).

Previous studies showed that K^+ mainly comes from biomass burning, sea salt and soil (Zhang et al., 2008a; Deng et al., 2011; Li et al., 2013). K^+ and Na^+ had a good correlation which can be seen in Table 4.8, meaning that Na^+ and K^+ could come from the similar sources.

4.3.2.3 Acidity of PM

The ion balance was usually used to indicate the acidity of PM by calculating the ratio of summed cation equivalent concentrations to summed anion equivalent concentrations(C/A).

The equivalent concentrations of anions (A) and cations (C) were calculated by atomic weights and charge number according to the following equations:

$$A = Cl^-/35.5 + NO_3^-/62 + (SO_4^{2-}/96) \times 2 \quad (4\text{-}5)$$

$$C = Na^+/23 + NH_4^+/18 + K^+/39 + (Mg^{2+}/24) \times 2 + (Ca^{2+}/40) \times 2 \quad (4\text{-}6)$$

$$R_{C/A} = C/A \quad (4\text{-}7)$$

In the above equation, $R_{C/A} \geq 1$ indicates that most acids can be neutralized, but if $R_{C/A} < 1$, it means that the PM is acidic.

Because there were no other cations available, except NH_4^+ in $PM_{4.3}$, therefore $R_{C/A}$ cannot be calculated for $PM_{4.3}$. For $PM_{2.5}$ at the IAP, the C/A ratio varied from 0.82 to 2.48 with the average of 1.30, which was higher than 1 and indicates that most of the acids, such as H_2SO_4, HNO_3 can be neutralized and most atmospheric particles in Beijing seems to be alkaline.

4.3.3 Mineral particles

Even though mineral particles are usually associated with coarse particles, their contribution to $PM_{2.5}$ cannot be ignored. This is because mineral particles can serve as the reactive surface during its global transportation (Dentener et al., 1996) and can also favor the formation of haze (Rahn et al., 1977).

The mass concentration of mineral particles in $PM_{2.5}$ is often estimated based on the following formulas (Chow et al., 1994; Malm et al., 1994):

$$[Mineral] = 1.89Al + 2.14Si + 1.40Ca + 1.43Fe \quad (4\text{-}8)$$

or

$$[Mineral] = 2.20Al + 2.49Si + 1.63Ca + 2.42Fe + 1.94Ti \quad (4\text{-}9)$$

However, because the filters used for collecting PM samples during two sampling campaigns were quartz fibre filters, there was a high level of background silicon. On the other hand, HF was used to digest PM samples during ICP-MS analysis. This can cause the formation of SiF_4 from volatilized Si. Therefore, Si has been estimated from Al by using Si/Al ratio of 4.0 in some previous studies (e.g. Sun et al., 2004a; Zhang et al., 2006). However, Si/Al mass ratios could have a significant difference between different Chinese regions (Zhang et al., 2013). Thus the following formula was used (Hsu et al., 2010; Deng et al., 2011; Zhang et al., 2013):

[Mineral] = Al/0.07 (4-10)

where 0.07 is the average contribution of Al in Asian dust sources (Zhang et al., 2003a).

Because Al in $PM_{4.3}$ samples collected at the CUGB cannot be analyzed by PEDXRF, no Al mass concentration data was available for $PM_{4.3}$ during the first campaign. Therefore, estimation of mineral particles in $PM_{4.3}$ cannot be performed here.

For $PM_{2.5}$ samples collected at the IAP, daily mean mass concentrations of mineral particles ranged from 3 to 84 μg m^{-3}, the average mineral particles mass concentration was 20.2 μg m^{-3} and the average mass percentage was 23.4%. The highest mineral particle mass concentration was observed on 19 May 2013, 84 μg m^{-3} and mass percentage of mineral particles in $PM_{2.5}$ was 55.6%. On this day, a re-suspended dust event was observed. Mg, Ca, Fe and Al which are recognized as indicators for natural source such as dust, reached peak mass concentrations on this day. The values were 2.2 μg m^{-3}, 6.8 μg m^{-3}, 4.6 μg m^{-3}, 5.9 μg m^{-3}, respectively.

4.3.4 Organic compounds

4.3.4.1 Levoglucosan

Levoglucosan originates from incomplete cellulose combustion and is widely used as an indicator for biomass burning (Zhang et al., 2008b; Wagener et al., 2012). During the sampling campaign in 2010-2011, levoglucosan had much higher mass concentrations in summer and autumn than in winter and spring (Table 4.3) which indicated that biomass burning contributed significantly to the particle loading in summer and autumn in Beijing. This agrees well with previous studies which pointed out that biomass burning usually happens in summer and autumn in Beijing and its surrounding area (Huang et al., 2012).

The contribution of biomass burning to OC can be implied by the mass ratio of levoglucosan to OC (Zhang et al., 2008b). The seasonal average mass ratios of levoglucosan to OC showed the highest was in summer 2010, followed by autumn 2010, then winter 2010 and spring 2011, and the values of these ratios were 0.04, 0.03, 0.02 and 0.01, respectively. The monthly average ratios in September, August and July 2010 had the first three highest ratios, reaching 0.042, 0.040 and 0.036, respectively. All these results indicated that biomass burning

contributed much more in summer and autumn than in winter and spring due to the combustion of agricultural waste and fallen leaves in summer and autumn.

4.3.4.2 Hopanes

Hopanes are usually considered to have originated from fossil fuel combustion, e.g. coal combustion and vehicle emissions (He et al., 2006; Schnelle-Kreis et al., 2007). Because of their high stability (He et al., 2006; Huang et al., 2006), the distribution of different hopanes, such as homohopane index and hopane index, are usually used to distinguish vehicle emission source from coal combustion source (Oros and Simoneit, 2000).

The homohopane index, 31abS/(31abS+31abR) was found to be 0.1 for lignite coal, 0.4 for bituminous coal, and 0.6 for fuel oil combustion (Oros and Simoneit, 2000; Schnelle-Kreis et al., 2007). The hopane index, 30ab/(30ab+30ba) is also used to distinguish the sources of hopanes. The ratio was found to be 0.1 for lignite coal, 0.5 for bituminous coal, 0.6 for brown coal (Oros and Simoneit, 2000) and greater than 0.9 for crude oil were found (El-Gayar et al., 2002). The homohopane index of $PM_{4.3}$ ranged from 0.14 to 0.78 with an annual average value of 0.53 and corresponding with 0.57, 0.58, 0.47 and 0.56 in summer 2010, autumn 2010, winter 2010 and spring 2010, respectively. In $PM_{4.3}$ at the CUGB, the hopane index varied from 0.29 to 0.95 with an annual average value of 0.72, corresponding with 0.86, 0.83, 0.61 and 0.82 in summer 2010, autumn 2010, winter 2010 and spring 2011, respectively. Both indexes in winter showed lower values compared with other seasons which indicated that coal combustion contributed more to hopanes in winter and a minor impact from coal combustion was found in summer, autumn and spring during the whole sampling period at the CUGB from June 2010 to June 2011. For $PM_{2.5}$, during spring 2013, the average homohopane index was 0.57, a similar value to that during spring 2011, and the average hopane index was 0.85. Therefore, both indexes data showed the same results. That is, hopanes in $PM_{4.3}$ and $PM_{2.5}$ mainly originated from fuel oil consumption while coal combustion made a greater contribution to hopanes during winter.

4.3.4.3 PAHs

PAHs are considered to have originated from incomplete combustion (He et al., 2006; Huang et al., 2006). In the past, the studies on PAHs have been widely carried out because of their

potential mutagenicity and carcinogenicity with regards to human health. As described in the above section 4.1.5, all PAHs in $PM_{4.3}$ samples collected at the CUGB during 2010-2011 had the highest mass concentrations in winter due to low temperatures and weak solar radiation which caused low volatility and degradation rates of PAHs (He et al., 2006). The increase in coal combustion during winter could be another reason for high PAHs mass concentration. PAHs can be divided into low molecular weight (LMW) and high molecular weight (HMW) on the basis of volatility. LMW PAHs (4 rings PAHs) are considered to be semi-volatile and are present in both the gas and particle phases, while HMW PAHs (5-7 rings PAHs) are mostly concentrated in the particle phase (Huang et al., 2006). As shown in Figure 4.23, LMW PAHs had a higher mass percentage in winter while HMW had a higher mass percentage in summer and autumn. This difference in distribution was caused by the gas-particle partitioning in the atmosphere (Zheng and Fang, 2000; Huang et al., 2006). The gas-to-particle ratio of PAHs was found to be related to the weather conditions and molecular weight of the compounds (Masclet et al., 1988).

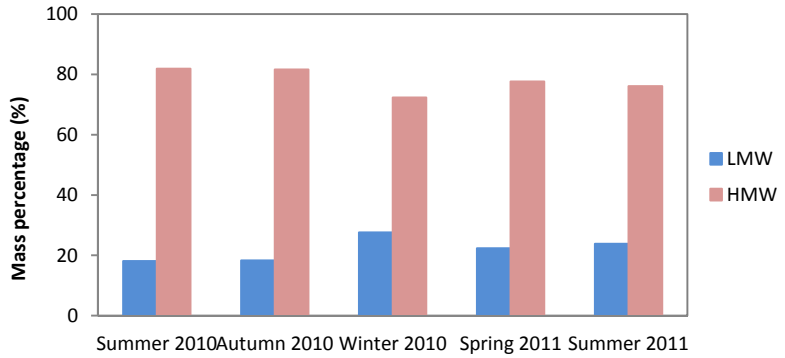

Figure 4.23: Seasonal variations of the LMW and HMW PAHs mass percentages in $PM_{4.3}$ at the CUGB during 2010-2011

PIC, which is used as a tracer for coal combustion (Oros and Simoneit, 2000), in $PM_{4.3}$ samples during 2010-2011, had the highest mass concentration in winter 2010, being 1.18 ng m^{-3}, which was 11 times higher than in summer 2010. This indicated that coal combustion contributed a large amount to PAHs mass in $PM_{4.3}$ in Beijing during winter.

Most PAHs are considered to have originated from anthropogenic sources, such as vehicle emissions and coal combustion (Hou et al., 2006). The diagnostic ratios of PAHs can be used to

trace the emission sources (Yunker et al., 2002). The average seasonal diagnostic ratios between PAHs in $PM_{4.3}$ and $PM_{2.5}$ are listed in Table 4.9.

Table 4.9: Average seasonal diagnostic ratios between PAHs in $PM_{4.3}$ at the CUGB and $PM_{2.5}$ at the IAP

	PM	BGH/BEP	IND/(IND+BGH)
Summer 2010	$PM_{4.3}$	1.57±0.40	0.57±0.07
Autumn 2010	$PM_{4.3}$	1.42±0.26	0.55±0.05
Winter 2010	$PM_{4.3}$	1.05±0.20	0.57±0.06
Spring 2011	$PM_{4.3}$	1.31±0.29	0.56±0.05
Spring 2013	$PM_{2.5}$	0.83±0.12	0.31±0.05

A high ratio of BGH to BEP is considered to be an indicator of vehicle emissions (Nielsen, 1996). In 2010-2011, the highest ratio of BGH to BEP was found in summer 2010 of 1.57, followed by autumn 2010 of 1.42, spring 2011 of 1.31, and then the lowest ratio was in winter 2010 of 1.05, suggesting that vehicle exhaust contributed much more to $PM_{4.3}$ in summer than in winter. This result agreed well with a previous study (Huang et al., 2006) in which the highest BGH/BEP ratio with the value of 1.2 was also observed in summer. In $PM_{2.5}$ at the IAP, 0.83 was found for the BGH/BEP ratio and was much lower than that in $PM_{4.3}$ during all seasons.

The IND/(IND+BGH) ratio can be used to differentiate sources of PAHs between traffic emissions and coal combustion (Li et al., 2011c). A ratio between 0.2 and 0.5 indicates liquid fossil fuel combustion, and greater than 0.5 is for grass, wood and coal combustion (Yunker et al., 2002). In $PM_{4.3}$ during the 2010-2011 sampling period, the averaged IND/(IND+BGH) ratios in summer 2010, autumn 2010, winter 2010 and spring 2010 were 0.57, 0.55, 0.57 and 0.56, respectively. The ratios of IND/(IND+BGH) in $PM_{4.3}$ during the whole year were close to coal burning ratios of 0.56 (Li et al., 2011c), so coal combustion were the dominant sources for PAHs in $PM_{4.3}$ at the CUGB. In $PM_{2.5}$, the averaged IND/(IND+BGH) ratio was 0.31, therefore, PAHs in $PM_{2.5}$ also originated from liquid fossil fuel.

4.3.5 Influences of meteorological parameters

Meteorological parameters, such as air pressure (P), temperature (T), precipitation, relative humidity (RH), wind speed (WS), wind direction (WD) and mixing layer height (MLH), influence transport, dispersion and transformation of atmospheric pollutants (Pang et al., 2009). Many studies have pointed out that meteorological parameters are important factors for PM loading (Sezer Turalıoğlu et al., 2005; Schäfer et al., 2006, 2011, 2014; Tai et al., 2010; Deng et al., 2012). Thus, investigating the meteorological parameters could provide a useful tool for understanding the variations in PM concentration and composition.

The meteorological parameters of the sampling campaign at the CUGB are listed in Table 4.10. Mass concentrations of $PM_{4.3}$ and the compounds in $PM_{4.3}$ are compared with meteorological parameters such as T, WS, RH and MLH. All correlation coefficients are shown in Table 4.11.

Table 4.10: Average values of meteorological parameters at the CUGB in Beijing from 2010.06.21 till 2011.06.20 (Apart from precipitation and MLH data were acquired by an automated weather station at IAP, the other meteorological data were obtained from ZBAA). The abbreviations are as follows: T_{Avg} = average temperature (°C), T_{Max} = maximum daily mean temperature (°C), T_{Min} = minimum daily mean temperature (°C), RH_{Avg} = average relative humidity (%), RH_{Max} = maximum daily mean relative humidity (%), RH_{Min} = minimum daily mean relative humidity (%), P_{Avg} = average air pressure (hPa), P_{Max} = maximum daily mean air pressure (hPa), P_{Min} = minimum daily mean air pressure (hPa), WS_{Avg} = average wind speed (m s^{-1}), WS_{Max} = maximum daily mean wind speed (m s^{-1}), WS_{Min} = minimum daily mean wind speed (m s^{-1}), Precip. = precipitation amount (mm), MLH_{Avg} = average mixing layer height (m), MLH_{Max} = maximum mixing layer height (m), MLH_{Min} = minimum mixing layer height (m).

	Summer 2010	Autumn 2010	Winter 2010	Spring 2011	Summer 2011	Annual
T_{Avg}	26.6	16.1	0.6	17.7	25.6	12.5
T_{Max}	32.9	25.2	13.7	25.6	27.4	32.9
T_{Min}	21.3	3.5	-9.6	8.5	21.2	-9.6
RH_{Avg}	67	68	41	40	56	52
RH_{Max}	89	92	93	73	79	93
RH_{Min}	27	32	13	12	25	12
P_{Avg}	1006	1018	1024	1011	1004	1016
P_{Max}	1015	1039	1042	1029	1008	1042
P_{Min}	996	1008	1009	999	996	996
WS_{Avg}	2.5	2.5	3.8	4.1	2.8	3.3
WS_{Max}	5.7	7.1	9.4	8.3	4.6	9.4
WS_{Min}	1.4	1.1	1.1	2.0	1.9	1.1
Precip.	200	118.6	10.6	34	32.6	395.8
MLH_{Avg}	735	670	696	1011	770	752
MLH_{Max}	1297	1559	1557	1875	1077	1875
MLH_{Min}	340	267	269	556	445	267

Table 4.11: Correlation coefficients (R) between $PM_{4.3}$ compounds and meteorological parameters at the CUGB during 2010-2011

	Temperature	Relative Humidity	Wind Speed	MLH
$PM_{4.3}$	0.07	0.29	-0.32	-0.27
OC	0.05	0.39	-0.44	-0.36
EC	0.01	0.44	-0.56	-0.45
Cl^-	-0.37	0.11	-0.30	-0.34
NH_4^+	0.02	0.40	-0.32	-0.30
NO_3^-	-0.14	0.23	-0.24	-0.26
SO_4^{2-}	0.16	0.43	-0.32	-0.27
Fe	0.001	0.01	-0.11	-0.10
S	0.26	0.54	-0.41	-0.29
K	-0.10	0.12	-0.25	-0.21
Ca	-0.05	-0.13	-0.08	-0.08
Ti	-0.02	-0.15	0.06	-0.001
Mn	-0.16	0.05	-0.18	-0.26
Cr	-0.02	0.22	-0.32	-0.27
Ni	-0.10	0.07	-0.20	-0.17
Cu	-0.08	0.28	-0.46	-0.40
Zn	0.11	0.40	-0.47	-0.32
As	0.03	0.21	-0.32	-0.21
Sn	0.11	0.09	-0.21	-0.004
Sb	-0.07	0.12	-0.10	-0.14
Ba	0.001	-0.01	-0.09	-0.10
Pb	-0.04	0.37	-0.46	-0.34
Ts	0.23	0.29	-0.25	-0.14
Tm	-0.41	0.14	-0.26	-0.33
29ab	-0.15	0.29	-0.41	-0.37
29ba	-0.49	0.11	-0.22	-0.35
30ab	0.05	0.39	-0.48	-0.37
30ba	-0.47	0.12	-0.24	-0.36
31abS	0.29	0.43	-0.45	-0.29
31abR	-0.09	0.26	-0.37	-0.34
32abS	-0.10	0.22	-0.26	-0.28
32abR	-0.07	0.20	-0.23	-0.23
BAA	-0.53	0.03	-0.20	-0.32
CRY	-0.54	0.04	-0.22	-0.34
BBKF	-0.54	0.09	-0.25	-0.37
BEP	-0.52	0.09	-0.25	-0.38
BAP	-0.49	0.09	-0.25	-0.34
PER	-0.44	0.08	-0.20	-0.36
DAH	-0.44	-0.10	-0.06	-0.34
IND	-0.52	0.08	-0.25	-0.40
PIC	-0.54	-0.04	-0.23	-0.44
BGH	-0.51	0.11	-0.27	-0.42
COR	-0.51	0.03	-0.21	-0.44
Levoglucosan	0.18	0.58	-0.43	-0.39

Temperature was found no significant correlation with $PM_{4.3}$ mass concentrations but Cl^-, all PAHs, Tm, 29ba and 30ba had a strong negative correlation and S, Ts and 31abS had a weakly positive correlation with temperature. A higher temperature is always accompanied by stronger solar radiation which can accelerate the degradation rate of PAHs. Cl^- is recognized as originating from coal burning for heating (Yao et al., 2002). Even though coal combustion for heating is not common in the city area any more, it still exists in the countryside. Therefore, it was expected that contribution from coal combustion to PM in Beijing increases with decreasing ambient temperatures.

Relative humidity had a weakly positive correlation with $PM_{4.3}$ mass concentrations which indicated a high RH could favor the growth of the particles because of their hygroscopicities which lead to the increase in PM mass concentration. Especially, EC, NH_4^+, SO_4^{2-}, S, Zn, 31abS and levoglucosan were found to have a strong positive correlation with RH while OC, NO_3^-, Cu, Cr, As, Pb, Ts, 29ab, 30ab, 31abR, 32abS and 32abR had a weakly positive correlation with RH which indicated that these compounds can increase under high RH.

Wind speed had a negative correlation with $PM_{4.3}$ mass concentration and most compounds which means that high wind speed could enhance the dispersion of pollutants.

MLH was found to have a negative correlation with $PM_{4.3}$ and most compounds which illustrated that a lower MLH could accelerate the accumulation of pollutants.

Wind direction and precipitation are also important factors for affecting PM mass concentrations in Beijing. The wind conditions during 2010-2011 are shown in Figure 4.24. The prevailing wind directions in spring were north, northwest, south and southeast. Dust storms which were blown from north and northwest can cause particularly higher PM concentrations. For instance, dust events which happened on 17 and 30 April 2011, raised the average $PM_{4.3}$ mass concentration in April, making it with the highest $PM_{4.3}$ mass concentration (Figure 4.2) during the whole year sampling at the CUGB from 21 June 2010 till 20 June 2010. In winter, the dominant wind direction was from the North and fresh air was brought into Beijing, thus reducing the pollutant mass concentrations which leaded to $PM_{4.3}$ mass concentration during winter was only a little bit higher than in summer and autumn (Figure 4.3). In summer, the $PM_{4.3}$ concentration was relatively low because there was a large amount of precipitation (58.8%) which can decrease the pollutant mass concentrations transported from the Southeast where an industrial area exists (Guinot et al., 2007). In autumn, the prevailing wind direction

was north and 30% precipitation happened in autumn so that the deposition of $PM_{4.3}$ was lower.

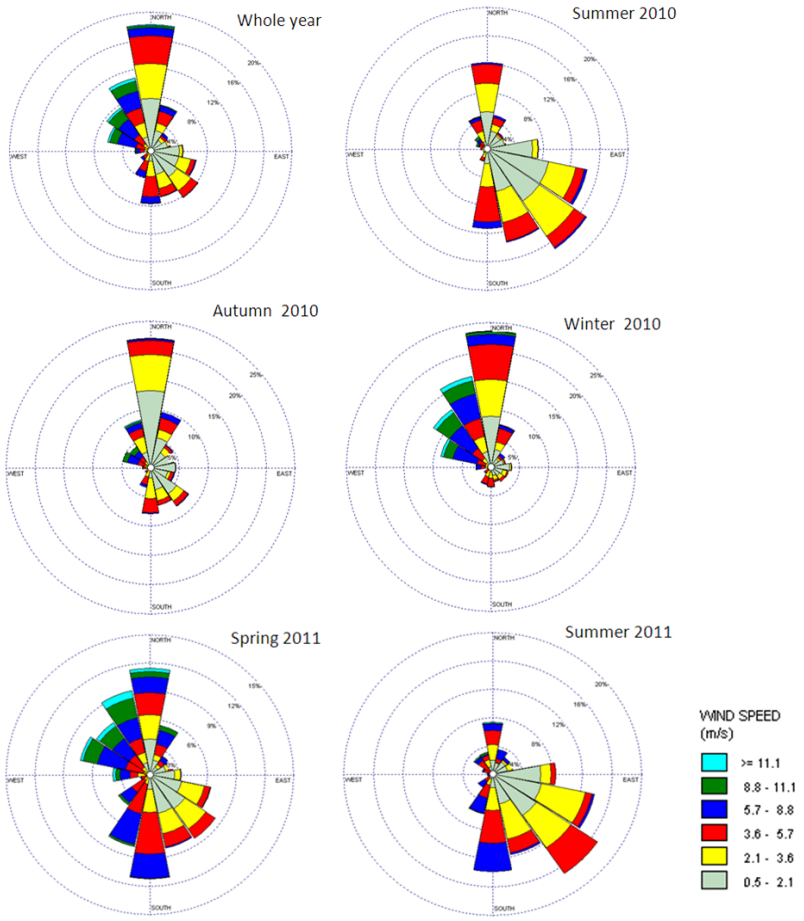

Figure 4.24: Wind rose (WRPLOT View Freeware, Lakes Environmental, Canada) for $PM_{4.3}$ sampling at the CUGB, Beijing (data obtained from ZBAA) from half hourly mean data during different seasons

Apart from the meteorological influence, human activities also play important role in the particles loading. For instance, January 2011 was found to have the lowest $PM_{4.3}$ mass concentration (Figure 4.2) over the whole year, as was found by colleagues from KIT/IMG who also collected $PM_{2.5}$ samples at the CUGB (Figure 3.9). The university winter holidays started in the middle of January. As CUGB is located in the area surrounded by different universities, air pollution from the surrounding area also decreased. During the Spring Festival holidays (starting from 2 February 2011), a large fraction of the population (the floating population of

Beijing was about 7 million and the total population was 19.6 million in 2010) departed for their hometowns, resulting in reduced human activities and reduced pollutants. That is why since November, when the period with residential heating started, the $PM_{4.3}$ concentration increased at first and decreased afterwards to be the lowest in January and but increased again in February (Figure 4.2).

During the $PM_{2.5}$ sampling campaign at the IAP, all correlation coefficients between mass concentrations of $PM_{2.5}$ and its compounds and meteorological parameters are listed in Table 4.12 and the wind conditions are shown in Figure 4.25. Dust events normally happen during spring in Beijing, but this year, except for several locally re-suspended dust events, no significant dust storm from the North or Northwest of Beijing (i.e. Gobi desert, Loess Plateau and Taklimakan desert) was observed.

Table 4.12: Correlation coefficients (R) between $PM_{2.5}$ compounds and meteorological parameters at the IAP

	Temperature	Relative Humidity	Wind Speed	MLH		Temperature	Relative Humidity	Wind Speed	MLH
$PM_{2.5}$	0.10	0.53	-0.36	-0.50	Cd	-0.25	0.41	-0.18	-0.33
Cl^-	-0.33	0.56	-0.27	-0.41	Ba	0.10	0.10	0.20	-0.01
NO_3^-	-0.15	0.70	-0.40	-0.52	Tl	0.16	0.65	-0.53	-0.59
SO_4^{2-}	0.16	0.76	-0.51	-0.57	Pb	0.03	0.67	-0.51	-0.54
Na^+	0.13	0.35	-0.30	-0.43	Ts	-0.15	-0.03	-0.09	-0.07
NH_4^+	0.06	0.80	-0.51	-0.59	Tm	-0.04	-0.04	-0.03	-0.26
K^+	0.07	0.64	-0.55	-0.56	29ab	-0.46	-0.06	-0.06	-0.25
Mg^{2+}	0.48	-0.26	-0.05	-0.10	29ba	-0.40	-0.11	0.001	-0.06
Ca^{2+}	0.14	-0.44	0.25	0.11	30ab	-0.36	-0.04	-0.09	-0.29
OC	0.20	0.22	-0.36	-0.42	30ba	-0.25	0.003	-0.01	-0.34
EC	0.34	0.58	-0.51	-0.60	31abS	-0.23	-0.14	-0.09	-0.16
Na	0.02	0.09	-0.06	-0.18	31abR	-0.19	0.03	-0.17	-0.37
Mg	0.05	-0.43	0.22	0.14	32abS	-0.15	-0.14	-0.10	-0.17
Al	0.23	-0.35	0.18	0.10	32abR	-0.26	-0.15	-0.01	0.10
K	0.09	0.37	-0.39	-0.42	BAA	-0.68	-0.01	0.12	-0.12
Ca	-0.02	-0.30	0.21	0.06	CRY	-0.57	0.18	-0.06	-0.28
Fe	0.22	-0.18	0.05	-0.01	BBKF	-0.32	0.14	-0.01	-0.33
V	0.23	0.41	-0.31	-0.31	BEP	-0.37	0.28	-0.15	-0.41
Cr	0.37	0.33	-0.32	-0.34	BAP	-0.54	0.23	-0.02	-0.34
Mn	0.15	0.06	-0.10	-0.25	PER	-0.32	0.36	0.09	-0.38
Co	0.23	-0.06	-0.06	-0.12	DAH	-0.19	0.31	-0.13	-0.34
Ni	0.35	0.45	-0.39	-0.39	IND	-0.33	0.25	-0.16	-0.38
Cu	0.05	0.34	-0.23	-0.36	PIC	-0.28	0.20	-0.12	-0.31
Zn	-0.04	0.64	-0.33	-0.52	BGH	-0.35	0.27	-0.14	-0.41
As	-0.13	0.37	-0.10	-0.30	COR	-0.14	0.33	-0.16	-0.36

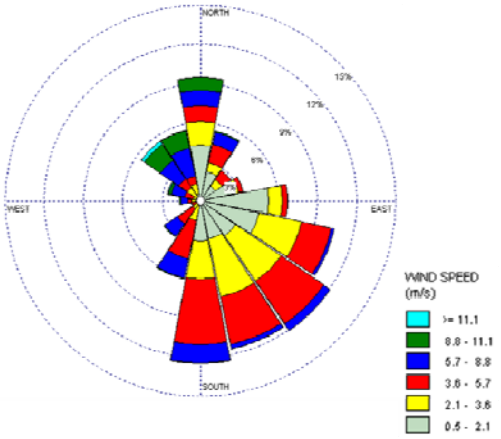

Figure 4.25: Wind rose (WRPLOT View Freeware, Lakes Environmental, Canada) for $PM_{2.5}$ sampling at the IAP, Beijing (data obtained from ZBAA) from half hourly mean data during the campaign

From Table 4.12, it's obvious that temperature had no significant correlation with $PM_{2.5}$ but had a negative correlation with NO_3^-, Cl^-, most hopanes and PAHs because ammonium nitrate, hopanes and PAHs are usually volatile under high temperatures.

Relative humidity was positively correlated with $PM_{2.5}$, especially NO_3^-, SO_4^{2-}, NH_4^+, K^+, EC, Zn, Tl and Pb. Because a high RH can increase the dissolution of hydrosoluble compounds, such as HNO_3 and NH_3, on the surface of moist particles, leading to the increase of NO_3^- and NH_4^+ in the PM (Pathak et al., 2009; Ianniello et al., 2010, 2011). Another reason is the heavy pollution days like haze, normally happened under high RH conditions, and secondary ions and anthropogenic elements contributed largely to PM in haze.

Wind speed had a negative correlation with $PM_{2.5}$ mass concentration indicated high wind speeds can increase the dilution of pollutants. But wind speed was found to have a positive correlation with Ca^{2+}, Mg, Al, Ca and Fe in this study. The reason is that high wind speeds can also cause re-suspended dust which includes much more crustal elements such as Ca^{2+}, Mg, Al, Ca and Fe.

MLH had a negative correlation with $PM_{2.5}$ and most of compounds, which means that a low MLH mainly enhanced the anthropogenic pollutant mass concentrations.

The main wind directions during these two months sampling period were north, northwest, south and southeast (Figure 4.25), which were similar to the wind directions in spring 2011.

Generally, in both campaigns, T was found no correlation with PM mass concentration, high RH and low MLH can enhance the PM mass concentration, while high WS can increase the dilution of pollutants. Specifically, the correlations between PM composition mass concentrations and meteorological parameters in $PM_{4.3}$ and $PM_{2.5}$ showed some small differences. This is because PM composition mass concentrations are not only influenced by one meteorological parameter, but also by an array of meteorological parameters. Another reason could be that the data set of $PM_{4.3}$ is one year but only 2 months for $PM_{2.5}$.

4.3.5 Effects on visibility

Visibility can be influenced by PM loading. The correlations between visibility and PM, as well as compounds in PM, at the CUGB and the IAP are listed in Table 4.13.

Table 4.13: Correlation coefficients (R) between PM compounds and visibility at the CUGB and the IAP

Species	CUGB	IAP	Species	CUGB	IAP	Species	CUGB	IAP
$PM_{4.3}$	-0.65	/	Ca	-0.18	0.18	29ba	-0.34	-0.14
$PM_{2.5}$	/	-0.71	Ti	-0.18	/	30ab	-0.47	-0.17
OC	-0.66	-0.39	Mn	-0.41	-0.09	30ba	-0.34	-0.12
EC	-0.62	-0.71	Cr	-0.39	-0.32	31abS	-0.38	-0.09
SOC	-0.51		Ni	-0.37	-0.52	31abR	-0.40	-0.18
Cl^-	-0.40	-0.67	Cu	-0.53	-0.38	32abS	-0.31	-0.03
NO_3^-	-0.47	-0.80	Zn	-0.68	-0.74	32abR	-0.33	-0.13
SO_4^{2-}	-0.71	-0.88	As	-0.47	-0.49	BAA	-0.27	-0.17
Na^+	/	-0.47	Sn	-0.22	/	CRY	-0.28	-0.29
NH_4^+	-0.66	-0.91	Sb	-0.22	/	BBKF	-0.33	-0.29
K^+	/	-0.65	V	/	-0.41	BEP	-0.35	-0.41
Mg^{2+}	/	0.29	Ba	-0.33	-0.17	BAP	-0.35	-0.35
Ca^{2+}	/	0.38	Pb	-0.65	-0.72	PER	-0.27	-0.41
Na	/	-0.27	Co	/	-0.02	DAH	-0.17	-0.42
Mg	/	0.34	Cd	/	-0.52	IND	-0.32	-0.39
Al	/	0.27	Tl	/	-0.70	PIC	-0.18	-0.21
Fe	-0.33	0.16	Ts	-0.26	-0.13	BGH	-0.37	-0.34
S	-0.84	/	Tm	-0.36	0.03	COR	-0.37	-0.37
K	-0.44	-0.45	29ab	-0.42	-0.13	Levoglucosan	-0.62	/

/: the compound was not available at the corresponding sampling site

At both sampling sites, visibility had a strong negative correlation with PM mass concentration which meant visibility decreased when PM mass concentration increased. Results from both sampling sites showed clearly that OC, EC, SOC, Cl^-, NO_3^-, SO_4^{2-}, NH_4^+, K, Cr, Ni, Cu, Zn, As, Pb and all PAHs had negative correlations with visibility. Besides this, S, levoglucosan, all hopanes in $PM_{4.3}$ samples at the CUGB and K^+, V, Cd and Tl in $PM_{2.5}$ samples at the IAP had a negative correlation with visibility. In general, visibility is highly correlated with most anthropogenic compounds.

In addition, correlations between visibility and meteorological parameters are also investigated. At both sampling sites, visibility showed a significant negative correlation with RH (R=-0.70 in 2010-2011 and R=-0.84 in 2013), indicating that with the increase in RH, visibility decreased.

4.4 Summary

According to the analysis of compounds of PM in Beijing, the temporal variations of PM and its compositions during several months, even one year, were shown and found to be mainly caused by emissions and secondary aerosol formation processes. Furthermore, meteorological parameters (temperature, wind speed, wind direction, precipitation, mixing layer height) also influence such variations, but the relationship is complex and parameters often interfered with each other.

In this study, SOC in $PM_{4.3}$ at the CUGB and $PM_{2.5}$ at the IAP were estimated. SOC contributed 55%, 47%, 25%, 22% and 42% to OC mass concentrations in winter 2010, summer 2010, spring 2011, autumn 2010 and spring 2013, respectively. Hence, SOC could be one important compound of PM, but as all the SOC data were only estimated but not measured, further research on SOC is necessary.

NO_3^-, SO_4^{2-} and NH_4^+ had strong negative correlations with visibility which illustrated that secondary inorganic ions were very important compounds in PM, making it important to control their concentrations for increasing the visibility.

The high levoglucosan mass concentrations in summer and autumn 2010 indicated that contributions from biomass burning to $PM_{4.3}$ are significant.

Both the homohopane index and hopane index showed the similar results that hopanes in $PM_{4.3}$ at the CUGB and $PM_{2.5}$ at the IAP in Beijing mainly originated from mixed sources (coal combustion and fuel oil consumption) and coal combustion contributed much more in winter than during other periods.

PAHs showed relatively high mass concentrations in winter 2010 and were dominated by 5-ring PAHs. LMW PAHs had a higher mass percentage in winter while HMW PAHs had a higher mass percentage in autumn and summer. Based on diagnostic ratios, coal combustion were found to be the dominant source of PAHs in $PM_{4.3}$ during 2010-2011, while liquid fossil fuel were the dominant source of PAHs in $PM_{2.5}$ during 2013 in Beijing.

Visibility was found to be mainly affected by most anthropogenic compounds, as well as RH.

Chapter 5 Haze and Dust

With the increase in energy combustion, haze events has become more frequent in some regions of the world recently, especially in Beijing (Sun et al., 2006; Wang et al., 2006a; Che et al., 2007). For instance, a severe haze pollution happened in Beijing in January 2013 during which the instantaneous $PM_{2.5}$ mass concentration even reached 1000 μg m^{-3} (Zhang et al., 2014a). Figure 5.1 shows the obviously reduction of visibility during haze days when comparing with clear day. Except for its influence on visibility, haze can also affect human health, therefore, haze has received much more attention during the past years (Okada et al., 2001; Chen et al., 2003; Yadav et al., 2003; Lee et al., 2006; Huang et al., 2011).

Figure 5.1: Pictures of a haze day and a clear day in Beijing, 2013

In addition to haze, dust is another typical and important pollution event in Beijing. Dust storms invade Beijing frequently in spring (Guo et al., 2004) because of its location downwind of Asian dust source regions (Figure 5.2). In spring, dust storms originate from sandy deserts, Loess plateau in Northern China, or Gobi Desert and Mongolia Desert (Zhang et al., 2003b), and are transported over long distances to Beijing (Zhuang et al., 2001; Zhang et al., 2009; Wang et al., 2010b). Dust particles have been found to affect the climate change (Tegen et al., 1996), the Earth's radiation budget (Wang et al., 2006b), visibility (Zhang et al., 2005),

biogeochemical processes (Cao et al., 2005; Wang et al., 2005a) and human health (Meng and Lu, 2007). Dust particles can serve as not only reactive surfaces for atmospheric chemical reaction, but also as carriers for the anthropogenic pollutants during long-range transport which make the interaction between various compounds possible (Wang et al., 2005a; Yuan et al., 2008). Beijing suffers from not only dust from non-local sources, such as Gobi desert and Mongolia desert, but also re-suspended dust from local sources, such as road dust and construction dust. Some studies reported that re-suspended dust is one of the most important contributions to dust pollution in Beijing and also to haze (Han et al., 2007).

Figure 5.2: Map of Asian dust source regions (Source: Google map)

In order to understand further the influences of haze and dust particles, knowledge of their chemical characteristics is required. In this chapter, the chemical characteristics of PM during haze episodes and dust events in Beijing are described, and the differences between haze, dust and clear days, and the possible sources for PM during haze and dust, are discussed. In this study, clear days referred to the days during which visibility is equal to or more than 10 km. Considering this study focused on polluted events, therefore threshold of PM mass concentration should be considered. Because both haze and dust can cause the decrease in visibility, therefore in this study, only sampling days with daily mean PM mass concentration higher than 90 μg m^{-3} (annual average value) and daily mean visibility lower than 10 km were

considered. Additionally, haze days corresponded with six hour visibilities were continuously lower than 5 km during one day. Dust days, including dust storms from non-local sources and re-suspended dust events from local sources, were identified by no precipitation and six hour wind speeds were continuously equal to or higher than 5 m s^{-1} which caused at least one hour visibility decreased during one day.

5.1 Results and discussion

5.1.1 PM mass concentrations during haze and dust episodes

5.1.1.1 Long-term daily mean sampling campaign at the CUGB (2010.06.21 – 2011.06.20)

During 2010-2011, most haze events happened in autumn and winter 2010 (Figure 5.3) which was the same observation as in the previous study (Sun et al., 2013a). Heating emissions and biomass burning in the rural area around Beijing were supposed to be the main reasons for frequent haze days in winter and autumn, respectively (Sun et al., 2013a). During the haze episodes of this campaign, 321 μg m^{-3} as the highest daily mean $PM_{4.3}$ mass concentration and 153 μg m^{-3} as the average daily mean $PM_{4.3}$ mass concentration were observed.

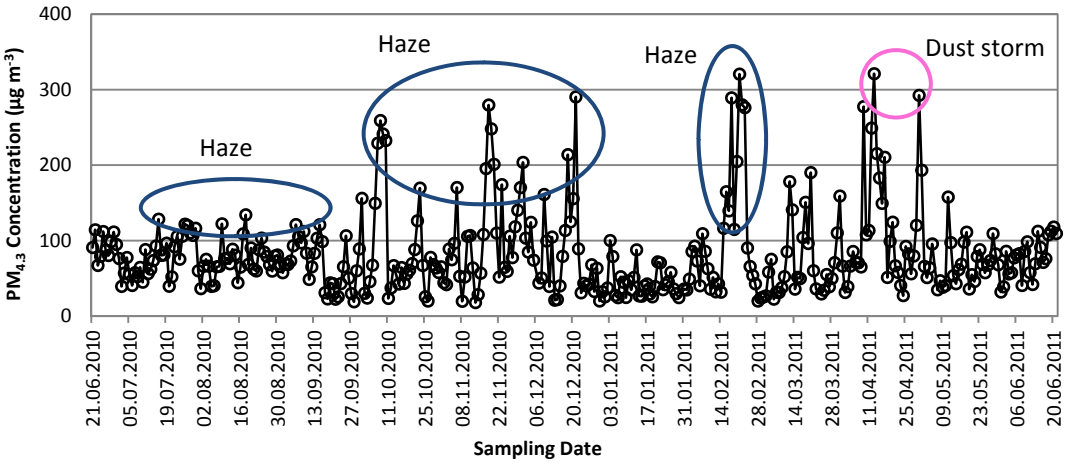

Figure 5.3: Annual variation of daily mean $PM_{4.3}$ mass concentrations at the CUGB from 2010.06.21 till 2011.06.20 with haze and dust episodes indicated

Dust events were concentrated in the spring season (Figure 5.3) and a dust storm happened on 30 April 2011 with maximum $PM_{4.3}$ mass concentration of 292 μg m^{-3}. During these dust events, the average daily mean $PM_{4.3}$ mass concentration was 173 μg m^{-3}.

Compared with clear days with the average daily mean $PM_{4.3}$ mass concentration of 43 μg m^{-3}, average daily mean $PM_{4.3}$ mass concentrations during haze days and dust days were 3.5 times and 4.0 times higher, respectively. It is evident that particulate pollution was extremely heavy during haze and dust events.

5.1.1.2 Short-term sampling campaign at the IAP (2013.04.10 – 2013.06.08)

In this campaign, several haze events were observed. The highest and average daily mean $PM_{2.5}$ mass concentration during haze days was 182 μg m^{-3} and 140 μg m^{-3}, respectively. Dust storms from the North or Northwest deserts did not happen during this spring campaign, but several locally re-suspended dust events were found. The highest and average daily mean $PM_{2.5}$ mass concentration during dust events were 151 μg m^{-3} and 126 μg m^{-3}, respectively. Daily mean $PM_{2.5}$ mass concentrations during haze days and dust days were 2.8 and 2.5 times that during clear days (average value: 51 μg m^{-3}), respectively and were 1.9 and 1.7 times higher than the 24 h average of Chinese Ambient Air Quality Standard for $PM_{2.5}$ (Grade II: 75 μg m^{-3}) (China State Environmental Protection Administration (SEPA), 2012), respectively.

As described in Chapter 4, three obvious accumulation and dissipation processes of haze episodes (HE, including clean days before and after) were found in this short term campaign (Figures 5.4, 5.5 and 5.6). They happened from 18 April till 25 April (HE1), 3 May till 9 May (HE2) and 1 June till 8 June (HE3). During haze episodes, the sampling time resolution was increased from 24 h to 4 h. Because it was difficult to predict the exact time when a haze episode would occur, the time resolution was sometimes increased in the middle of the haze episode.

The first accumulation and dissipation process of haze episode (HE1, Figure 5.4) started from 18 April with $PM_{2.5}$ mass concentration of 20 μg m^{-3} and increased until 23 April with the peak $PM_{2.5}$ mass concentration of 182 μg m^{-3}. The mass concentration then decreased to 33 μg m^{-3} on 25 April. During this process, the time resolution of all the sampling was 24 h.

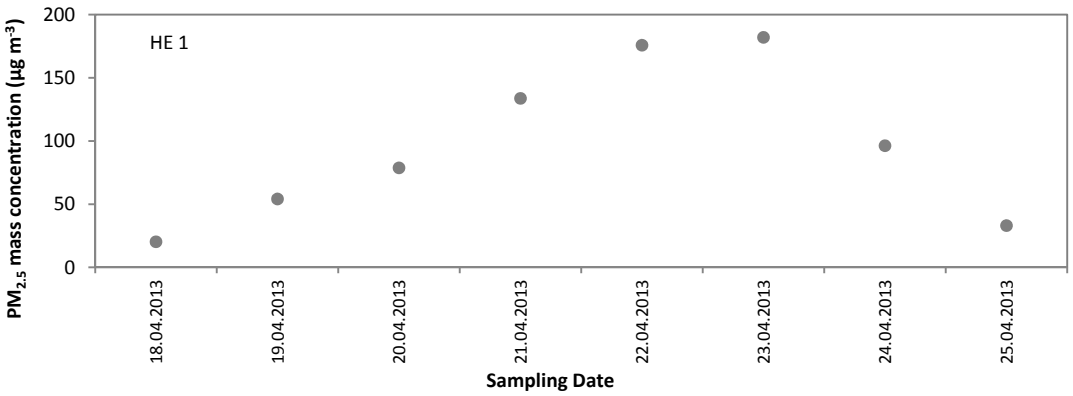

Figure 5.4: Variation of daily mean $PM_{2.5}$ mass concentrations during the first haze episode at the IAP from 2013.04.18 till 2013.04.25

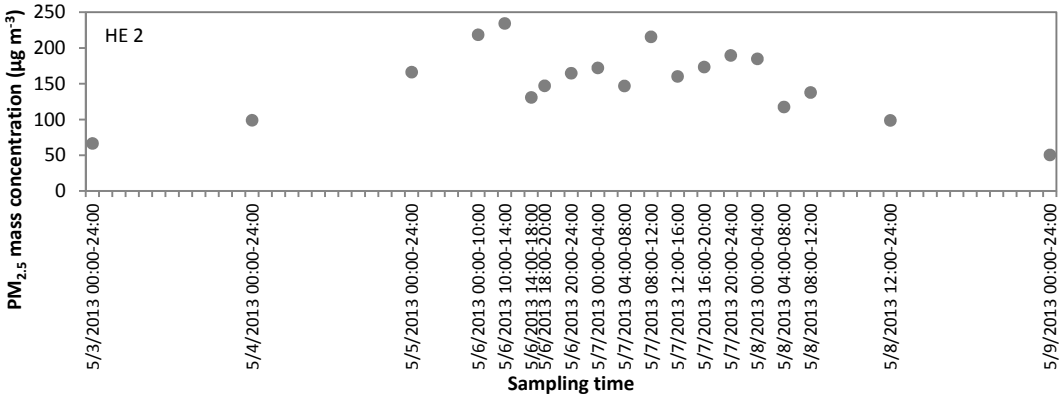

Figure 5.5: Variation of $PM_{2.5}$ mass concentrations during the second haze episode at the IAP from 2013.05.03 till 2013.05.09

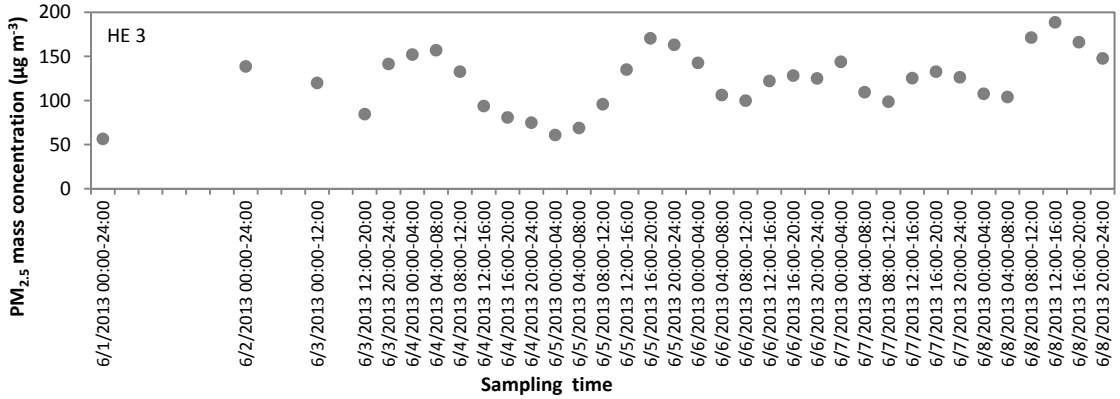

Figure 5.6: Variation of $PM_{2.5}$ mass concentrations during the third haze episode at the IAP from 2013.06.01 till 2013.06.08

The second observed haze episode (HE2, Figure 5.5) started on 3 May, then the $PM_{2.5}$ mass concentration reached a peak value of 234 μg m^{-3} between 10 am and 2 pm on 6 May, and then fluctuated around 170 μg m^{-3} until 8 May midnight (00:00-04:00). Later on, $PM_{2.5}$ mass concentration started to decrease and reached the lowest value of 51 μg m^{-3} on 9 May.

The third observed haze episode (HE3, Figure 5.6) showed two obvious accumulation processes. One started from 1 June, and reached the peak value of $PM_{2.5}$ mass concentration in the early morning of 4 June (04:00-08:00), 157 μg m^{-3}. Thereafter, $PM_{2.5}$ mass concentration decreased and reached a minimum value of 61 μg m^{-3} on 5 June (00:00-04:00). The $PM_{2.5}$ mass concentration then started to increase again and arrived at the peak value of 171 μg m^{-3} on 5 June afternoon (16:00-20:00), fluctuating around 120 μg m^{-3} thereafter.

5.1.2 Comparison of daily mean PM chemical characteristics during haze, dust and clear days

5.1.2.1 Mass variation

In order to get the variation of each compound mass concentration and mass percentage during haze, dust and clear days, the ratios of haze/clear and dust/clear during two campaigns were calculated and shown in Figures 5.7, 5.8, 5.9 and 5.10, respectively.

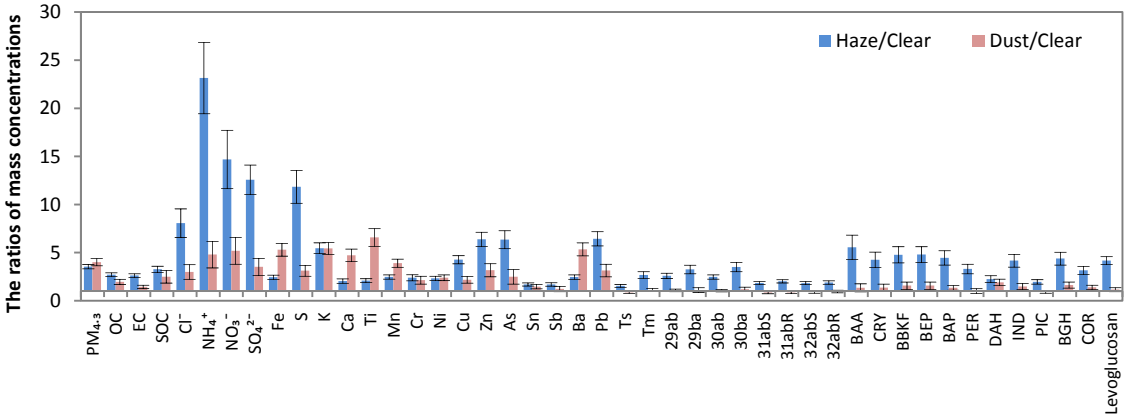

Figure 5.7: The ratios of average daily mean $PM_{4.3}$ and each compound mass concentration during haze and clear days, dust and clear days at the CUGB from 2010.06.21 till 2011.06.20

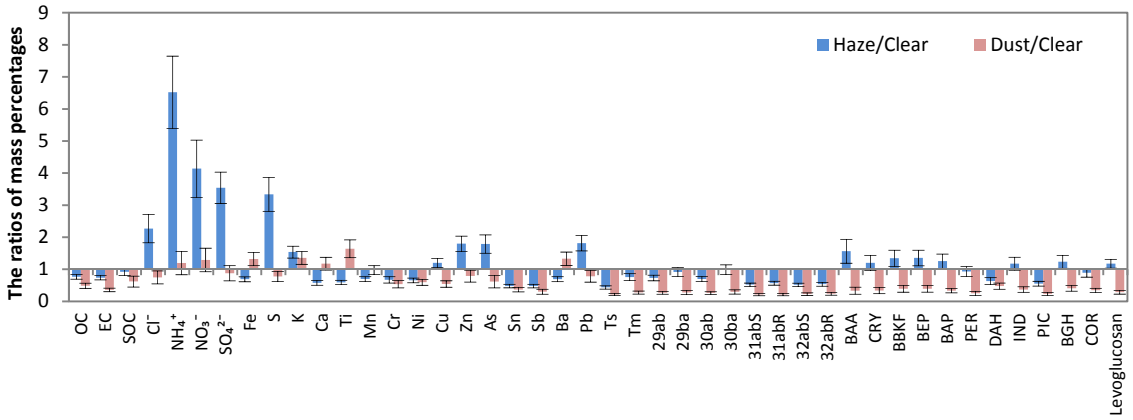

Figure 5.8: The ratios of average daily mean $PM_{4.3}$ and each compound mass percentage during haze and clear days, dust and clear days at the CUGB from 2010.06.21 till 2011.06.20

During 2010-2011, all chemical compound mass concentrations during haze days were higher than those during clear days. However, during dust days, EC, OC, SOC, all water soluble ions, all inorganic elements and most organic compound mass concentrations except Ts, 30ab, 31abS, 31abR, 32abS, 32abR, PER and PIC were higher than during clear days. The variation for EC, OC, SOC, Cl^-, NH_4^+, NO_3^-, SO_4^{2-}, S, Cr, Cu, Zn, As, Sn, Sb and Pb mass concentrations were the same, decreasing from haze, through to dust, to clear days. However, for Fe, Ca, Ti, Mn and Ba, the mass loading increased from clear, to haze, and to dust days. K and Ni displayed the similar mass concentrations during haze and dust days, and higher than that during clear days. Most organic compounds except Ts, 30ab, 31abS, 31abR, 32abS, 32abR, PER and PIC showed the variation as the highest during haze days and the lowest during clear days. The ratios of haze/clear and dust/clear for each compound mass percentage showed that Cl^-, NH_4^+, NO_3^-, SO_4^{2-}, S, Cu, Zn, As, Pb, BAA, CRY, BBKF, BEP, BAP, IND, BGH and levoglucosan increased significantly during haze days, while Fe, Ti and Ba increased sharply during dust days. K increased obviously during both haze and dust days. This indicates that compounds which increased more rapidly during haze days were mainly anthropogenic compounds, while during dust days they were mainly crustal compounds. NH_4^+ and NO_3^- mass percentage were also found to increase during dust days which indicated that dust particles can bring anthropogenic pollutants or supply the surface for chemical formation.

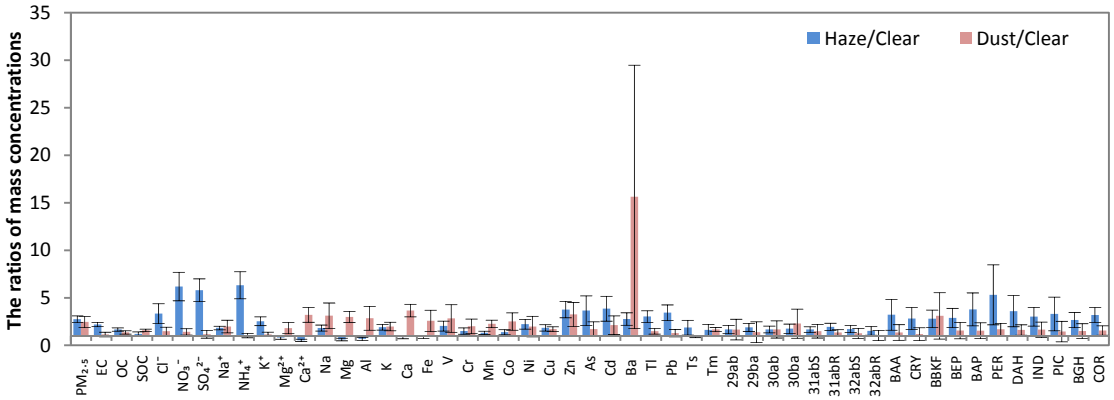

Figure 5.9: The ratios of average daily mean $PM_{2.5}$ and each compound mass concentration during haze and clear days, dust and clear days at the IAP from 2013.04.10 till 2013.06.08, organic compounds (Ts to COR) were only available from 2013.04.10 till 2013.05.31

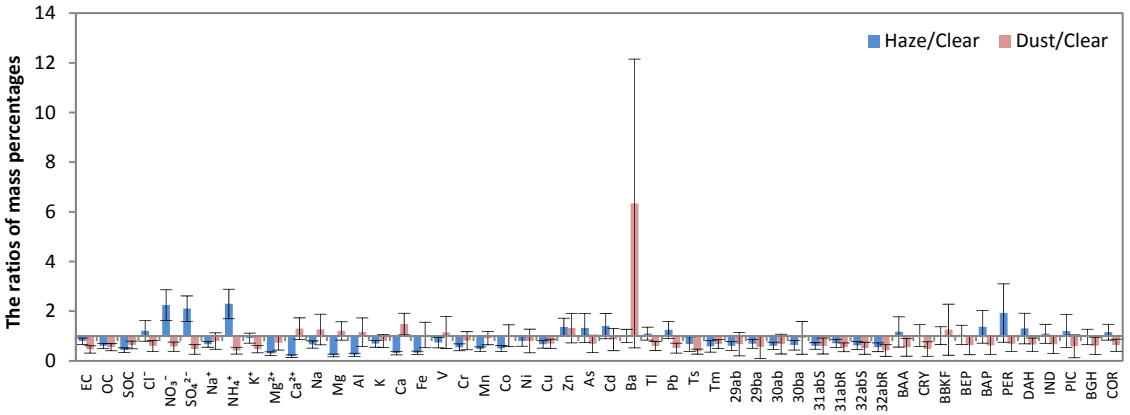

Figure 5.10: The ratios of average daily mean $PM_{2.5}$ and each compound mass percentage during haze and clear days, dust and clear days at the IAP from 2013.04.10 till 2013.06.08, organic compounds (Ts to COR) were only available from 2013.04.10 till 2013.05.31

During spring 2013, average daily mean mass concentrations of most chemical compounds during haze and dust days were higher than those during clear days. Compared with clear days, average daily mean mass concentrations of Mg^{2+}, Ca^{2+}, Mg, Al, Ca and Fe were lower during haze days. Average daily mean mass concentrations of EC, OC, Cl^-, NO_3^-, SO_4^{2-}, NH_4^+, K^+, Cu, Ni, Zn, As, Cd, Tl, Pb, most hopanes and PAHs showed the same variation, decreasing from haze days, through dust days, to clear days. For SOC, Mg^{2+}, Ca^{2+}, Na^+, Na, Mg, Al, Ca, Fe, V, Cr, Mn, Co, Ba, 30ba and BBKF mass concentrations were more elevated during dust days. Comparing the ratios of haze/clear and dust/clear for each compound mass percentage, NO_3^-, SO_4^{2-}, NH_4^+,

As, Zn, Cd, Pb, BAP and PER mass percentages increased sharply during haze days while Ca^{2+}, Na, Mg, Al, Ca and Ba during dust days increased rapidly.

5.1.2.2 Water soluble ions

The mass percentages of secondary inorganic ions in $PM_{4.3}$ at the CUGB from June 2010 till June 2011 were 41.4%, 13.2% and 13.2% during haze, dust and clear days, respectively. In 2013, mass percentages of secondary inorganic ions in $PM_{2.5}$ were 56.6%, 12.9% and 24.2% during haze, dust and clear days, respectively. Both campaigns showed the same variation of secondary inorganic ions mass percentages in PM with the highest during haze days. Mass concentrations and mass percentages of secondary inorganic ions in PM enhanced sharply during haze days which showed that the chemical formation of sulfate and nitrate was accelerated under haze conditions. During dust days, mass concentrations of secondary inorganic ions increased slightly above those during clear days illustrated that dust particles can carry anthropogenic pollutants during transportation or function as the reactive surfaces for atmospheric chemical formation.

At the CUGB from 2010 till 2011, Cl^- mass percentages in $PM_{4.3}$ were 2.7%, 1.1% and 1.5% during haze, dust and clear days, respectively. As depicted in Chapter 4, Cl^- in $PM_{4.3}$ could be sourced from coal combustion from 2010 till 2011, and therefore coal combustion could be an important source for haze pollution. During 2013 at the IAP, Cl^- and K^+ mass concentrations increased rapidly during haze days. K^+ can be used as a tracer for biomass burning (Duan et al., 2004). Sun et al. (2013a) found that K^+ and Cl^- were strongly correlated during autumn haze days, but not significantly correlated during spring haze days in Beijing. In this study, K^+ and Cl^- were only found to be weakly correlated during haze days. This is because Cl^- not only originates from biomass burning (Sun et al., 2013a), but also from coal combustion (Yao et al., 2002). Na^+, Mg^{2+} and Ca^{2+} had the highest mass concentrations during dust days. Ca^{2+} mass concentrations especially increased during dust days to about 3.2 times that value measured on clear days. This is the evidence that Mg^{2+} and Ca^{2+} were mainly from crustal sources, like construction dust. Na^+ increased during both haze and dust days, but only a little higher during dust days, also indicating that Na^+ mostly like originated from crustal sources.

5.1.2.3 Acidity of PM

Different chemical composition was found in the different pollution events, and could lead to different particle acidities. Therefore, the study on the acidities of particles in different pollution events is necessary. All the details about the calculation of the acidity were described in Chapter 4.

During the 2010-2011 campaign, only data of one cation (NH_4^+) is available, the cation/anion ratio cannot be calculated.

During the 2013 campaign, the average equivalent concentration ratios of C/A during haze, dust and clear days were 1.1, 1.8 and 1.6, respectively, which indicates that the particles were more alkaline during dust days than during clear and haze days. Ca^{2+} and Mg^{2+} mass concentrations increased very rapidly during dust days which could be the reason for the alkalinity of particles during these days. The average C/A ratio of 1.1 during haze days was close to unity, suggesting that most of the acids can be neutralized.

5.1.2.4 Inorganic elements

During the first campaign at the CUGB in 2010-2011, all the measured inorganic elements mass concentrations increased during haze and dust days. Comparing the ratios of haze/clear and dust/clear for each element mass percentage, S, Cu, Zn, As and Pb increased more during haze days, but Fe, Ca, Ti and Ba enhanced more during dust days. K increased during both haze and dust. Based on the variation characteristics of mass percentage during haze and dust days, two kinds of particles were found: crustal particles (represented by Fe, Ca, Ti and Ba) and haze particles (represented by S, Cu, Zn, As and Pb). Increased ratios of K mass percentage showed no significant difference between during dust days and haze days, indicating the mixture of sources.

In 2013, the increase in Ni, Cu, Zn, As, Cd, Tl and Pb mass concentrations during haze days were higher than those during dust days. The other measured elements showed the opposite variation. As with the first campaign, on the basis of mass percentage ratios for each compound, crustal particles could be represented by Na, Mg, Al, Fe, Ca, V, Co and Ba, and haze particles could be represented by Zn, As, Cd, Tl and Pb. Zn and Cu mass concentration and percentage did not show much change during both haze and dust days. The reason could be

that the dust events in 2013 were only re-suspended dust, which was influenced more by local road particles, for instance, from vehicle exhaust.

In general, considering the inorganic elements which were measured in both campaigns, Fe, Ca and Ba were proposed to represent dust particles, and Zn, As and Pb were suggested to indicate haze particles.

5.1.2.5 Organic compounds

During 2010-2011, levoglucosan and PAHs showed the same variation during haze, dust and clear days, the highest mass concentrations during haze days, less during dust days and the lowest during clear days. The mass concentrations of levoglucosan during haze, clear and dust days were 847 ng m^{-3}, 203 ng m^{-3}, 234 ng m^{-3}, respectively. PAHs had mass concentrations of 60 ng m^{-3}, 13 ng m^{-3} and 18 ng m^{-3} during haze, clear and dust days while the mass concentrations of hopanes during haze, clear and dust days were 42 ng m^{-3}, 18 ng m^{-3} and 17 ng m^{-3}, respectively. The mass percentages of all organic compounds in $PM_{4.3}$ during haze days were higher than during dust days. Mass percentages of BAA, CRY, BBKF, BEP, BAP, IND, BGH and levoglucosan in $PM_{4.3}$ during haze days were higher than during clear days, and all the others were lower. All organic compounds mass percentages during dust days were lower than during clear days.

During spring 2013, most hopanes and all PAHs mass concentrations during both haze and dust days were higher than during clear days, except for Ts and 32abR which had equal or lower mass concentrations during dust days than clear days. Mass percentages showed that BAP and PER increased rapidly during haze days.

As described in Chapter 4, some ratios between organic compounds can be used to distinguish PM sources. These ratios during haze, dust and clear days are listed in Table 5.1.

The contribution of biomass burning to OC in $PM_{4.3}$ can be estimated by the mass ratio of levoglucosan to OC (Zhang et al., 2008b). Table 5.1 showed that haze days had higher ratios than dust and clear days while dust days had the lowest ratio. This indicated that biomass burning is an important source of haze in Beijing.

Table 5.1: Ratios between organic compounds in $PM_{4.3}$ at the CUGB (2010.06.21-2011.06.20) and in $PM_{2.5}$ at the IAP (2013.04.10-2013.05.31) during haze, dust and clear days

	$PM_{4.3}$			$PM_{2.5}$		
	Haze	Dust	Clear	Haze	Dust	Clear
Levoglucosan/OC	0.03	0.01	0.02	/	/	/
Homohopane index	0.52	0.53	0.52	0.55	0.57	0.58
Hopane index	0.73	0.74	0.71	0.85	0.81	0.86
BGH/BEP	1.27	1.15	1.23	0.79	0.80	0.83
IND/(IND+BGH)	0.55	0.54	0.57	0.32	0.32	0.32

/: No data available

In $PM_{4.3}$, the homohopane index 31abS/(31abS+31abR) and the hopane index 30ab/(30ab+30ba) showed a similar variation. Haze, dust and clear days had similar hopane index and homohopane index. This indicated that the sources of hopanes during haze, dust and clear days are stable. In $PM_{2.5}$, the similar variation hopane index and homohopane index were also found. But both homohopane and hopane indexes had the higher value in $PM_{2.5}$. The different results were found in two campaigns could be caused by the different sampling durations.

In $PM_{4.3}$, the ratios of BGH to BEP during haze, dust and clear days were similar, but the ratio during haze days showed slightly higher value than during dust and clear days. Because the high ratio of BGH to BEP indicates the presence of particles from vehicle emissions (Nielsen, 1996), fuel oil combustion contributed more to haze particles. In $PM_{2.5}$, BGH/BEP ratio was the highest during clear days, which showed the same results as the homohopane and hopane indexes.

The ratios of IND/(IND+BGH) of $PM_{4.3}$ during haze, dust and clear days were all higher than 0.5. As discussed in Chapter 4, one can conclude that coal combustion were dominant sources for $PM_{4.3}$ during haze, dust and clear days at the CUGB. In $PM_{2.5}$, IND/(IND+BGH) showed the same value during haze, dust and clear days, the liquid fossil fuel was found to be the main source for PAHs in $PM_{2.5}$. No obvious variation of these ratios was observed during haze, dust and clear days, indicating the sources of PAHs are stable.

5.1.2.6 The ratios of $PM_{2.5}/PM_{10}$

During the sampling campaign in 2010-2011 at the CUGB, $PM_{4.3}$ samples were collected on the filters at the CUGB while PM_{10} data were obtained from TEOM at the IAP. Unfortunately, there is a disadvantage in using filter weighing data and online mass concentration data to get the ratio because of different methods. Therefore, considering that CUGB is not far away from IAP (3 km), TEOM $PM_{2.5}$ and TEOM PM_{10} data obtained at the IAP were used to get the $PM_{2.5}/PM_{10}$ ratio. The $PM_{2.5}/PM_{10}$ ratios during haze, dust and clear days were 0.56, 0.31 and 0.35, respectively, indicating that more fine particles were present during haze days.

During the sampling campaign at the IAP in 2013, even though the filter weighing data and TEOM data were obtained at the same sampling site, they were still different. Therefore, only $PM_{2.5}$ TEOM data and PM_{10} TEOM data were used as a ratio. The $PM_{2.5}/PM_{10}$ ratios during haze, dust and clear days were 0.68, 0.25, and 0.38, respectively.

The $PM_{2.5}/PM_{10}$ ratios during both campaigns indicated that fine particles were the dominant particles during haze pollution. The variation of $PM_{2.5}/PM_{10}$ ratios shows the different transformation efficiency into secondary aerosols (fine particles) which is the highest during haze days. This is in agreement with the increased mass concentration and percentage of secondary inorganic ions during haze.

5.1.2.7 Meteorological parameters

Meteorological parameters can influence the particle mass loading. In order to better understand the variations of particle mass concentration and composition during the different pollution events, investigations on the influences of meteorological parameters are necessary. Meteorological conditions during haze, dust and clear days at the CUGB in 2010-2011 and at the IAP in 2013 are listed in Table 5.2.

For both campaigns, haze days had the highest relative humidity at 69% in 2010-2011 and 70% in 2013, compared with dust and clear days. The previous studies showed that a high relative humidity could favor the formation of secondary inorganic ions (Sun et al., 2006). Dust days are always accompanied by a high wind speed. The average wind speed reached 5.3 m s^{-1} in 2010-2011 and 5.8 m s^{-1} in 2013. The very low wind speed during haze days (2.1 m s^{-1} in 2010-

2011 and 2.5 m s^{-1} in 2013) was not supportive of pollutant dispersion, but accelerated the increase in pollutants.

Table 5.2: Average values of meteorological parameters during haze, dust and clear days at the CUGB and the IAP

	CUGB			IAP		
	Haze	Dust	Clear	Haze	Dust	Clear
Temperature (°C)	16	14	10	19	18	18
Relative Humidity (%)	69	37	35	70	39	31
Air pressure (hPa)	1011	1011	1021	1011	1002	1011
Wind speed (m s^{-1})	2.1	5.3	4.4	2.5	5.8	4.1
Mixing Layer Height (m)	582	822	916	682	1234	1407

Mixing layer height decreased from clear days, through dust days and to haze days: 916 m, 822 m and 582 m, respectively in 2010-2011 and 1407 m, 1234 m and 682 m, respectively in 2013. Low MLH could also favor the accumulation of pollutants which leads to a high mass concentration of particles and the formation of haze days. Temperature and air pressure did not show large differences among these three categories in 2010-2011 and 2013.

The main meteorological differences between haze and clear days were the relative humidity and mixing layer height.

5.1.2.8 Influence on visibility

Both haze and dust can reduce visibility. In 2010-2011, the average visibilities during haze and dust days were 3.8 km and 7.6 km, respectively. In 2013, the average visibility during haze days was 4.5 km. Compared with the average visibility of dust days in 2010-2011, the visibility of dust days in 2013 was higher, reaching 8.5 km. This is because dust events in 2013 were only locally re-suspended dust which was only lasted for a short period.

5.1.3 Haze episodes

5.1.3.1 Seasonal variation of haze particles characteristics at the CUGB in 2010-2011

$PM_{4.3}$ average daily mean mass concentrations during haze events in summer 2010, autumn 2010, winter 2010, and spring 2011 were 108, 162, 197 and 147 μg m^{-3}, respectively. All the main chemical compound mass percentages are listed in Table 5.3.

Table 5.3: Chemical compound mass percentages in $PM_{4.3}$ (unit:%) during haze days and the haze/clear ratios of these mass percentages in different seasons at the CUGB in 2010-2011

	Summer 2010		Autumn 2010		Winter 2010		Spring 2011	
	Mass percentage	Haze/Clear	Mass percentage	Haze/Clear	Mass percentage	Haze/Clear	Mass percentage	Haze/Clear
OC	18.6	0.5	21.2	0.7	22.5	0.8	20.8	0.7
EC	4.2	0.7	4.5	0.7	4.1	0.7	4.5	0.8
SOC	7.8	0.4	6.0	0.7	13.8	0.9	2.1	0.2
K	1.6	1.6	1.3	0.8	2.5	1.7	2.1	1.7
Fe+Ca+Ti+Ba	2.9	0.6	2.9	0.5	4.1	0.7	5.2	0.9
Zn+Pb+As	0.7	2.3	0.6	1.3	0.7	2.3	0.9	2.6
NO_3^-+SO_4^{2-}+NH_4^+	49.0	5.2	49.0	4.1	33.9	2.2	31.1	2.5
Hopane	0.02	0.6	0.02	1.2	0.04	1.1	0.01	0.5
PAH	0.01	1.0	0.01	0.6	0.07	1.2	0.02	1.5
Levoglucosan	1.0	1.8	0.6	0.8	0.4	0.7	0.3	1.2

EC and OC showed no large variation during the whole year. SOC and K had the highest mass percentages in winter 2010. The sum of crustal element mass percentages, such as Fe, Ca, Ti and Ba, was the highest in spring 2011. The sum of anthropogenic element mass percentages, such as Zn, As and Pb, varied little during the whole year. Secondary inorganic ions showed the highest mass percentage in summer 2010 and autumn 2010. The mass percentages of hopanes and PAHs were the highest during winter time while levoglucosan had the highest mass percentage in summer 2010.

Compared with mass percentage in $PM_{4.3}$ during clear days, K increased during summer, winter and spring haze days. Zn, Pb, As and secondary inorganic ions increased during haze days in the whole year which indicated they are very important compounds for haze particles. The ratio of crustal elements during haze and clear days increased rapidly during spring when compared with other seasons. Mass concentration and mass percentage of PAHs and

levoglucosan increased rapidly during winter and summer haze days, respectively. Generally, secondary inorganic ions were found to be the dominant fraction of PM during haze days in the whole year.

As described in Chapter 4, some indexes were also used here in order to find out the main sources for particles during haze days in different seasons. The ratio of IND/(IND+BGH) during haze events in different seasons had a similar value, 0.55-0.56. Based on the knowledge mentioned in Chapter 4, coal combustion were stable sources of PAHs in $PM_{4.3}$ during haze days in the whole year. In addition, the ratio of levoglucosan to OC was the highest in summer 2010 with the value of 0.06, while it was only 0.03, 0.02, and 0.02 in autumn 2010, winter 2010 and spring 2011, respectively which indicates that $PM_{4.3}$ during haze days in summer had mainly originated from biomass burning. Both the homohopane and hopane indexes were the lowest in winter 2010, at 0.45 and 0.58, respectively and showed little variation in other three seasons. The homohopane indexes in summer 2010, autumn 2010 and spring 2011 were 0.57, 0.58 and 0.52, respectively and the hopane index were 0.86, 0.84 and 0.84, respectively during those same seasons. Therefore, coal combustion contributed more to $PM_{4.3}$ during haze days in winter when compared with other seasons. Because crustal element mass percentages increased significantly during haze days in spring, it is concluded that mineral dust was one important source of spring haze. During haze events in autumn, secondary inorganic ions showed the highest mass percentage, indicating the main sources of the haze particles were secondary inorganic ions.

In general, coal combustion, fuel oil combustion, biomass burning, secondary inorganic ions and mineral dust are the main sources for PM of haze pollution in Beijing.

5.1.3.2 Comparison of different haze episodes at the IAP in 2013

During spring 2013, three accumulation and dissipation processes of haze episodes were found at the IAP: from 18 April till 25 April (HE1), 3 May till 9 May (HE2), 1 June till 8 June (HE3) (Figures 5.4, 5.5 and 5.6). During these episodes, haze polluted (HP) days were from 21 till 23 April (HP1), 5 till 8 May (HP2) and 2 till 8 June (HP3). Previous studies have pointed out three types of haze: biomass burning, secondary inorganic ions pollution and dust (Huang et al., 2012). To get better understand of haze, the differences and agreements among these three haze pollution events are discussed in this section.

The average daily mean $PM_{2.5}$ mass concentration during HP1, HP2 and HP3 was 164 μg m^{-3}, 164 μg m^{-3} and 125 μg m^{-3}, respectively. Hence, HP1 and HP2 had higher $PM_{2.5}$ daily mean mass concentration than HP3. Precipitation could be one reason for the lower $PM_{2.5}$ mass concentration during HP3. The total precipitation during HP3 was 39.6 mm which was much higher than that during HP1 (0.0 mm) and HP2 (0.8 mm).

The mass percentages of chemical compounds in $PM_{2.5}$ during these three haze polluted events are shown in Table 5.4. Even though HP3 had the lowest $PM_{2.5}$ mass concentration, the mass percentage of secondary inorganic ions was the highest, compared with other two haze pollution events. The secondary inorganic ions contributed 56%, 54% and 61% to $PM_{2.5}$ mass concentration during HP1, HP2 and HP3, respectively, and the mass percentages of secondary inorganic ions were more than 50% during all three haze pollution events, which were much higher than that during haze events in spring 2011 (31%), indicating that the secondary inorganic ions were the most important compounds for $PM_{2.5}$ during haze in spring 2013. Some difference of secondary inorganic ions during these three haze polluted events can be observed, HP1 was affected much more by nitrate while HP2 and HP3 were influenced much more by sulfate because HP1 had the highest NO_3^- mass percentage while HP2 and HP3 had higher SO_4^{2-} mass percentages. The mass percentage of summed Zn, As and Pb was also the highest during HP1, with a value of 0.7%. The mass percentage of Ca, Mg, Al and Fe showed the highest value of 3.7% during HP2, but Cl^- contributed less to $PM_{2.5}$ mass than that during the other two haze polluted events.

Table 5.4: Mass percentages of chemical compounds in $PM_{2.5}$ during different haze polluted events at the IAP in spring 2013 (unit: %)

	Cl^-	NO_3^-	SO_4^{2-}	NH_4^+	OC	EC	Ca+Mg+Al+Fe	Zn+As+Pb	Other
HP1	2.1	24.1	19.7	12.4	10.1	2.3	2.6	0.7	25.9
HP2	0.6	16.1	24.5	13.3	12.0	3.6	3.7	0.4	25.7
HP3	2.3	17.4	26.0	17.2	10.0	4.0	2.8	0.6	19.7

The average equivalent concentration ratios of C/A during HP1, HP2 and HP3 were 0.9, 1.0 and 1.1, respectively, which indicates that the aerosols were more acidic during HP1 and more alkaline during HP3.

In section 5.1.2.7, MLH, RH and wind speed were found to be the most important meteorological parameters which can affect the PM loading. Therefore, in the following sections, these three parameters will be discussed in each haze episode. In section 5.1.2, secondary inorganic ions, Cl^-, As, Zn and Pb mass percentage were found to increased significant during haze days when compared with clear days. Therefore, these compounds will be also discussed in each haze episode in the following sections. Ca, Mg, Al and Fe will be also discussed because they originate from crustal sources. Additionally, in order to study the characteristics of particle transportation during the different haze polluted events, 72 h backward trajectories at three altitudes above the ground level (100 m, 500 m and 1000 m) were also computed in this section.

(1) HE1

In Figure 5.11, the variation of daily mean $PM_{2.5}$ mass concentration, MLH, RH and wind speed are shown. Obviously, MLH and wind speed decreased from 18 April to 20 April, which was one day before HP started, and became stable during HP, then increased again. RH showed the opposite variation. It increased from 18 April, and reached the highest value on 23 April, which had the highest $PM_{2.5}$ mass concentration, then started to decrease. With the variation of MLH, RH and wind speed, $PM_{2.5}$ mass concentration increased from 18 April and reached the highest value on 23 April. From this variation, one can concluded that, low MLH, low wind speed and high RH are not favorable for the dilution of pollutants, in other words, favorable for the form of haze.

The variation of chemical compound mass percentage in $PM_{2.5}$ during HE1 are shown in Figure 5.12 and seventy-two hours backward trajectories during HE1 are shown in Figure 5.13.

On 18 April (Figure 5.13 (a)), air flow came from the North at three altitudes of 100 m, 500 m and 1000 m. Secondary inorganic ions, Cl^-, and sum of Zn, As and Pb had low mass percentages in $PM_{2.5}$ on this day. Because air flow passed Inner Mongolian sandy lands, crustal elements had the highest mass percentages. From this day on, secondary inorganic ion, Cl^-, and sum of Zn, As and Pb mass percentages started to increase while crustal element mass percentage started to decrease. Cl^-, NH_4^+ and sum of Zn, As and Pb mass percentages reached their first peak value on 19 April.

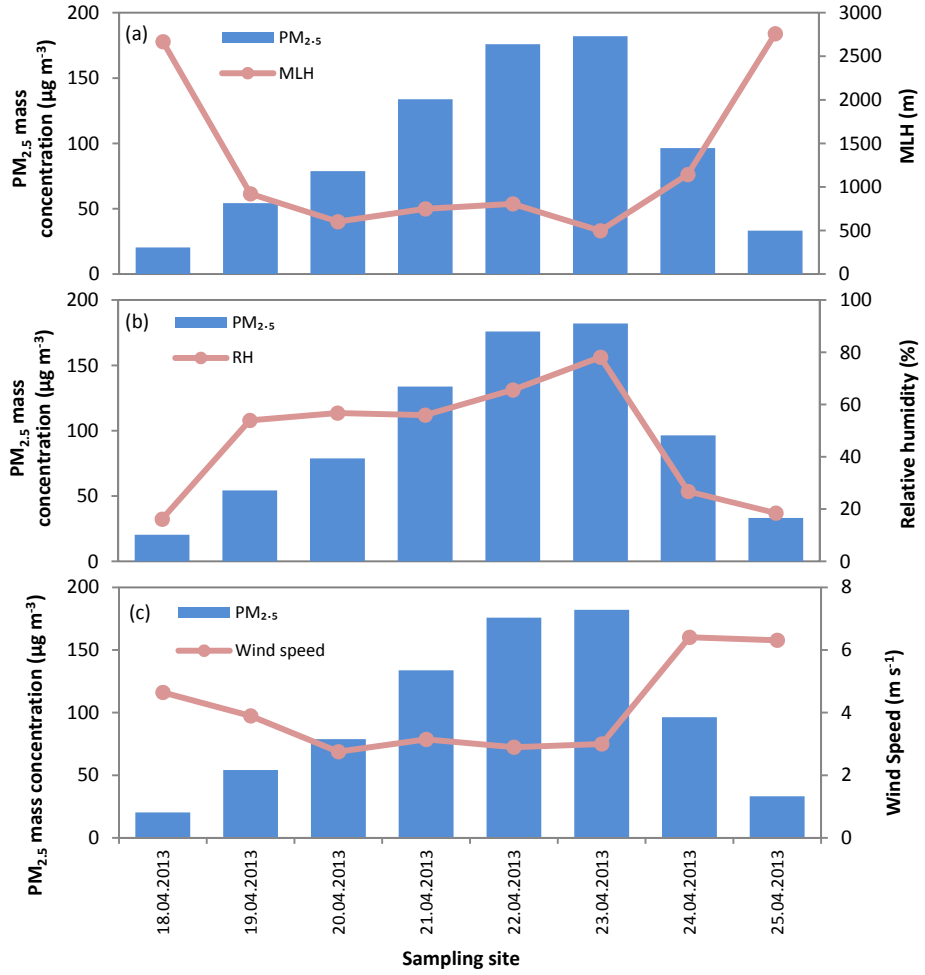

Figure 5.11: Variation of daily mean $PM_{2.5}$ mass concentration, (a)MLH, (b)RH and (c)wind speed during HE1 at the IAP in spring 2013

Figure 5.13 (b) shows air flow at three altitudes originated from the North, passed Bohai Sea, Tangshan city and Tianjin Municipality, and arrived at Beijing from the South. Air flow from Bohai sea can transport Cl^- to Beijing while Tangshan city and Tianjin Municipality, which are heavy industrial cities, can pass Zn, As and Pb to Beijing. On 20 April (Figure 5.13 (c)), air flows at three altitudes were still from the North but there was a little difference from 19 April. Air flow at 1000 m passed Tangshan city, then turned to north again and arrived at Beijing from the North. Air flow at 500 m passed Bohai Sea, Tangshan city and Tianjin Municipality to Beijing from the South. Air flow at 100 m passed Tangshan city and Tianjin Municipality to Beijing from the South. SO_4^{2-} and NO_3^- reached their first peak value of mass percentages. On 21 April, mass percentage of summed Ca, Mg, Al and Fe increased a little and mass growth rate

reached 109.5%. Figure 5.13 (d) shows that the air flow at 1000 m was from the Southeast, turned to the North which can bring crustal elements from Inner Mongolian sandy lands and reached Beijing from the Southwest.

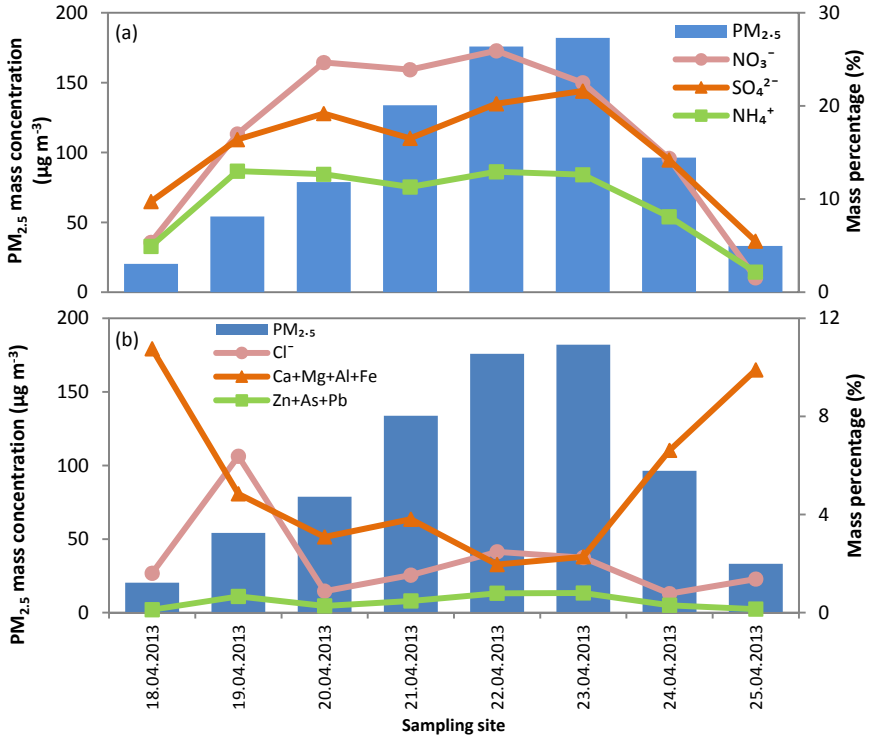

Figure 5.12: Variation of daily mean chemical compound mass percentage in $PM_{2.5}$ during HE1 at the IAP in spring 2013

On 22 April (Figure 5.13 (e)), Cl^-, NH_4^+, NO_3^- and sum of Zn, As and Pb showed the second peak value of their mass percentages. Air flow at 100 m was from the South, and air flow at 500 m came from the Southeast and reached Beijing from the South. These two air flows passed Baoding and Shijiazhuang cities which are industrial city can bring the pollutant from these cities. During HE1, Cl^- and K^+ correlated well with the correlation coefficients (R) of 0.89, which suggested that biomass burning could have been the source for Cl^-. Mass percentages of Cl^-, $NH_4^+$and NO_3^- decreased on 23 April. Air flows at 100 m and 500 m were still from the South but air flow at 1000 m came from the Northwest (Figure 5.13 (f)). SO_4^{2-} mass percentage reached the second peak value on this day. It could be caused by the emission from Zhangjiakou fossil-fuel power station located on the Northwest of Beijing which can produce

the precursor of SO_4^{2-}. Crustal element mass percentage increased again on this day, especially increased rapidly on 24 and 25 April because the air flows at three altitudes on these two days came from the Northwest of Beijing (Figure 5.13 (g) and (h)), Gobi Desert which can transport crustal elements to Beijing.

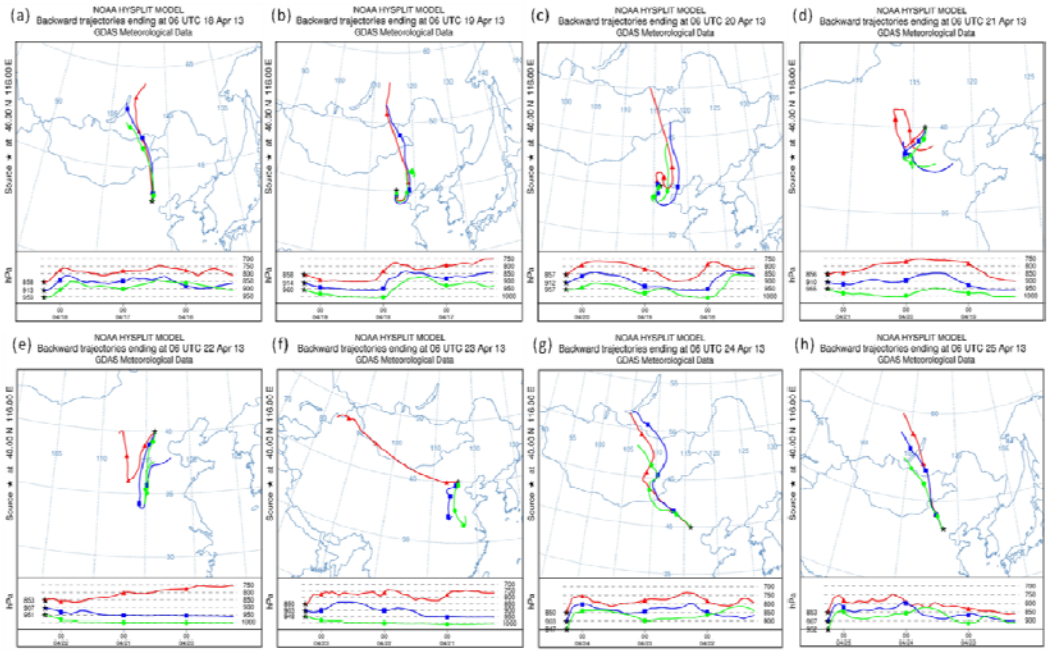

Figure 5.13: 72 h backward trajectories at different altitudes above ground level (red: 1000 m; blue: 500 m; green: 100 m) of HE1 calculated by the NOAA HYSPLIT model

(2) HE2

The second haze episode (HE2) was from 3 May April till 9 May April. The haze polluted days occurred on 5 May April and lasted until 8 May April. The variation of daily mean $PM_{2.5}$ mass concentration, MLH, RH and wind speed are shown in Figure 5.14.

Compared with HE1, from Figure 5.14, the same results were found. With low MLH, low wind speed and high RH, high $PM_{2.5}$ mass concentration was found. Even though low MLH, low wind speed and high RH was observed on 9 May, $PM_{2.5}$ mass concentration was not high on that day. This result could be caused by precipitation which can favor the wet deposition of PM. The amount of precipitation on 8 May and 9 May was 0.6 mm and 0.2 mm, respectively.

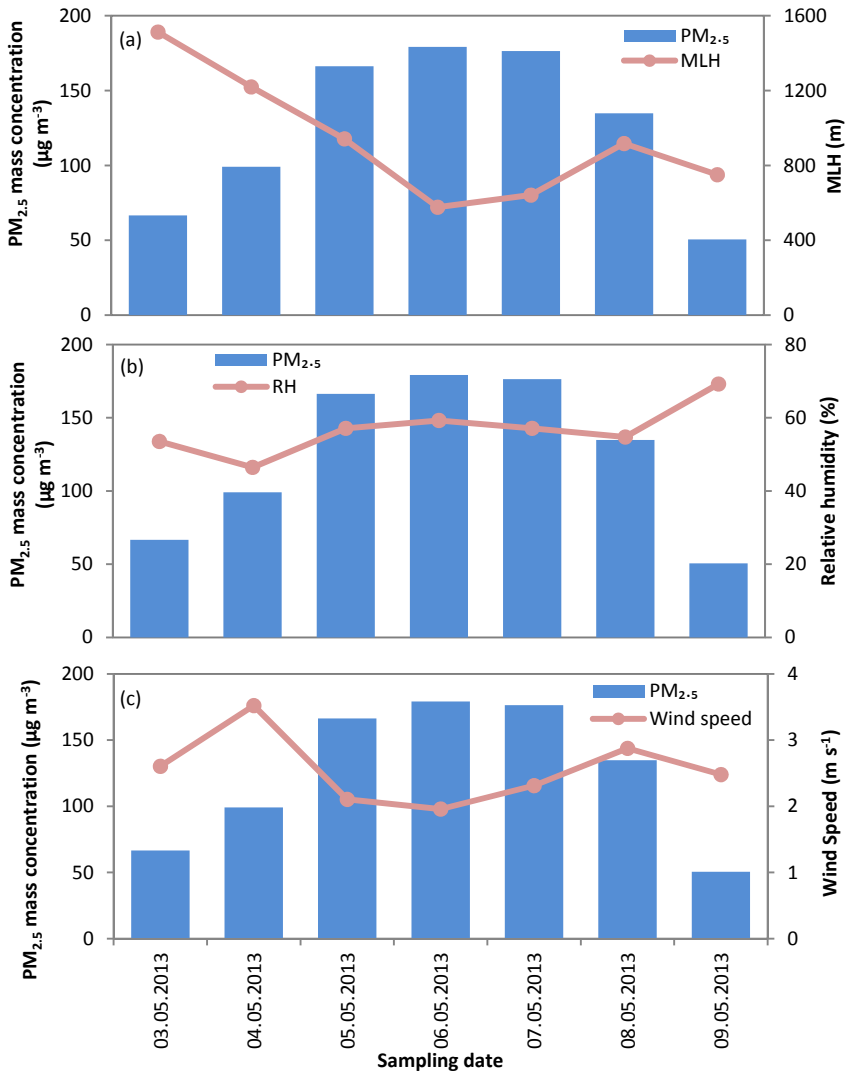

Figure 5.14: Variation of daily mean $PM_{2.5}$ mass concentration, (a)MLH, (b)RH and (c)wind speed during HE2 at the IAP in spring 2013

The variation of chemical compound mass percentage in $PM_{2.5}$ during HE2 are shown in Figure 5.15 and seventy-two hours backward trajectories during HE2 are shown in Figure 5.16. All air flows at the altitudes of 100 m, 500 m and 1000 m were found to come from the Southeast of Beijing, except for air flow at 1000 m on 9 May.

Compared with the variation of the same compound mass percentage during HE1, the difference is NO_3^- and NH_4^+ had the highest mass percentage on 9 May which was non-haze day with low $PM_{2.5}$ mass concentration. The reason could be relative humidity on 9 May was

the highest during HE2. As mentioned in Chapter 4, high relative humidity can enhance NO_3^- and NH_4^+ mass concentration (Pathak et al., 2009; Ianniello et al., 2010, 2011). SO_4^{2-} mass percentage increased with the increase in $PM_{2.5}$ mass concentration. Mass percentage of summed Zn, As and Pb showed little variation during HE2, because air flows during the whole HE2 were from the similar direction, southeast, indicating that when air flows were from the similar direction, the mass percentage of Zn, As and Pb was stable. Mass percentage of summed Ca, Mg, Al and Fe had two peaks. One was on 4 May and the other one was on 8 May. No air flows on these two days were observed from desert area or sandy area. Therefore, this is probably caused by the local source, such as reconstruction activities on the roof on these two days. Cl^- mass percentage increased rapidly on 8 May. From the Figure 5.16, air flow on each day during HE 2 passed Bohai Sea to Beijing and wind speed on 8 May was relative high which can bring more Cl^- to Beijing. During HE2, the correlation coefficient of Cl^- and K^+ was 0.5. Therefore, Cl^- probably originated from the Sea.

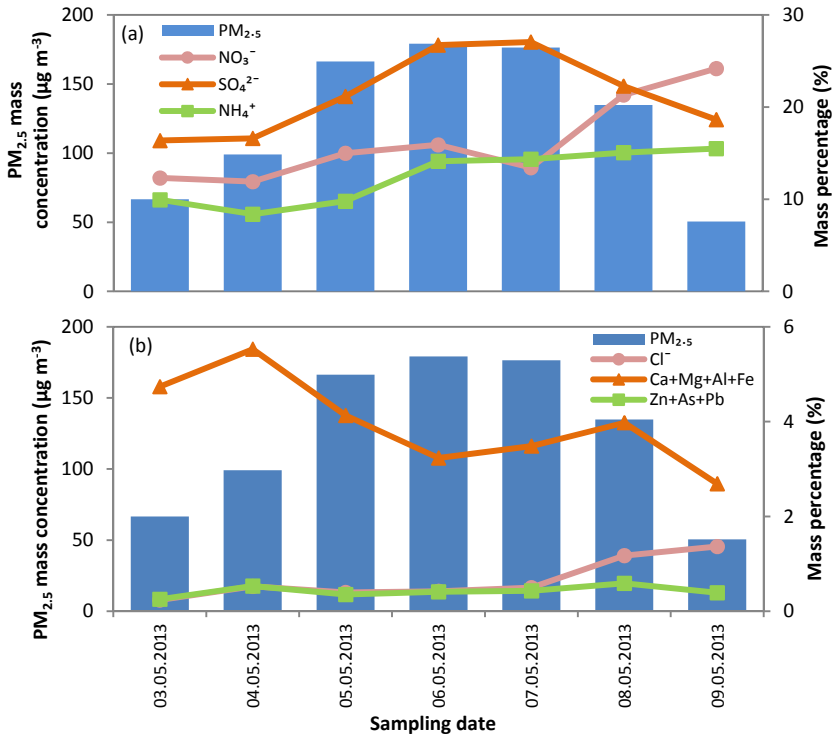

Figure 5.15: Variation of daily mean chemical compound mass percentage in $PM_{2.5}$ during HE2 at the IAP in spring 2013

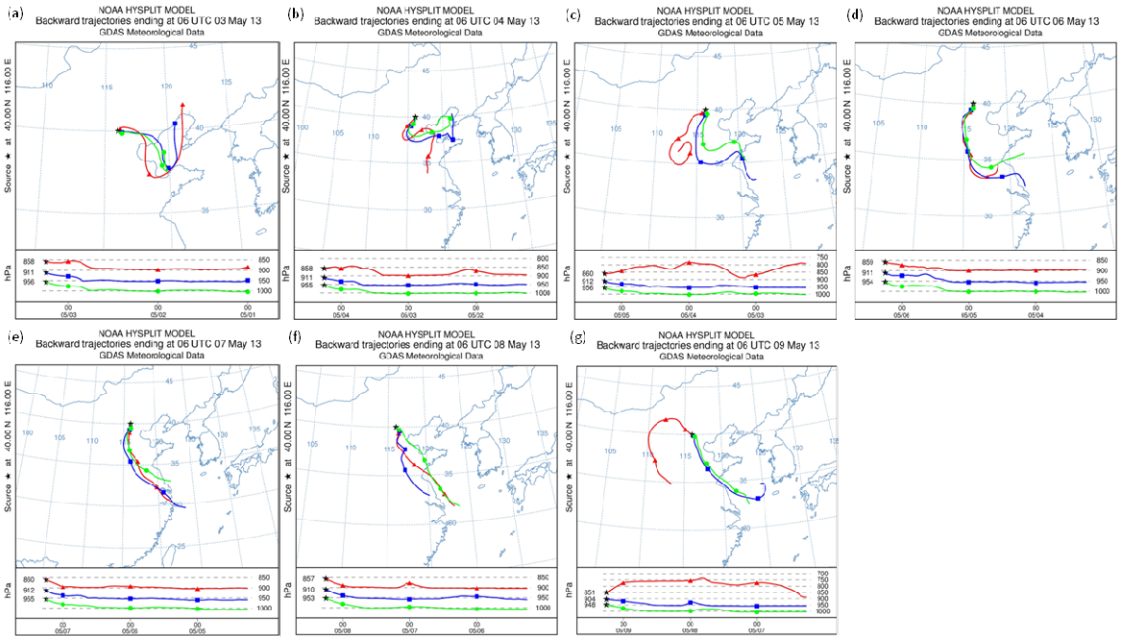

Figure 5.16: 72 h backward trajectories at different altitudes above ground level (red: 1000 m; blue: 500 m; green: 100 m) of HE2 calculated by the NOAA HYSPLIT model

(3) HE3

The daily mean variation during HE1 and HE2 was discussed above. However, the sampling frequency was increased from 24 h to 4 h intervals, to further understand the characteristics of $PM_{2.5}$ during haze episodes. In this study, the sampling period was only changed during HE2 and HE3. As the time change was only carried out in the middle of HE2, therefore, more attention on high time resolution sampling was focused on HE3 in this section.

Considering incomparable between different sampling time, so the discussion only included data from 4 h sampling. In Figure 5.6, the sampling frequency with 4 h intervals started since on 3 June 20:00 - 24:00. The variation of average 4 h $PM_{2.5}$ mass concentration, MLH, RH, precipitation and wind speed are shown in Figure 5.17.

Obviously, compared with HE1 and HE2, the correlations of $PM_{2.5}$ mass concentration and meteorological parameters during HE3 are different. RH during HE3 was higher than during HE1 and HE2. One reason was precipitation which can cause high RH, and the other reason was HE3 was not only haze days, but also fog days. RH was found to have negative correlation with $PM_{2.5}$ mass concentration. The main reason could be that the amount of precipitation

during HE3 (39.6 mm) was much higher than during HE1 (0 mm) and HE2 (1 mm). The influence of MLH and wind speed on $PM_{2.5}$ mass loading was not significant.

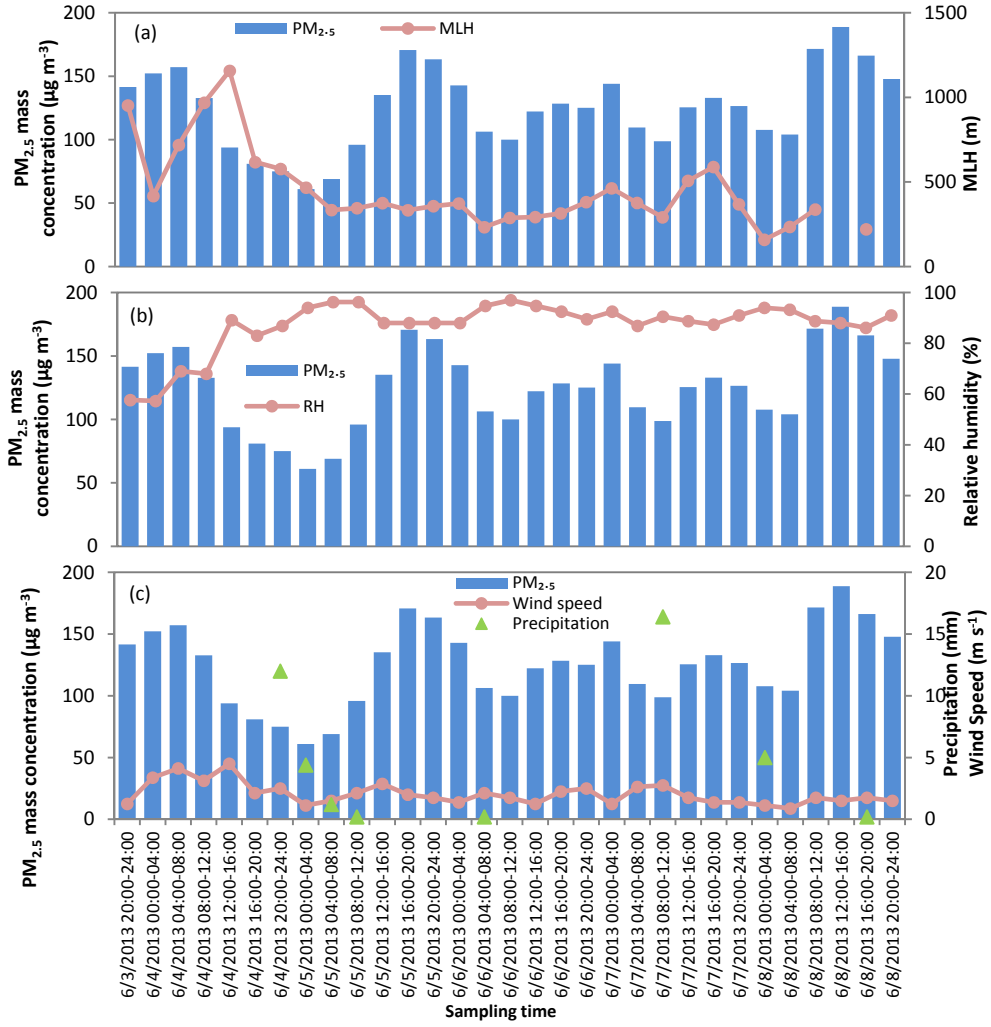

Figure 5.17: Variation of daily mean $PM_{2.5}$ mass concentration, (a)MLH, (b)RH and (c)wind speed and precipitation during HE3 4 h sampling period at the IAP in spring 2013

Seventy-two hours backward trajectories of 4 h sampling period during HE3 were used to analyze the influence from the regional area (Figure 5.18). For each 4 h, the middle time was used as the ending time to trace backward. Therefore, backward trajectories ending at local time 02:00, 06:00, 10:00, 14:00, 18:00 and 22:00 every day were obtained. The regional

dominant air flow was found to be from the Southeast (Figure 5.18). Except for the regional wind direction, local wind direction is also very important for $PM_{2.5}$ mass loading (Figure 5.19).

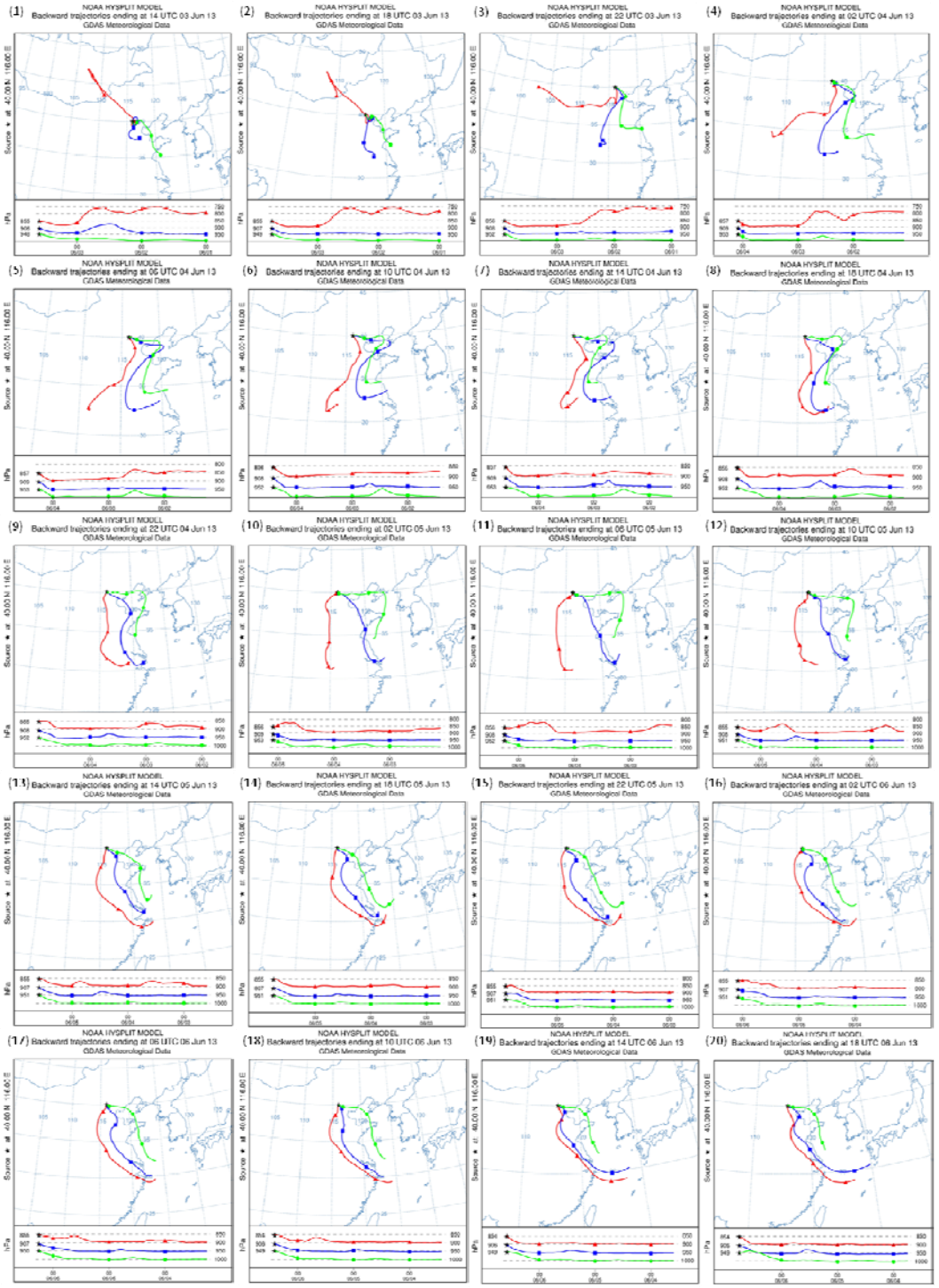

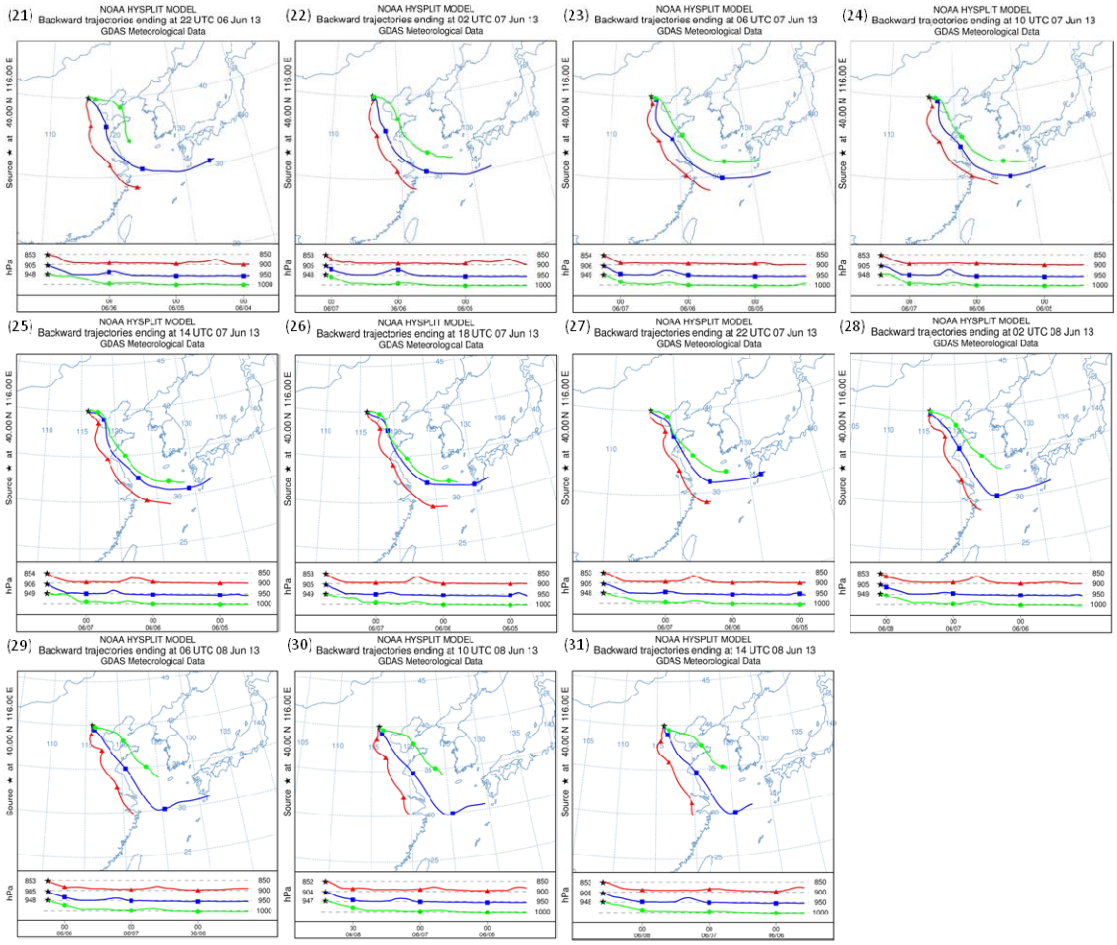

Figure 5.18: 72 h backward trajectories at different altitudes above ground level (red: 1000 m; blue: 500 m; green: 100 m) of HE3 4 h sampling period calculated by the NOAA HYSPLIT model: (1)2013-06-03 22:00; (2)2013-06-04 02:00; (3)2013-06-04 06:00; (4)2013-06-04 10:00; (5)2013-06-04 14:00; (6)2013-06-04 20:00; (7) 2013-06-04 22:00; (8)2013-06-05 02:00; (9)2013-06-05 06:00; (10)2013-06-05 10:00; (11)2013-06-05 14:00; (12)2013-06-05 20:00; (13) 2013-06-05 22:00; (14)2013-06-06 02:00; (15)2013-06-06 06:00; (16)2013-06-06 10:00; (17)2013-06-06 14:00; (18)2013-06-06 20:00; (19) 2013-06-06 22:00; (20)2013-06-07 02:00; (21)2013-06-07 06:00; (22)2013-06-07 10:00; (23)2013-06-07 14:00; (24)2013-06-07 20:00; (25) 2013-06-07 22:00; (26)2013-06-08 02:00; (27)2013-06-08 06:00; (28)2013-06-08 10:00; (29)2013-06-08 14:00; (30)2013-06-08 20:00; (31) 2013-06-08 22:00.

During this 4 h sampling period, three times increase and decrease processes of $PM_{2.5}$ mass concentration was found. Three peaks during this 4 h sampling period: on 4 June 4:00 – 8:00, on 5 June 16:00 – 20:00 and on 8 June 12:00 – 16:00 (Figure 5.17). $PM_{2.5}$ mass concentration increased from 3 June 20:00 - 24:00 and reached the first peak on 4 June 4:00 – 8:00, 157 μg m^{-3}. After 12:30, the wind direction changed to the North and very strong instantaneous wind speed was found (11 m s^{-1}), which led to a decrease in $PM_{2.5}$ mass concentration. Precipitation

also favored the wet deposition of $PM_{2.5}$. The $PM_{2.5}$ mass concentration continued decreasing until 0:00 – 4:00 on 5 June with the value of 61 μg m^{-3}. At 5:00 on 5 June the prevailing wind direction changed to the Southeast again. The $PM_{2.5}$ mass concentration kept increasing thereafter and attained the second peak at 16:00 – 20:00 on 5 June, 171 μg m^{-3}. After this, the $PM_{2.5}$ mass concentrations fluctuated around 120 μg m^{-3}. Since 8 June 9:00, wind direction changed to the Southeast again and $PM_{2.5}$ mass concentration increased again from 8 June 8:00 on and reached the third peak value of $PM_{2.5}$ mass concentration (189 μg m^{-3}). During 8 June evening, wind direction changed to the North once again. As a result, $PM_{2.5}$ mass concentration started to decrease. From the discussion above, it can be seen that meteorological parameters are very important for determining the $PM_{2.5}$ mass loading.

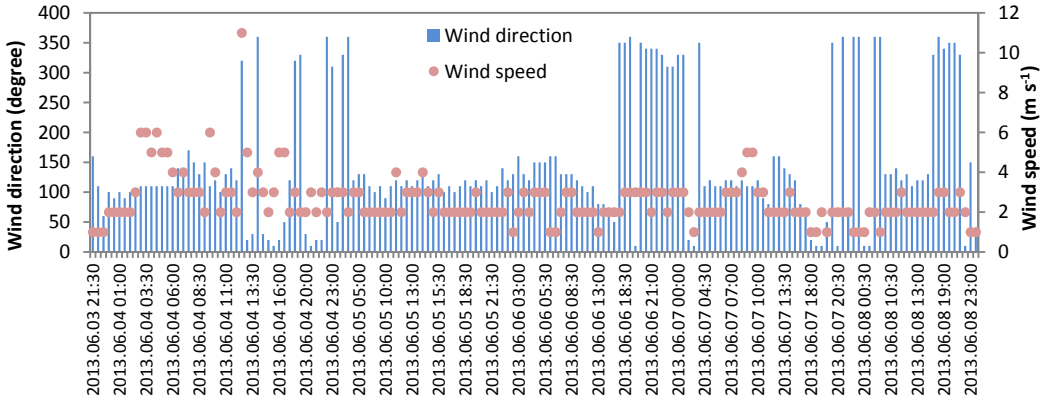

Figure 5.19: Wind direction and wind speed (ZBAA data) during HE3 4 h sampling period at the IAP in spring 2013

The average $PM_{2.5}$ mass concentration of each 4 h in one whole day showed that the highest $PM_{2.5}$ mass concentration was during 16:00 – 20:00 (Figure 5.20). The possible reason was that the period of 16:00 – 20:00 was rush hours when people had departed from work, thus causing even more traffic emission. Elemental carbon contributed 4.4% (the third highest mass percentage of EC in $PM_{2.5}$ during the whole day) to $PM_{2.5}$ during this time period which also supported this reasoning.

During midnight, $PM_{2.5}$ mass concentration remained at a high level, because of heavy-duty trucks passing Beijing which also contributed significantly to $PM_{2.5}$ mass. According to the rules of truck management, the trucks of Beijing only can pass along the 5th ring from 23:00 till 6:00

every second day, while the trucks of other cities from 0:00 till 6:00 every second day (Song et al., 2012). During 0:00 – 4:00, EC contributed 4.9% to $PM_{2.5}$ mass, which was the highest sampled during all periods. The second highest EC mass percentage was 4.5% on 20:00 – 24:00. Previous studies have pointed out that heavy-duty truck emissions is an important source of EC in Beijing (Wang et al., 2009a; Song et al., 2012).

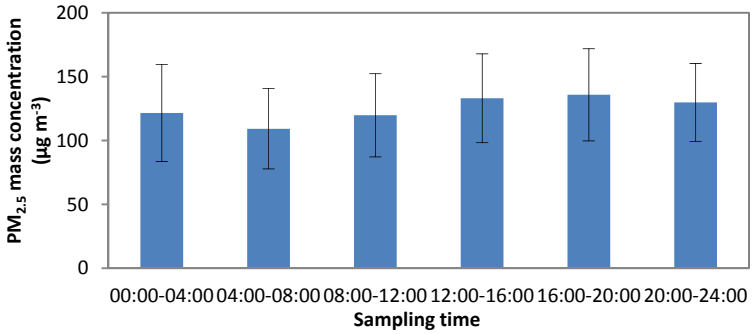

Figure 5.20: The average $PM_{2.5}$ mass concentration during HE3 4 h sampling period at the IAP in spring 2013

The variations of chemical compound mass percentages in $PM_{2.5}$ during HE3 4 h sampling period are shown in Figure 5.21. NO_3^- mass percentage showed an obvious variation that had a high value during night and early morning (0:00 – 8:00) and a low value during day (12:00 – 20:00). Because during day, the temperature is high when comparing with during night, which accelerate the volatilization of NO_3^- and destruction into NO_x. In addition, much more precursors of NO_3^- (NO_x) are emitted by the heavy-duty trucks during night which can enhance the mass percentage of NO_3^-. SO_4^{2-} mass percentage varied with $PM_{2.5}$ mass concentration basically and had the highest values between about 12:00 and 20:00. This is caused by stronger solar radiation during day which accelerates the formation of secondary sulfates from SO_2. NH_4^+ showed no clear daily variation.

Crustal elements were found to have a high value of mass percentage during low $PM_{2.5}$ mass concentration (Figure 5.21 (b)). This was caused by the decrease in mass percentage of other compounds. The variation of anthropogenic elements, Zn, As and Pb, showed a little variation means that the sources of these elements are stable. This is supported by the back trajectories which showed that the air flows originated from the Southeast. Cl^- had two peaks on 3 June

20:00 – 24:00 and 7 June 8:00 – 12:00, respectively (Figure 5.21 (b)). Figure 5.18 (1) indicated that Cl^- on 3 June 20:00 – 24:00 could be from coal combustion, because 1000 m height air flow passed through Zhangjiakou city which has fossil-fuel power station. Even though air flow on the same height was also from the Northwest on 4 June 0:00 – 4:00, because wind speed was much higher (Figure 5.17 (c)) which can speed up the dilution of pollutant, Cl^- mass concentration and percentage decreased. On 7 June 8:00 – 12:00, Figure 5.18 (22) showed that air flows originated from the Southeast, but the molar ratio of Cl^- and Na^+ was 8.6, much higher than during sea water (1.17) which indicated Cl^- originated from other sources. K^+ had the highest mass concentration at the same time, which indicated that Cl^- could originate from biomass burning.

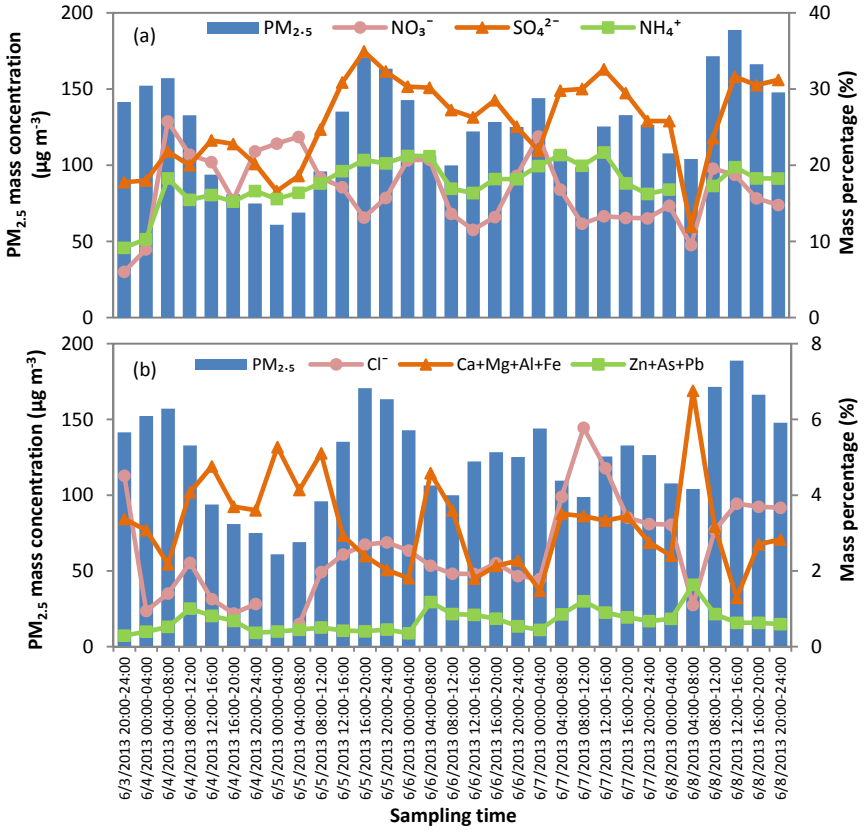

Figure 5.21: Variation of chemical compound mass percentage in $PM_{2.5}$ during 4 h sampling period of HE3 at the IAP in spring 2013

In general, secondary inorganic ions were the most important fraction of $PM_{2.5}$ during these three haze episodes in spring 2013. Biomass burning and re-suspended crustal elements from local or non-local sources could also be the sources.

5.1.4 Dust storm

5.1.4.1 Comparison between different dust events

In spring 2011, there were two dust storms with a higher $PM_{4.3}$ mass concentration on 17 and 30 April, but there were also differences between these two events. The mass percentages of each element are given in Figure 5.22.

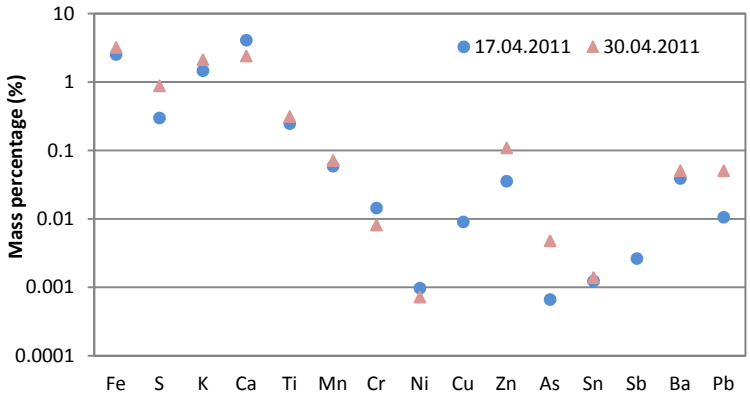

Figure 5.22: The mass percentage of each inorganic element in $PM_{4.3}$ at the CUGB during dust storm events in spring 2011

The mass percentage of Ca in $PM_{4.3}$ on 17 and 30 April was 4.1% and 2.4%, respectively, because Ca had originated from not only geogenic sources, but also construction materials, such as mortar and concrete. On 17 April, there was the roof of a supermarket under re-construction located about 100 m to the North of the sampling site. The 72 h backward trajectories of the 17 and 30 April dust events were calculated (Figure 5.23) and showed that the air pollutants on 17 and 30 April were transported from the North and Northwest, respectively. Dust was observed on 30 April coming from the Gobi desert and passing through the Shanxi and Hebei Provinces which can then bring further pollution from these two

provinces to Beijing. That is why S, Zn, As and Pb showed higher mass concentrations on 30 April. In general, the air pollutants on 17 and 30 April originated from the sandy lands and Gobi Desert, respectively.

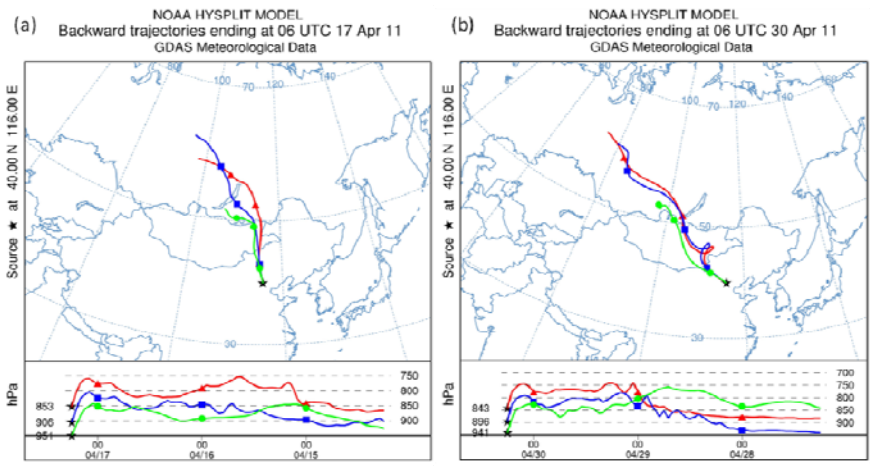

Figure 5.23: 72 h backward trajectories at different altitudes above the ground level (red: 1000 m; blue: 500 m; green: 100 m) of two dust events on (a) 17 April and (b) 30 April in 2011 which were calculated with the NOAA HYSPLIT model

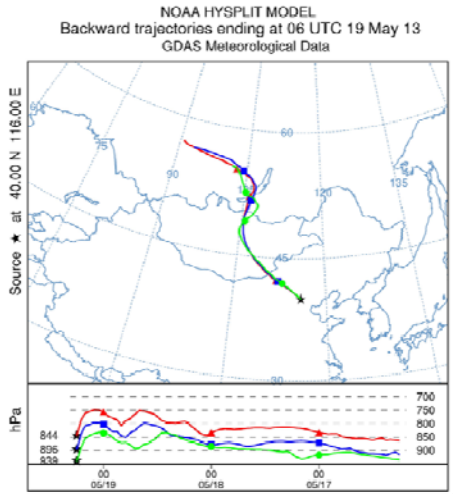

Figure 5.24: 72 h backward trajectories at different altitudes above the ground level (red: 1000 m; blue: 500 m; green: 100 m) of the dust event on 19 May 2013 14:00 (local time) which were calculated with the NOAA HYSPLIT model

In spring 2013, one dust event was observed on 19 May mixed with haze. The 72 h backward trajectories (Figure 5.24) showed air flows at different altitudes above ground level (100 m (red line), 500 m (blue line) and 1000 m (green line)) came from the Northwest of Beijing and indicated that it can bring dust from Gobi Desert to Beijing.

5.1.4.2 Element ratio Mg/Al

The mineral particles in Beijing are affected by not only the sources inside, but also the sources from outside of Beijing. Estimating the contributions of the sources from inside and outside of Beijing is useful for managing the air pollution in Beijing.

The ratio of Mg/Al has been used as a reliable tracer to differentiate dust sources (e.g. Sun et al., 2004a; Han et al., 2005), and the estimation of the relative contributions of mineral particles from different sources (inside and outside Beijing) to total mineral particles was calculated based on the following equations (Sun et al., 2004a):

$$(Mg/Al)_{Particle} = m \times (Mg/Al)_{Local} + n \times (Mg/Al)_{Non\text{-}local} \quad (5\text{-}1)$$

$$m + n = 1 \quad (5\text{-}2)$$

where $(Mg/Al)_{Particle}$ is the mass ratio of Mg/Al in the PM samples in Beijing, $(Mg/Al)_{Local}$ is the average mass ratio of Mg/Al in Beijing soil samples, $(Mg/Al)_{Non\text{-}local}$ is the average mass ratio of Mg/Al in soil samples from outside of Beijing, and m and n are the contributions of mineral particles from inside and outside of Beijing to the total mineral particles, respectively.

The values of $(Mg/Al)_{Local}$ and $(Mg/Al)_{Non\text{-}local}$ were given in the previous study (Sun et al., 2004a) as 0.45 and 0.175, respectively.

During the first campaign at the CUGB, no Mg and Al data is available, the estimation cannot be done. During the second campaign at the IAP, an obvious a dust event happened on 19th May 2013. The mass ratio of Mg to Al was 0.38. According to the formula mentioned above, during this event, the sources from outside and inside Beijing contributed 25.5% and 74.5% to the total mineral particles in $PM_{2.5}$, respectively.

5.2 Summary

The characteristics of particles during haze, dust and clear days at the CUGB in 2010-2011 and at the IAP in 2013 were discussed and a comparison between haze, dust and clear days was also performed in this chapter.

Particle pollution was extremely heavy during haze and dust events. $PM_{4.3}$ mass concentration showed a decreasing trend from dust, through haze, to clear days while $PM_{2.5}$ mass concentration was in the sequence of haze > dust > clear which indicated that dust particles were mainly coarse particles while haze particles were dominated by fine particles.

Secondary inorganic ion concentrations increased rapidly during the haze days. Mass percentages of secondary inorganic ions in $PM_{4.3}$ were 41.4%, 13.2% and 13.2% during haze, dust and clear days, respectively and reached 56.6%, 12.9% and 24.2% in $PM_{2.5}$ during haze, dust and clear days, respectively. The highest mass percentages of secondary inorganic ions was found during haze days in both size of particles which indicated that haze particles were also dominated by fine particles. This result was support by the $PM_{2.5}/PM_{10}$ ratio.

In $PM_{2.5}$, the average equivalent concentration ratios of C/A during haze, dust and clear days were 1.1, 1.8 and 1.6, respectively, which indicated that the particles were more alkaline during dust days than those during clear and haze days.

By comparing the inorganic elements mass ratio of haze/clear and dust/clear, Fe, Ca and Ba were proposed to represent dust particles, and Zn, As and Pb were suggested to indicate haze particles.

Secondary inorganic ions were found to be the most important part of PM during the whole year haze days. Additionally, biomass burning was an important source for summer haze, coal combustion was an important source for winter haze, dust was an important source for spring haze.

Meteorological parameters are important for influencing particle mass loading and the affection of meteorological parameters are complicate and interaction. With low MLH, low wind speed and high RH, high $PM_{2.5}$ mass concentration was always found. Precipitation was also found to reduce the PM mass concentration. Influence of regional and local wind cannot be ignored. Air flows from the Northerly during night bring less pollutant to Beijing than from the Southerly.

Backward trajectories showed the different air flows during three haze episodes in 2013. Basically, air flows from the Southerly were the dominant sources of haze in 2013. Data from 4 h sampling was investigated in detail. Average $PM_{2.5}$ mass concentration had the highest value during 16:00 – 20:00 in one day. NO_3^- mass percentage showed an obvious variation that had a high value during night and early morning (0:00 – 8:00) and a low value during day (12:00 – 20:00) while SO_4^{2-} mass percentage varied with $PM_{2.5}$ mass concentration basically and had high value between 12:00 and 20:00.

Backward trajectories were also used to distinguish the sources of different dust events. The back trajectories showed that the air pollutants were transported from the North and Northwest on 17 and 30 April, respectively, suggesting that the air pollutants on 17 and 30 April had originated from the sandy lands and Gobi Desert, respectively. The dust event on 19 May, 2013 was investigated and sources from outside and inside Beijing contributed 25% and 75% to the total mineral particles in $PM_{2.5}$, respectively, during the dust event on 19 May 2013 as identified by the ratio of Mg/Al.

Chapter 6 Source apportionment

PM has been found to affect the environment, climate and human health in previous studies (Satheesh et al., 2005; Shao et al., 2006; Cao et al., 2012; Dimitrova et al., 2012; IPCC 2013). In order to make the development of effective control strategies to improve the air quality of Beijing, a clear understanding of the potential PM sources is required.

6.1 Positive matrix factorization (PMF)

PMF has been applied extensively worldwide, such as in Hong Kong, China (Lee et al., 1999), Toronto, Canada (Lee et al., 2003), Seoul, Korea (Heo et al., 2009), Navarra, Spain (Aldabe et al., 2011), Augsburg, Germany (Gu et al., 2011), St Louis, USA (Amato and Hopke, 2012), and the Northern Yellow Sea, China (Wang et al., 2013). PMF has also been used widely in the studies of $PM_{2.5}$ in Beijing and the review of source apportionment of Beijing $PM_{2.5}$ by PMF are listed in Table 6.1.

Previous studies (Table 6.1) used EC, OC, inorganic elements, ions, and PAHs data for source apportionment. The major sources of $PM_{2.5}$ in Beijing from these studies can be concluded as: dust, biomass burning, coal combustion, industry, vehicle emission and secondary particles. Unfortunately, these studies only used inorganic or organic compounds when they performed source apportionment and the durations of sampling were short or discontinuous. Source apportionments of PM in Beijing by using PMF with continuous long-term inorganic and organic compounds are quite rare. Therefore, a full year of continuous data is needed to obtain a precise source apportionment. In this study, continuous one year daily mean PM samples were analyzed for inorganic elements, water soluble ions, EC/OC, hopanes, PAHs and levoglucosan to perform source appointment by PMF. The detailed description of PMF and data treatment is presented in Chapter 3.

Source apportionment

In this chapter, source apportionments of $PM_{4.3}$ at the CUGB during 2010-2011 and $PM_{2.5}$ at the IAP during 2013 by using PMF are presented.

Table 6.1: Previous studies of source apportionment on $PM_{2.5}$ in Beijing by using PMF

Sampling site	Sampling period	Measured components	Major sources	Reference
Suburban	2002.03.18-2002.05.10	Inorganic elements	Two area types and four source types, as soil, limestone quarry, crop burning and mixture of residue motor and coal burning	Lei et al., 2004
Five locations	January, April, July, and October 2000	Inorganic elements; Ions; EC/OC	Biomass burning (11%); Secondary sulfates (17%); Secondary nitrates (14%); Coal combustion (19%); Industry (6%); Motor vehicles (6%); Road dust (9%); Others (18%)	Song et al., 2006a
Five urban sites and one rural site	January and August 2004	Inorganic elements; Ions; EC/OC	Coal combustion; Secondary sulfate; Secondary nitrate; Biomass burning; Vehicle emissions; Road dust	Song et al.,2007
Beijing Normal University	Dry and wet seasons, 2001-2004	Inorganic elements and ions	Soil dust (20%); Biomass burning (12%); Secondary particles (19%); Coal combustion (14%); Vehicle emission (28%); Industry (5%); Unknown (2%)	Zhang et al., 2007
Beijing Normal University	Summer and winter, 2001-2006	Inorganic elements and ions	Coal combustion (17%); Biomass burning (12%); Non-local dust (7%); Local dust (9%); industry (9%); Secondary nitrate (15%); Secondary sulfate (13%); vehicle emission (6%); Others (12%)	Wang et al., 2008b
Northwest suburb	Summer and winter, 2005-2007	Inorganic elements; Ions; EC/OC; PAHs	Biomass burning (4%); Coal combustion (21%); Secondary ions (28%); Road dust (17%); Soil (2%); Manufacture activities (9%); Vehicle emission (4%); Unidentified source associated with F^- (10%); Others (5%)	Wang et al., 2009b
Beijing Normal University	2010.01.01-2010.12.31	Inorganic elements	Secondary sulphur (27%); Vehicle emission (17%); Fossil fuel combustion (16%); Road dust (13%); Biomass burning (11%); Soil dust (10%); Metal processing (6%)	Yu et al., 2013
North 4^{th} Ring Road	Summer and winter, 2008-2009	PAHs	Diesel vehicles; Gasoline vehicles; Coal combustion	Wu et al., 2014

6.2 Results and discussion

6.2.1 Source apportionment of $PM_{4.3}$ at the CUGB (2010.06.21 – 2011.06.21)

6.2.1.1 PMF

Based on the data selection criterion which were mentioned in Chapter 3.4, 321 daily mean $PM_{4.3}$ samples with 31 species collected at the CUGB from June 2010 till June 2011 were used in the PMF analysis. Although it was found that 46% of Cl^- values and 60% of PIC values were lower than LOQ, both were not be excluded from PMF analysis because Cl^- and PIC are important tracers for coal combustion, but set as weak variables to reduce their influence on the model. A summary of chemical compounds which were used in PMF is listed in Table 6.2.

The $PM_{4.3}$ mass concentration was also included in PMF to apportion mass concentration of factors, but it was marked as "total variable" which was grouped into "weak category" automatically by model in order to reduce its influence on PMF solution. PMF was run several times with different factor numbers (4-12) to determine the most reasonable number of factors. Finally, six factors were determined to be the most meaningful result. After a reasonable solution was selected, a 100 bootstrap was run (minimum R^2 = 0.6) to check its stability. Of the 100 runs, factor 1, factor 2 and factor 6 only had 2, 2 and 3 bootstraps unmapped, respectively, while all the remaining three factors had all bootstraps mapped. Therefore, the solution with six factors was considered as stable result.

The comparison between daily mean modeled $PM_{4.3}$ mass concentrations by PMF and daily mean measured $PM_{4.3}$ mass concentrations is shown in Figure 6.1. It shows that the model can adequately reproduce the measured $PM_{4.3}$ mass concentration with a correlation (R^2) of 0.93 and a slope of 0.96.

Six factors including mixture of secondary sulfate formation and biomass burning, secondary nitrate formation, mineral dust, industry, coal combustion and traffic were determined. These sources had average mass contributions of 18%, 11%, 36%, 11%, 6% and 18%, respectively (Figure 6.2). The species mass concentration (g g^{-1}, the species mass contained in 1 g particles in each factor) and mass percentage (%, the species mass concentration contained in one factor divided by the total mass concentration in all factors) are shown in Figure 6.3. The time

series variation of each factor mass concentration is shown in Figure 6.4. The seasonal mass contributions of six factors are listed in Table 6.3.

Table 6.2: A summary of chemical compounds in $PM_{4.3}$ at the CUGB from 2010.06.21 till 2011.06.20

Species	S/N[a]	Category	<LOQ[b]	Missing[c]
$PM_{4.3}$	4.8	Weak	0	0
OC	10.9	Strong	0	0
EC	10.8	Strong	0	0
Cl^-	5.2	Weak	147	0
NH_4^+	4.9	Strong	58	1
NO_3^-	5.7	Strong	3	0
SO_4^{2-}	5.7	Strong	2	0
Fe	6.2	Strong	1	0
K	6.8	Strong	4	0
Ca	7.1	Strong	1	0
Ti	6.2	Strong	1	0
Mn	5.8	Strong	1	0
Cu	1.1	Weak	35	36
Zn	8.8	Strong	1	0
As	5.5	Strong	78	0
Ba	4.1	Strong	3	1
Pb	5.8	Strong	27	0
29ab	1.8	Strong	0	12
29ba	1.2	Weak	40	39
30ab	1.9	Strong	0	11
30ba	1.3	Weak	22	38
31abS	1.1	Weak	2	34
31abR	1.2	Weak	2	34
BAA	4.7	Strong	5	3
CRY	4.3	Strong	1	3
BBKF	4.2	Strong	0	3
BEP	4.1	Strong	0	3
BAP	4.2	Strong	4	3
IND	3.2	Strong	11	4
PIC	1.6	Weak	191	6
BGH	3.2	Strong	9	4
Levoglucosan	1.1	Weak	0	45

[a]S/N, the ratio of signal to noise.

[b]<LOQ, number of samples, below the limit of quantification, from total number n =321.

[c]Missing, number of samples, which were not analyzed, from total number n=321.

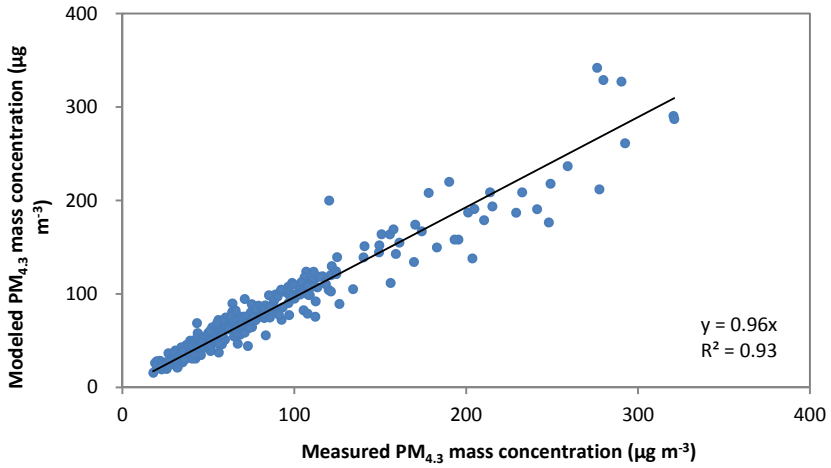

Figure 6.1: Comparison between measured $PM_{4.3}$ mass concentration at the CUGB and modeled $PM_{4.3}$ mass concentration by PMF

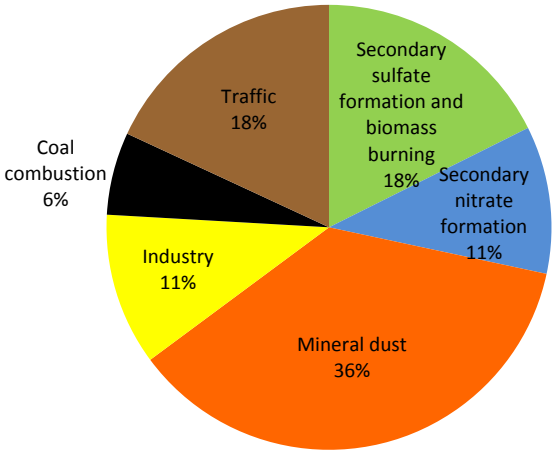

Figure 6.2: The contribution of six sources to $PM_{4.3}$ at the CUGB in Beijing during 2010-2011

Table 6.3: Seasonal contributions of 6 factors to $PM_{4.3}$ during 2010-2011 (unit: µg m^{-3})

	Secondary sulfate formation and biomass burning	Secondary nitrate formation	Mineral dust	Industry	Coal combustion	Traffic
Summer 2010	35.8	0.8	17.1	7.3	0.3	16.3
Autumn 2010	13.7	13.2	20.7	9.0	1.1	17.5
Winter 2010	8.6	10.4	27.7	8.9	10.2	13.4
Spring 2011	8.5	8.1	53.6	9.9	0.7	9.8

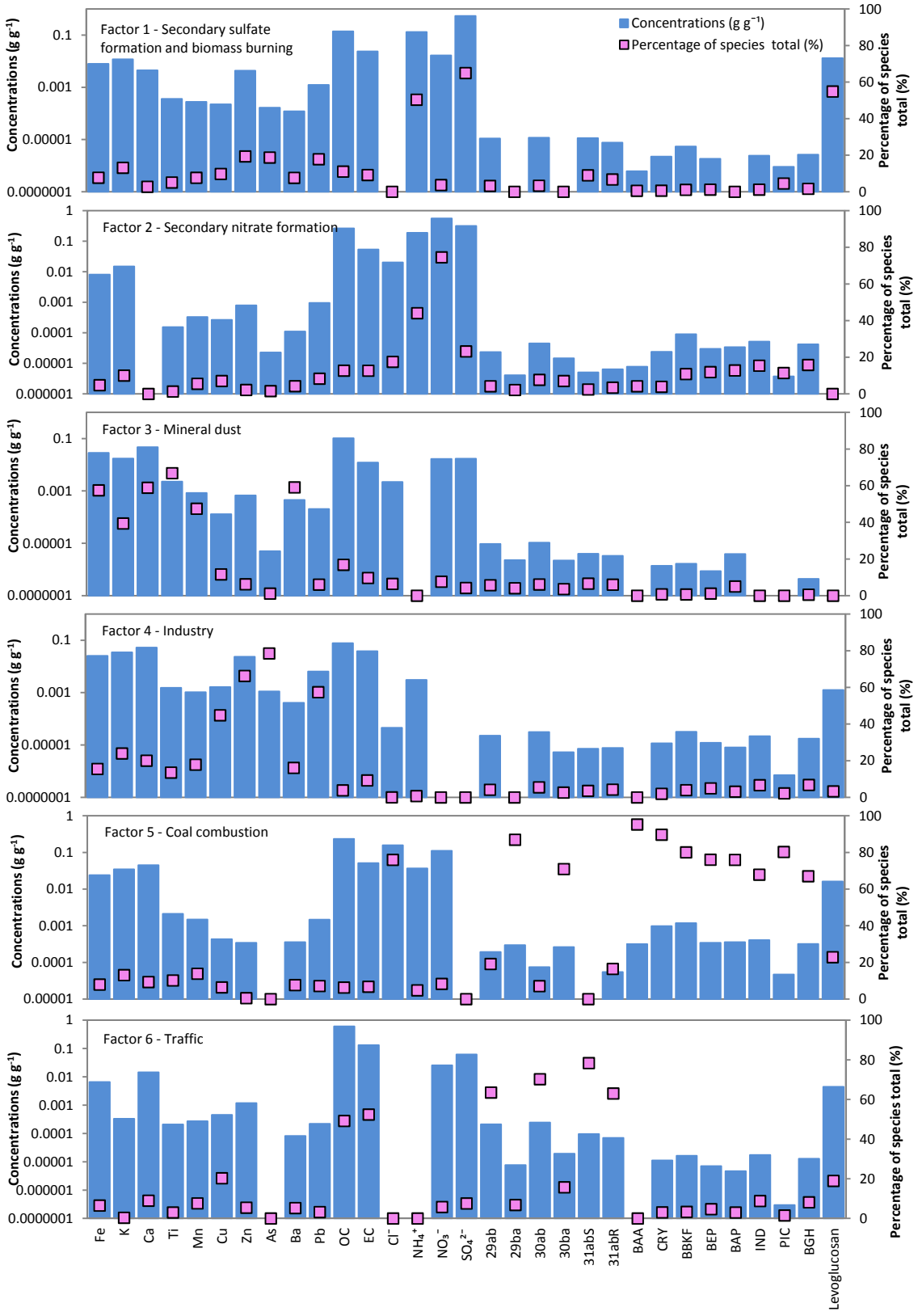

Figure 6.3: PMF factor profiles from chemical compounds data in $PM_{4.3}$ during 2010-2011 at the CUGB

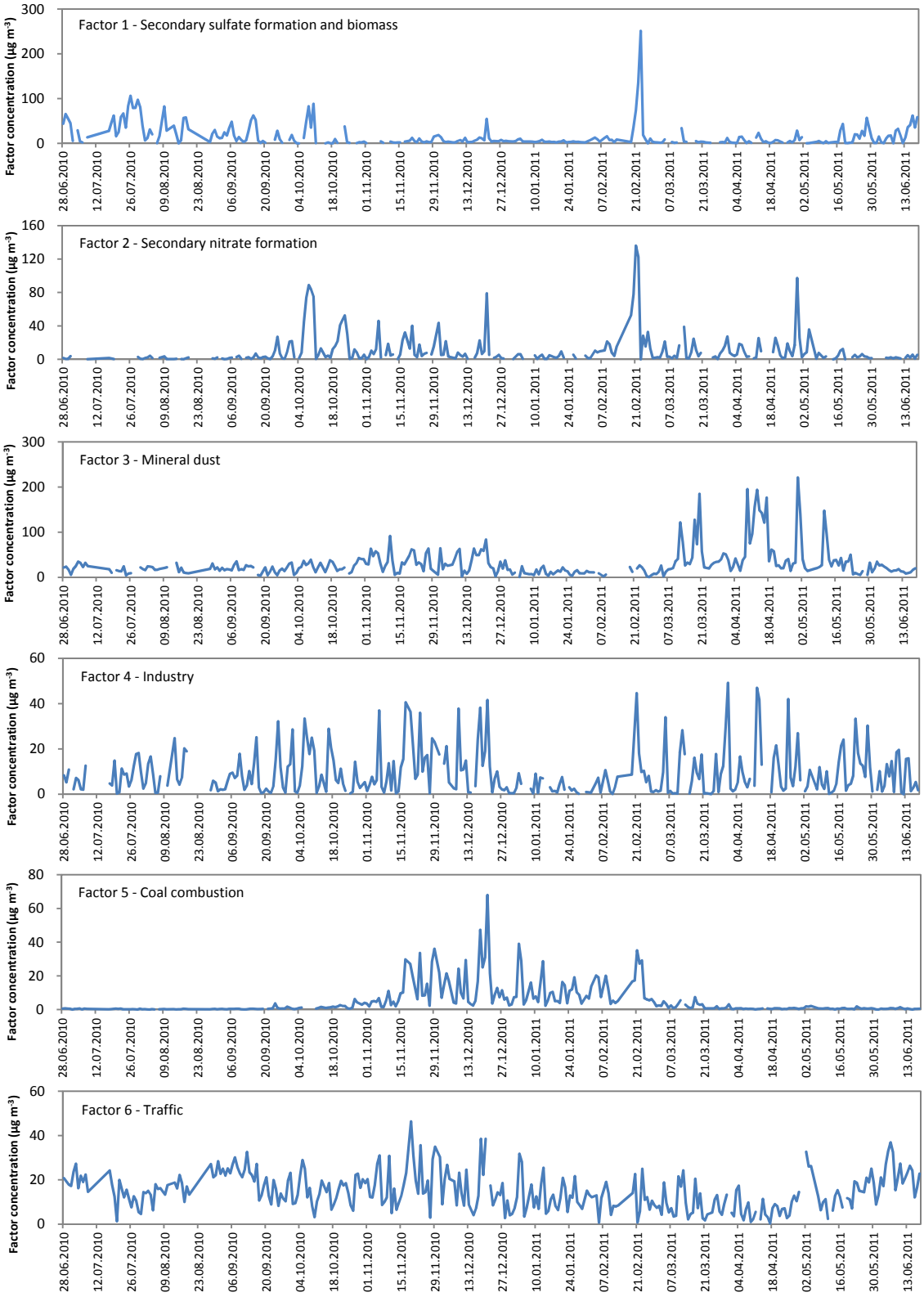

Figure 6.4: Daily mean contributions of six sources from the PMF analysis for $PM_{4.3}$ at the CUGB in Beijing during 2010-2011

The first factor contained 65.0% of SO_4^{2-}, 50.4% of NH_4^+ and 54.9% of levoglucosan. Levoglucosan is widely used as a tracer for biomass burning (Zhang et al., 2008b; Wagener et al., 2012). From Figure 6.4 and Table 6.3, the time series variation shows that this factor concentrated during summer (35.8 μg m^{-3}), followed by autumn (13.7 μg m^{-3}). This is because biomass burning usually happens during summer and autumn in Beijing and its surrounding areas (Huang et al., 2012) and the secondary sulfate is easily formed under strong solar radiation and high temperature, especially in summer (Seinfeld and Pandis, 2006). In addition, previous studies showed that SO_4^{2-} mass concentration increased during biomass burning episodes (Cheng et al., 2014; Rastogi et al., 2014). Therefore this factor can be explained by biomass burning and secondary sulfate formation.

The second factor was characterized by high concentrations of nitrate and ammonium, which can be considered as a secondary nitrate formation. The time series shows that this factor had low concentration during summer, because nitrate is volatile under high temperature. Table 6.3 shows that this factor concentrated during autumn and winter.

The third factor had a high contribution from Fe (57.5%), Ca (58.9%), Ti (66.9%), Mn (47.5%), and Ba (59.1%). All of these elements are mainly from soil. The time series of this factor contribution showed that high concentrations of this factor were concentrated during spring time when dust storms occurred very often. For example, the factor had a peak value on 30 April 2011 when a dust storm happened. Therefore, this factor is indicative of mineral dust, which includes dust storm, re-suspended road dust and construction dust.

The fourth factor was characterized by relative high contributions of As (78.6%), Zn (66.3%), Pb (57.4%), Cu (44.8%). As was found to originate from smelter and base-metal refinery industries (Wang and Mulligan, 2006). Zn and Cu can originate from industrial metallurgical process (Xu et al., 2012). Tangshan city and Tianjin Municipality are important industrial cities which are located to the Southeast of Beijing. The main industry in Tangshan is Iron and steel. In Tianjin, metalworking is one kind of important industries. Pb was considered to have originated from the ceramic industry, the manufacturing of insecticides, paints, glass and storage batteries (Soriano et al., 2012). Porcelain is another important industry in Tangshan city and producing photovoltaic cells is a kind of important industry in Baoding city which is located to the Southwest of Beijing. In addition to surrounding cities, inside of Beijing has also smelter industry which locates to the Northwest of CUGB sampling site, called “Changping smelter”. All the above indicates that this factor is representative of industrial based sources. The time

series shows that the contribution of this factor to PM is stable during the whole year, except for January 2011. This agrees well with $PM_{4.3}$ mass concentration variation. The reason could be it was influenced by meteorological parameters and holiday periods.

The fifth factor was dominated by PAHs (BAA (95.3%), CRY (89.7%), BBKF (80.1%), BEP (76.1%), BAP (76.0%), IND (67.9%), PIC (80.3%) and BGH (67.0%)), 29ba (87.0%), 30ba (70.1%), Cl^- (76.0%), and levoglucosan (22.9%). Levoglucosan was found not only from biomass burning, but also from lignite combustion (Fabbri et al., 2008, 2009). Cl^- originates from coal combustion (Yao et al., 2002) and PIC is also used as a tracer for coal combustion (Oros and Simoneit, 2000). The hopane index 30ab/(30ab+30ba) is also used to distinguish the sources of hopanes also. This ratio was found to be 0.1 for lignite coal, 0.5 for bituminous coal, 0.6 for brown coal (Oros and Simoneit, 2000) and greater than 0.9 for crude oil were found (El-Gayar et al., 2002). For this factor, the hopane index is 0.2. Hence, this factor can be interpreted as coal combustion. Contribution of this factor was found to be concentrated during winter (Figure 6.4), indicating that coal combustion for heating during winter is the main reason. Additionally, organic compounds being volatile under higher temperature is also the reason.

The sixth factor was characterized by EC (52.4%), OC (49.2%), 29ab (63.5%), 30ab (70.3%), 31abS (78.4%) and 31abR (63.1%). In this factor, the homohopane index 31abS/(31abS+31abR) was 0.6 and the hopane index 30ab/(30ab+30ba) was 0.9. Both indexes indicated that this factor can be explained by oil combustion. Hopanes are considered to be an organic tracer for the lubricating oil which is usually used for gasoline or diesel engine vehicles (Rogge et al., 1993b; Phuleria et al., 2006; Kleeman et al., 2009). Therefore this factor can be considered as traffic. Time series shows that the contribution of this factor to PM is stable during the whole year.

6.2.1.2 Backward trajectory and cluster analysis

The 72 h backward trajectories at 500 m AGL prior to arriving in Beijing at 14:00 local time each day were calculated by HYSPLIT 4. Four trajectory clusters were found (Figure 6.5).

Cluster 1 (red line) expressed the air flow from the South of Beijing, showing that many air pollutants had orignated from the Hebei province, and can be called as the “South flow” (S flow). Cluster 2 (dark blue line) was the air flow which had originated from the North of Beijing.

This cluster can be named as the “North flow” (N flow). Cluster 3 (green line) represented air flow coming from the Northwest, passing Mongolia, Inner Mongolia, Gobi desert and Hebei province and can be named as the “Northwest flow” (NW flow). Cluster 4 (light blue line) was similar to Cluster 3, the difference with Cluster 4 being the long range transport. This cluster can be named as the “Long-range Northwest flow” (Long-range NW flow). The S, N, NW and long-range NW flows accounted 33%, 17%, 35% and 15% of all air flows in 2010-2011, respectively. The S flow showed very short trajectories in Figure 6.5 compared with other trajectories, which indicated the presence of a relatively stagnant atmosphere and also the strong influence of regional transport.

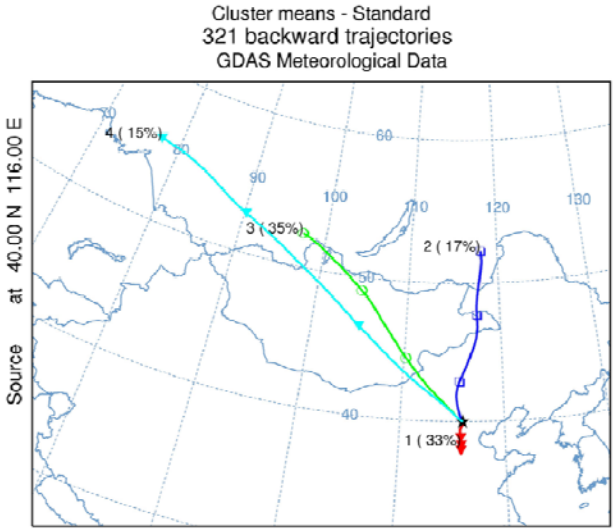

Figure 6.5: Clusters of backward trajectories during 2010-2011

Based on these four air flow directions, all sampling days were also classified into four groups (Table 6.4). The highest $PM_{4.3}$ mass concentration of 103 µg m^{-3} was found in the S flow, followed by the long-range NW flow with 95 µg m^{-3}, the NW flow with 63 µg m^{-3} and the N flow was of the lowest mass concentration at 57 µg m^{-3}. The mixture of secondary sulfate formation and biomass burning, secondary nitrate formation and industry were mainly from S flows with the highest mass concentrations of 33.5 µg m^{-3}, 14.2 µg m^{-3} and 12.8 µg m^{-3}, respectively. The highest contributions from mineral dust with 43.9 µg m^{-3} and from coal combustion with 10.8 µg m^{-3} were found in long-range NW flows. From Figure 6.5, one can see that long-range NW flow was the longest trajectory which indicates that wind speed of this air flow was the highest.

In addition, this air flow passed Russia, Mongolia, Inner Mongolia and Hebei Province. Therefore, high wind speed could bring the dust from Gobi desert in Mongolia and sandy lands in Inner Mongolia to Beijing as well as raise the local road dust and construction dust. Coal is widely used for heating during winter in Mongolia, Inner Mongolia and Hebei Province, and 75% sampling days from long-range NW flows were in winter period. Zhangjiakou fossil-fuel power station, by which coal is mainly used, is also located on the trajectory of this cluster. Therefore, the highest contribution from coal combustion was found from long-range NW flows coincidentally. Traffic showed little variation in all four backward trajectory clusters, indicating that it was mainly impacted from local sources.

Table 6.4: Summary of source distribution to $PM_{4.3}$ and corresponding $PM_{4.3}$ mass concentration on different directions of air flows during 2010-2011 (unit: μg m^{-3}). S is South, etc.

Direction	Secondary sulfate formation and biomass burning	Secondary nitrate formation	Mineral dust	Industry	Coal combustion	Traffic	$PM_{4.3}$
S	33.5	14.2	22.6	12.8	3.3	16.7	103
N	5.5	5.9	23.6	6.6	2.5	12.6	57
NW	3.4	4.7	31.6	5.9	4.7	13.0	63
Long-range NW	6.9	8.8	43.9	9.5	10.8	15.1	95

6.2.1.3 Haze

Possible sources of PM during haze obtained from particle characteristics were discussed in Chapter 5. In this chapter, mass distribution and contribution from different sources to $PM_{4.3}$ during haze days in different seasons on the basis of source appointment are described in Table 6.5 and Figure 6.6.

From Table 6.5 and Figure 6.6, the mixture of secondary sulfate formation and biomass burning was found to be the dominant source of $PM_{4.3}$ during summer haze, secondary nitrate formation and the mixture of secondary sulfate formation and biomass burning were the dominant sources of $PM_{4.3}$ during autumn haze, mineral dust was the main source for spring haze, winter haze was dominated by a mixture of different sources. Compared with other season haze events, winter haze had the highest contribution from coal combustion. During

the four seasons, mineral dust had the highest mass concentrations and percentages during spring haze, while coal combustion showed the highest mass concentrations and percentages during winter haze. The mixture of secondary sulfate and biomass burning and secondary nitrate had the highest mass concentrations and percentages during summer haze and autumn haze, respectively. These results are in agreement with the results from Chapter 5.

Table 6.5: Source distributions of $PM_{4.3}$ during haze days in different seasons (unit: $\mu g\ m^{-3}$)

	Secondary sulfate formation and biomass burning	Secondary nitrate formation	Mineral dust	Industry	Coal combustion	Traffic
Summer	69.9	0.9	12.9	10.0	0.4	13.3
Autumn	42.2	40.5	22.3	18.8	0.6	16.5
Winter	36.3	40.0	39.0	29.5	26.0	23.3
Spring	31.4	29.0	59.0	27.7	0.7	8.5

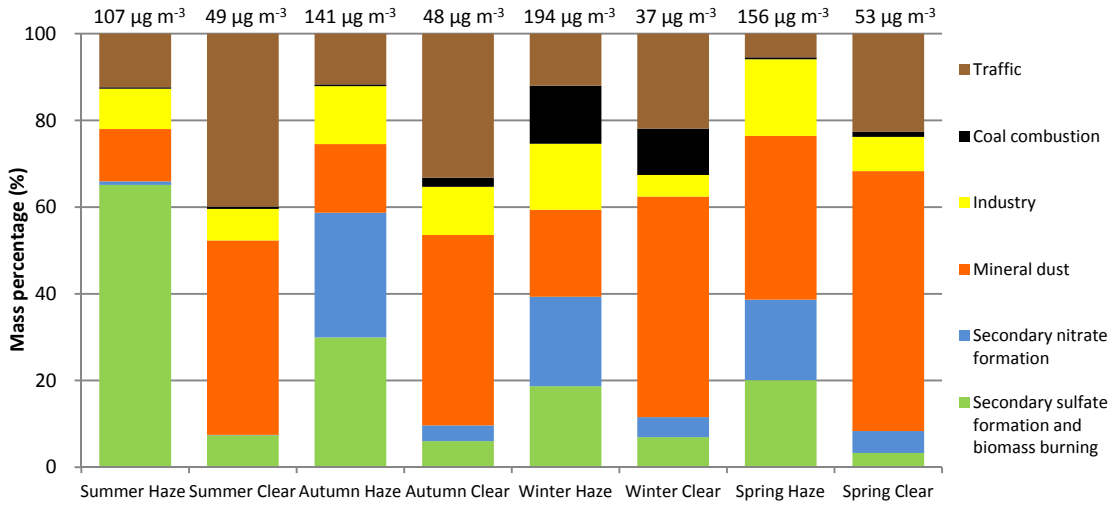

Figure 6.6: Mass contribution of different sources to $PM_{4.3}$ during haze and clear days in different seasons (unit: %)

The comparison between mass contribution of different sources to $PM_{4.3}$ during haze and clear days in different seasons is also shown in Figure 6.6. In all seasons, the dominant sources of $PM_{4.3}$ are traffic and mineral dust in clear days while contributions of secondary sulfate and

nitrate formation, biomass burning and industry increased in haze days. In summer, contribution of the mixture of secondary sulfate formation and biomass burning during haze days (65.1%) was 9 times of during clear days (7.4%). In autumn, contributions of secondary nitrate formation and the mixture of secondary sulfate formation and biomass burning increased 8 and 5 times during haze days when compared with clear days, respectively. In winter, contributions from 6 sources became more evenly. In spring, dust was the dominant source in both haze and clear days.

From all haze days, 77% occurred with a S flow, 17% with a long-range NW flow, and 6% with a NW flow. No haze happened from a N flow. Therefore, S flow was the main source for Beijing haze $PM_{4.3}$. Figure 6.7 shows that the directions of air flow during haze days in different seasons. It points out 100% of air flows during haze days in summer, autumn and spring were from the South. During winter haze, the air flows were mainly from the South and long-range Northwest. Additionally, average relative humidity from S flow was higher than other directions. Higher RH can be favor for the formation of haze.

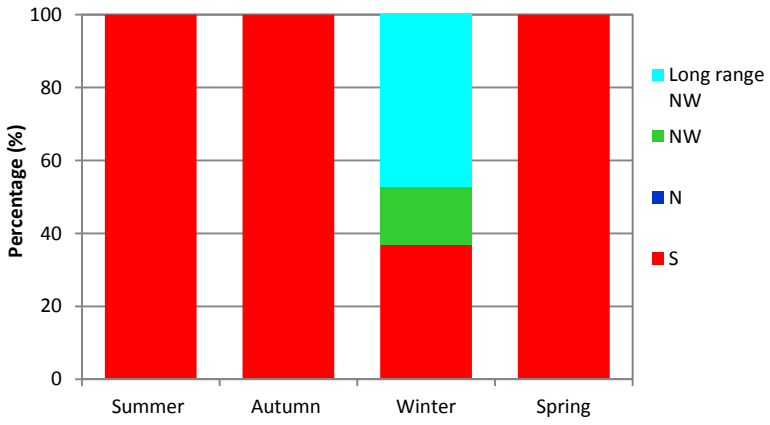

Figure 6.7: Percentages of different clusters during haze days in different seasons

6.2.2 Source apportionment of $PM_{2.5}$ at the IAP (2013.04.10 – 2013.06.08)

6.2.2.1 Source apportionment of daily mean $PM_{2.5}$

(1) PMF

60 daily mean $PM_{2.5}$ data with 23 species were used in the PMF analysis. Barium (Ba) was excluded from this analysis because it was poorly modeled by PMF. As $PM_{4.3}$, the $PM_{2.5}$ mass concentration was also included in PMF to apportion mass concentration of factors, but it was marked as "total variable" in order to reduce its influence on PMF solution. A summary of the chemical compounds used in the PMF is listed in Table 6.6.

Table 6.6: Summary of chemical compounds in $PM_{2.5}$ at IAP from 2013.04.10 till 2013.06.08

Species	S/N[a]	Category	<LOQ[b]	Missing[c]
$PM_{2.5}$	2.00	Weak	0	2
OC	11.30	Strong	0	0
EC	11.37	Strong	0	0
Cl^-	7.33	Weak	0	0
NO_3^-	7.33	Strong	0	0
SO_4^{2-}	7.33	Strong	0	0
NH_4^+	7.33	Strong	0	0
Na	11.49	Strong	0	0
Mg	11.50	Strong	0	0
Al	11.50	Strong	0	0
K	11.50	Strong	0	0
Ca	11.50	Strong	0	0
Fe	11.50	Strong	0	0
V	11.50	Strong	0	0
Cr	11.50	Strong	0	0
Mn	11.50	Strong	0	0
Co	11.46	Strong	0	0
Ni	11.49	Strong	0	0
Cu	11.50	Strong	0	0
Zn	11.50	Strong	0	0
As	11.50	Strong	1	0
Cd	11.50	Strong	1	0
Tl	11.50	Strong	0	0
Pb	11.50	Strong	0	0

[a]S/N, the ratio of signal to noise.
[b]<LOQ, number of samples below the limit of quantification from total number n =60.
[c]Missing, number of samples which were not analyzed, from total number n=60.

In order to find the most reasonable numbers of sources, a different number of factors (4-12) were tested. After a reasonable solution was selected, a 100 bootstrap was run (minimum R^2 = 0.6) to check its stability. Of the 100 runs, factor 2, factor 4 and factor 5 only had 2, 2 and 11

bootstraps unmapped, respectively, while all the other factors had all bootstraps mapped. Therefore, the solution with five factors which include industry, secondary inorganic ions formation, mineral dust, fuel oil combustion and traffic was considered as stable result. These sources had an average contribution of 12%, 31%, 20%, 16% and 21%, respectively (Figure 6.8). Daily mean modeled $PM_{2.5}$ mass concentrations by PMF are compared with daily mean measured $PM_{2.5}$ mass concentrations in Figure 6.9. It shows that the measured $PM_{2.5}$ mass can be well reproduced by the model with a correlation (R^2) of 0.94 and a slope of 0.99. The species mass concentration (g g^{-1}) and mass percentage (%) in different factors are shown in Figure 6.10. The time series of each factor are shown in Figure 6.11.

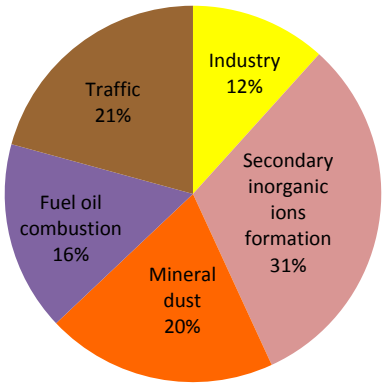

Figure 6.8: The contribution of five sources to $PM_{2.5}$ at the IAP in Beijing in spring 2013

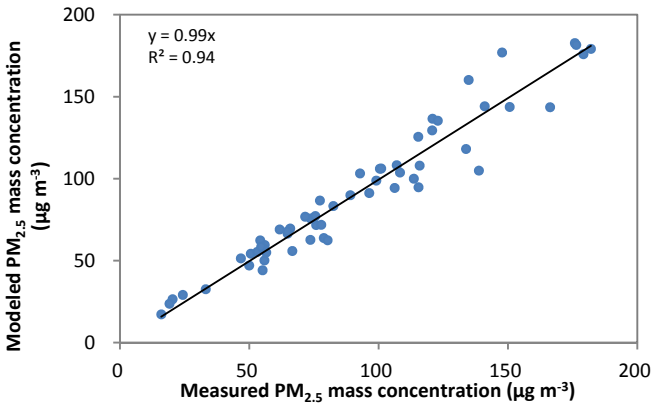

Figure 6.9: Comparison between measured $PM_{2.5}$ mass concentrations and modeled $PM_{2.5}$ mass concentrations at the IAP by PMF

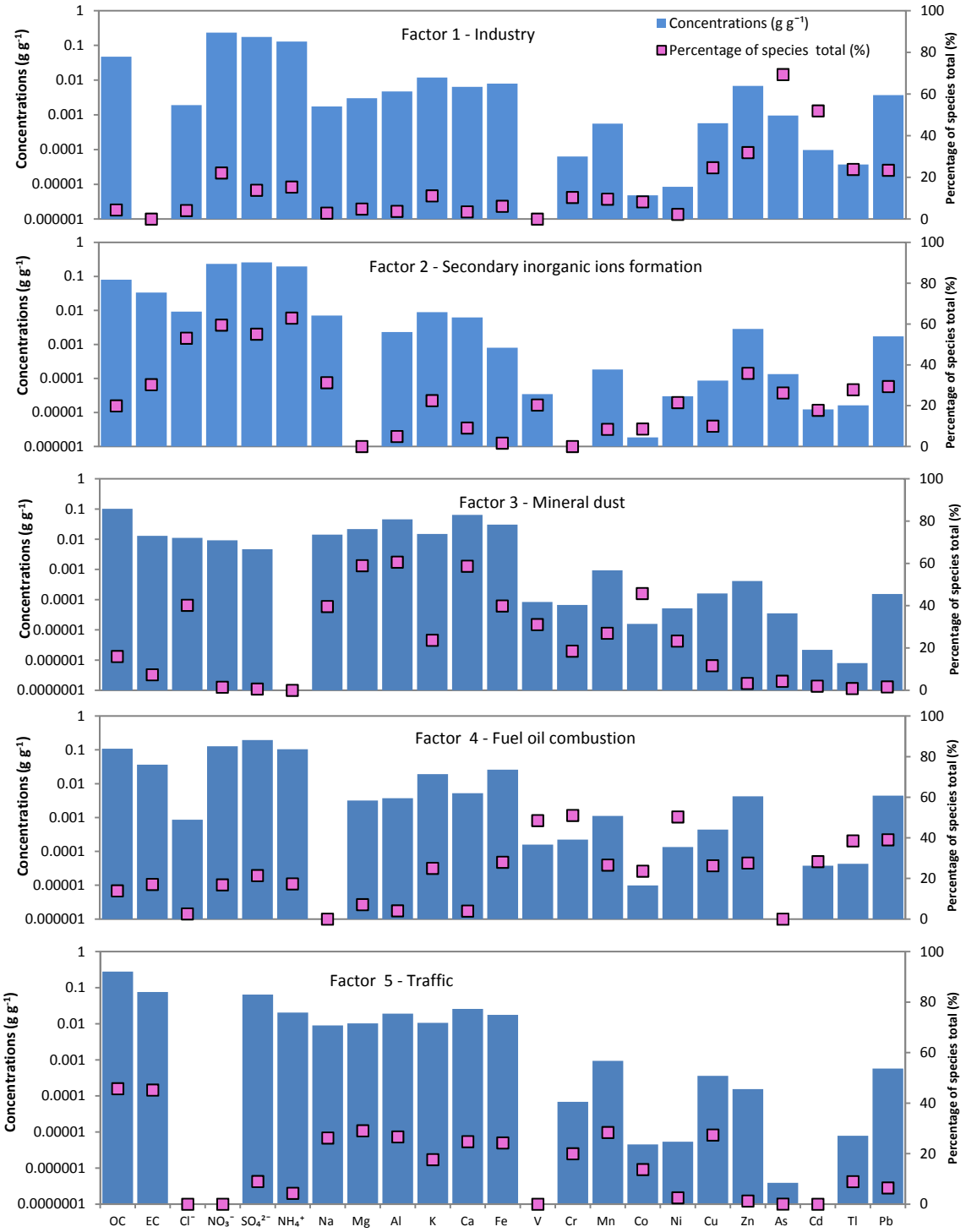

Figure 6.10: PMF factor profiles from chemical compounds data in $PM_{2.5}$ during spring 2013 at the IAP in Beijing 10 April till 8 June 2013

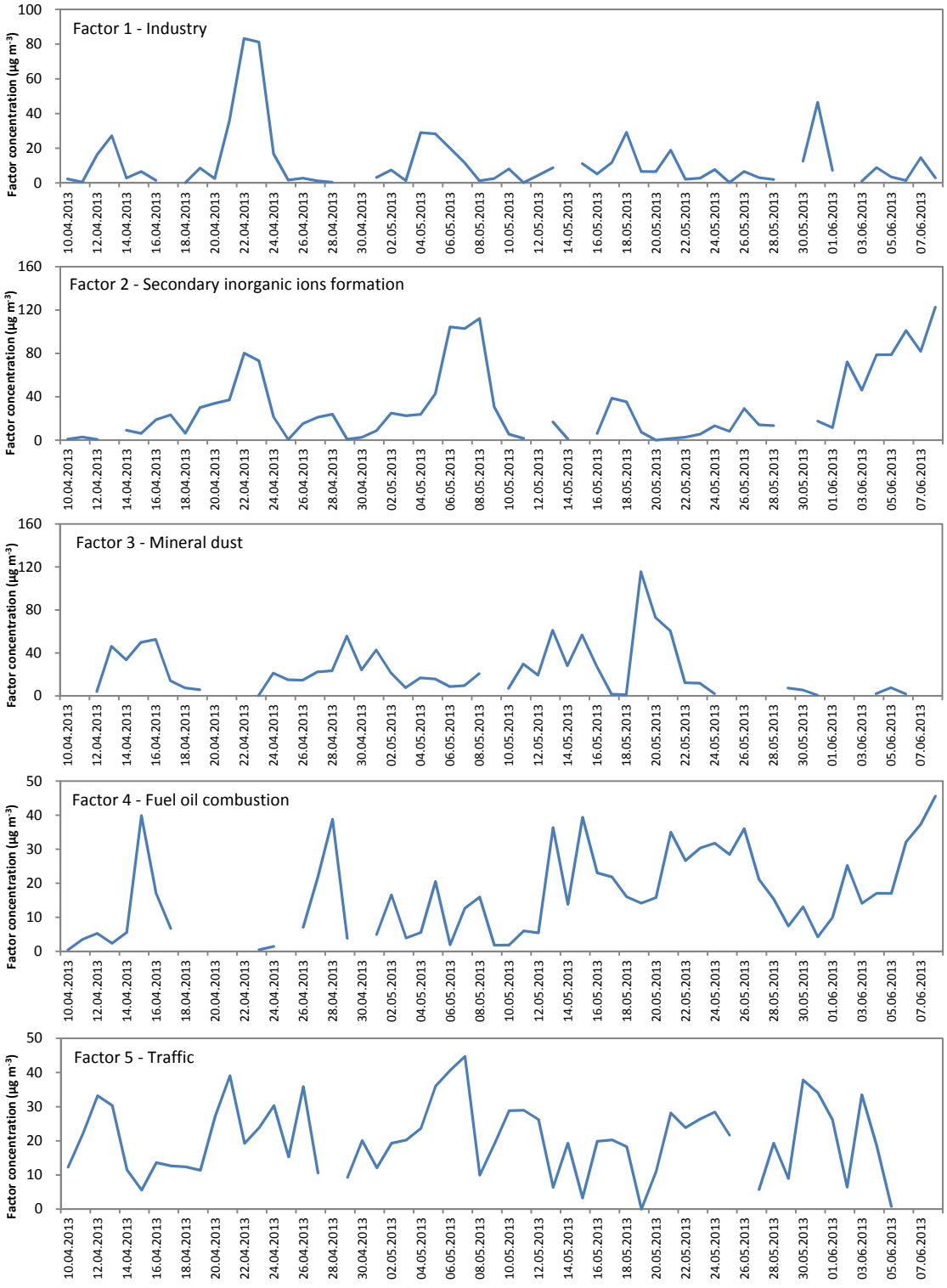

Figure 6.11: Daily mean contributions of five sources from the PMF analysis of $PM_{2.5}$ at the IAP in Beijing from 10 April till 8 June 2013

The first factor was dominated by As (70%) and contained a high concentration of Cd (52%). As and Cd was found to originate from nonferrous metal smelter (Lee et al., 1999). Therefore, this factor can be explained as industry.

The second factor with high loading of NO_3^-, SO_4^{2-} and NH_4^+ represented the secondary inorganic ion formation source which was the largest contributor (31%) to $PM_{2.5}$ in spring 2013. The peaks of secondary inorganic ion source contributions showed good agreement within time periods when haze pollution happened. Therefore, secondary inorganic ions are an important fraction of $PM_{2.5}$ during haze episodes.

The third factor was typically characterized by a high contribution from crustal elements, such as Mg, Al, Ca, Co and Fe. Fifty-nine percent of Mg, 61% of Al, 59% of Ca, 46% of Co and 40% of Fe were present in this factor. High Ca mass concentrations can be associated with the re-construction works in Beijing. The main sources of these species were re-suspended road dust, construction dust, and fugitive dust. The time series of this factor contribution showed that the highest mass concentration contribution happened on 19 May 2013 which was an obvious re-suspended dust event. Therefore this factor can be interpreted as mineral dust.

The fourth factor was related to V, Cr and Ni, where 49% of V, 51% of Cr and 50% of Ni contributed to this factor. V, Cr and Ni are usually considered as tracers for fuel oil combustion (Fang et al., 2010; Yang et al., 2013) used in steam boilers and oil-fired power plants (Yang et al., 2013). So this factor can be explained as fuel oil combustion.

The fifth factor was characterized by EC, OC and Cu, and could explain 46%, 45% and 27% of them, respectively. EC and OC are recognized as indicators for tail pipe emission (Gu et al., 2011) and Cu is widely used in vehicle brake linings and pump systems (Lee et al., 1999; Xu et al., 2012). In this factor, crustal elements such as Na, Mg, Al, Ca,Fe and Mn also showed a relative high loading. The common source for these compounds was considered to be the re-suspension of road dust due to traffic activity, including wear and tear of tires, brake wear and oil burning. Previous studies also found the combination between the vehicle source and road dust (Hedberg et al., 2005; Aldabe et al., 2011). So this factor can be explained as traffic.

(2) Backward trajectory and cluster analysis

Backward trajectories were also calculated in the 2013 campaign. 72 h backward trajectories at an altitude of 500 m AGL arriving at Beijing at local time 14:00 every day were calculated by HYSPLIT 4. Four trajectory clusters were found (Figure 6.12). Cluster 1 (red line) represented air flow coming from the North, passing Mongolia, Inner Mongolia and Hebei province, so this cluster can be named as “North flow” (N flow). Cluster 2 (dark blue line) was the air flow orignated from the Northwest of Beijing by long-range transport and named as “Long-range Northwest flow” (long-range NW flow). Cluster 3 (green line) shows the air flow came from the North but reached Beijing from the Southeast. This cluster can be named as “North-Southeast flow” (N-SE flow). Cluster 4 (light blue line) expresses the air flow from the Southeast of Beijing, and many of which were orignated from the Hebei province and Tianjin Municipality. This cluster was called “Southeast flow” (SE flow). Consequently, N, long-range NW, N-SE, and SE flows accounted for 27%, 17%, 15% and 42% of all air flows in spring 2013, respectively.

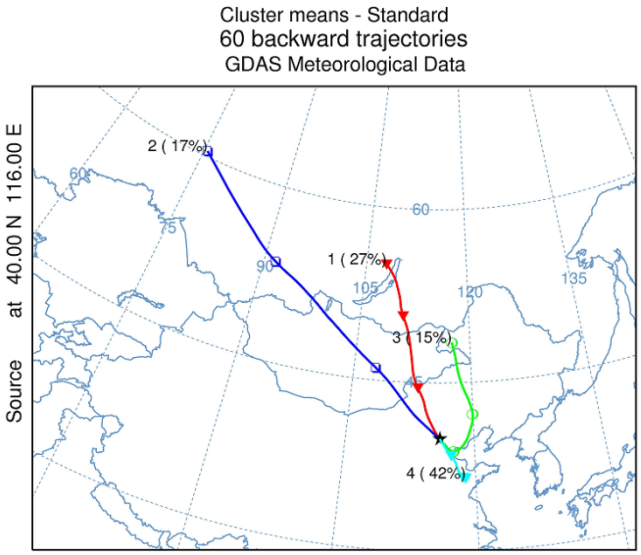

Figure 6.12: Clusters of backward trajectories at the IAP in spring 2013

Based on these clusters from different directions, all the sampling days were divided into four groups (Table 6.7). The highest $PM_{2.5}$ mass concentration (118 μg m^{-3}) was found in SE flow, followed by long-range NW flow with 81 μg m^{-3}, N-SE flow with 78 μg m^{-3} and N flow with 59 μg m^{-3}. The SE flow was the shortest trajectory as shown in Figure 6.12, indicating the presence

of a relatively stagnant atmosphere which is favorable for the accumulation of air pollutants leading to high $PM_{2.5}$ mass concentration.

As described in Table 6.7, the highest mass concentration (18 μg m^{-3}) contributed by industry was from SE flow, and little difference was found from other three directions. The reason could be that the SE air flow passed through Tianjin Municipality (industrial city) and brought pollutants from industry to Beijing.

Table 6.7: Summary of source distributions to $PM_{2.5}$ and corresponding $PM_{2.5}$ mass concentration from different directions in spring 2013 (unit: μg m^{-3}). N is North, etc.

Direction	Industry	Secondary inorganic ions formation	Mineral dust	Fuel oil combustion	Traffic	$PM_{2.5}$
N	4.8	8.6	15.4	8.7	21.5	59
Long-range NW	5.4	6.6	43.0	9.0	17.0	81
N-SE	5.4	22.7	17.6	17.4	14.9	78
SE	18.0	51.6	9.9	20.0	19.1	118

Secondary inorganic ions mainly came from SE flows. The contribution of secondary inorganic ions from this direction was 51.6 μg m^{-3}. It was almost around 6-8 times the contributions from N and long-range NW flows. Therefore, the cluster analysis indicated that secondary inorganic ions increased quickly when air flow had originated from SE with stagnant atmospheric conditions. Beijing was thus significantly affected by secondary inorganic ions originating from cities located to the south in the Hebei Province and Tianjin Municipality.

The long-range NW, N-SE, N and SE flows contributed 43.0 μg m^{-3}, 17.6 μg m^{-3}, 15.4 μg m^{-3}, and 9.9 μg m^{-3} to mineral dust mass concentration, respectively. Long-range NW flow is the longest trajectory as shown in Figure 6.12, indicating the wind speed from this direction is the highest. Therefore, long-range NW flow could bring more dust particles to Beijing when it passed through the Gobi desert in Mongolia with high wind speed.

Fuel oil combustion source had the highest mass concentration with a value of 20.0 μg m^{-3} from the SE flow. This is in good agreement with the location of industries. Especially Tangshan

city, which is located to the Southeast of Beijing, is a industrial city. The concentrations of fuel oil combustion from N and long-range NW had no significant difference.

Compared with other sources, traffic had the minimum variation among these four directions of air flows, which indicated that this source was mainly from local. Nonetheless, the N and SE flows still contributed relatively high concentrations to the traffic sources with values of 21.5 μg m^{-3} and 19.1 μg m^{-3}, respectively.

(3) Haze

During spring 2013, secondary inorganic ions contributed 75.6 μg m^{-3} to $PM_{2.5}$ mass concentration during haze days, followed by industry (20.9 μg m^{-3}), traffic (19.6 μg m^{-3}), fuel oil combustion (17.4 μg m^{-3}), and mineral dust (5.2 μg m^{-3}). Therefore, secondary inorganic ions were the dominant source for $PM_{2.5}$ during haze days in spring 2013.

Three haze pollution events were discussed in Chapter 5. The comparison of mass contribution of different sources between these three haze pollution events and clear days is shown in Figure 6.13. Obviously, traffic and dust were the dominant sources of $PM_{2.5}$ during the clear days while secondary inorganic ions increased rapidly during haze days. In addition, some difference among these three haze pollution events were also found. For HP1, industry was another important source. Compared with HP1 and HP3, dust had relative higher contribution in HP2. Fuel oil combustion was the second important source of $PM_{2.5}$ in HP3.

During all haze days in spring 2013, 88% had originated from SE flow, 6% came from N-SE flow and 6% came from N flow. No haze days were from long-range NW flow. Therefore, SE flow was the main source for haze in spring 2013.

From Figure 6.12, SE flow was found that could be affected by the air from the Bohai Sea. So the relative humidity from SE flow was the highest with the value of 64% in all four directions and 29%, 34% and 49% in N flow, long-range NW flow and N-SE flow, respectively. So pollutants were brought to Beijing from industrial cities which located to the South of Beijing, such as Tangshan city and Tianjin Municipality, and blocked by mountains which lie to the North, Northwest and West of Beijing. Under high relative humidity, these pollutants grew up, caused the decrease in visibility and led to the forming of haze.

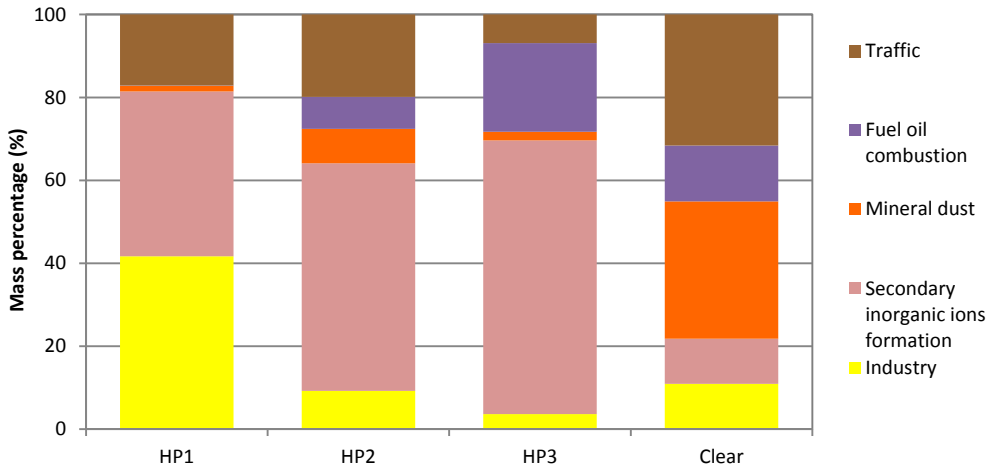

Figure 6.13: Mass contribution of different sources to $PM_{2.5}$ during three haze pollution events and clear days at the IAP in Beijing in spring 2013 (unit: %)

6.2.2.2 Source apportionment of 4 h sampling $PM_{2.5}$

In order to get better understanding of sources of $PM_{2.5}$ during haze days, the investigation on the high time resolution sampling $PM_{2.5}$ samples is also done. But the results from PMF are not stable. This is could be caused by small amount of 4 h sampling $PM_{2.5}$ samples, only 41 samples. Generally the amount of samples should be much larger than the amount of species which were used in PMF. Therefore, the results cannot be used here.

6.3 Summary

Source apportionments were carried out for $PM_{4.3}$ collected at the CUGB during 2010-2011 and $PM_{2.5}$ collected at the IAP in spring 2013 by using a PMF model together with PM chemical composition data in this study.

Six sources were found for $PM_{4.3}$ at the CUGB in Beijing during 2010-2011: mixture of secondary sulfate formation and biomass burning, secondary nitrate formation, mineral dust, industry, coal combustion and traffic. These sources had average contributions of 18%, 11%, 36%, 11%, 6% and 18%, respectively. Four backward trajectory clusters have been found: south (33%), northwest (35%), north (17%) and long-range northwest (15%). In general, S flow contributed mostly to $PM_{4.3}$ mass concentration and N flow was a relatively cleaner air.

Summer and autumn haze were mainly caused by secondary sulfate formation and biomass burning, except for this, secondary nitrate formation was another main source for autumn haze. Winter haze was dominated by a mixture of different sources, especially coal combustion while spring haze was caused by mineral dust.

Five sources were determined for $PM_{2.5}$ at the IAP in Beijing during springtime 2013: industry, mineral dust, secondary inorganic ions formation, fuel oil combustion and traffic which showed average contributions of 12%, 20%, 31%, 16% and 21%, respectively. Four backward trajectory clusters, North, long-range Northwest, North-Southwest and Southeast were grouped. The highest $PM_{2.5}$ mass concentration was found from SE flow due to industry, secondary inorganic ions and fuel oil combustion while a higher $PM_{2.5}$ mass concentration was found from long-range NW flows due to dust. In general, SE flow is the main sources for high $PM_{2.5}$ mass concentration in Beijing while N flow is a relatively clean air. Secondary inorganic ions were found to be the dominant source for $PM_{2.5}$ during spring haze 2013.

In general, dust and traffic were found to be the main sources of PM during clear days and secondary inorganic ions were the dominant source of PM during haze days for whole year. The backward trajectory from the South was always found to be short and with high PM mass concentration. Therefore, southerly flow were the main source of PM during haze days in Beijing.

Chapter 7 Conclusion and outlook

Studies on continuous annual PM composition, including inorganic and organic composition, especially during haze events in different seasons are rare. In this thesis, systematically comprehensive investigation on the complete chemical composition of continuously one year collected PM and source appointment based on these data are performed. The main objective was to find out the long-term characteristics of PM in Beijing after the Olympic Summer Games 2008 and to identify the main sources of PM, especially during haze episodes in different seasons and weather conditions. A large unique dataset including EC, OC, inorganic elements, water soluble ions and organic compounds was analyzed for $PM_{4.3}$ collected at the CUGB during one year in 2010-2011 and $PM_{2.5}$ collected at the IAP during two months in springtime 2013.

The temporal variations of PM and its compounds were investigated and the results showed that the PM mass concentrations after the emission reduction measures during the Olympic Summer Games 2008 were still high, approximately 2.5 times higher than the annual average of Chinese Ambient Air Quality Standard for $PM_{2.5}$ (Grade II: 35 μg m^{-3}) (China State Environmental Protection Administration (SEPA), 2012). Not only emissions but also meteorological parameters were found to be important factors influencing PM and its compounds mass variations and often interfered with each other. High relative humidity and low MLH can enhance PM mass concentration while high wind speed and precipitation can reduce pollutants. But high wind speed can also probably cause resuspended dust pollution. In addition, different wind directions can bring different pollutants to Beijing from different regions, such as northerly winds during spring transports dust to Beijing and southerly winds carry pollution from industrial area to Beijing (see Figure 7.1).

Organic matters (OM) and secondary inorganic ions were found to be the major fractions of PM in Beijing which contributed 22-41% and 25-37% to PM mass, respectively, indicating that the contribution of anthropogenic PM to total PM is very important. SOC was found to be the most important fraction in OM and SOC/OC ratio was higher in winter than in summer in Beijing which is different from previous study results. The reason could be the increase in the emission from coal combustion for heating during winter in Beijing and surrounding area

which leads to the increase in organic compound emissions. Especially, SOC mass contributions had a significant positive correlation with PM mass concentrations during winter time which indicates that SOC was the key compound in PM during winter time. Secondary inorganic ions were found to be the main compounds during haze days in all seasons, especially their mass percentages increased rapidly from 19% during clear days to 49% during haze days. In addition, secondary inorganic ions were found to have significant negative correlations with visibility. Therefore, in order to increase the visibility, controlling the precursors of secondary inorganic ions, such as SO_2, NO_x and NH_3, becomes more and more important. Considering SO_2, which mainly originates from coal combustion, and NO_x, which is mainly caused by vehicle exhaust emissions, the improvement of the quality of fossil fuel (reduction of sulfur) and vehicle exhaust cleaning (reduction of NO_x) become necessary.

Sources of PM were estimated by characteristics of compounds in PM. For instance, the high levoglucosan concentrations in summer and autumn indicated that contributions of biomass burning to PM exposure are significant. The homohopane index, hopane index and diagnostic ratios of PAHs illustrated that coal combustion and fuel oil consumption were the main sources for hopanes and PAHs in PM. Similar sources of PM were obtained by source apportionment: industry, secondary nitrate formation, secondary sulfate formation, coal combustion, traffic, dust and biomass burning. Therefore all these findings from the wide range of speciation of PM support that the consideration of source apportionment results from mostly all chemical compounds of PM provides reliable results finally. This is also supported by the similar results from previous studies which are listed in Table 6.1. The major sources of $PM_{2.5}$ in Beijing from these previous studies can be concluded as: dust, biomass burning, coal combustion, industry, vehicle emission and secondary particles formation. The difference to these studies is that the contribution of each source is different. The reason could be that in previous studies, only inorganic or organic compounds were used for source apportionment and the duration of sampling was short or discontinuous, such as only summer and winter or one month in each season. Source apportionment of PM in Beijing by using PMF with continuous one year inorganic and organic compounds in this study is performed for the first time. Therefore, the contribution of each source given in this study is more reliable when compared with other studies.

A special focus is on haze episodes because these are related to the highest PM pollution. Not only the nucleation and Aitken mode particles (primary pollutants), whose ratio to fine and coarse particles increased during the last years, originated this situation but also the

accumulation mode particles (secondary pollutants), as shown here, are a reason. This agrees well with hypothesis 2 (see Chapter 2). The different sources of haze particles during different seasons were given here for the first time. Source apportionment pointed out that haze in summer and autumn was mainly caused by secondary inorganic ions formation and biomass burning, winter haze was dominated by a mixture of different sources especially by coal combustion which contributed mainly to winter haze, while spring haze was caused by mineral dust mainly. In general, sources of PM in clear days was dominated by dust and traffic while in haze days was dominated by secondary inorganic ions formation during the whole year. These results were in good agreement with the analysis of the characteristics of particles composition and also agreed well with hypothesis 3 (see Chapter 2). But the sources of $PM_{2.5}$ during spring haze in 2013 showed the difference, because it was mainly caused by secondary inorganic ions formation. In general, southerly air flow was found to be the main source for PM during haze days in Beijing. This agrees well with previous studies (e.g. Sun et al., 2006). Therefore emission reduction measures should not only consider Beijing but also the whole region, including Tianjin Municipality and Hebei province, which is one of the most important coal producing and consuming provinces and has a lot of industrial cities such as Tangshan city, Shijiazhuang city and Baoding city (Figure 7.1). All these cities, which are located in the South of Beijing, are sources of pollutants from industrial emissions which are transported to Beijing when southerly air flow passes them, especially coal is used as the most important energy for industries. Coal accounted 88.8% of primary energy consumption in Hebei Province in 2012 (Hebei economic yearbook, 2013) and 53.0 million tonnes of coal in Tianjin Municipality in 2012, making coal as the most consumed energy source (Tianjin statistical yearbook, 2013). The location of Beijing is favorable for the accumulation of pollutants during air flow from southerly directions because mountains to the North, Northwest and West block the transportation of pollutants (Figure 7.1). In addition, Beijing has its own industries, such as electricity and heat production, supply industry and petroleum processing, which can also produce pollutants. Even though the amount of coal consumption decreased in Beijing recently, it was still high in 2012 with an amount of 22.7 million tonnes coal (Beijing statistical yearbook 2013). Hohhot city and Zhangjiakou city, which have fossil fuel power stations, are located in the Northwest of Beijing. Because wind from the Northwest was always accompanied with high wind speed (Figure 4.26), which is favorable for the dilution of pollutants, but on the other hand high wind speed also easily brings dust particles to Beijing from long distance. In addition, 75% of sampling days from long-range NW flows were found in winter period. Therefore, the highest contribution from coal combustion (used for heating)

was found from long-range NW flows coincidentally. Hypothesis 1 is supported by these conclusions. Even though, the influences on air quality from the Northwest air flow was still smaller than from the southerly air flow.

Except for the pollutants from regional and local sources, stagnant weather conditions were also favorable for the formation of haze, such as high relative humidity, low mixing layer height and low wind speed.

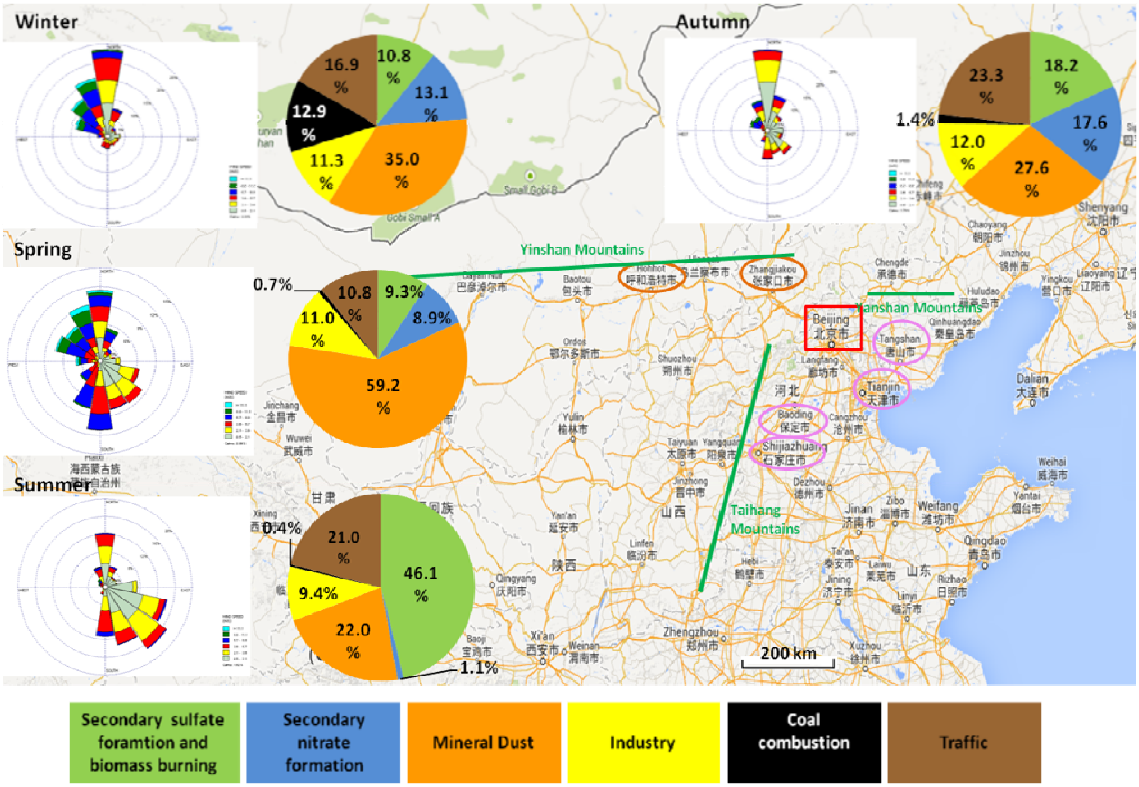

Figure 7.1: The orographic condition and emissions in the surroundings of Beijing (Source: Google map)

The government did a lot of work in the past so as to improve the air quality of Beijing, such as moving the heavy industries to Hebei Province, enforcing vehicle license plates number rule, but these measures did not lead to sustainable reduction of pollution in Beijing. Because air pollution becomes to be the regional problem now, moving the polluted industries to surrounding cities cannot solve the problem ultimately. Therefore, control strategies should be performed in a regional scale (Beijing-Tianjin-Hebei Metropolitan Region). This is also

formulated by other researchers (Ji et al., 2014; Wang et al., 2014a). The results from source appointment in this study showed that secondary inorganic ions were the main source for haze particles which indicate that changing the energy structure (reducing the coal consumption and changing into clean energies) is necessary. At the same time, the quality of coal and the cleaning of coal combustion exhausts should be improved. Coal in China has a large amount of sulfur, which can produce large SO_2 amount when it is burning and SO_2 is the precursor of SO_4^{2-} which is the important fraction of PM during haze days. Additionally, improving the fuel quality standard and vehicle emission standard are also important. Un-cleaned vehicle emissions lead to high emissions of NO_x, which is the precursor of NO_3^-, which is another important fraction of PM during haze days. Therefore, improving the purity of fuel and vehicle exhaust cleaning are helpful for the decrease of sulfur emissions and NO_3^-, respectively. At the moment, except Beijing where used GB5 vehicle emission regulation (equivalent to Euro 5 emission standard), all the other cities in China still use GB4 (equivalent to Euro 4). Now, Euro 6 is being introduced in EU member countries. So implementing GB6 (equivalent to Euro 6) not only in Beijing but also in other provinces becomes necessary. In addition, abandoning old high emission vehicles is also important. Industry emission is another important source for NO_x and SO_2. So installation of cleaning equipment in industrial exhaust vents also becomes important. Similar suggestions are also given by Ji et al. (2014). In this study, dust, which includes dust storm, resuspended dust and construction dust, is found to be the third important source of haze particles. Improving road cleaning standards, reducing construction dust and increasing vegetation coverage can help to reduce the dust particles influences. The fourth consideration should be improving the emission standard for waste incineration and biomass burning in order to reduce the influence from these activities.

In the history, similar air pollution events had happened worldwide, such as Meuse Valley fog event in 1930 (Belgium) caused by heavy industry, Los Angeles photochemical smog event in 1943 (U.S.) caused by road traffic emissions, Donora smog in 1948 (U.S.) caused by industrial emissions, London's Great Smog in 1952 (U.K.) from household heating (sulfur pollution), Ruhr area smog episodes in 1962 and 1985 (Germany) by soot from industry. Haze pollution events in China now just repeated what already had happened in these developed countries during past years. The advantages are that we can learn the experiences to avoid these haze episodes and introduce developed technology from these countries.

At the moment, Beijing government announced the PM reduction targets to the public: annual PM_{10} and $PM_{2.5}$ mass concentrations shell reach 100 μg m^{-3} and 60 μg m^{-3} in 2015 and 80 μg m^{-3}

and 50 μg m^{-3} in 2020, respectively (http://zhengwu.beijing.gov.cn/gzdt/gggs/t1225355.htm). Considering that the population in Beijing and surrounding cities is huge, the corresponding human activities, which can affect air quality, are huge. Therefore, it is a long way to go for improving the air quality and reach WHO or EC or EPA standards.

By summarizing the PhD thesis, the following points can be under consideration for further studies:

1) Concluding that fine particles are the dominant fraction in PM during haze pollution, the research on finer particles, e.g. PM_1, is necessary. So at least one year continuously sampling and analysis of PM_1, including organic and inorganic compounds, is required.

2) In this study, proposals to reduce the precursors of secondary inorganic ions are given. But the reduction of organic compounds and inorganic toxic elements of PM is also important. So emission reduction measures are necessary and reasonable suggestions for the development of strategies for reducing air pollution are necessary.

3) In order to better understand the sources of PM during haze days, high time resolution (4 h) of PM sampling was used during haze days in 2013. Unfortunately in this study, the amount of 4 h $PM_{2.5}$ samples was not enough to perform source apportionment by PMF. In order to investigate the different source and mechanisms contributing during different periods in one day, sampling should be continued during haze days with high time resolution. If all needed compounds can be analyzed above the limit of quantification, 2 h sampling should be done by priority.

4) Health influences should be studied further. In 2013, the International Agency for Research on Cancer (IARC) had classified outdoor air pollution as carcinogenic to humans (IARC Monographs, 2013). So what is the influence of particles during haze days? What is the DNA damage ratio of haze particles? This is a topic to find out certain PM compounds which influence human health most.

5) A numerical modeling of dust influence of Beijing air quality together with application of satellite-based remote sensing data systems and coupling was done by PhD thesis work of S. Schrader (2014) “Assessment of the impact of mineral dust on air quality in Northern China by using the COSMO-ART model in conjunction with satellite and ground-based data” in KIT. The next step is to investigate PM in Beijing on both modeling and experiment results.

Appendix

A. Standard Operation Procedure for filter weighing

1. Objectives

The quartz fibre filters of sampler B which will be used to measure mass concentration of filter samples and to analyze inorganic elements by PEDXRF or ICP-MS. The empty filters will be weighed in an air conditioned room at the DWD Freiburg. This standard operation procedure bases on the VDI 2463 page21.

2. Aluminum foil preparation

(1) Tools needed

① Spray bottle

② Acetone

③ Gloves (non-powder)

(2) Clean Aluminum foil

① Decide how much aluminum foil you need for one filter

②Use the spray bottle with acetone to clean the inside of aluminum foil and dry them by air.

3. Filter weighing

(1) Tools needed

① Balance

② Tweezers (non - metal)

③ Knife (ceramic)

④ Plastic divide tool

⑤ Static electricity eliminator

⑥ Gloves (non-powder)

(2) Weighing before sampling

① Before weighing, all the filters are individually packed in aluminum foil. Each aluminum foil is labeled with filter number, for example, B-1, B-2, B-3….. All the filters with aluminum foils are put in the condition room (temperature is 22°C and relative humidity is 42 %) at the DWD in Freiburg for 48 hours for an equilibrium of filters with ambient air.

② Open the balance and the static electricity eliminator. Calibrate the balance by using weights. Preheat the balance for 10 - 20 minutes.

③ Use the tweezers to make the filter to go through the static electricity eliminator 3 times, open the door of the balance, and then put the filter on the plate of the balance slightly. Please notice to keep the filter away from the walls of the balance.

④ Until the reading on the screen of the balance is stable, you can write this number down. This takes normally 1 min. At the same time, it is better that you also write down the temperature and humidity at that moment.

⑤ Use the tweezers to get the filter out of the balance and put it into the cleaned aluminum foil back.

⑥ Close the door of the balance and wait the reading on the screen to turn back to zero. Then you can weigh the next filter.

⑦ After taking the first round weighing, repeat ③-⑥ for twice again.

⑧ Each filter has its own aluminum foil and every 7 filters or 8 filters was packaged in one aluminum foil. The first week is 7 filters and then the second week is 8 filters, the third week is 7 weeks again, and so on.

⑨ After 5 hours weighing, the balance should be calibrated by using weights once more.

(3) Weighing after sampling

① Before weighing, all the filters with aluminum foil are put in the condition room (temperature is 22℃ and relative humidity is 42 %) at the DWD in Freiburg for 48 hours for equilibrium. Aluminum foil should be opened to make the filter to be touched by air.

② Open the balance and the static electricity eliminator. Calibrate the balance by using weights. Preheat the balance for 10 - 20 minutes.

③ Use the tweezers to get the filter out of the aluminum foil according to the filter number.

④ Make the filter to go through the static electricity eliminator 3 times, open the door of the balance, and then put the filter on the plate of the balance slightly. Please notice to keep the filter away from the walls of the balance.

⑤ Until the reading on the screen of the balance is stable, you can write this number down. This takes normally 1 min. Use the tweezers to get the filter out of the balance and put it back into the aluminum foil.

⑥ Close the door of the balance and wait the reading on the screen to turn back to zero. Then you can weigh the next filter.

⑦ After taking the first round weighing, repeat ③-⑥ for 2 rounds again.

4. Notice

During the whole weighing, do not touch the filter and the inside of aluminum foil even though you already wear the gloves.

B. Standard Operation Procedure for sampling

1. Background

Two DHA-80 samplers will be used in parallel to collect PM samples automatically at the ground at the CUGB nearby the measurement systems of KIT/IMG (low-volume $PM_{2.5}$ sampler) and DWD (passive sampler).

The DHA-80 samplers will be operated at flow rate of 500 l min^{-1} for 24 hours per day (00:00 – 24:00). Quartz fibre filters with 150 mm diameter will be used as sampling substrates. The duration of the sampling campaign is one year.

2. Objectives

The filters of sampler A will be used to apply GC-MS at the HMGU for organic compounds and water soluble ions. These filters will be also analyzed for EC/OC together with the University of Rostock. Further, these filters will be analyzed for DNA assay by CUMTB.

The quartz fibre filters of sampler B will be used to measure mass concentration of filter samples and to analyze for trace elements. The empty filters will be weighed in an air conditioned room at the DWD Freiburg. Before analysis of composition, the loaded filters have been weighed once more at the DWD.

3. Filter handling

(1) Pretreatment of filters

The filters of sampler A have been baked at 500°C for 6 hours before being sampled. Each filter of sampler B has been weighed in a pre-conditioned, clean environment. All the filters for sampler A and B are individually packed in aluminium foil which are labelled with filter number. 7 filters (each wrapped in pre-cleaned aluminium foil) for one sampling week have been packed together with one field blank filter (every second week) and wrapped in a pre-cleaned aluminium foil. Then all filters are sent to the CUMTB and stored there in clean environment.

(2) Preparation for sampling

1) Tools needed: gloves (non-powder), tweezers, pincer, de-ionized water, aluminum foil, ultrasonic bath, beaker (3L, Ø>170mm), oven, spray bottle, solvent (Methanol, GC Ultra Grade), pasteur pipettes, erlenmeyer flask, suction cup

2) Preparation/cleaning of filter holders

① Wear gloves while filter holders are being cleaned.

② Put the pincer into the two small holes at the both ends of the filter holder ring to get the filter holder ring out.

③ Use the de-ionized water (in spray bottle) to wash the filter holders and rings for twice.

④ Put the filter holders and rings into the beaker.

⑤ Put the de-ionized water into the beaker to cover the filter holders and rings.

⑥ Put the beaker into the ultrasonic bath for 20 min for twice.

⑦ Use the de-ionized water (in spray bottle) to wash the filter holders and rings again for 1 time.

⑧ Put the filter holders and rings on a clean plate and put them into the oven for 1 h at 110℃.

⑨ Put filter holders and rings in clean beakers and close beakers with cleaned aluminum foil.

⑩ Store cleaned filter holders and rings in clean environment until being used.

3) Preparation of work space

① The work table must be cleaned by Methanol before being used every time.

② Pre-cleaned aluminum foil has to be put on the table where you will work on. Use methanol to clean it for 2-3 times.

③ Clean the plate of the container with methanol for one time.

4) Cleaning of tweezers

① The tweezers should be cleaned before being used every time.

② Use de-ionized water (in spray bottle) to wash the tweezers for 3 times.

③ Use Methanol by Pasteur Pipettes to wash them for 3 times.

④ Put them on the clean aluminium foil and wait them to be dry.

⑤ Store cleaned tweezers in clean erlenmeyer flask and close erlenmeyer flask with cleaned aluminum foil.

5) Installation of filters of sampler A/B into holders

① Wear the gloves while preparing filters for sampling.

② Take clean filter holder from beaker and place it on cleaned aluminum foil on the table.

③ Open filter pack (7 or 8 filters) and put the filter in the filter holder by tweezers, then put the filter holder ring on the top of the filter and press the ring lightly into neck of the holder to lock the filter.

Remind to take a pack including field blank filter every second week. Please keep the aluminum foils which pack the filters clean, especially the inside which touches the filters directly. Don’t touch the inner face of aluminum foils and filters.

④ After putting one filter into the corresponding holder, write down the number of filter, the number of corresponding filter holder and the corresponding sampling date on the record form. The number of the filter holder for sampler A is from 1 to 30 and for sampler B is from 31 to 60.

⑤ Put seven or eight (when field blank is included) filter holders with filter into the container and bring the container to the sampling site. If you prepare the filters in the filter holders for several hours up to 1-2 days in advance, please use pre-cleaned aluminium foil to pack them before putting them into the container.

⑥ Wrap the aluminum foils from the individual filters in cleaned aluminum foil.

6) Putting the filter holders with filter into the samplers

① Open the door of the sampler.

② Take the filter holders out from the container and put them into the changer magazine one by one on the basis of the set time order on the record form. From the bottom up, the sampling dates of the filters are from near to far.

③ Get the memory card from the sampler. Put the memory card into the computer and copy them out and name them by the date when you copy. After that, you can open the original file in the memory card, and delete the data except the headline of the row. Put the memory card back into the sampler.

④ Start the sampling program.

⑤ Close the door of the sampler.

(3) Treatment for loaded filters

① Take out all loaded filter holders from the sampler, put them into the container and bring them back to the work table.

② Wear the gloves when handling loaded filters.

③ Take collected filter holders with filter from container and place them on cleaned aluminum foil on the work table.

④ Unwrap aluminum foils which packs filter before.

⑤ Use the pincer to get the filter holder ring out and get the filter out from the filter holder by cleaned tweezers, and then put it back into the corresponding aluminium foils (for sampler A and B) on the basis of the record form. Then wrap the aluminum foils.

⑥ Make a record about the date and time of sampling for each filter on the surface of the corresponding aluminium foil (for sampler A and B).

⑦ 7 (or 8) filters for one sampling week of sampler A or B which are wrapped in one aluminium foil again to be packed together with field blank filter every two weeks and are stored in a clean deep freezer at -20°C.

⑧ All packed filters which will be sent to Germany must be also stored under cooled conditions at -20°C. They will be put into the foamed plastic box with ice during the transport from China to Germany. Alternatively, the filters of sampler B can be transported un-cooled in a separate box.

4. Notice

(1) During the whole campaign, do not touch the filters and inner face of aluminum foils with (gloved) hands.

(2) Reading out the memory card is required once per week i.e. during the filter holders change.

(3) If something special happens, just like flood, rain, dust storm, hail etc. Please notice these things in “Remarks” on record form.

(4) The baffle pot in the sampler head should be cleaned every week. Use a plastic spatula to clean the plate at first. After that, use a cloth with methanol, not too wet, to clean the particles on the plate carefully. Last step is using brush to put some grease on the surface of the baffle pot.

(5) The sampling head with tubes should be cleaned every three months. The sampling head must be removed before cleaning. The cleaning is performed with water and some cleaning agent.

(6) The battery of the memory card should be changed every 3 months.

(7) Do not mix the filters and memory cards for sampler A and B.

Acronyms

PM: Particulate matter
POC: Polymeric organic compound
EC: Elemental carbon
OC: Organic carbon
TC: Total carbon
CM: Carbonaceous matter
OM: Organic matter
SO_2: Sulfur dioxide
NO_x: Nitrogen oxides
NH_3: Ammonia
O_3: Ozone
Cl^-: Chloride
Na^+: Sodium
K^+: Potassium
Mg^{2+}: Magnesium
Ca^{2+}: Calcium
SO_4^{2-}: Sulfate
NO_3^-: Nitrate
NH_4^+: Ammonium
Li: Lithium
Na: Sodium
Mg: Magnesium
Al: Aluminum
Si: Silicon
S: Sulfur
K: Potassium
Ca: Calcium
Sc: Scandium
Ti: Titanium
V: Vanadium
Cr: Chromium
Mn: Manganese
Fe: Iron
Co: Cobalt
Ni: Nickel

Cu: Copper
Zn: Zinc
Ge: Germanium
As: Arsenic
Mo: Molybdenum
Y: Yttrium
Cd: Cadmium
In: Indium
Sn: Tin
Sb: Antimony
Ba: Barium
W: Tungsten
Tl: Thallium
Pb: Lead
Bi: Bismuth
PAHs: Polycyclic aromatic hydrocarbons
MSA: Methane sulfuric acid
OPC: Optical pyrolyzed carbon
He: Helium
O_2: Oxygen
PTFE: Poly tetra fluoro ethylene
MSTFA: N-Methyl-N-trimethylsilyltrifluoroacetamide
Ts: 18α(H)-22,29,30-Trisnorneohopane
Tm: 17α(H)-22,29,30-Trisnorhopane
27b: 17β(H)-22,29,30-Trisnorhopane
29ab: 17α(H)21β(H)-30-Norhopane
29ba: 17β(H)21α(H)-30-Norhopane
30ab: 17α(H)21β(H)-Hopane
30ba: 17β(H)21α(H)-Hopane (Moretan)
31abS: 22S-17α(H)21β(H)-Homohopane
31abR: 22R-17α(H)21β(H)-Homohopane
32abS: 22S-17α(H)21β(H)-Bishomohopane
32abR: 22R-17α(H)21β(H)-Bishomohopane
PHE: Phenanthrene
ANT: Anthracene
PYR: Pyrene
FLU: Fluoranthene
BAA: Benz(a)anthracene
CRY: Chrysene
BBKF: Benz(bk)fluoranthene
BEP: Benzo(e)pyrene

BAP: Benzo(a)pyrene
PER: Perylene
DAH: Dibenz(a,h)anthracene
IND: Indeno(1,2,3,c,d) pyrene
PIC: Picene
BGH: Benz(g,h,i)perylene
COR: Coronen
VOC: Volatile organic compound
SOC: Secondary organic carbon
POM: Particulate organic matter
PCB: Polychlorinated biphenyl
SOA: Secondary organic aerosol

WHO: World Health Organization
EC: European Commission
US-EPA: United States Environmental Protection Agency
BTH: Beijing-Tianjin-Hebei
CUGB: China University of Geosciences (Beijing)
IAP: Institute of Atmospheric Physics
CAS: Chinese Academy of Sciences
DWD: Air Quality Department, Research Center Human Biometeorology, German Meteorological Service
KIT/IMG: Institute of Mineralogy and Geochemistry, Karlsruhe Institute of Technology
HMGU: Helmholtz Zentrum München
CUMTB: China University of Mining and Technology (Beijing)
UR: University of Rostock
BGC: Research Unit Analytical BioGeoChemistry
NOAA: US National Oceanic and Atmospheric Administration
IARC: International Agency for Research on Cancer

SEM: Scanning electron microscopy
TEM: Transmission electron microscopy
EDX: Energy dispersive X-ray
PIXE: Proton induced X-ray emission analysis
ICP-MS: Inductively coupled plasma mass spectrometry
IC: Ion chromatography
HPLC-MS: High performance liquid chromatography–mass spectrometry
GC-MS: Gas chromatography–mass spectrometry

TEOM: Tapered Element Oscillating Microbalance
PEDXRF: Polarized Energy Dispersive X-ray Fluorescence
LEM: Laboratory for Electron Microscopy
CFA: Continuous Flow Analyzer
HVS: High volume sampler
MVS: Mini-Volume sampler
LVS: Low volume sampler
IMPROVE: Interagency Monitoring of Protected Visual Environments
DTD-GC-TOFMS: Direct thermal desorption gas chromatography time-of-flight mass spectrometry

P: Air pressure
T: Temperature
RH: Relative humidity
WS: Wind speed
WD: Wind direction
MLH: Mixing layer height

SA: Source appointment
PCA: Principal component analysis
FA: Factor analysis
CMB: Chemical mass balance
PMF: Positive matrix factorization
EV-CMB: Effective Variance Chemical Mass Balance
HYSPLIT: Hybrid Single Particle Lagrangian Integrated Trajectory

SCE: Standard coal equivalent
SOP: Standard operation procedure
LOQ: Limits of quantification
S/N: Signal-to-noise
GDAS: Global Data Assimilation System
AGL: Above ground level
QA/QC: Quality assurance / quality control
S/W: Jet-to-plate distance to jet width
Re: Reynolds number
T/W: Nozzle throat length to jet width

LMW: low molecular weight
HMW: High molecular weight
HE: Haze episodes
HP: Haze polluted days

List of Figures

List of Tables

References

Adamson, I. Y. R., Prieditis, H., Hedgecock, C., et al. (2000). "Zinc Is the Toxic Factor in the Lung Response to an Atmospheric Particulate Sample." Toxicology and Applied Pharmacology 166(2): 111-119.

Aldabe, J., Elustondo, D., Santamaría, C., et al. (2011). "Chemical characterisation and source apportionment of $PM_{2.5}$ and PM_{10} at rural, urban and traffic sites in Navarra (North of Spain)." Atmospheric Research 102(1–2): 191-205.

Allen, J. O., Dookeran, N. M., Smith, K. A., et al. (1996). "Measurement of Polycyclic Aromatic Hydrocarbons Associated with Size-Segregated Atmospheric Aerosols in Massachusetts." Environmental Science & Technology 30(3): 1023-1031.

Alpert, P., Kaufman, Y. J., Shay-El, Y., et al. (1998). "Quantification of dust-forced heating of the lower troposphere." Nature 395(6700): 367-370.

Amato, F. and Hopke, P. K. (2012). "Source apportionment of the ambient $PM_{2.5}$ across St. Louis using constrained positive matrix factorization." Atmospheric Environment 46(0): 329-337.

Arditsoglou, A. and Samara, C. (2005). "Levels of total suspended particulate matter and major trace elements in Kosovo: a source identification and apportionment study." Chemosphere 59(5): 669-678.

Arimoto, R., Duce, R. A., Savoie, D. L., et al. (1996). "Relationships among aerosol constituents from Asia and the North Pacific during PEM-West A." Journal of Geophysical Research: Atmospheres 101(D1): 2011-2023.

Aymoz, G., Jaffrezo, J. L., Chapuis, D., et al. (2007). "Seasonal variation of PM_{10} main constituents in two valleys of the French Alps. I: EC/OC fractions." Atmospheric Chemistry and Physics 7(3): 661-675.

Beijing Statistic Yearbook, 2004-2013.

Bi, X., Sheng, G., Peng, P. A., et al. (2005). "Size distribution of n-alkanes and polycyclic aromatic hydrocarbons (PAHs) in urban and rural atmospheres of Guangzhou, China." Atmospheric Environment 39(3): 477-487.

Bodzek, D., Luks-Betlej, K. and Warzecha, L. (1993). "Determination of particle-associated polycyclic aromatic hydrocarbons in ambient air samples from the upper Silesia region of Poland." Atmospheric Environment. Part A. General Topics 27(5): 759-764.

Borja-Aburto, V. H., Castillejos, M., Gold, D. R., et al. (1998). "Mortality and ambient fine particles in southwest Mexico City, 1993-1995." Environmental Health Perspectives 106(12): 849-855.

Brorström-Lundén, E. and Lindskog, A. (1985). "Characterization of organic compounds on airborne particles." Environment International 11(2–4): 183-188.

Cabada, J. C., Pandis, S. N., Subramanian, R., et al. (2004). "Estimating the Secondary Organic Aerosol Contribution to $PM_{2.5}$ Using the EC Tracer Method Special Issue of Aerosol Science and Technology on Findings from the Fine Particulate Matter Supersites Program." Aerosol Science and Technology 38(Sup1): 140-155.

Cao, J. J., Lee, S. C., Chow, J. C., et al. (2007). "Spatial and seasonal distributions of carbonaceous aerosols over China." Journal of Geophysical Research: Atmospheres 112(D22): D22S11.

Cao, J. J., Lee, S. C., Zhang, X. Y., et al. (2005). "Characterization of airborne carbonate over a site near Asian dust source regions during spring 2002 and its climatic and environmental significance." Journal of Geophysical Research: Atmospheres 110(D3): D03203.

Cao, J. J., Wang, Q. Y., Chow, J. C., et al. (2012). "Impacts of aerosol compositions on visibility impairment in Xi'an, China." Atmospheric Environment 59(0): 559-566.

Cao, T., An, L., Wang, M., et al. (2008). "Spatial and temporal changes of heavy metal concentrations in mosses and its indication to the environments in the past 40 years in the city of Shanghai, China." Atmospheric Environment 42(21): 5390-5402.

Castro, L. M., Pio, C. A., Harrison, R. M., et al. (1999). "Carbonaceous aerosol in urban and rural European atmospheres: estimation of secondary organic carbon concentrations." Atmospheric Environment 33(17): 2771-2781.

Chan, C. K. and Yao, X. (2008). "Air pollution in mega cities in China." Atmospheric Environment 42(1): 1-42.

Chang, D., Song, Y. and Liu, B. (2009). "Visibility trends in six megacities in China 1973–2007." Atmospheric Research 94(2): 161-167.

Che, H., Zhang, X., Li, Y., et al. (2007). "Horizontal visibility trends in China 1981–2005." Geophysical Research Letters 34(24): L24706.

Chen, A. L. W., Watson, J. G., Chow, J. C., et al. (2010). "Chemical mass balance source apportionment for combined $PM_{2.5}$ measurements from U.S. non-urban and urban long-term networks." Atmospheric Environment 44(38): 4908-4918.

Chen, J., Tan, M., Li, Y., et al. (2008). "Characteristics of trace elements and lead isotope ratios in $PM_{2.5}$ from four sites in Shanghai." Journal of Hazardous Materials 156(1–3): 36-43.

Chen, L. W., Chow, J. C., Doddridge, B. G., et al. (2003). "Analysis of a summertime $PM_{2.5}$ and haze episode in the mid-Atlantic region." Journal of the Air & Waste Management Association 53(8): 946-956.

Cheng, Y., Engling, G., He, K. B., et al. (2014). "The characteristics of Beijing aerosol during two distinct episodes: Impacts of biomass burning and fireworks." Environmental Pollution 185(0): 149-157.

Chester, R. (1990). "Marine Geochemistry." Cambridge University Press, London: 698 pp.

China State Environmental Protection Administration of China. Ambient Air Quality Standard of People's Republic of China (GB3095-2012).

References

Chow, J. C., Watson, J. G., Chen, L. W. A., et al. (2007). "The IMPROVE_A Temperature Protocol for Thermal/Optical Carbon Analysis: Maintaining Consistency with a Long-Term Database." Journal of the Air & Waste Management Association 57(9): 1014-1023.

Chow, J. C., Watson, J. G., Crow, D., et al. (2001). "Comparison of IMPROVE and NIOSH Carbon Measurements." Aerosol Science and Technology 34(1): 23-34.

Chow, J. C., Watson, J. G., Fujita, E. M., et al. (1994). "Temporal and spatial variations of $PM_{2.5}$ and PM_{10} aerosol in the Southern California air quality study." Atmospheric Environment 28(12): 2061-2080.

Chow, J. C., Watson, J. G., Lu, Z., et al. (1996). "Descriptive analysis of $PM_{2.5}$ and PM_{10} at regionally representative locations during SJVAQS/AUSPEX." Atmospheric Environment 30(12): 2079-2112.

Chow, J. C., Watson, J. G., Pritchett, L. C., et al. (1993). "The dri thermal/optical reflectance carbon analysis system: description, evaluation and applications in U.S. Air quality studies." Atmospheric Environment. Part A. General Topics 27(8): 1185-1201.

Cusack, M., Pérez, N., Pey, J., et al. (2013). "Source apportionment of fine PM and sub-micron particle number concentrations at a regional background site in the western Mediterranean: a 2.5 year study." Atmospheric Chemistry and Physics 13(10): 5173-5187.

Cyrys, J., Dietrich, G., Kreyling, W., et al. (2001). "$PM_{2.5}$ measurements in ambient aerosol: comparison between Harvard impactor (HI) and the tapered element oscillating microbalance (TEOM) system." Science of The Total Environment 278(1-3): 191-197.

Dan, M., Zhuang, G., Li, X., et al. (2004). "The characteristics of carbonaceous species and their sources in $PM_{2.5}$ in Beijing." Atmospheric Environment 38(21): 3443-3452.

Deng, C., Zhuang, G., Huang, K., et al. (2011). "Chemical characterization of aerosols at the summit of Mountain Tai in Central East China." Atmospheric Chemistry and Physics 11(14): 7319-7332.

Deng, X., Shi, C., Wu, B., et al. (2012). "Analysis of aerosol characteristics and their relationships with meteorological parameters over Anhui province in China." Atmospheric Research 109–110(0): 52-63.

Deng, X., Tie, X., Wu, D., et al. (2008). "Long-term trend of visibility and its characterizations in the Pearl River Delta (PRD) region, China." Atmospheric Environment 42(7): 1424-1435.

Dentener, F. J., Carmichael, G. R., Zhang, Y., et al. (1996). "Role of mineral aerosol as a reactive surface in the global troposphere." Journal of Geophysical Research: Atmospheres 101(D17): 22869-22889.

Dimitrova, R., Lurponglukana, N., Fernando, H. J. S., et al. (2012). "Relationship between particulate matter and childhood asthma - basis of a future warning system for central Phoenix." Atmospheric Chemistry and Physics 12(5): 2479-2490.

Dockery, D. W., Cunningham, J., Damokosh, A. I., et al. (1996). "Health Effects of Acid Aerosols on North American Children: Respiratory Symptoms." Environmental Health Perspectives 104(5): 500-505.

Dockery, D. W., Pope, C. A., Xu, X., et al. (1993). "An Association between Air Pollution and Mortality in Six U.S. Cities." New England Journal of Medicine 329(24): 1753-1759.

Doyle, M. and Dorling, S. (2002). "Visibility trends in the UK 1950–1997." Atmospheric Environment 36(19): 3161-3172.

Duan, F., He, K., Ma, Y., et al. (2005). "Characteristics of carbonaceous aerosols in Beijing, China." Chemosphere 60(3): 355-364.

Duan, F., Liu, X., Yu, T., et al. (2004). "Identification and estimate of biomass burning contribution to the urban aerosol organic carbon concentrations in Beijing." Atmospheric Environment 38(9): 1275-1282.

Duan, F. K., He, K. B., Ma, Y. L., et al. (2006). "Concentration and chemical characteristics of $PM_{2.5}$ in Beijing, China: 2001–2002." Science of The Total Environment 355(1–3): 264-275.

Duan, J. and Tan, J. (2013). "Atmospheric heavy metals and Arsenic in China: Situation, sources and control policies." Atmospheric Environment 74(0): 93-101.

Duan, J., Tan, J., Wang, S., et al. (2012). "Size distributions and sources of elements in particulate matter at curbside, urban and rural sites in Beijing." Journal of Environmental Sciences 24(1): 87-94.

Eatough, D. J., Long, R. W., Modey, W. K., et al. (2003). "Semi-volatile secondary organic aerosol in urban atmospheres: meeting a measurement challenge." Atmospheric Environment 37(9–10): 1277-1292.

El-Gayar, M. S., Abdelfattah, A. E. and Barakat, A. O. (2002). "Maturity-dependent geochemical markers of crude petroleums from Egypt." Petroleum Science and Technology 20(9-10): 1057-1070.

Engler, C., Birmili, W., Spindler, G., et al. (2012). "Analysis of exceedances in the daily PM_{10} mass concentration (50 µg m^{-3}) at a roadside station in Leipzig, Germany." Atmospheric Chemistry and Physics 12(21): 10107-10123.

Fabbri, D., Marynowski, L., Fabiańska, M. J., et al. (2008). "Levoglucosan and Other Cellulose Markers in Pyrolysates of Miocene Lignites: Geochemical and Environmental Implications." Environmental Science & Technology 42(8): 2957-2963.

Fabbri, D., Torri, C., Simoneit, B. R. T., et al. (2009). "Levoglucosan and other cellulose and lignin markers in emissions from burning of Miocene lignites." Atmospheric Environment 43(14): 2286-2295.

Fang, G. C., Huang, Y. L. and Huang, J. H. (2010). "Study of atmospheric metallic elements pollution in Asia during 2000–2007." Journal of Hazardous Materials 180(1–3): 115-121.

Finkelman, R. B., Belkin, H. E. and Zheng, B. (1999). "Health impacts of domestic coal use in China." Proceedings of the National Academy of Sciences 96(7): 3427-3431.

Fu, F., Shinohaya, N., Ito, M., et al. (2008). "Difference between low-volume and high-volume Andersen samplers in measuring atmospheric aerosols." Particuology 6(3): 218-222.

Fu, H., Zhang, M., Li, W., et al. (2012). "Morphology, composition and mixing state of individual carbonaceous aerosol in urban Shanghai." Atmos. Chem. Phys. 12(2): 693-707.

Gao, L., Jia, G., Zhang, R., et al. (2011). "Visual Range Trends in the Yangtze River Delta Region of China, 1981–2005." Journal of the Air & Waste Management Association 61(8): 843-849.

Gao, Y., Nelson, E. D., Field, M. P., et al. (2002). "Characterization of atmospheric trace elements on $PM_{2.5}$ particulate matter over the New York–New Jersey harbor estuary." Atmospheric Environment 36(6): 1077-1086.

Garland, R. M., Schmid, O., Nowak, A., et al. (2009). "Aerosol optical properties observed during Campaign of Air Quality Research in Beijing 2006 (CAREBeijing-2006): Characteristic differences between the inflow and outflow of Beijing city air." Journal of Geophysical Research: Atmospheres 114(D2): D00G04.

Green, D. and Fuller, G. W. (2006). "The implications of tapered element oscillating microbalance (TEOM) software configuration on particulate matter measurements in the UK and Europe." Atmospheric Environment 40(29): 5608-5616.

Gu, J. w., Pitz, M., Schnelle-Kreis, J., et al. (2011). "Source apportionment of ambient particles: Comparison of positive matrix factorization analysis applied to particle size distribution and chemical composition data." Atmospheric Environment 45(10): 1849-1857.

Gu, Z. P., Feng, J. L., Han, W. L., et al. (2010). "Diurnal variations of polycyclic aromatic hydrocarbons associated with $PM_{2.5}$ in Shanghai, China." Journal of Environmental Sciences 22(3): 389-396.

Guinot, B., Cachier, H., Sciare, J., et al. (2007). "Beijing aerosol: Atmospheric interactions and new trends." Journal of Geophysical Research: Atmospheres 112(D14): D14314.

Guo, H., Lee, S. C., Ho, K. F., et al. (2003). "Particle-associated polycyclic aromatic hydrocarbons in urban air of Hong Kong." Atmospheric Environment 37(38): 5307-5317.

Guo, J., Rahn, K. A. and Zhuang, G. (2004). "A mechanism for the increase of pollution elements in dust storms in Beijing." Atmospheric Environment 38(6): 855-862.

Guo, S., Hu, M., Guo, Q., et al. (2013). "Quantitative evaluation of emission controls on primary and secondary organic aerosol sources during Beijing 2008 Olympics." Atmospheric Chemistry and Physics 13(16): 8303-8314.

Guo, S., Hu, M., Guo, Q., et al. (2012). "Primary Sources and Secondary Formation of Organic Aerosols in Beijing, China." Environmental Science & Technology 46(18): 9846-9853.

Guo, S., Hu, M., Wang, Z. B., et al. (2010). "Size-resolved aerosol water-soluble ionic compositions in the summer of Beijing: implication of regional secondary formation." Atmospheric Chemistry and Physics 10(3): 947-959.

Guo, Y., Jia, Y., Pan, X., et al. (2009). "The association between fine particulate air pollution and hospital emergency room visits for cardiovascular diseases in Beijing, China." Science of The Total Environment 407(17): 4826-4830.

Gussman, R. A. (1969). "On the Aerosol Particle Slip Correction Factor." Journal of Applied Meteorology 8(6): 999-1001.

Han, L., Zhuang, G., Cheng, S., et al. (2007). "Characteristics of re-suspended road dust and its impact on the atmospheric environment in Beijing." Atmospheric Environment 41(35): 7485-7499.

Han, L., Zhuang, G., Sun, Y., et al. (2005). "Local and non-local sources of airborne particulate pollution at Beijing." Science in China Series B: Chemistry 48(3): 253-264.

Haywood, J. and Boucher, O. (2000). "Estimates of the direct and indirect radiative forcing due to tropospheric aerosols: A review." Reviews of Geophysics 38(4): 513-543.

He, K., Yang, F., Ma, Y., et al. (2001). "The characteristics of $PM_{2.5}$ in Beijing, China." Atmospheric Environment 35(29): 4959-4970.

He, K., Zhao, Q., Ma, Y., et al. (2012). "Spatial and seasonal variability of $PM_{2.5}$ acidity at two Chinese megacities: insights into the formation of secondary inorganic aerosols." Atmospheric Chemistry and Physics 12(3): 1377-1395.

He, L. Y., Hu, M., Huang, X. F., et al. (2006). "Seasonal pollution characteristics of organic compounds in atmospheric fine particles in Beijing." Science of The Total Environment 359(1–3): 167-176.

Hedberg, E., Gidhagen, L. and Johansson, C. (2005). "Source contributions to PM_{10} and arsenic concentrations in Central Chile using positive matrix factorization." Atmospheric Environment 39(3): 549-561.

Hebei economic yearbook, 2013.

Heo, J. B., Hopke, P. K. and Yi, S. M. (2009). "Source apportionment of $PM_{2.5}$ in Seoul, Korea." Atmospheric Chemistry and Physics 9(14): 4957-4971.

Hitzenberger, R., Berner, A., Galambos, Z., et al. (2004). "Intercomparison of methods to measure the mass concentration of the atmospheric aerosol during INTERCOMP2000—influence of instrumentation and size cuts." Atmospheric Environment 38(38): 6467-6476.

Holmes, N. S. and Morawska, L. (2006). "A review of dispersion modelling and its application to the dispersion of particles: An overview of different dispersion models available." Atmospheric Environment 40(30): 5902-5928.

Hopke, P. K., Ito, K., Mar, T., et al. (2006). "PM source apportionment and health effects: 1. Intercomparison of source apportionment results." Journal of Exposure Science and Environmental Epidemiology 16(3): 275-286.

Hou, X., Zhuang, G., Sun, Y., et al. (2006). "Characteristics and sources of polycyclic aromatic hydrocarbons and fatty acids in $PM_{2.5}$ aerosols in dust season in China." Atmospheric Environment 40(18): 3251-3262.

Hsu, S. C., Liu, S. C., Arimoto, R., et al. (2010). "Effects of acidic processing, transport history, and dust and sea salt loadings on the dissolution of iron from Asian dust." Journal of Geophysical Research: Atmospheres 115(D19): D19313.

Huang, K., Zhuang, G., Lin, Y., et al. (2012). "Typical types and formation mechanisms of haze in an Eastern Asia megacity, Shanghai." Atmospheric Chemistry and Physics 12(1): 105-124.

Huang, K., Zhuang, G., Lin, Y., et al. (2010). "Relation between optical and chemical properties of dust aerosol over Beijing, China." Journal of Geophysical Research: Atmospheres 115(D7): D00K16.

Huang, K., Zhuang, G., Lin, Y., et al. (2013). "How to improve the air quality over megacities in China: pollution characterization and source analysis in Shanghai before, during, and after the 2010 World Expo." Atmospheric Chemistry and Physics 13(12): 5927-5942.

Huang, L., Yuan, C. S., Wang, G., et al. (2011). "Chemical characteristics and source apportionment of PM_{10} during a brown haze episode in Harbin, China." Particuology 9(1): 32-38.

Huang, X. F., He, L. Y., Hu, M., et al. (2006). "Annual variation of particulate organic compounds in $PM_{2.5}$ in the urban atmosphere of Beijing." Atmospheric Environment 40(14): 2449-2458.

Hussein, T., Puustinen, A., Aalto, P. P., et al. (2004). "Urban aerosol number size distributions." Atmospheric Chemistry and Physics 4(2): 391-411.

Ianniello, A., Spataro, F., Esposito, G., et al. (2011). "Chemical characteristics of inorganic ammonium salts in $PM_{2.5}$ in the atmosphere of Beijing (China)." Atmospheric Chemistry and Physics 11(21): 10803-10822.

Ianniello, A., Spataro, F., Esposito, G., et al. (2010). "Occurrence of gas phase ammonia in the area of Beijing (China)." Atmospheric Chemistry and Physics 10(19): 9487-9503.

IARC Monographs, Volume 109 (2013): Outdoor air pollution. Retrieved from "http://monographs.iarc.fr/".

IPCC, 2013: Climate Change 2013: The Physical Science Basis. Contribution of Working Group I to the Fifth Assessment Report of the Intergovernmental Panel on Climate Change (Stocker, T. F., Qin, D., Plattner G. K., et al. (eds.)]. Cambridge, United Kingdom and New York, NY, USA: Cambridge University Press.

Jacobson, M. Z. (2001). "Strong radiative heating due to the mixing state of black carbon in atmospheric aerosols." Nature 409(6821): 695-697.

Jahn, H. J., Kraemer, A., Chen, X. C., et al. (2013). "Ambient and personal $PM_{2.5}$ exposure assessment in the Chinese megacity of Guangzhou." Atmospheric Environment 74(0): 402-411.

Ji, D. S., Li, L., Wang, Y. S., et al. (2014). "The heaviest particulate air-pollution episodes occurred in northern China in January, 2013: Insights gained from observation." Atmospheric Environment 92(0): 546-556.

Jung, C. H. and Kim, Y. P. (2006). "Numerical estimation of the effects of condensation and coagulation on visibility using the moment method." Journal of Aerosol Science 37(2): 143-161.

Kadıoğlu, Y. K., Üstündağ, Z., Solak, A. O., et al. (2010). "Sources of Environmental Pollution in Ankara (Turkey): Geochemistry and Traffic Effects—PEDXRF Applications." Spectroscopy Letters 43(3): 247-257.

Kan, H., London, S. J., Chen, G., et al. (2007). "Differentiating the effects of fine and coarse particles on daily mortality in Shanghai, China." Environment International 33(3): 376-384.

Kang, Y., Liu, G., Chou, C. L., et al. (2011). "Arsenic in Chinese coals: Distribution, modes of occurrence, and environmental effects." Science of The Total Environment 412–413(0): 1-13.

Keuken, M. P., Jonkers, S., Zandveld, P., et al. (2012). "Elemental carbon as an indicator for evaluating the impact of traffic measures on air quality and health." Atmospheric Environment 61(0): 1-8.

Kim, K. H., Jahan, S. A., Kabir, E., et al. (2013). "A review of airborne polycyclic aromatic hydrocarbons (PAHs) and their human health effects." Environment International 60(0): 71-80.

Kleeman, M. J., Riddle, S. G., Robert, M. A., et al. (2009). "Source apportionment of fine ($PM_{1.8}$) and ultrafine ($PM_{0.1}$) airborne particulate matter during a severe winter pollution episode." Environmental Science & Technology 43(2): 272-279.

Kramar, U. (1999). "1999 Methods and Instrumentation - X ray fluorescence Spectrometers." Encyclopedia of Spectroscopy and Spectrometry: 2467-2477.

Lee, C. G., Yuan, C. S., Chang, J. C., et al. (2005). "Effects of aerosol species on atmospheric visibility in Kaohsiung City, Taiwan." Journal of the Air & Waste Management Association 55(7): 1031-1041.

Lee, E., Chan, C. K. and Paatero, P. (1999). "Application of positive matrix factorization in source apportionment of particulate pollutants in Hong Kong." Atmospheric Environment 33(19): 3201-3212.

Lee, K. H., Kim, Y. J. and Kim, M. J. (2006). "Characteristics of aerosol observed during two severe haze events over Korea in June and October 2004." Atmospheric Environment 40(27): 5146-5155.

Lee, P. K. H., Brook, J. R., Dabek-Zlotorzynska, E., et al. (2003). "Identification of the Major Sources Contributing to $PM_{2.5}$ Observed in Toronto." Environmental Science & Technology 37(21): 4831-4840.

Lei, C., Landsberger, S., Basunia, S., et al. (2004). "Study of $PM_{2.5}$ in Beijing suburban site by neutron activation analysis and source apportionment." Journal of Radioanalytical and Nuclear Chemistry 261(1): 87-94.

Li, W., Peng, Y., Shi, J., et al. (2011c). "Particulate polycyclic aromatic hydrocarbons in the urban Northeast Region of China: Profiles, distributions and sources." Atmospheric Environment 45(40): 7664-7671.

Li, W., Shao, L., Shen, R., et al. (2011b). "Internally Mixed Sea Salt, Soot, and Sulfates at Macao, a Coastal City in South China." Journal of the Air & Waste Management Association 61(11): 1166-1173.

Li, W., Zhou, S., Wang, X., et al. (2011a). "Integrated evaluation of aerosols from regional brown hazes over northern China in winter: Concentrations, sources, transformation, and mixing states." Journal of Geophysical Research: Atmospheres 116(D9): D09301.

Li, W. J. and Shao, L. Y. (2009). "Observation of nitrate coatings on atmospheric mineral dust particles." Atmospheric Chemistry and Physics 9(6): 1863-1871.

Li, W. J., Shao, L. Y. and Buseck, P. R. (2010b). "Haze types in Beijing and the influence of agricultural biomass burning." Atmospheric Chemistry and Physics 10(17): 8119-8130.

Li, X., Wang, L., Ji, D., et al. (2013). "Characterization of the size-segregated water-soluble inorganic ions in the Jing-Jin-Ji urban agglomeration: Spatial/temporal variability, size distribution and sources." Atmospheric Environment 77(0): 250-259.

Li, X., Wang, L., Wang, Y., et al. (2012). "Chemical composition and size distribution of airborne particulate matters in Beijing during the 2008 Olympics." Atmospheric Environment 50(0): 278-286.

Li, X., Wang, S., Duan, L., et al. (2007). "Particulate and Trace Gas Emissions from Open Burning of Wheat Straw and Corn Stover in China." Environmental Science & Technology 41(17): 6052-6058.

Li, Y., Wang, W., Kan, H., et al. (2010a). "Air quality and outpatient visits for asthma in adults during the 2008 Summer Olympic Games in Beijing." Science of The Total Environment 408(5): 1226-1227.

Li, Z., Hopke, P. K., Husain, L., et al. (2004). "Sources of fine particle composition in New York city." Atmospheric Environment 38(38): 6521-6529.

Lim, H. J. and Turpin, B. J. (2002). "Origins of Primary and Secondary Organic Aerosol in Atlanta: Results of Time-Resolved Measurements during the Atlanta Supersite Experiment." Environmental Science & Technology 36(21): 4489-4496.

Lin, J. J. and Tai, H. S. (2001). "Concentrations and distributions of carbonaceous species in ambient particles in Kaohsiung City, Taiwan." Atmospheric Environment 35(15): 2627-2636.

Lin, P., Hu, M., Deng, Z., et al. (2009). "Seasonal and diurnal variations of organic carbon in $PM_{2.5}$ in Beijing and the estimation of secondary organic carbon." Journal of Geophysical Research: Atmospheres 114(D2): D00G11.

Lippmann, M., Ito, K., Hwang, J. S., et al. (2006). "Cardiovascular effects of nickel in ambient air." Environ Health Perspect 114(11): 1662-1669.

Liu, Z. R., Wang, Y. S., Liu, Q., et al. (2013). "Source apportionment of ambient fine particle from combined size distribution and chemical composition data during summertime in Beijing." Atmospheric Chemistry and Physics Discussion 13(1): 1367-1397.

Lohmann, U. and Feichter, J. (2005). "Global indirect aerosol effects: a review." Atmospheric Chemistry and Physics 5(3): 715-737.

Magari, S. R., Schwartz, J., Williams, P. L., et al. (2002). "The association of particulate air metal concentrations with heart rate variability." Environmental Health Perspectives 110(9): 875-880.

Malm, W. C., Sisler, J. F., Huffman, D., et al. (1994). "Spatial and seasonal trends in particle concentration and optical extinction in the United States." Journal of Geophysical Research: Atmospheres 99(D1): 1347-1370.

Marple, V. A. and Liu, B. Y. H. (1974). "Characteristics of laminar jet impactors." Environmental Science & Technology 8(7): 648-654.

Marple, V. A. and Willeke, K. (1976). "Impactor design." Atmospheric Environment 10(10): 891-896.

Masclet, P., Pistikopoulos, P., Beyne, S., et al. (1988). "Long range transport and gas/particle distribution of polycyclic aromatic hydrocarbons at a remote site in the Mediterranean Sea." Atmospheric Environment 22(4): 639-650.

Meng, Z. and Lu, B. (2007). "Dust events as a risk factor for daily hospitalization for respiratory and cardiovascular diseases in Minqin, China." Atmospheric Environment 41(33): 7048-7058.

Menon, S., Hansen, J., Nazarenko, L., et al. (2002). "Climate Effects of Black Carbon Aerosols in China and India." Science 297(5590): 2250-2253.

Misra, N. L. and Singh Mudher, K. D. (2002). "Total reflection X-ray fluorescence: A technique for trace element analysis in materials." Progress in Crystal Growth and Characterization of Materials 45(1–2): 65-74.

Morawska, L., Thomas, S., Bofinger, N., et al. (1998). "Comprehensive characterization of aerosols in a subtropical urban atmosphere: particle size distribution and correlation with gaseous pollutants." Atmospheric Environment 32(14–15): 2467-2478.

Münkel, C., Eresmaa, N., Rasanen, J., et al. (2007). "Retrieval of mixing height and dust concentration with lidar ceilometer." Boundary-Layer Meteorology 124(1): 117-128.

Mutlu, A., Lee, B. K., Park, G. H., et al. (2012). "Long-term concentrations of airborne cadmium in metropolitan cities in Korea and potential health risks." Atmospheric Environment 47(0): 164-173.

Nielsen, T. (1996). "Traffic contribution of polycyclic aromatic hydrocarbons in the center of a large city." Atmospheric Environment 30(20): 3481-3490.

Norris, G., Vedantham R., Wade, K., et al. (2008). EPA Positive Matrix Factorization (PMF) 3.0 Fundamentals & User Guide.

Okada, K., Ikegami, M., Zaizen, Y., et al. (2001). "The mixture state of individual aerosol particles in the 1997 Indonesian haze episode." Journal of Aerosol Science 32(11): 1269-1279.

Omar, N. Y. M. J., Abas, M. R. B., Ketuly, K. A., et al. (2002). "Concentrations of PAHs in atmospheric particles (PM_{10}) and roadside soil particles collected in Kuala Lumpur, Malaysia." Atmospheric Environment 36(2): 247-254.

Orasche, J., Schnelle-Kreis, J., Abbaszade, G., et al. (2011). "Technical Note: In-situ derivatization thermal desorption GC-TOFMS for direct analysis of particle-bound non-polar and polar organic species." Atmospheric Chemistry and Physics 11(17): 8977-8993.

Oros, D. R. and Simoneit, B. R. T. (2000). "Identification and emission rates of molecular tracers in coal smoke particulate matter." Fuel 79(5): 515-536.

Ostro, B., Broadwin, R., Green, S., et al. (2006). "Fine particulate air pollution and mortality in nine California counties: results from CALFINE." Environmental Health Perspectives 114(1): 29-33.

Paatero, P. (1997). "Least squares formulation of robust non-negative factor analysis." Chemometrics and Intelligent Laboratory Systems 37(1): 23-35.

Paatero, P. and Hopke, P. K. (2003). "Discarding or downweighting high-noise variables in factor analytic models." Analytica Chimica Acta 490(1–2): 277-289.

Paatero, P. and Tapper, U. (1993). "Analysis of different modes of factor analysis as least squares fit problems." Chemometrics and Intelligent Laboratory Systems 18(2): 183-194.

Paatero, P. and Tapper, U. (1994). "Positive matrix factorization: A non-negative factor model with optimal utilization of error estimates of data values." Environmetrics 5(2): 111-126.

Pakkanen, T. A., Loukkola, K., Korhonen, C. H., et al. (2001). "Sources and chemical composition of atmospheric fine and coarse particles in the Helsinki area." Atmospheric Environment 35(32): 5381-5391.

Pan, Y., Wang, Y., Sun, Y., et al. (2013). "Size-resolved aerosol trace elements at a rural mountainous site in Northern China: Importance of regional transport." Science of The Total Environment 461-462: 761-771.

Pandis, S. N., Harley, R. A., Cass, G. R., et al. (1992). "Secondary organic aerosol formation and transport." Atmospheric Environment. Part A. General Topics 26(13): 2269-2282.

Pang, X., Mu, Y., Lee, X., et al. (2009). "Influences of characteristic meteorological conditions on atmospheric carbonyls in Beijing, China." Atmospheric Research 93(4): 913-919.

Park, S. S. and Kim, Y. J. (2004). "$PM_{2.5}$ particles and size-segregated ionic species measured during fall season in three urban sites in Korea." Atmospheric Environment 38(10): 1459-1471.

Park, S. S., Kim, Y. J. and Fung, K. (2001). "Characteristics of $PM_{2.5}$ carbonaceous aerosol in the Sihwa industrial area, Korea." Atmospheric Environment 35(4): 657-665.

Parmar, R. S., Satsangi, G. S., Kumari, M., et al. (2001). "Study of size distribution of atmospheric aerosol at Agra." Atmospheric Environment 35(4): 693-702.

Pathak, R. K., Wu, W. S. and Wang, T. (2009). "Summertime $PM_{2.5}$ ionic species in four major cities of China: nitrate formation in an ammonia-deficient atmosphere." Atmospheric Chemistry and Physics 9(5): 1711-1722.

Penttinen, P., Timonen, K. L., Tiittanen, P., et al. (2001). "Number Concentration and Size of Particles in Urban Air: Effects on Spirometric Lung Function in Adult Asthmatic Subjects." Environmental Health Perspectives 109(4): 319-323.

Phuleria, H. C., Geller, M. D., Fine, P. M., et al. (2006). "Size-resolved emissions of organic tracers from light- and heavy-duty vehicles measured in a California roadway tunnel." Environmental Science & Technology 40(13): 4109-4118.

Piña, A. A., Villaseñor, G. T., Jacinto, P. S., et al. (2002). "Scanning and transmission electron microscope of suspended lead-rich particles in the air of San Luis Potosi, Mexico." Atmospheric Environment 36(33): 5235-5243.

Polissar, A. V., Hopke, P. K., Paatero, P., et al. (1998). "Atmospheric aerosol over Alaska: 2. Elemental composition and sources." Journal of Geophysical Research: Atmospheres 103(D15): 19045-19057.

Pope, C. A. and Dockery, D. W. (2006). "Health Effects of Fine Particulate Air Pollution: Lines that Connect." Journal of the Air & Waste Management Association 56(6): 709-742.

Pope, C. A., Dockery, D. W. and Schwartz, J. (1995). "Review of Epidemiological Evidence of Health Effects of Particulate Air Pollution." Inhalation Toxicology 7(1): 1-18.

Qu, W. J., Arimoto, R., Zhang, X. Y., et al. (2010). "Spatial distribution and interannual variation of surface PM_{10} concentrations over eighty-six Chinese cities." Atmospheric Chemistry and Physics 10(12): 5641-5662.

Raes, F., Dingenen, R. V., Vignati, E., et al. (2000). "Formation and cycling of aerosols in the global troposphere." Atmospheric Environment 34(25): 4215-4240.

Rahn, K. A., Borys, R. D. and Shaw, G. E. (1977). "The Asian source of Arctic haze bands." Nature 268(5622): 713-715.

Ramanathan, V., Crutzen, P. J., Kiehl, J. T., et al. (2001). "Aerosols, Climate, and the Hydrological Cycle." Science 294(5549): 2119-2124.

Rastogi, N., Singh, A., Singh, D., et al. (2014). "Chemical characteristics of $PM_{2.5}$ at a source region of biomass burning emissions: Evidence for secondary aerosol formation." Environmental Pollution 184(0): 563-569.

Reff, A., Eberly, S. I. and Bhave, P. V. (2007). "Receptor modeling of ambient particulate matter data using positive matrix factorization: review of existing methods." Journal of the Air & Waste Management Association 57(2): 146-154.

Richter, P., Griño, P., Ahumada, I., et al. (2007). "Total element concentration and chemical fractionation in airborne particulate matter from Santiago, Chile." Atmospheric Environment 41(32): 6729-6738.

Rodríguez, S., Van Dingenen, R., Putaud, J. P., et al. (2005). "Nucleation and growth of new particles in the rural atmosphere of Northern Italy—relationship to air quality monitoring." Atmospheric Environment 39(36): 6734-6746.

Rogge, W. F., Hildemann, L. M., Mazurek, M. A., et al. (1993b). "Sources of fine organic aerosol. 2. Noncatalyst and catalyst-equipped automobiles and heavy-duty diesel trucks." Environmental Science & Technology 27(4): 636-651.

Rogge, W. F., Mazurek, M. A., Hildemann, L. M., et al. (1993a). "Quantification of urban organic aerosols at a molecular level: Identification, abundance and seasonal variation." Atmospheric Environment. Part A. General Topics 27(8): 1309-1330.

Rosenfeld, D., Lohmann, U., Raga, G. B., et al. (2008). "Flood or Drought: How Do Aerosols Affect Precipitation?" Science 321(5894): 1309-1313.

Ross, G. (2004). "The public health implications of polychlorinated biphenyls (PCBs) in the environment." Ecotoxicology and Environmental Safety 59(3): 275-291.

Satheesh, S. K. and Krishna Moorthy, K. (2005). "Radiative effects of natural aerosols: A review." Atmospheric Environment 39(11): 2089-2110.

Seinfeld, J. H. and Pandis, S. N. (2006). Atmospheric Chemistry and Physics: From Air Pollution to Climate Change, 2nd edition, John Wiley & Sons Inc., New Jersey, U.S..

Schäfer, K., Elsasser, M., Arteaga-Salas, J. M., et al. (2014). Source apportionment and role of meteorological conditions in the assessment of air pollution exposure due to urban emissions. Atmospheric Chemistry and Physics Discussion 14: 2235-2275.

Schäfer, K., Emeis, S., Hoffmann, H., et al. (2006). Influence of mixing layer height upon air pollution in urban and sub-urban area. Meteorologische Zeitschrift 15: 647-658.

Schäfer, K., Emeis, S., Schrader, S., et al. (2011). A measurement based analysis of the spatial distribution, temporal variation and chemical composition of particulate matter in Munich and Augsburg. Meteorologische Zeitschrift 21 (1): 47-57.

Schleicher, N., Norra, S., Chai, F., et al. (2012). Mobility of trace metals in urban atmospheric particulate matter from Beijing, China. Urban Environment. S. Rauch and G. M. Morrison, Springer Netherlands. 19: 191-200.

Schleicher, N., Norra, S., Chai, F., et al. (2010). Seasonal Trend of Water-Soluble Ions at One TSP and Five PM2.5 Sampling Sites in Beijing, China. Highway and Urban Environment. S. Rauch, G. M. Morrison and A. Monzón, Springer Netherlands. 17: 87-95.

Schleicher, N., Norra, S., Dietze, V., et al. (2011). "The effect of mitigation measures on size distributed mass concentrations of atmospheric particles and black carbon concentrations during the Olympic Summer Games 2008 in Beijing." Science of The Total Environment 412–413(0): 185-193.

Schnelle-Kreis, J., Sklorz, M., Orasche, J., et al. (2007). "Semi volatile organic compounds in ambient PM2.5. Seasonal trends and daily resolved source contributions." Environmental Science & Technology 41(11): 3821-3828.

Schrader, S. (2014). “Assessment of the impact of mineral dust on air quality in Northern China by using the COSMO-ART model in conjunction with satellite and ground-based data”. PhD thesis, Karlsruhe Institute of Technology (KIT), submission on May 23, 2014.

Schwartz, J. (1994). "Air Pollution and Daily Mortality: A Review and Meta Analysis." Environmental Research 64(1): 36-52.

Schwartz, J., Dockery, D. W. and Neas, L. M. (1996). "Is daily mortality associated specifically with fine particles?" Journal of the Air & Waste Management Association 46(10): 927-939.

See, S. W., Balasubramanian, R. and Wang, W. (2006). "A study of the physical, chemical, and optical properties of ambient aerosol particles in Southeast Asia during hazy and nonhazy days." Journal of Geophysical Research: Atmospheres 111(D10): D10S08.

Sezer Turalıoğlu, F., Nuhoğlu, A. and Bayraktar, H. (2005). "Impacts of some meteorological parameters on SO_2 and TSP concentrations in Erzurum, Turkey." Chemosphere 59(11): 1633-1642.

Shao, L., Li, J., Zhao, H., et al. (2007a). "Associations between particle physicochemical characteristics and oxidative capacity: An indoor PM_{10} study in Beijing, China." Atmospheric Environment 41(26): 5316-5326.

Shao, L., Li, W., Yang, S., et al. (2007b). "Mineralogical characteristics of airborne particles collected in Beijing during a severe Asian dust storm period in spring 2002." Science in China Series D: Earth Sciences 50(6): 953-959.

Shao, L., Shi, Z., Jones, T. P., et al. (2006). "Bioreactivity of particulate matter in Beijing air: Results from plasmid DNA assay." Science of The Total Environment 367(1): 261-272.

Shen, Z., Cao, J., Arimoto, R., et al. (2009). "Ionic composition of TSP and $PM_{2.5}$ during dust storms and air pollution episodes at Xi'an, China." Atmospheric Environment 43(18): 2911-2918.

Shi, G., Chen, Z., Bi, C., et al. (2010). "Comprehensive assessment of toxic metals in urban and suburban street deposited sediments (SDSs) in the biggest metropolitan area of China." Environmental Pollution 158(3): 694-703.

Shi, Z., Shao, L., Jones, T. P., et al. (2005). "Microscopy and mineralogy of airborne particles collected during severe dust storm episodes in Beijing, China." Journal of Geophysical Research: Atmospheres 110(D1): D01303.

Shi, Z., Shao, L., Jones, T. P., et al. (2003). "Characterization of airborne individual particles collected in an urban area, a satellite city and a clean air area in Beijing, 2001." Atmospheric Environment 37(29): 4097-4108.

Shi, Z., Shao, L., Jones, T. P., et al. (2004). "Oxidative stress on plasmid DNA induced by inhalable particles in the urban atmosphere." Chinese Science Bulletin 49(7): 692-697.

Shon, Z. H., Kim, K. H., Song, S. K., et al. (2012). "Relationship between water-soluble ions in $PM_{2.5}$ and their precursor gases in Seoul megacity." Atmospheric Environment 59(0): 540-550.

Sokolik, I. N. and Toon, O. B. (1996). "Direct radiative forcing by anthropogenic airborne mineral aerosols." Nature 381(6584): 681-683.

Song, S., Wu, Y., Jiang, J., et al. (2012). "Chemical characteristics of size-resolved $PM_{2.5}$ at a roadside environment in Beijing, China." Environmental Pollution 161: 215-221.

Song, Y., Tang, X., Xie, S., et al. (2007). "Source apportionment of $PM_{2.5}$ in Beijing in 2004." Journal of Hazardous Materials 146(1–2): 124-130.

Song, Y., Xie, S., Zhang, Y., et al. (2006b). "Source apportionment of $PM_{2.5}$ in Beijing using principal component analysis/absolute principal component scores and UNMIX." Science of The Total Environment 372(1): 278-286.

Song, Y., Zhang, Y., Xie, S., et al. (2006a). "Source apportionment of $PM_{2.5}$ in Beijing by positive matrix factorization." Atmospheric Environment 40(8): 1526-1537.

Sørensen, M., Schins, R. P. F., Hertel, O., et al. (2005). "Transition Metals in Personal Samples of $PM_{2.5}$ and Oxidative Stress in Human Volunteers." Cancer Epidemiology, Biomarkers & Prevention 14(5): 1340-1343.

Soriano, A., Pallarés, S., Pardo, F., et al. (2012). "Deposition of heavy metals from particulate settleable matter in soils of an industrialised area." Journal of Geochemical Exploration 113(0): 36-44.

Stone, R. (2008). "Beijing's Marathon Run to Clean Foul Air Nears Finish Line." Science 321(5889): 636-637.

Strader, R., Lurmann, F. and Pandis, S. N. (1999). "Evaluation of secondary organic aerosol formation in winter." Atmospheric Environment 33(29): 4849-4863.

Sun, Y., Song, T., Tang, G., et al. (2013c). "The vertical distribution of $PM_{2.5}$ and boundary-layer structure during summer haze in Beijing." Atmospheric Environment 74(0): 413-421.

Sun, Y., Wang, Z., Dong, H., et al. (2012). "Characterization of summer organic and inorganic aerosols in Beijing, China with an Aerosol Chemical Speciation Monitor." Atmospheric Environment 51(0): 250-259.

Sun, Y., Zhuang, G., Wang, Y., et al. (2004a). "The air-borne particulate pollution in Beijing—concentration, composition, distribution and sources." Atmospheric Environment 38(35): 5991-6004.

Sun, Y., Zhuang, G., Wang, Y., et al. (2005). "Chemical composition of dust storms in Beijing and implications for the mixing of mineral aerosol with pollution aerosol on the pathway." Journal of Geophysical Research: Atmospheres 110(D24): D24209.

Sun, Y., Zhuang, G., Yuan, H., et al. (2004b). "Characteristics and sources of 2002 super dust storm in Beijing." Chinese Science Bulletin 49(7): 698-705.

Sun, Y. L., Wang, Z. F., Fu, P. Q., et al. (2013b). "Aerosol composition, sources and processes during wintertime in Beijing, China." Atmospheric Chemistry and Physics 13(9): 4577-4592.

Sun, Y. L., Zhuang, G. S., Tang, A. H., et al. (2006). "Chemical characteristics of $PM_{2.5}$ and PM_{10} in haze-fog episodes in Beijing." Environmental Science & Technology 40(10): 3148-3155.

Sun, Z., Mu, Y., Liu, Y., et al. (2013a). "A comparison study on airborne particles during haze days and non-haze days in Beijing." Science of The Total Environment 456–457(0): 1-8.

Tai, A. P. K., Mickley, L. J. and Jacob, D. J. (2010). "Correlations between fine particulate matter ($PM_{2.5}$) and meteorological variables in the United States: Implications for the sensitivity of $PM_{2.5}$ to climate change." Atmospheric Environment 44(32): 3976-3984.

Tan, J. H., Bi, X. H., Duan, J. C., et al. (2006). "Seasonal variation of particulate polycyclic aromatic hydrocarbons associated with PM_{10} in Guangzhou, China." Atmospheric Research 80(4): 250-262.

Tang, I. N., Fung, K. H., Imre, D. G., et al. (1995). "Phase Transformation and Metastability of Hygroscopic Microparticles." Aerosol Science and Technology 23(3): 443-453.

Tegen, I., Lacis, A. A. and Fung, I. (1996). "The influence on climate forcing of mineral aerosols from disturbed soils." Nature 380(6573): 419-422.

Tian, H. Z., Wang, Y., Xue, Z. G., et al. (2010). "Trend and characteristics of atmospheric emissions of Hg, As, and Se from coal combustion in China, 1980–2007." Atmospheric Chemistry and Physics 10(23): 11905-11919.

Tianjin statistical yearbook, 2013.

Turpin, B. J. and Huntzicker, J. J. (1991). "Secondary formation of organic aerosol in the Los Angeles basin: A descriptive analysis of organic and elemental carbon concentrations." Atmospheric Environment. Part A. General Topics 25(2): 207-215.

Turpin, B. J. and Huntzicker, J. J. (1995). "Identification of secondary organic aerosol episodes and quantitation of primary and secondary organic aerosol concentrations during SCAQS." Atmospheric Environment 29(23): 3527-3544.

Turpin, B. J., Huntzicker, J. J., Larson, S. M., et al. (1991). "Los Angeles summer midday particulate carbon: primary and secondary aerosol." Environmental Science & Technology 25(10): 1788-1793.

Turpin, B. J. and Lim, H. J. (2001). "Species Contributions to $PM_{2.5}$ Mass Concentrations: Revisiting Common Assumptions for Estimating Organic Mass." Aerosol Science and Technology 35(1): 602-610.

VDI, 1996. VDI-guideline 2463, Blatt 11. Particulate Matter Measurement. Measurement of Mass concentration in Ambient air. Filter Method – Digitel DHA-80 Filter Changer.

VDI/DIN, 2005. DIN EN 14907. Ambient air quality – Standard gravimetric measurement method for the determination of the $PM_{2.5}$ mass fraction of suspended particulate matter (ICS 13.040.20).

Viana, M., Kuhlbusch, T. A. J., Querol, X., et al. (2008). "Source apportionment of particulate matter in Europe: A review of methods and results." Journal of Aerosol Science 39(10): 827-849.

Viana, M., Querol, X., Alastuey, A., et al. (2006). "Identification of PM sources by principal component analysis (PCA) coupled with wind direction data." Chemosphere 65(11): 2411-2418.

Wagener, S., Langner, M., Hansen, U., et al. (2012). "Spatial and seasonal variations of biogenic tracer compounds in ambient PM_{10} and PM_1 samples in Berlin, Germany." Atmospheric Environment 47(0): 33-42.

Wang, F., Chen, D. S., Cheng, S. Y., et al. (2010b). "Identification of regional atmospheric PM_{10} transport pathways using HYSPLIT, MM5-CMAQ and synoptic pressure pattern analysis." Environmental Modelling & Software 25(8): 927-934.

Wang, H., Shi, G., Li, S., et al. (2006b). "The impacts of optical properties on radiative forcing due to dust aerosol." Advances in Atmospheric Sciences 23(3): 431-441.

Wang, H., Zhou, Y., Zhuang, Y., et al. (2009b). "Characterization of $PM_{2.5}$/$PM_{2.5–10}$ and source tracking in the juncture belt between urban and rural areas of Beijing." Chinese Science Bulletin 54(14): 2506-2515.

Wang, H., Zhuang, Y., Wang, Y., et al. (2008b). "Long-term monitoring and source apportionment of $PM_{2.5}$/PM_{10} in Beijing, China." Journal of Environmental Sciences 20(11): 1323-1327.

Wang, L., Qi, J. H., Shi, J. H., et al. (2013). "Source apportionment of particulate pollutants in the atmosphere over the Northern Yellow Sea." Atmospheric Environment 70(0): 425-434.

Wang, Q., Liu, Y. and Pan, X. (2008a). "Atmosphere pollutants and mortality rate of respiratory diseases in Beijing." Science of The Total Environment 391(1): 143-148.

Wang, S. and Mulligan, C. N. (2006). "Occurrence of arsenic contamination in Canada: Sources, behavior and distribution." Science of The Total Environment 366(2–3): 701-721.

Wang, S., Zhao, M., Xing, J., et al. (2010a). "Quantifying the Air Pollutants Emission Reduction during the 2008 Olympic Games in Beijing." Environmental Science & Technology 44(7): 2490-2496.

Wang, X., Westerdahl, D., Chen, L. C., et al. (2009a). "Evaluating the air quality impacts of the 2008 Beijing Olympic Games: On-road emission factors and black carbon profiles." Atmospheric Environment 43(30): 4535-4543.

Wang, Y. S., Zhou, L., Wang, M. X., et al. (2001). "Trends of atmospheric methane in Beijing." Chemosphere - Global Change Science 3(1): 65-71.

Wang, Y., Ren, X., Ji, D., et al. (2012). "Characterization of volatile organic compounds in the urban area of Beijing from 2000 to 2007." Journal of Environmental Sciences 24(1): 95-101.

Wang, Y., Yao, L., Wang, L., et al. (2014a). "Mechanism for the formation of the January 2013 heavy haze pollution episode over central and eastern China." Science China Earth Sciences 57(1): 14-25.

Wang, Y., Zhuang, G., Sun, Y., et al. (2005a). "Water-soluble part of the aerosol in the dust storm season—evidence of the mixing between mineral and pollution aerosols." Atmospheric Environment 39(37): 7020-7029.

Wang, Y., Zhuang, G., Sun, Y., et al. (2006a). "The variation of characteristics and formation mechanisms of aerosols in dust, haze, and clear days in Beijing." Atmospheric Environment 40(34): 6579-6591.

Wang, Y., Zhuang, G., Tang, A., et al. (2005b). "The ion chemistry and the source of $PM_{2.5}$ aerosol in Beijing." Atmospheric Environment 39(21): 3771-3784.

Wang, Z., Li, J., Wang, Z., et al. (2014b). "Modeling study of regional severe hazes over mid-eastern China in January 2013 and its implications on pollution prevention and control." Science China Earth Sciences 57(1): 3-13.

Wehner, B. and Wiedensohler, A. (2003). "Long term measurements of submicrometer urban aerosols: statistical analysis for correlations with meteorological conditions and trace gases." Atmospheric Chemistry and Physics 3(3): 867-879.

Wei, Y., Han, I. K., Hu, M., et al. (2010). "Personal exposure to particulate PAHs and anthraquinone and oxidative DNA damages in humans." Chemosphere 81(10): 1280-1285.

World Health Organisation (WHO), Global Health Observatory (GHO), 2012. Available from: http://www.who.int/gho/phe/outdoor_air_pollution/burden_text/en/index.html

Wu, C. F., Li, Y. R., Kuo, I. C., et al. (2012a). "Investigating the association of cardiovascular effects with personal exposure to particle components and sources." Science of The Total Environment 431(0): 176-182.

Wu, J., Fu, C., Zhang, L., et al. (2012b). "Trends of visibility on sunny days in China in the recent 50 years." Atmospheric Environment 55(0): 339-346.

Wu, Y., Yang, L., Zheng, X., et al. (2014). "Characterization and source apportionment of particulate PAHs in the roadside environment in Beijing." Science of The Total Environment 470–471(0): 76-83.

Xiao, H. Y. and Liu, C. Q. (2004). "Chemical characteristics of water-soluble components in TSP over Guiyang, SW China, 2003." Atmospheric Environment 38(37): 6297-6306.

Xie, C., Nishizawa, T., Sugimoto, N., et al. (2008). "Characteristics of aerosol optical properties in pollution and Asian dust episodes over Beijing, China." Applied Optics 47(27): 4945-4951.

Xu, L., Chen, X., Chen, J., et al. (2012). "Seasonal variations and chemical compositions of $PM_{2.5}$ aerosol in the urban area of Fuzhou, China." Atmospheric Research 104-105: 264-272.

Yadav, A. K., Kumar, K., Kasim, A. M. b. H. A., et al. (2003). "Visibility and Incidence of Respiratory Diseases During the 1998 Haze Episode in Brunei Darussalam." Pure and applied geophysics 160(1-2): 265-277.

Yang, F., Huang, L., Duan, F., et al. (2011a). "Carbonaceous species in $PM_{2.5}$ at a pair of rural/urban sites in Beijing, 2005–2008." Atmospheric Chemistry and Physics 11(15): 7893-7903.

Yang, F., Tan, J., Zhao, Q., et al. (2011b). "Characteristics of $PM_{2.5}$ speciation in representative megacities and across China." Atmospheric Chemistry and Physics 11(11): 5207-5219.

Yang, F., Ye, B., He, K., et al. (2005). "Characterization of Atmospheric Mineral Components of $PM_{2.5}$ in Beijing and Shanghai, China." Science of The Total Environment 343(1–3): 221-230.

Yang, G., Ma, L., Xu, D., et al. (2012). "Levels and speciation of arsenic in the atmosphere in Beijing, China." Chemosphere 87(8): 845-850.

Yang, L., Cheng, S., Wang, X., et al. (2013). "Source identification and health impact of $PM_{2.5}$ in a heavily polluted urban atmosphere in China." Atmospheric Environment 75: 265-269.

Yang, Y., Wang, Y., Wen, T., et al. (2009). "Elemental composition of $PM_{2.5}$ and PM_{10} at Mount Gongga in China during 2006." Atmospheric Research 93(4): 801-810.

Yao, X., Chan, C. K., Fang, M., et al. (2002). "The water-soluble ionic composition of $PM_{2.5}$ in Shanghai and Beijing, China." Atmospheric Environment 36(26): 4223-4234.

Yu, L. D., Wang, G. F., Zhang, R. J., et al. (2013). "Characterization and Source Apportionment of $PM_{2.5}$ in an Urban Environment in Beijing." Aerosol and Air Quality Research 13(2): 574-583.

Yuan, C. S., Lee, C. G., Liu, S. H., et al. (2006). "Correlation of atmospheric visibility with chemical composition of Kaohsiung aerosols." Atmospheric Research 82(3–4): 663-679.

Yuan, H., Zhuang, G., Li, J., et al. (2008). "Mixing of mineral with pollution aerosols in dust season in Beijing: Revealed by source apportionment study." Atmospheric Environment 42(9): 2141-2157.

Yunker, M. B., Macdonald, R. W., Vingarzan, R., et al. (2002). "PAHs in the Fraser River basin: a critical appraisal of PAH ratios as indicators of PAH source and composition." Organic Geochemistry 33(4): 489-515.

Zhang, J. K., Sun, Y., Liu, Z. R., et al. (2014a). "Characterization of submicron aerosols during a month of serious pollution in Beijing, 2013." Atmospheric Chemistry and Physics 14(6): 2887-2903.

Zhang, L., Vet, R., Wiebe, A., et al. (2008a). "Characterization of the size-segregated water-soluble inorganic ions at eight Canadian rural sites." Atmospheric Chemistry and Physics 8(23): 7133-7151.

Zhang, R., Arimoto, R., An, J., et al. (2005). "Ground observations of a strong dust storm in Beijing in March 2002." Journal of Geophysical Research: Atmospheres 110(D18): D18S06.

Zhang, R., Han, Z., Cheng, T., et al. (2009). "Chemical properties and origin of dust aerosols in Beijing during springtime." Particuology 7(1): 61-67.

Zhang, R., Jing, J., Tao, J., et al. (2013). "Chemical characterization and source apportionment of $PM_{2.5}$ in Beijing: seasonal perspective." Atmospheric Chemistry and Physics 13(14): 7053-7074.

Zhang, R., Li, Q. and Zhang, R. (2014b). "Meteorological conditions for the persistent severe fog and haze event over eastern China in January 2013." Science China Earth Sciences 57(1): 26-35.

Zhang, T., Claeys, M., Cachier, H., et al. (2008b). "Identification and estimation of the biomass burning contribution to Beijing aerosol using levoglucosan as a molecular marker." Atmospheric Environment 42(29): 7013-7021.

Zhang, W., Guo, J., Sun, Y., et al. (2007). "Source apportionment for urban PM_{10} and $PM_{2.5}$ in the Beijing area." Chinese Science Bulletin 52(5): 608-615.

Zhang, W., Zhuang, G., Guo, J., et al. (2010). "Sources of aerosol as determined from elemental composition and size distributions in Beijing." Atmospheric Research 95(2–3): 197-209.

Zhang, W. J., Sun, Y. L., Zhuang, G. S., et al. (2006). "Characteristics and seasonal variations of $PM_{2.5}$, PM_{10}, and TSP aerosol in Beijing." Biomedical and Environmental Sciences 19(6): 461-468.

Zhang, X. Y., Gong, S. L., Shen, Z. X., et al. (2003a). "Characterization of soil dust aerosol in China and its transport and distribution during 2001 ACE-Asia: 1. Network observations." Journal of Geophysical Research: Atmospheres 108(D9): 4261.

Zhang, X. Y., Gong, S. L., Zhao, T. L., et al. (2003b). "Sources of Asian dust and role of climate change versus desertification in Asian dust emission." Geophysical Research Letters 30(24): 2272.

Zhang, X. Y., Wang, Y. Q., Zhang, X. C., et al. (2008c). "Carbonaceous aerosol composition over various regions of China during 2006." Journal of Geophysical Research: Atmospheres 113(D14): D14111.

Zhao, P. S., Dong, F., Yang, Y., et al. (2013a). "Characteristics of carbonaceous aerosol in the region of Beijing, Tianjin, and Hebei, China." Atmospheric Environment 71(0): 389-398.

Zhao, P. S., Dong, F., He, D., et al. (2013b). "Characteristics of concentrations and chemical compositions for $PM_{2.5}$ in the region of Beijing, Tianjin, and Hebei, China." Atmospheric Chemistry and Physics 13(9): 4631-4644.

Zhao, X. J., Zhao, P. S., Xu, J., et al. (2013c). "Analysis of a winter regional haze event and its formation mechanism in the North China Plain." Atmospheric Chemistry and Physics 13(11): 5685-5696.

Zhao, Y. and Gao, Y. (2008). "Mass size distributions of water-soluble inorganic and organic ions in size-segregated aerosols over metropolitan Newark in the US east coast." Atmospheric Environment 42(18): 4063-4078.

Zheng, M. and Fang, M. (2000). "Particle-associated Polycyclic Aromatic Hydrocarbons in the Atmosphere of Hong Kong." Water, Air, and Soil Pollution 117(1-4): 175-189.

Zheng, M., Salmon, L. G., Schauer, J. J., et al. (2005). "Seasonal trends in $PM_{2.5}$ source contributions in Beijing, China." Atmospheric Environment 39(22): 3967-3976.

Zhou, Y., Wu, Y., Yang, L., et al. (2010). "The impact of transportation control measures on emission reductions during the 2008 Olympic Games in Beijing, China." Atmospheric Environment 44(3): 285-293.

Zhu, L., Huang, X., Shi, H., et al. (2011). "Transport pathways and potential sources of PM_{10} in Beijing." Atmospheric Environment 45(3): 594-604.

Zhuang, G., Guo, J., Yuan, H., et al. (2001). "The compositions, sources, and size distribution of the dust storm from China in spring of 2000 and its impact on the global environment." Chinese Science Bulletin 46(11): 895-900.